UNIVERSIDADE
BEIRA INTERIOR

Developing Energy Harvest Efficient Strategies with Microbial Fuel Cells

Pedro Miguel Domingos Serra

Tese para obtenção do Grau de Doutor em
Engenharia Electrotécnica e de Computadores
(3º ciclo de estudos)

Orientador: Prof. Doutor António Eduardo Vitória Espírito Santo

novembro de 2021

Provas realizadas a 26 de outubro de 2021 pelas 14h30.

O júri das referidas provas foi constituído pelo Doutor António João Marques Cardoso, professor catedrático da Universidade da Beira Interior, Doutor Senentxu Lanceros-Mendez, professor associado da Universidade do Minho, Doutor António José Guerreiro de Brito, professor associado do Instituto Superior de Agronomia da Universidade de Lisboa, Doutora Maria do Rosário Alves Calado, professora associada da Universidade da Beira Interior, Doutor António Eduardo Vitória do Espírito Santo, professor auxiliar da Universidade da Beira Interior.

Dedication

A work such as this is pervaded by challenges and self-conquests. Although being a process of great intellectual independence, finishing it with merit and pleasure is impossible without friends, family and mentors. My friends have my appreciation: they are the keepers of secrets, tears and smiles, most of them a stress exhaust. I can't forget the patience, gratitude and unconditional support of my family which, more frequent than not, were treated unfairly due to my unease. My mentors have my acknowledgement since advising in comfort does not contribute to growth. I got close with several emotions, good and bad. Fortunately, my friend, accomplice and partner for life, Joana Santos, never let me go. And although slowly, I've grown tremendously.

I thank you all. From the bottom of my heart.

Dedicatória

Um trabalho desta natureza é permeado por desafios e conquistas. Apesar de ser um processo de grande independência intelectual, concluí-lo com mérito e prazer é impossível sem se fazer acompanhar de amigos, família e mentores. Aos primeiros deixo o meu agradecimento: guardam confissões e sorrisos cúmplices que são escape. À família é impossível esquecer o reconhecimento, a paciência e o apoio incondicional: não são poucas as vezes em somos injustos por fruto do incómodo. Aos mentores entrego a minha gratidão, porque aconselhar em conforto não é estimular o crescimento. Por tudo isto agarrei e larguei a mão a várias emoções. Felizmente, a minha amiga, cúmplice e namorada, Joana Santos, nunca quis largar-me a mão. E este processo fez-me crescer de formas inimagináveis. A ela rendo o meu amor. A todos, agradeço. Do fundo do coração: obrigado!

Acknowledgments

I received significative help to finish this work. In the academic and professional community, my acknowledgments go to Professor António Albuquerque, to Professor António Magrinho, and to João Pereira, PhD. From the University of Minho, I also thank to Professor Senentxu Lanceros-Mendez and Carlos Costa, PhD. I would also like to recognize the contributions of the company Águas da Serra, through the help of the engineer Orlanda Carvalho and the analysts Ângela Rito and Ana Matos.

A special thank you to my supervisor, Professor António Eduardo Vitória Espírito Santo that was available to guide me through this journey: we did not always agree and that stimulated my patience, my perseverance and my judgment and critical thinking.

A final acknowledgement for the funding received from the Telecommunications Institute and the Portuguese Foundation for Science and Technology (ERANETMED/0004/2014).

Agradecimentos

A ajuda que me foi prestada para a conclusão desta formação tem contribuições várias. No meio académico e profissional, agradeço ao Professor Doutor António Albuquerque, ao Professor Doutor António Magrinho, ao Doutor João Pereira. Da Universidade do Minho, agradeço também ao Professor Doutor Senentxu Lanceros-Mendez e ao Doutor Carlos Costa. Agradeço ainda a ajuda da empresa Águas da Serra, na pessoa da Engenheira Orlanda Carvalho e das Analistas Ângela Rito e Ana Matos.

Deixo um agradecimento especial ao meu orientador, Professor Doutor António Eduardo Vitória Espírito Santo, por se ter disponibilizado a acompanhar neste trajeto: nem sempre estivemos de acordo, o que estimulou a minha paciência, perseverança, capacidade argumentativa, organizativa e pensamento crítico.

Agradeço ainda ao Instituto de Telecomunicações e à Fundação para a Ciência e Tecnologia (ERANETMED/0004/2014) pelo financiamento prestado no apoio à elaboração deste projeto.

Resumo

Pensar em economia energética é, hoje, considerar soluções para a redução de consumo e reutilização de recursos. Esta preocupação é importante ao examinar a utilização dos recursos hídricos. O consumo de água potável está a crescer insustentavelmente e, apesar de grande parte desse consumo ser restituído ao meio ambiente, a qualidade da água é afetada por poluentes ou impurezas.

A utilização de água residual, um produto da nossa rotina e qualidade de vida, como um recurso é, por isso, uma mais valia. É ainda mais evidente ao considerar os elevados consumos energéticos de uma estação de tratamento de água residual.

As hipóteses abordadas neste trabalho mostram como é possível atingir este objetivo usando células microbianas de combustível. A composição orgânica desta água faz com que o seu potencial energético possa ser explorado, usando o metabolismo bacteriano para produzir energia e, simultaneamente, auxiliar na limpeza da água.

Este documento está dividido em 5 capítulos. O posicionamento do tema ocorre no capítulo 1. O capítulo 2 observa os principais elementos da tecnologia das células microbianas de combustível, permitindo compreender o seu funcionamento e conhecer que variáveis afetam o seu funcionamento. No capítulo 3 são apresentadas as tipologias de abordagem à gestão energética para esta pilha bacteriológica, discutindo-se as vantagens e otimizações de cada sistema. O penúltimo capítulo corresponde à exploração de resultados experimentais e à validação de hipóteses, orientadas para a maior eficiência energética. Surgem assim recomendações que servirão para guiar os trabalhos futuros, discutidos no capítulo final. Este, o capítulo 5, conta ainda com a apresentação das principais conclusões e das tendências de pesquisa. O trabalho termina com um exemplo de aplicação que solidifica a validade e utilidade da aplicação desta tecnologia.

Palavras-chave

Nexus energia-água; Água residual; Recolha energia de baixa potência; Células microbiológicas de combustível.

Abstract

Nowadays, thinking of energetic efficiency is to determine how to decrease consumption and to reuse resources. This is a major concern when addressing hydric resources. The consumption of drinking water is seeing an unaffordable growth and, although most of it is replenished to the environment, the water quality is affected by pollutants and impurities.

As such, using wastewater, a by-product of our routine and way of life, as resource is an asset. Even more when thinking about the heightened energy costs of a wastewater treatment station.

The hypotheses of this work show how to achieve this goal by using microbial fuel cells. The organic composition of this water increases its energy production potential, where the bacterial metabolism can be used to, simultaneously, produce energy and help to clean the water.

This document is divided in 5 chapters. The strategic positioning of the theme happens in chapter 1. Chapter 2 explains how the main elements of microbial fuel cell technology can work and determine its operation. In chapter 3, the power management systems used with microbial fuel cells are presented and discussed, with the identification of optimization strategies. The second-to-last chapter corresponds to the experimental results discussion and validation, while focusing improved energy production efficiencies. The outputs of this chapter pilot the future work analysis on chapter 5, together with the main conclusions and research trends. The validity and usefulness of this work is cleared with an application example.

Keywords

Energy-water nexus; Wastewater; Low-power energy harvesting; Microbial Fuel Cells.

Resumo alargardo

Introdução

Esta secção apresenta o resumo alargado, em português, do trabalho de investigação da Tese de doutoramento intitulada de "Developing Energy Harvesting Efficient Strategies with MFCs". Em primeiro lugar é feito o posicionamento geral do trabalho de investigação, seguido da análise dos problemas abordados e respetivas conclusões. As direções para trabalhos futuros colmatam esta secção.

Enquadramento

É cada vez mais evidente a interdependência entre água, energia e alimento. Estes três elementos são fundamentais para a nossa sobrevivência e desenvolvimento, suprimindo necessidades fundamentais. A utilização da tecnologia na otimização de processos e reciclagem de recursos tem conduzido a grandes conquistas, mas há ainda muito trabalho a desenvolver na relação entre água e energia.

Os custos diretos com energia estão associados à exploração, tratamento ou produção, distribuição e taxas ambientais. No que diz respeito à água, grande parte dos custos estão concentrados no tratamento e distribuição. O peso das despesas em cada um destes setores pode ser mitigado com estratégias adequadas à potencialização dos contributos de cada um dos recursos entre si: é utilizada água na produção de energia (por exemplo, para refrigeração de centrais termoelétricas) e essa energia pode ser, por exemplo, utilizada para alimentar estações de tratamento de águas residuais.

No exemplo acima é identificada uma utilização partilhada de um recurso. Este ponto de partida é muito vantajoso precisamente nas estações de tratamento de água residual: o tratamento da água residual para retorno ao consumo é uma necessidade com um custo energético elevado. Ainda assim, é possível extrair energia de água residual por vários métodos: pela exploração da sua composição orgânica, composição química, pelo aproveitamento da sua energia térmica e ainda pela reciclagem de alguns elementos nutricionais, como o azoto e o fósforo (que têm grande aplicabilidade na agricultura). A energia térmica pode ser recolhida usando bombas de calor, apesar dessa recolha estar dependente da temperatura da água residual. A produção de metano através de água residual também possível, podendo depois ser utilizado como fonte de energia. A recolha de energia tirando partido da composição orgânica da água residual é um processo simbiótico, uma vez que é necessário manipular as bactérias deste substrato para a

produção de eletricidade. Recorrendo a reações de oxidação-redução, é possível produzir energia e limpar a água residual, o âmago do nexus água-energia.

A materialização deste objetivo é alcançada recorrendo às células microbiológicas de combustível, do inglês Microbial Fuel Cell (MFC). São cinco os elementos mais importantes numa MFC: o ânodo, o cátodo, o substrato, a membrana e as bactérias. A produção de energia tem início quando as bactérias oxidam o substrato e libertam os eletrões finais resultantes para o ânodo. A diferença de potencial entre este elétrodo e o cátodo, exposto ao oxigénio ou outro aceitador final de eletrões, promove o fluxo de eletrões e a concomitante produção de energia. A membrana é responsável por impedir que as bactérias tenham contacto com aceitador final de eletrões disponível no cátodo: doutra forma, não haveria vantagem energética na entrega dos eletrões finais ao primeiro elétrodo.

Por ser uma tecnologia com aproximadamente 100 anos e, pelo menos, uma variável de difícil controlo (o metabolismo bacteriológico), é possível conduzir investigações em diferentes temas. No que diz respeito ao reator em si, é possível avaliar, por exemplo, diferentes materiais, geometrias, substratos e famílias de bactérias. Ao considerar a MFC como um bloco indistinguível, a atenção é concentrada nos dispositivos a ela ligados, originando trabalhos relacionados com sistemas de gestão de energia.

Problemas abordados e respetivas conclusões

Nesta tese, foram primeiramente definas as configurações ótimas para uma proposta de MFC: um reator de câmara simples, com cátodo exposto ao ar e substrato de água residual artificial com acetato. Depois de confirmadas as configurações ótimas para uma proposta de MFC, o problema abordado em seguida focou-se nas metodologias de colonização do ânodo. A resolução deste desafio, quer por colonização primária ou por colonização secundária (a partir de uma colónia já existente), é determinante para a efetiva produção de energia da MFC. Houve também lugar a uma breve pesquisa sobre os fatores internos que podem impactar a produção de energia: parâmetros bioquímicos, temperatura, alteração das características dos elétrodos e métodos de disponibilização do substrato.

Tendo encontrado um compromisso ótimo para os parâmetros acima discutidos, procedeu-se ao estudo de estratégias de otimização da recolha de energia a partir destas fontes. O primeiro esclarecimento para este objetivo tratou de criar um modelo elétrico para a MFC, quer para respostas estabilizadas, quer para respostas transitórias. Este modelo possibilitou quantificar a resistência interna da célula, permitindo concretizar a

operação no ponto máximo de funcionamento. Através da correspondência de impedância entre a MFC e os dispositivos a si ligados, foi também possível determinar quais os modos de operação da célula mais favoráveis à produção de energia. Estudaram-se associações série e paralelo de reatores, bem como funcionamentos contínuos e comutados. Nas associações de reatores, ficou claro que a associação em série produz maiores valores de tensão e que a associação em paralelo leva à produção de valores de corrente mais interessantes. Seja qual for a tipologia de associação, a potência elétrica é sempre maior. Nos estudos dos modos de funcionamento, verificou-se que a ligação comutada, com a célula em circuito aberto por períodos de tempo superiores ou iguais a 30 minutos é mais vantajosa para os primeiros 5 minutos de operação comutada. Todavia, esta operação comutada tem também parâmetros ótimos de configuração, com um ciclo de funcionamento de 95% para uma frequência de 500 Hz.

Foi depois estabelecida uma correspondência para a ligação de condensadores diretamente à célula, comparando o seu perfil de carregamento para um funcionamento contínuo e um funcionamento comutado. Verificou-se que o funcionamento contínuo provoca grandes variações de tensão, representantes das profundas adaptações provocadas ao biofilme exoeletrogénico do reator. Por outro lado, a operação comutada não só previne essas variações, mantendo o valor de tensão do reator, como conduz a um carregamento mais rápido e para maiores valores de tensão.

Estas considerações e estudos anteriores culminam na proposta de um sistema de gestão de energia adequado a MFC. O valor máximo de tensão de uma MFC é inferior a 0,8 V quando opera em circuito aberto, ou seja, quando a célula não fornece corrente, e, por isso, a impedância interna não provoca uma queda de tensão. Com o aumento da corrente fornecida pela célula, a tensão de saída tende a diminuir. Esta característica pode fazer com que a tensão de saída da célula não seja suficiente para fazer arrancar um conversor DC/DC, necessário para regular a tensão para um nível capaz de ser utilizado para alimentar outros dispositivos. A solução deste problema passa por recorrer a um andar intermédio, que implementa um mecanismo capaz de elevar a tensão para um valor suficiente que permita o arranque do conversor DC/DC. Esta tensão regulada e elevada para um nível adequado poderá então ser utilizada para alimentar outros dispositivos.

Trabalhos futuros

Considerando a aplicação desta tecnologia em estações de tratamento de águas residuais, é de manifesto interesse a reutilização da energia, desta forma recuperada, na mesma localização. Na verdade, estas infraestruturas concretizam pesados investimentos energéticos e financeiros e uma solução deste género contribui para diminuir este peso. Apesar da energia produzida não ser grande, a sua gestão e utilização adequada pode garantir a alimentação de sensores de qualidade, obrigatórios para cumprir com as normas e regras de tratamento destas estações. Conceptualizando um formato de sensor inteligente, onde o sensor de qualidade é alimentado por uma MFC e tem capacidades de comunicação, é possível idealizar uma rede de sensores sem fios capaz de instrumentar uma estação de tratamento de águas residuais, eventualmente sem requisitos energéticos adicionais. Terá ainda a mais valia de não requerer ou estar sujeito à disponibilidade de operadores humanos. Se os dados forem armazenados numa estrutura de dados online, na cloud, é ainda possível diminuir as restrições de acesso, sem comprometer gravemente a segurança, a estes dados. Assim, a única restrição de aplicação desta tecnologia tem a ver com a disponibilidade do substrato. Tendo sido feito estudo de caso com as estações de tratamento de águas residuais, existem outras possibilidades para aplicar esta tecnologia. São exemplo todos os pontos de águas paradas (lagos ou lagoas, poços) e/ou outros com composição orgânica (pontos de rega, canalizações domésticas).

List of publications

1. P. M. D. Serra, A. Espírito-Santo and A. Albuquerque, "An experimental setup for energy efficiency evaluation of microbial fuel cells," *2015 IEEE International Conference on Industrial Technology (ICIT)*, Seville, 2015, pp. 902-907, doi: 10.1109/ICIT.2015.7125212.
2. P. Serra and A. V. Espirito-Santo, "Harvesting Energy from Microbial Fuel Cells: Powering Wireless Sensor Networks Operating in Wastewater Treatment Plants," in *Biologically-Inspired Energy Harvesting through Wireless Sensor Technologies*, Hershey, PA, USA: IGI Global, 2016, pp. 121–171.
3. A. Espírito-Santo, P. Serra, S. Albuquerque, B. Ribeiro, F. Santos and J. Páscoa, "Low-power smart sensing in energy and water systems integration," *2017 IEEE International Workshop on Measurement and Networking (M&N)*, Naples, 2017, pp. 1-6, doi: 10.1109/IWMN.2017.8078408.
4. P. M. Domingos Serra, A. Esoírito-Santo and M. Magrinho, "Energy Harvesting from Wastewater with a Single-Chamber Air-Cathode Microbial Fuel Cell," *IECON 2018 - 44th Annual Conference of the IEEE Industrial Electronics Society*, Washington, DC, 2018, pp. 3847-3851, doi: 10.1109/IECON.2018.8592827.
5. P. M. D. Serra, A. Espírito-Santo, J. Bonifácio and F. S. Relvas, "Capacitive Level Smart Sensors in the Management of Wastewater Treatment Processes," *2019 IEEE International Symposium on Measurements & Networking (M&N)*, Catania, Italy, 2019, pp. 1-6, doi: 10.1109/IWMN.2019.8804993.
6. A. Espírito-Santo, S. Ambrósio, P. M. D. Serra and R. J. C. Pinto, "Water pH Monitoring with a Smart Sensor Powered by a Thermoelectric Generator with a Phase-Change Material," *IECON 2019 - 45th Annual Conference of the IEEE Industrial Electronics Society*, Lisbon, Portugal, 2019, pp. 5550-5555, doi: 10.1109/IECON.2019.8927259.
7. P.M.D. Serra, A. Espírito-Santo, M. Magrinho, A steady-state electrical model of a microbial fuel cell through multiple-cycle polarization curves, *Renew. Sustain. Energy Rev.* (2020), https://doi.org/10.1016/j.rser.2019.109439 (IF 10.556, Q1 Renewable Energy, Sustainability and the Environment)
8. Serra, P.M., Espírito-Santo, A. & Magrinho, M. An Experimental Setup for Microbial Fuel Cells Construction, Evaluation, and Study. *Instrum Exp Tech* 63, 567–576 (2020), https://doi.org/10.1134/S0020441220040326 (IF 0.443, Q3 Instrumentation)
9. P.M.D. Serra, E.-S. A, Sourcing power with microbial fuel cells: A timeline, *J. Power Sources*. 482 (2021) 228921, https://doi.org/https://doi.org/10.1016/j.jpowsour.2020.228921 (IF 7.467, Q1 Electrical and Electronic Engineering)
10. P. M. D. Serra, A. Espírito-Santo, Electrical energy produced by microbial fuel cells using wastewater to power a network of smart sensors, in *Delivering Low-Carbon Biofuels with Bioproduct Recovery* (December 2020), Elsevier.

Contents

List of Figures

Chapter 1

Chapter 2

Chapter 3

Chapter 4

Chapter 5

List of tables

Chapter 2

Chapter 3

Chapter 4

Acronyms

ABS	Acrylonitrile Butadiene Styrene
AD	Anaerobic Digesters
AEM	Anion Exchange Membrane
AS-MFC	Air-cathode Single-chambered MFC
ATT	Advanced Thermal Treatments
AW	Artificial Wastewater
BES	Bio-Electrochemical Systems
BMFC	Benthic Microbial Fuel Cell
BO	Blocking Oscillator
BOSV	Blocking Oscillator Voltage Oscillator
CCC	Charge pump-Capacitor-Converter
CDC	Capacitor engaged Duty Cycling
CEM	Cathode Exchange Membrane
CFC	Capacitor-Transformer-Converter
CHP	Combined mode of Heat and Power
DCM	Discontinuous Conduction Mode
DO	Dissolved Oxygen
EET	Extracellular Electron Transfer
EFCs	Enzymatic Fuel Cells
EH	Energy Harvesting
ELVs	End-of-Life vehicles
EM	Exchange Membranes
ESC	Extremum Seeking Control Method
FFT	Fast Fourier Transform
HRT	Hydraulic Retention Time
IncCon	Incremental Conductance Method
IP	Instrumentation Plataform
IVP	Current-Voltage-Power Conditioner
LCA	Life Cycle Assessments
LP	Low Power
MCP-H	Maximum Current with Active Energy harvesting

MCP-R	Maximum Current Point with Passive Resistor
MCU	Microcontroller Unit
MEAs	Membrane Electrode Assemblies
MFCs	Microbial Fuel Cells
MPP	Maximum Power Point
MPP-H	Maximum Power Point with Active Energy Harvesting
MPP-R	Maximum Power Point with Passive Resistor
MPPT	Maximum Power Point Tracking
MU	Multiunit optimization method
MVP-R	Maximum Voltage Point with Passive Resistor
NV	Nonvolative memory
OCV	Open Circuit Voltage
ORP	Oxidation-Reduction Potential
ORR	Oxygen Reduction Reaction
P&O	Perturbation and Observe method
PBS	Phosphate Buffer Solution
PCB	Printed Circuit Board
PCP	Platinized Carbon Paper
PGM	Platinum-Group-Metal
PLA	Polylactic Acid
PMMA	Poly(methyl methacrylate)
PMS	Power Management System
PMU	Power Management Unit
POR-PG	Power-on-reset pulse generator
PTFE	Polytetrafluoroethylene
PV	Photovoltaic systems
PVDF	Poly(vinylidene fluoride)
PWM	Pulse Width Modulation
RF	Radio Frequency
RH	Região Hidrográfica
RVC	Reticulated Vitreous Carbon
SCC	Short Circuit Current
SEAs	Separator Electrode Assemblies
SV	Voltage Supervisor
ULP	Ultra-Low Power
UPEM	Ultra-low Power Energy harvesters for MFCs

VC	Voltage Comparator
WEEE	Waste from Electrical and Electronic Equipment
WSN	Wireless Sensor Network
WWTP	Wastewater Treatment Plants

Chapter 1

Waste, wastewater, and energy-water nexus

Few are the human acts free from waste production. Waste, garbage, or unused materials almost seem to happen as a product of our actions. Throughout history, there are even some events that result from unmanaged waste: the bubonic plague, cholera, and typhoid fever became major health incidents resulting from disposing of waste without following any set of rules. Cats, dogs, and rodents roamed freely, and fleas were large in number, becoming disease vectors in several instances. In the Mayan culture, trash was usually covered up with dirt, at home, when its size became too big. The very first record of a municipal dump was around 500 BC, in Athens: residents were obliged to dispose of waste outside the city limits, at a fixed distance. Around 1400, in Paris, garbage piles became so big that they started to interfere with the city's defense. With industrialization, waste levels increased: historic records point to a direct relationship between waste production and product availability. The urban quality of life decreased and proposals for waste collection and removal were heard [1].

Nowadays, waste-related issues are on top of political, social, and economic agendas. The European union waste hierarchy [2] is organized according to Figure 1.1.

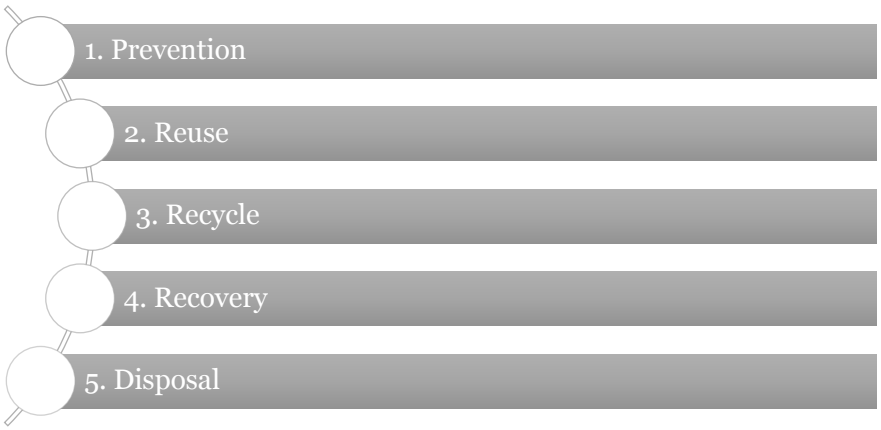

Figure 1.1 – European Union waste hierarchy.

While there are records showing that Native Americans produced about two and a half kilograms of undifferentiated waste per day, a 500 grams cut was achieved by 1911 [1]. With the advent of municipal waste management systems and overall public awareness, today's data points to about one and a half kilograms of municipal solid waste production per capita [3]. If waste is left unmanaged, or if its management is of poor quality, besides contributing to health issues, it also leads to environmental problems, non-efficient resource use, and landscape deterioration [2]. Waste easily contributes to an increase in greenhouse gases, water, soil, and air pollution levels. Waste dumps are still a reality for the majority of low-income countries: they are the easiest and

cheapest way of garbage disposal but pose significant threats to landscape deterioration and all-round pollution. Diseases like Malaria or even the spreading of the recent Ebola outbreak can also be tied to poor waste management systems. The Sierra Leone civil war, which lasted until 2002 and serves as an example, forced a lot of rural residents to move to major cities, namely Freetown. The Sierra Leone capital city waste management system has always struggled with insufficient coverage and service issues. This population increase did nothing to help the issue. Garbage piles can retain water, which acts as a pool for the breeding of viruses and bacteria. These infectious agents, transported by mosquitos or other animal vectors, pose a significant public health threat [4]. Major concerns are also with the average 580 million Sub-Saharan Africans currently living in slums, environments where this is quite frequent [5], [6]. In 2025, the United Nations estimate that, out of the 8 billion world inhabitants, about 1.5 billion people will be living in these environments. The poor qualities of the waste management systems in these areas will uttermost undermine the sustainability of health levels and the improvement of the average environmental and life quality levels. First world countries can also make negligent choices: the U.S.A. public service determined that the Ebola patients (treated in U.S.A. soil) bodily waste was to be discharged to the public sewer system [7]. Though it is expected that waste management practices can safely remove any traces of the infection, there is a study, from 2003, stating the U.S.A. tap water is at risk due to old pipes and outdated treatment strategies. Atlanta, the U.S.A. state where the patients were treated, has been reported as having severe water quality problems [8]. Recent investigations also point to grave concerns regarding plastic contamination in drinking water, all around the world [9].

For any given country, waste amount volumes are deeply related to its population numbers and consumption patterns. Either for first or third world country cities', waste management services tend to be the heaviest item in their budget. The lower the income of a country, the higher will be its costs with waste management. Low-income countries spend most of their waste management budgets on waste collection rather than on disposal (which happens in high-income countries). Current trends show that the rates of waste production are increasing quicker than the rates of urbanization. While countries urbanize, their economic wealth, standards of living, and consumption of goods and services increases. And so do the produced waste volumes: From 2012 until 2025, municipal solid waste is expected to increase 40%, with a 0.69% increase per each 1% of the gross domestic product [3], [5]. By 2025, 375.5 billion dollars will be spent only on municipal waste management systems. Efforts have already begun to be made to improve awareness and to lower waste volume numbers: in San Francisco, economic incentives and public awareness initiatives achieved a 77% cut in the waste to landfill percentage rate; in Belgium, similar outputs were achieved with tough waste standards; Taiwan and Spain are two major examples that even social pressure, this time from the general public to official organisms, can be used to better official waste management programs [10].

Between 2011 and 2013, the Portuguese urban waste levels dropped by 7.4%. Each Portuguese made a daily contribution to the waste levels of 1.24 kg and the highest waste production levels

were found on Lisbon and the Northern region (37.6 and 32.5% respectively). According to the European panorama, Portugal still registers a per capita waste level lower than the average of the 27 European countries. Even so, more than half of the garbage was deposited on landfills, with only 18.2% being converted to energy. Legislation is in place to guarantee that by 2020, only 35% of all the produced waste can be directed to landfills. The remaining waste should be used for energy production, compost, and recycling [11]. In 2015, despite the increase in the produced garbage per capita (1.26 kg per capita), only 34% of the 4.52 million tons of garbage ended up in landfills, a value below the 2020 target. The energetic valuing of garbage also improved to 21%. These records show that current policies and legislation are helping to achieve the established goals, aiding in decreasing the environmental damage of our daily activities [12].

Waste streams and their management

According to its composition, waste can be fitted in several different categories. First and foremost, and according to its physical properties, it can be liquid or solid. These two major classes can encompass 10 (according to European policy) other sub-classifications:

1. Municipal waste: also referred to as community waste, totals about 14% of the total European waste. Paper and cardboard, organic compounds and plastics make up the majority of municipal waste, either from households and/or commercial sources;
2. Industrial waste: major contributors for this category are manufacturing plants, like those used for the production of foods and beverages or basic metals;
3. Hazardous waste: materials identified as toxic (poisonous to humans and animals), flammable (can easily catch fire), reactive (exploding materials) or corrosive (that eat through metal) are all named as hazardous. About 1% of all the 2017 European waste is hazardous;
4. Construction and demolition waste: all construction and demolition materials contribute about 25% of the total waste percentage. These materials and their treatment have been marked as a priority due to their resource value and their considerable size contribution in a landfill;
5. Mining waste: totaling 29% of the European waste, this is a residue type with the largest volumes and hazardous potentials;
6. Waste from electrical and electronic equipment (WEEE): all electrical and electronic materials from every source fit in this category. According to recent trends, waste levels of this residue are quickly rising and becoming a serious contribution to landfills and incineration. Mainly because of recent customization technologies, which decrease the reuse of devices by different people;
7. Biodegradable municipal waste: this waste type is usually a product of municipal waste treatment systems and is routed to suitable treatment stations;
8. Packaging waste: waste with a relatively short life that makes up 17% of the total municipal waste;

9. End-of-Life vehicles (ELVs) and tires: end-of-life vehicles are all the passenger and vehicles that are no longer of viable use. Their materials are separated, and each follows a suitable route;
10. Agricultural waste: majorly composed of organic waste, plastics, fencing, pesticides, waste oils, and veterinary medicines.

Aside from the above categories, residues can also be put in one more category: air pollutants. Primary air pollutants are substances that enter the atmosphere directly from a source. Examples of primary pollutants are hydrocarbons, nitrogen, and sulfur oxide derivatives. Secondary air pollutants result as an interaction between primary air pollutants with each other or other atmosphere existing substances. Ozone, for instance, is a result of unburned hydrocarbons and nitrogen oxide compounds in the presence of UV light.

Physical, chemical, biological, and thermal technologies can all be applied to treat waste residues. Physical methods use waste physical characteristics to separate it and further treat it. Chemical methods like, for instance, electrolysis, chemical precipitation or combustion, change the waste properties to treat it and decrease its pollutant potential. Biological methods are a particular implementation of chemical treatments as the reactions are applied by microorganisms and/or plants. Lastly, thermal techniques, like incineration and phytoremediation, use heat to destroy waste.

Energy from waste

Treatment strategies, although much needed to limit waste reactiveness, are also being approached from an energy recovery perspective.

In Europe, the Directive 2008/98/EC on waste (waste framework directive) establishes the waste management hierarchy, as presented in Figure 1.1. Recovery mechanisms are vital to maintaining a sustainable waste management system. Energy recovery, either to produce heat or electricity, is the last step before disposal. This option provides alternatives to the use of fossil fuels and the landfilling of residues. Energy from waste, sometimes referred to as low carbon energy source, can be recovered as heat, electricity, diesel, or natural gas [13]. The conversion process happens at waste-to-energy plants: high-tech incinerators equipped with energy recovery and cleaning mechanisms, submitted to very strict emission regulations, with the lowest emission rates of the industrial sector. Until 2005, waste-to-energy plants were directly associated with the production of dioxins from the burning of the waste.

Flue gas treatments were implemented and, today, these plants are the best way to achieve energy recovery from municipal solid waste [14]. The recovery process can be divided into four major steps, as represented in Figure 1.2:

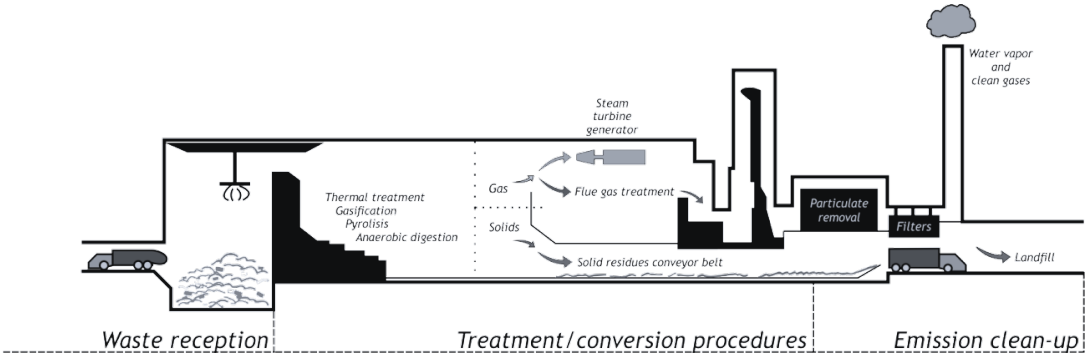

Figure 1.2 – Typical waste-to-energy plant.

1. Waste reception;
2. Treatment procedure(s);
3. Conversion to a transportable form of energy;
4. Emissions clean-up.

The most common thermal treatment is incineration. With it, steam is produced and is used to run a turbine generator for electricity production. The process starts with direct combustion of waste: the gas volume on the incineration chamber increases and the burner is turned off. The process continues and is self-sustained due to the reaction of the gases and oxygen, which generates more heat. With the produced heat, water is boiled, and steam is produced to run the turbine generator. The overall efficiency of the process is about 15-27%.

Gasification and pyrolysis are two types of Advanced Thermal Treatments (ATT). ATT processes are more common in smaller facilities. The products of ATTs can be used to boil water (following the same path as incineration) or burnt directly as fuel. This last option, however, is technically more challenging and has reduced overall benefits since part of the recovered energy has to be used to power the process. Syngas, the gas byproduct of ATTs, is produced by limiting the oxygen amount on the incineration chamber: the produced gas cannot react with oxygen, and energy available in the chemical form increases. The available oxygen is just enough to keep the process going. Clean syngas can be used for direct combustion, presenting higher efficiencies than steam turbines.

Anaerobic digesters are used on solid waste residues with high organic content. The produced energy is typically in the form of heat.

Most of the European waste-to-energy plants are built to function in a combined mode of heat and power (CHP), but the direct use of heat is conditioned to the availability of heat customers (buildings or facilities needing higher temperatures) and the relative costs of other heating alternatives. Since these plants are not usually built near enough heat customers, they usually end up operating in the power mode only.

Energy from wastewater

In rural locations, electric energy sources are not as readily available as they are in cities and urban settings. By rural locations, we can be referring to underdeveloped countries or peripheral sites around big urban centers. These places are, by default and due to their characteristics, chosen for the installation of wastewater treatment plants. Wastewater treatment and collection systems are among the highest energy consumers per municipality, having a major role in environmental protection and health standards. Although needing treatment, wastewater has untapped energetic potential, and, political pressure created by the need for sustainable societies, can change its label from waste to resource. Methane (CH_4) production from anaerobic digesters is still the greatest chunk of energy production with wastewater. Even so, the net balance for obtaining this product is low: the dissolved organic content cannot be recovered and has to be removed by aerobic, energy-consuming, processes.

For developed countries, wastewater treatment can spend as much as 3% of the country's total electrical load. A wastewater plant of aerobic activated sludge and anaerobic sludge digestion can spend between 0.5 and 2 kWh per cubic meter of treated wastewater, having at least 0.3 kWh of energy spent on aeration processes (these processes can account for as much as 60% of the total wastewater plant energy consumption). Wastewater has energy in three major forms:

1. In its organics;
2. In its thermal content: energy captured and used with low-energy heat pumps;
3. In its nitrogen and phosphorous contents.

The organic contents of wastewater have the energy potential to exceed by 10 times the energy used to treat it. The suspended, biodegradable solids are used for methane production. Other organics, even though needing further treatment and unbalancing the energy gains, can also lead to CH_4 production. Dissolved organics, on the other hand, can go through energy-expensive aerobic processes or, as applied more recently, through anaerobic treatments, leading to significant energy savings. Anaerobic treatments are even capable of electricity production, though only containing between 30 to 40% of the original energy potential in the biodegradable wastewater organics. Microbial fuel cells (MFCs) are a particular type of anaerobic process capable of retrieving about 44% of the energy from the wastewater organics.

Using MFCs as replacements for anaerobic digesters is still under evaluation, although using them to continuously harvest and store small amounts of energy at remote locations is a more immediate scenario for their application. Their usefulness becomes clearer if we think about using them to aid in quality monitoring. Reusing wastewater is only possible if strict quality standards are met. Considering that higher quality standards imply more energy expenditure, that water reuse is becoming more frequent due to its limited supply and that untreated wastewater release onto clean water is a dangerous source of contamination, energy-efficient technology capable of mitigating such effects will help preserve this valuable natural resource. Information on the

physical and chemical properties of the wastewater is, therefore, paramount for decision-making on the collection, treatment, and disposal of these types of waste.

Current wastewater quality monitoring techniques are dependent on manual collection, indirect techniques or fixed position, heavy and energetically dependent systems. Being repetitive and predictive tasks, these processes can be optimized and have their cost lowered if replaced by a smart sensors network. A network of such devices would allow for autonomous, precise, and versatile data collection, precisely because a smart sensor has a wider range of application. Beyond the sensing element, a smart sensor also comprises a filtering and amplifying stage, a processing unit, and two additional modules, one for communication and another for power. This last item can be more detailed as having a power source and an energy regulation and storage stage. In wastewater treatment stations, an MFC can be used as the power source, rendering the smart-sensor self-powered since it makes use of the wastewater organics to produce energy.

Figure 1.3 outlines how electrochemical energy sources compare with ultra-low power (ULP) and low power (LP) sensors regarding energy production and energy needs. There is a growing interest in the energy-water connection and wastewater research activities are being encouraged to address all water-related issues.

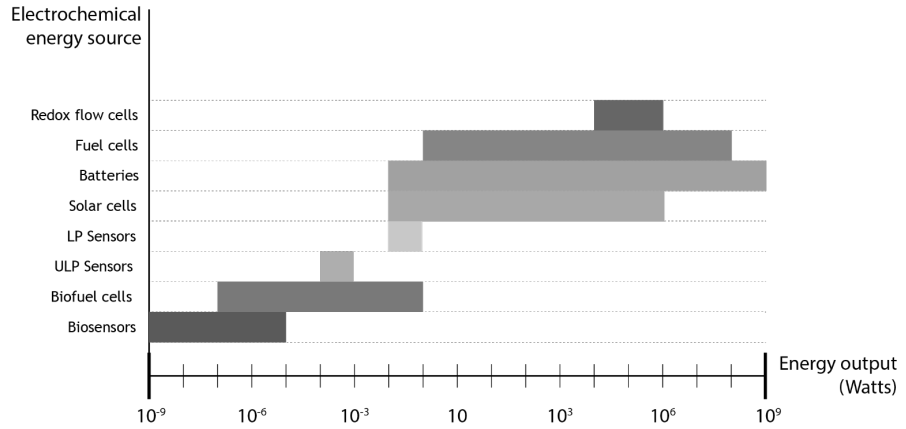

Figure 1.3 - Energy production levels of electrochemical sources relative to the energy needs of two types of low-power sensor technologies.

The energy-water nexus: Global view

The human population is thriving and its numbers continue to grow, even in developing countries, reaching 9 billion people in 2050 [15]. Our planet's natural resources continue being explored and, more frequently than not, irresponsibly spent. In some developed countries, technological advancements are being thought of with environmental-friendly concerns gaining ground to disposable solutions and counterbalancing negligent behavior. Food, water, and energy supplies are also being studied for adequate management, being the most fundamental necessities for the sustainability and development of life. Food can't be produced without water, water can't be made available without energy, and energy and electricity production are extremely limited without water. Considering current trends of resource depletion and climate changes, water and energy

will leverage food production, resource sustainability, and technology development, balancing supply and demand [16].

The business of energy implies more money than the water counterpart: direct costs with energy are related to exploration, treatment or generation, distribution, and environmental taxes while water-related costs are mostly connected with treatment and distribution. On top of this, energy expenditure data is richer than water expenditure and distribution [17]. By 2012, around 700 million people didn't have access to an improved water source, while 1.3 billion people had no access to electricity [17], [18]. All these factors have a significant influence on policies, ensuing stricter energy management procedures than water regulations. However, a closer look at the energy or water expenditure data shows their relationship, and recent data points to the need of applying similar control strategies to hinder resource and water scarcity.

Water for energy

Water is used in almost every sector of human activity, but, from them all, the energy sector comes in second. Only water use for irrigated cultures comes first. In Europe, in 2015, of 247 000 million cubic meters of water, 44 % was spent on energy production. For energy-related activities, water is used for fuel extraction, refining, and processing. It also plays a significant part in the cooling of thermal power plants, accounting for 50% of the total of freshwater withdrawals in the U.S.A. and over 10% in China. It is also vital for bioenergy and biofuel feedstock crops, an energy solution easily believed to be eco-friendly and that is estimated to achieve 7.5% of global electricity production by 2050 [17]–[20].

Portugal and water usage

In Portugal, water is managed according to 8 hydrographic regions ("RH", *regiões hidrográficas*):

- RH1 – Hidrographic region of Minho and Lima;
- RH2 - Hidrographic region of Cávado, Ave and Leça;
- RH3 – Hidrographic region of Douro;
- RH4 - Hidrographic region of Vouga, Mondego and Lis;
- RH5 - Hidrographic region of Tejo and Ribeira do Oeste;
- RH6 - Hidrographic region of Sado and Mira;
- RH7 - Hidrographic region of Guadiana;
- RH8 - Hidrographic region of Ribeiras do Algarve.

Figure 1.4 presents the distribution of each region on the country's map.

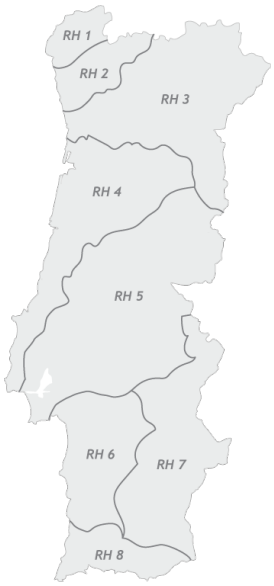

Figure 1.4 – General overview of the Portuguese hydrographic regions.

The most water-intensive sector is Agriculture, spending 73% of all the mainland freshwater. Of all regions, RH5 presents the highest consumption levels, also being the most densely populated. The remaining 19% if water consumption happens in the urban sector. Although most of the water ends at its appropriate use, almost half of it is lost in leakages in storage, transport, and distribution. Of all water used in urban settings and for agriculture, 40% is lost. For industry, levels of inefficiency drop to around 30% [12], [21].

Energy for water

Water extraction, distribution, treatment, and disposal are very different in countries with and without limited energy access. By 2050, water used for irrigation will be surpassed by the water withdrawn for energy, industrial processes, and municipal applications. Energy is needed to extract and convey water, from source to destination, and depends mostly on topography, distance, and the relationship between the source's volume of water and the amount needed at the destination (small aquifers imply more energy for water pumping). Water treatment also deals with large amounts of energy to convert wastage, rain or seawater to a useful and safe version, both for humans and for the environment: the dirtier the water, the more energy is needed to clean it [17]–[19], [21].

Portugal and energy usage

Portugal has a history with high levels of imported energy: while, in 2013, the imported energy levels decreased, from 2014 to 2015 an increase of 19.4% was registered. The energy consumed in 2015 also increased by around 1%, with fossil fuels having a significant role in this, and being one of the main primary power sources (42.6%) [12].

Strategies for energy and water management

The concept of energy-water nexus was first explored by Gleick PH, in 1994 [22]. For some time, since then, several events have highlighted the need for stricter regulations in water management. In 2001, there was a significant period of water shortage in California, in an event known as "The Californian Energy Crisis". Political decisions taken at the time favored short-term human comfort in detriment for the environment and a more sustainable water management. This incident, and the likes of these, show that if no policies are applied to water management, the onset of water scarcity will happen sooner. China, the Middle East, North Africa, and Spain are in the regions at most peril. Simple measures like efficient water appliances and reduced leaks in water distribution are a good way to start. Sourcing water bodies far from its destination, more energy will be spent on water transport. This is happening all across Europe, making water supply more energy-intensive in these territories than in Asian countries. Trailing this, governments should invest in augmenting the water supply with additional sources, treating and reusing stormwater, and investigating technological solutions for freshwater production, with reverse osmosis water recycling systems and desalination plants. On power plants, alternative water sources can be used for cooling and wastewater can also be used for energy recovery [17], [19], [23].

In Europe, legislation is in place for energy management, with the European directive 2012/27/EU (the "Energy Efficiency Directive") and the adoption of the ISO50001. This directive establishes energy utilization targets, enforces periodical energy audits, and requires sustained upgrades on energy management and delivery tools. For water, similar directives are being studied and implemented. The water footprint assessment is a concept, very similar to the carbon footprint, used to quantify the water used based on life cycle assessments (LCA) and implemented with an international standard, the ISO14046. ISO14046 evaluates the water expenditure and its impact on the environment in different life cycle stages, informing users and industry players of the water impacts of their activities and choices [17], [24].

By adopting the ISO50001, several organizations showed significant decreases in energy and water usage levels as well. In Ireland, for instance, the University of Cork, which adopted the standard in 2011, saw an 18% reduction of the spent water, though an increased student activity was registered during that year. This decrease could have been higher if the standard had similar measures for water-related issues, like leakages, old pipes, faulty meters, and operation of sanitary facilities in low occupation periods. The implementation of this same standard by Coca Cola resulted in a 10% decrease in water and 16.5% in energy consumption [17], [25].

While this report shows that water consumption can be decreased by energy-efficient management strategies, much more is possible by implementing suitable measures and initiatives for water management. By 2025, 800 million people will live in water-scarce regions and around 65% of the global population will live in severe water stress conditions.

Wastewater management and energy potential

Water and energy flows are extremely complex and interdependent which accounts for serious difficulties in acquiring data figures for each system's diagnose [26]. Strict water quality parameters are being applied to limit the environmental impact of wastewater recovery, clean-up, and disposal. In Portugal, the Decree-Law 236/98, from the Environmental Ministry, establishes clear standards, criteria, and quality objectives to protect the hydrosphere and improve water quality according to its main uses. This law also distinguishes wastewater according to its origins:

1. Domestic wastewater – water produced mainly from human metabolism and domestic activities;
2. Industrial wastewater – all the raw sewage deriving from activities that cannot be classified as producing domestic wastewater or rainwater;
3. Urban wastewater – domestic wastewater mixed with industrial wastewater and/or rainwater.

Annex XVIII of this Decree-Law imposes emission limit values for wastewater disposal from wastewater treatment stations [27].

Wastewater treatment and collection systems are among the highest energy consumers per municipality. They play a major role in environmental protection and health standards but, for its treatment, require around 0.5 to 2 kWh of energy per cubic meter of wastewater. However, there is an untapped potential for energy retrieval in wastewater. The untapped potential resides on the organic content, the thermal energy and nutritional elements, like nitrogen and phosphorous, on the wastewater itself [28]. Wastewater is progressively being approached more as a resource than just waste, mostly due to political pressure created by the need for sustainable societies [29], [30]. Thermal energy can be retrieved with heat pumps, although being dependent on the source's temperature [28]. Chemical energy is difficult to retrieve and methane production from anaerobic digesters is the process closest to resource recycling. Harvesting energy from the organic contents on wastewater must follow a symbiotic approach, where particular strains of bacteria are manipulated to use wastewater for energy production. By taking advantage of specific oxidation-reduction reactions, wastewater can simultaneously be cleaned and produce energy. This is particularly interesting when considering solutions where no energy input is needed, allowing to expand the energy sources portfolio for wastewater treatment plants.

Rationale behind microbial fuel cells as low power renewable energy sources

The ecological awareness of our society is growing. The impact that the human species had on the planet in the last century has contributed to this. The result is visible in the continued degradation of natural environments, some beyond possible recovery. The study of the energy-water nexus has contributed to identify processes where there is a direct relationship between these two essential resources for humans.

Electric energy availability in rural and remote locations is very different from that in cities and urban settings, due to distance and investment unbalances. Having the ability to increase that energy availability without the need to install large infrastructures or to change landscapes or water flow is of particular interest. This goal may be achieved by unlocking the full energetic potential of wastewater.

This work will demonstrate that Microbial Fuel Cells (MFCs) represent the most direct and cheap path for energy extraction from the wastewater organic content. As a new technology with a plethora of variables and a mutable element – the bacteria – research on this subject can take many forms: it can be focused on one, or several, fuel cell elements or it can target external optimization strategies.

This document discusses the development of energy harvesting efficient strategies with external devices. There are five chapters structured to allow the reader to bridge between the technology need and usefulness. Chapter 1 was used to introduce the interdependence between energy and water, zeroing in the unexploited energetic potential of wastewater. This analysis was initiated by pointing towards waste production and its impact when unmanaged. To complement this point of view, the benefits of waste recycling were immediately presented, supporting how waste can be used as a resource, specifically wastewater for energy production. Microbial fuel cells were also briefly introduced but its relationship with wastewater management is further explored in chapter 2. In fact, this second part lays ground for the technology discussion. The operation principle ensues and is followed by a deep state-of-the-art review addressing an historical perspective and each of the main research achievements for every element of a microbial fuel cell reactor. The role of the main players in power development for this fuel cell type is fundamental: it is only through this that an adequate discussion of how power develops can be pursuit. An abstraction layer is achieved in chapter 3, where the reactor is treated as a black box. The issue of energy harvesting with microbial fuel cells is firstly viewed through the lens of the strategies used with photovoltaic systems (PV). The decision to compare both technologies was based on the fact that, in MFCs, the substrate availability changes in time and that the sun radiance also changes throughout the day, for photovoltaic systems. The algorithms used to improve the time spent at the maximum power point operation for PV systems are briefly presented as a comparison on the strategies that could be explored for MFC power conditioning. A similar analysis on the energy optimization mechanics studied with MFCs is then put forth, with a major focus on the state-of-the-art review. A

comprehensive analysis of energy harvesting techniques applied to MFCs tracks the developments with passive components, maximum power point tracking algorithms, power and energy management systems and series and parallel grouping of MFCs. This work is of paramount importance to steer the experimental procedures exploited in chapter 4. A roadmap of the core experimental research introduces this section. The MFC technology is tested in two major subjects: reactor and biofilm development studies and power production. The power production research is further divided into how internal and external variables impact it. Amongst the internal variables are biochemical parameters, biofilm age and electrode fouling and substrate feeding strategies. On the matter of external factors, the technology was studied through polarization trials applied at different settings. Modulating the electrode connection was also a research topic: the retrieved experimental data shows promising results that clear different operation alternatives for the MFC as a power source. The external variables impact culminates in a power management solution proposal, with a detailed discussion on the weight of each element and how they contribute to convert the unregulated MFC power to a regulated and reliable energy source. The last chapter, chapter 5, is presented as a sum of the full work, dealing with the main discoveries and key contributions, pointing to unexplored research paths and future works and reviewing the current research trends.

References

[1] R. Barbalace, “The History of Waste: Do you want to be a garbologist?” [Online]. Available: https://environmentalchemistry.com/yogi/environmental/wastehistory.html. [Accessed: 08-Aug-2014].

[2] European Commission, “Landfill waste - Environment - European Commission.” [Online]. Available: http://ec.europa.eu/environment/waste/. [Accessed: 08-Aug-2014].

[3] D. Hoornweg and P. Bhada-Tata, “What a waste : a global review of solid waste management - IWA Water Wiki - Open Access Information for the Global Water Community,” 2012.

[4] A. O. Bockarie, “Garbage and Malaria, two bedfellows?” [Online]. Available: http://standardtimespress.org/?p=2316. [Accessed: 09-Aug-2014].

[5] A. Mavropoulos, “Waste management 2030+,” *Waste Management World*, 2011.

[6] European Parliament, “Note on Urbanisation Challenges, Waste Management, and Development,” 2014.

[7] B. Goodman, “American Ebola Patient Kent Brantly Improving.” [Online]. Available: http://www.webmd.com/news/20140801/american-ebola-patients-returning-us#1. [Accessed: 09-Aug-2014].

[8] E. Olson, “What’s on tap - Grading drinking water in U.S. cities.”

[9] D. Carrington, “Plastic fibres found in tap water around the world, study reveals,” *The Guardian*, 2017. [Online]. Available: https://www.theguardian.com/environment/2017/sep/06/plastic-fibres-found-tap-water-around-world-study-reveals. [Accessed: 20-Sep-2017].

[10] C. Allen *et al.*, “On The Road to Zero Waste Successes and Lessons from around the World,” 2012.

[11] A. M. Dias *et al.*, “Relatório do estado do ambiente 2013,” 2013.

[12] A. C. Fernandes, M. D. Guerra, R. Ribeiro, and S. Rodrigues, “Relatórios do Estado do Ambiente 2016,” *Agência Port. do Ambient.*, p. 204, 2016.

[13] E. S. of W. to E. T. ESWET, “Everything you always wanted to know about Waste-to-Energy,” 2012.

[14] E. S. of W. to E. T. ESWET, “Everything you always wanted to know about Waste-to-Energy,” 2012. [Online]. Available: http://www.eswet.eu/tl_files/eswet/Handbook/ESWET_Handbook_Waste-to-Energy.pdf. [Accessed: 09-Sep-2014].

[15] WWAP, “The United Nations World Water Development Report 2014: Water and Energy,” 2014.

[16] US Department of Energy, “The Water Energy Nexus: Challenges and Opportunities,” *Report*, p. 238, 2014.

[17] B. P. Walsh, S. N. Murray, and D. T. J. O’Sullivan, “The water energy nexus, an ISO50001 water case study and the need for a water value system,” *Water Resour. Ind.*, vol. 10, pp. 15–28, 2015.

[18] M. Halstead, T. Kober, and B. van der Zwaan, “Understanding the Energy-Water Nexus,” 2014.

[19] M. Wakeel, B. Chen, T. Hayat, A. Alsaedi, and B. Ahmad, “Energy consumption for water use cycles in different countries: A review,” *Appl. Energy*, vol. 178, pp. 868–885, 2016.

[20] M. Hightower and S. A. Pierce, “The energy challenge,” *Nature*, vol. 452, no. 7185, pp. 285–286, Mar. 2008.

[21] A. P. do Ambiente, “Programa Nacional para o Uso Eficiente da Água,” Ministério da Agricultura, do Mar, do Ambiente e do Ordenamento do Território, 2012.

[22] P. H. Gleick, “Water and Energy,” *Annu. Rev. Energy Environ.*, vol. 19, no. 1, pp. 267–299, Nov. 1994.

[23] A. M. Hamiche, A. B. Stambouli, and S. Flazi, “A review of the water-energy nexus,” *Renewable and Sustainable Energy Reviews*, vol. 65. pp. 319–331, 2016.

[24] International Organization for Standardization, “ISO 14046:2014 - Environmental management -- Water footprint -- Principles, requirements and guidelines.” [Online]. Available: https://www.iso.org/standard/43263.html. [Accessed: 20-Sep-2017].

[25] I. Johnson, P. Fullerton, R. Razeen, and M. Ahern, “ISO 50001 ‘on fire’ - Energy management standard goes global,” 2012. [Online]. Available: https://www.iso.org/news/2012/03/Ref1537.html. [Accessed: 20-Sep-2017].

[26] C. Copeland, “Energy-Water Nexus : The Water Sector ’ s Energy Use,” 2014.

[27] Ministério do Ambiente, *Decreto-Lei nº236/98, relativo aos critérios a observar para proteger o meio aquático e melhorar a qualidade das águas em função dos seus usos*. Portugal, 1998.

[28] V. G. Gude, "Wastewater treatment in microbial fuel cells - An overview," *J. Clean. Prod.*, vol. 122, pp. 287–307, 2016.

[29] L. T. Angenent, K. Karim, M. H. Al-Dahhan, B. A. Wrenn, and R. Domíguez-Espinosa, "Production of bioenergy and biochemicals from industrial and agricultural wastewater.," *Trends Biotechnol.*, vol. 22, no. 9, pp. 477–85, Sep. 2004.

[30] P. L. McCarty, J. Bae, and J. Kim, "Domestic wastewater treatment as a net energy producer--can this be achieved?," *Environ. Sci. Technol.*, vol. 45, no. 17, pp. 7100–6, Sep. 2011.

Chapter 2

Microbial Fuel Cells

Microbial Fuel Cells and wastewater management systems

The use of microbial fuel cells (MFC) with wastewater substrates is currently of great interest. A wastewater treatment plant spends almost half of its energy supply in the aeration basins of the activated sludge treatment, around 0.33 to 0.60 kwh/m^3 [1]. Having the ability to clean wastewater and, at the same time, produce power or retrieve added value compounds from these residues is now turning heads and gathering attention. Particularly due to the increasing global energy needs and water scarcity episodes [2]–[5].

One of the first studies to report the use of microbial fuel cells and real wastewater substrate is from 2004 [6]. Before that, laboratory experiments would only use synthetic wastewater or simpler substrates (as described along this section). The data retrieved with these trials pointed to estimate power production levels capable of powering wastewater substations, like aerobic trickling filters [7]. Yet, when using real wastewater, it became clear that these energy achievements were lower. A power decrease of about 30% was even reported when comparing the functioning of an air-cathode MFC with real and synthetic wastewater [8]. More recently, other wastewater sources, like dairy and potato wastewater, were also evaluated as energy sources [9]. These preliminary results showed that further optimization of the MFC technology was possible and needed.

The main limiting factors for electricity generation with MFC on real wastewater applications are related with inadequate microbial communities and methanogenesis. There are some researchers who point to the need of a pre-fermentation stage, on the substrate, so as to guarantee that all the fermentable compounds (which give rise to methanogenesis) are converted to non-fermentable compounds [10]. All these challenges are under investigation. It is expected that an adequately dimensioned, continuous flow, MFC behaves effectively [11]. It may even not be a large MFC system but rather a modular type solution, more adequate for powering instrumentation, wireless nodes and small signal devices used for quality monitoring [12]–[16].

Nevertheless, the advantages on using an MFC on wastewater treatment plants are undeniable: an MFC allows energy recovery, limits energy input to the wastewater treatment system and decreases the sludge production levels. No other current technology can achieve such goals with these characteristics. Furthermore, MFC technology (and, on a broader sense, bio-electrochemical systems) is also capable of biologically produce methane, hydrogen and other chemical compounds of interest. The byproducts of MFC are non-pollutant and single MFCs can be stacked to increase the power production capabilities of this technology [2], [3], [17]–[19]. MFCs have also been compared to anaerobic digesters (AD). Both technologies have the same

inputs (wastewater) and outputs (electricity). Even so, the AD's final product is biogas and, for electricity production, this byproduct needs further processing. Also, AD power requirements easily amount to 45-75% of the whole wastewater power plant energy costs. Converting an aeration tank to an MFC equivalent would eliminate these energy costs and could also lead to 10-20% more power production (a total energy balance of about 55-95% more) [20], [21].

Operation principle

Electrochemical devices can be partitioned into three categories: batteries, fuel cells and solar cells. An electrochemical device converts chemical or light energy to electrical energy through a chemical reaction: if the device uses incident light to produce electricity then it corresponds to a solar cell; if not, then the device can either be a battery or a fuel cell. Batteries have limited lifetime cycles and cannot be recycled: their internal fuel cannot be replaced and, once spent, the battery has no more use, making them, at least, as pollutant as fuel cells. Fuel cells, on the other hand, can have their fuel replaced, being able to run for a very long time (provided that no other element is damaged). Fuel cells and batteries can be inorganic or organic. For organic types, the devices get the denomination of bio-electrochemical systems (BES) and get subdivided into three types:

- Cells using an organic material to generate a byproduct, like hydrogen, which is then used as fuel for a conventional, for instance hydrogen/oxygen, fuel cell;
- Cells using an organic material and enzymes or whole microorganisms to produce electricity;
- Cells using photochemically active systems and biological partners to convert sunlight to electricity.

Microbial fuel cells (MFCs) and enzymatic fuel cells (EFCs) are two examples of the second type: the latter having catalysts (reaction facilitators) act on isolated and purified enzymes and the first on microbes [17], [22]–[25]. The development of these devices came as an alternative to fossil fuels, complementing the clean energy alternatives. These alternatives are of dire need, both to limit the green-house effect and particularly for the developing countries. In India, for instance, it is quite frequent to find people in the rural areas, with limited access to western common energy sources, burning organic waste to have a flame source for cooking [26].

A microbial fuel cell can be described in terms of five major components: the anode, the cathode, the substrate, the membrane and the bacteria. The anode experiences an oxidation reaction (the loss of electrons) and the cathode a reduction reaction (the gain of electrons). These reactions are possible because of the substrate and an external circuitry, responsible for maintaining the conditions for electrons and ions to flow. In a typical fuel cell, electrons produced by the oxidation reaction (at the anode) travel to the cathode, through the external circuit, where they reduce another component. For microbial fuel cells, bacteria are responsible for oxidizing an electron donor and oxygen is frequently the acceptor at the cathode. The membrane keeps both chambers separated and is usually proton permeable, guarantying the filtering of protons from the anode to

the cathode chamber where, with the electrons and oxygen, water is produced [27], [28]. Figure 2.1 presents a schematic of a double-chamber MFC with acetate as a substrate.

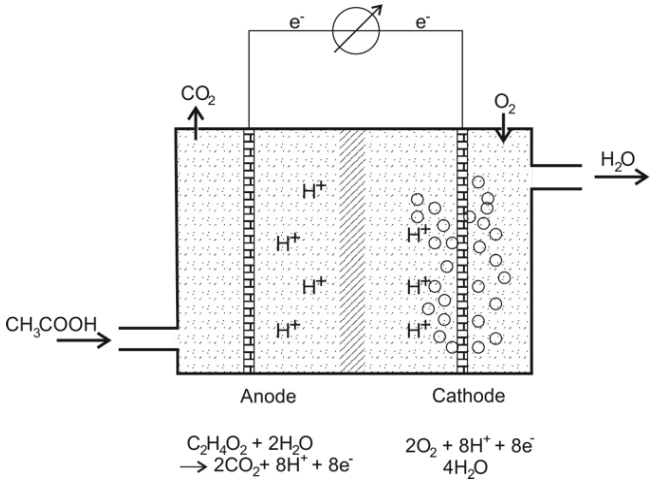

Figure 2.1 - Microbial fuel cell with acetate as a substrate. With the substrate oxidation, electrons flow from the anode to the cathode through the external circuit. Protons rising from the oxidation reaction are then selectively chosen to go to the cathode chamber through a proton exchange membrane. Adapted from [27].

Although double chamber reactors are standard for laboratory studies, these fuel cells can have other arrangements. Irrespective of those arrangements, an MFC always has a cathode, an anode and an external circuitry. The use of a separator, or membrane, is not mandatory.

Power density is the default figure of merit for comparing fuel cell's performance. MFCs are no different. Considering power is the product between the cell's voltage and the current density, power density has a dimensioning factor that accounts for area or volume. In MFC's, double chamber and single-chamber reactors don't have the same reactor volume and, in order to compare different reactor topologies, power density is usually reported in W/m^2 or mW/cm^2, almost always referring to the cathode's size. Earlier studies presented power normalized to anode area, since it was thought that the available space for bacteria to interface with the electrode was the limiting factor for power production [29]–[31]. However, further studies concluded that both the membrane and the cathode exerted far more influence on the power production levels [30], [32]–[34], which led to power being reported according to the cathode area. The maximum power density corresponds to the cell's maximum power point and equals the product of a specific combination of current and voltage values. Having a cell working at this point guarantees the highest power production levels, albeit possibly occurring at low voltages [29], [35]–[37].

An historical overview

If the first connection between biology and electricity was made by Galvani, the first fuel cell concept is Grove's responsibility. While Galvani, in 1790, demonstrated that an electrical current can influence a biological response – by the famous frog leg's twitching experiment [38] – Grove, by 1839 [39], was able to force the combination of hydrogen and oxygen to produce water and electricity, reversing electrolysis [22]. It was not until early in the 20th century that electro-physiology truly gained momentum. Researchers in Germany and in the US were leading the way on findings related with the association, unclear at the time, between chemical changes and electrical changes on vegetable physiological processes. Haacke [40] and Klein [41], with investigations 6 years apart, showed the relationship between electrical currents in plants and their physiological processes, being also able to modulate the electrical current characteristics by changing particular aspects of the plant's biological phenomena. The Americans, by Waller, pointed to the possibility that both vegetable [42] and animal [43] protoplasm could give rise to an electrical response. By 1910, a British investigator named Michael Cresse Potter made several experiments so as to determine if one of Waller's conceptions had a more inclusive meaning [44]. According to Waller, in biology, a dissociation process would give rise to an electrical current whereas an association process would need an electrical current. Potter set out to find if there were electrical effects on fermentation or putrefaction by bacteria and if they, as a dissociation process, had the announced effects. He developed a device using a glass jar containing a porous cylinder, a galvanometer, a capacitor and a Morse key, as shown in Figure 2.2. Using some copper wires he made the connections between the elements and chose to use platinum for his electrodes. As for the fermentation process, he elected the fermentation of yeast upon glucose, mostly because it was a well-known process and had few conditional restraints. Having made all the choices, he poured a glucose solution to the cylinder and added a pre-planned amount of yeast to the outer glass jar. After several studies, made so as to remove any possible sources of mistakes or measurement inaccuracies, he observed a gradually increasing voltage (later on found to be dependent on the concentration of the glucose solution, the temperature and the quantity of yeast added) [45].

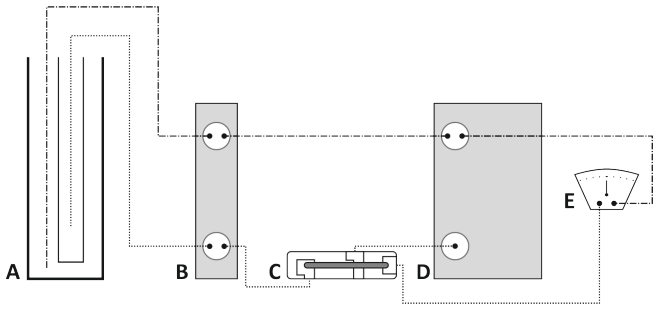

Figure 2.2 - Schematic representing the experimental set up for Potter's work: (A) – The cell; (B) – Mercury cups to facility connections with different cells; (C) – Morse key; (D) – Capacitor; (E) – Galvanometer (Adapted from [44]).

This work was highly underestimated and needed bigger results and a higher impact to get the attention it deserved. By 1931, another researcher brought this work to the spotlight: Barnet Cohen [46] created several fuel cells and connected them in series to evaluate their behavior and electrical output. He was able to produce a 35 V potential but only a 2-mA current. Even so, his work drew the attention of at least one major player in the energy field: NASA. By 1960, one year after the creation of Project Mercury and the X-15 rocket plane, NASA clearly stated its objective of developing a technology that could generate electricity while organic waste produced by the astronauts was decomposed [47]. More recently, in 2012, they reaffirmed their intentions [48]. Rohrback and his team made another contribution in 1962 [49]: they reported the use of the bacteria *Clostridium butyricum* as a catalyst for producing hydrogen trough glucose fermentation. The cell's hydrogen could then be used, as reported by DelDuca et al [50], in an oxygen/hydrogen fuel cell. From then onwards, several efforts were developed so as to understand what factors would have an effect on MFCs electrical output. In 1966 the attention was on the cell's substrate [51]: rice chaff was used in microbial fuel cells connected in series to produce 40 mA at 6 V, a significant improvement, current-wise, from Cohen's work.

The development of photovoltaic cells, a more technically feasible technology, put a brake on the research work in BES. Though the oil crisis stroke in the 80s and renewed the interest in MFCs, true advances and revolutions were only seen around the 90s and the beginning of the 21st century (between 1980 and 1990 the only significant contributions were more theoretical and even so, over enzymatic fuel cells: researchers like Wingard [52], and Davis and Turner [53], [54] were head names in the field at the time). Researchers like Benetto (who laid the core funding for the understanding of MFCs' functioning) were responsible for increasing the current density and power output by adding recently investigated electron mediators (works reported in [55]–[57] are just a few examples). By 1991 there were already attempts to apply MFCs to domestic waste water treatment and concomitant energy production [22], [23], [27], [28], [45], [58]. It was not until 1999 that the use of electron mediators was set aside and its use practically discarded: a team led by Kim B. H. reported the development of a mediator-less fuel cell and their achievements were so remarkable that this was considered a landmark for MFC's development [59]. If, until then, only two generations of MFCs devices could be identified – generation I (Gen-I) with synthetic mediators and generation II (Gen-II) with naturally occurring mediators – this discovery gave rise to the third generation (Gen-III): mediator-less MFCs [29], [60]. After approximately 10 years, around 2009, MFCs' power reporting shifted from being exclusively normalized to the electrode surface to also being normalized to power per volume. This change was natural, since there was a need to compare different power outputs reported by several researchers. As years have passed, attention was redirected from exploring materials and factors limiting power on an area basis to the same factors influence on the overall volumetric power achievable. It is expected, in the next couple of years, to achieve power levels similar to what is produced with anaerobic digesters, making this technology strong enough to be more diversely applied. Reactor geometries

Microbial fuel cell reactors can be grouped in six major configurations – single chamber [8], double chamber [61], flat plate [62], membrane-less [63], up-flow [7] and stacked [64]. Other arrangements are also possible, although not so common, like nested [6] and in-plane [65]. This section will address construction characteristics disregarding electrodes, membranes, bacteria or substrate choices.

Bennetto and his team [66] were among the first investigators to report a low cost MFC device. This construction was mostly used for demonstrations and proof of concept studies. In its simplest form, the container was a large glass tube. The electrodes were recycled from old batteries and the connections made using an ordinary copper wire. A dialysis membrane, in a shape similar to a bag, was applied to the anode to separate it from the cathode. The anodic bag had the microorganisms, a mediator and a small amount of glucose. In spite of this cell not producing useful amounts of energy it did, and still does, establish the building grounds for an MFC [66]. One year before, in 1989, Sell et al reported the first air-cathode MFC [67]. The development of different designs spread through time and pinpointing when and which architecture came to be is a rather unfair task. As shown in Figure 2.3, MFC designs can be highlighted by the number of chambers - single and two-chambered MFCs; geometry of electrodes - air-cathode MFCs, MFCs with soluble catholytes or poised potentials and tubular MFCs; or number of cells – stacked constructions [23], [27]–[29], [66].

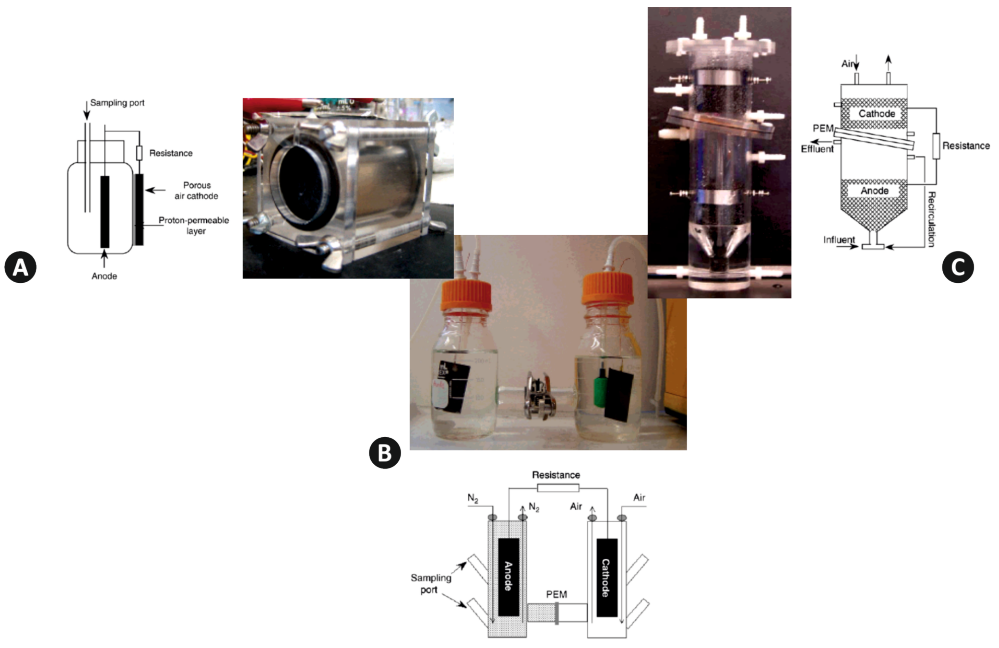

Figure 2.3 - The three major types of architectures for MFCs. In (A), single cell (air-chatode) geometry; (B) represents the dual chamber disposition and part C refers to the tubular devices (Adapted from [28] and [30]).

Two-chamber MFCs are the typical construction for laboratory studies. Bottle reactors, usually in a H-shape, and cube reactors, as reported by Bennetto et al [66], are a classical two-chamber MFC example. They are easily autoclaved and sterilized and can be run in batch or continuous mode. They are useful to determine whether or not power generation is possible and can also be used to establish a timeline relationship for the development of microbial communities. They are not adequate to improve or investigate which factors affect power output, albeit being a commercially viable MFC design [28], [66]. The separation between chambers is guaranteed by the membrane and, if oxygen is chosen as the terminal electron acceptor, the cathodic chamber needs aeration. Other examples of two-chambered devices are:

- Bottle type - You et al, in 2006, described a bushing MFC [68]: a plastic bottle with 4 bars had a cathode exchange membrane (CEM) hot pressed in them and a cathode concentrically placed inside the bottle;
- Tubular devices – built to run in continuous flow mode: the substrate in these designs flows from the anode to the cathode, either in a bottom to top configuration or in an outer to inner path (for cylindrical designs). For vertical constructions, up-flow, the first devices had their chambers separated by glass wool and glass beds. Rabaey and his team, in 2005, presented a tubular device made using a granular graphite anode delimited by a PEM sleeve and a sacrificial cathode [69]. Up-flow MFCs are mainly used in wastewater treatment since the energy needs for fluid recirculation are greater than the power output [23], [27]–[29], [70].

Single-compartment MFCs have simpler and cheaper designs. The cathode is frequently exposed to air leaving behind the aeration need. Bottle type devices are also the simplest examples. The most typical constructions consist of a single laboratory bottle with a side-arm where the cathode (generally associated with a membrane) is placed. The side arm has a larger diameter than usual to increase oxygen exposure. Cube reactors are also a mainstream choice for single-chamber designs: the geometry reported by Liu and Logan, in 2004, described the construction from a 4-cm block of acrylic drilled to produce a cylindrical chamber with a radius of 3 cm [8]. The reactor was oxygen free and sealed to prevent any leaks. Ringeisen's team, in 2006, proved the design can be scaled down [71]. More recently, Serra et al [72] also presented a larger volume variation on this design. Currently, this is the most frequent choice for reactor geometries due to its low cost, easy manufacturing and versatility [73]–[77].

Other constructions have been reported. Of particular interest is a flat plate device (built to mimic a hydrogen fuel cell and follow similar power outputs) built by Min et al [62]. Their main objective was to come up with a construction of decreased space between the electrodes. The two plates were 15 cm wide and 15 cm long with only 2 cm of height. The characteristic serpentine flow path had only 0.7 cm wide and 0.4 cm deep. In [78], flat-plate, air-breathing, microbial fuel cells have been used to evaluate different separators. 3D printed reactors have also been studied, with evident benefits regarding their availability and readiness [79], [80].

Stacked MFCs can be seen as another type of constructions. They can be described has the connection, in parallel or series, of individual MFCs which can, in turn, be of any type. These devices are most common in applications where a single device can't power the application for what it was devised [29]. Current research is being directed at efficient and scalable designs for increased power production and wastewater clean-up [81]–[83].

Membranes and separators

Membranes are used to selectively conduct chemical compounds, allowing for the isolation of electrodes from task hindering species, exerting some control on the electrolyte characteristics. On double chamber MFCs, specifically, membranes lead protons from the anode to the cathode chamber, separating the anolyte from the catholyte (fuel crossover) and the anode from oxygen exposure. Membranes are a semi-permeable type of separator and can be classified according to their morphology and/or driving force. Morphology wise, membranes can be porous or non-porous, symmetric or asymmetric and neutral or charged. Regarding the driving force, membranes can work through pressure differences, concentration unbalances or electrical potential dissimilarities [28], [31], [84]–[87].

Microbial fuel cells' membranes are charged and work through an electrical potential gradient: these ion-exchange membranes transport fixed charge particles according to the polarity of their internal charged groups: cation exchange membranes (CEM) allow cation diffusion and repel anions because of their matrix negative charge; anion exchange membranes (AEM) allow anion diffusion and repel cations due to their internal positive charge. The schematics for a CEM and an AEM are shown in Figure 2.4.

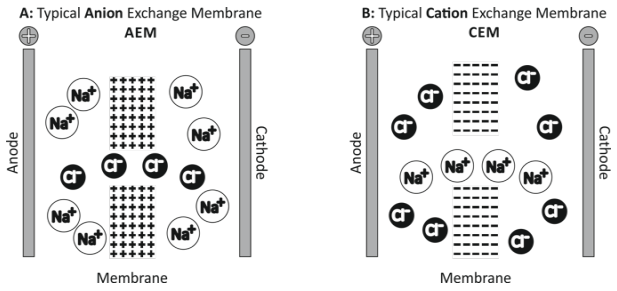

Figure 2.4 - On left (A), anion exchange membrane (AEM). On right (B), cathode exchange membrane (CEM). Negative ions are conceptually represented by chloride ions (Cl-) and positive ions with sodium ions (Na+).

Bipolar membranes are also available for use with MFCs: they consist of an anion and a cation membrane joined in series. Instead of proton flow, a voltage is developed across the membrane and that results in the transport of anions (OH^-) to the anode and cations (H^+) to the cathode. Comparatively to other membranes, this type has a higher internal resistance and decreases the cell's power output [28], [85], [88].

Membrane efficiency can be evaluated according to its end-use and pore size, porosity and ion-exchange capability. The ideal characteristics of an ion exchange membrane can be summed up to high permselectivity, low electrical resistance, good mechanical and form stability, high chemical stability and low price. On MFCs, these features mean no oxygen diffusion to the anode chamber, no bacterial growth on the membrane surface and weak electrolyte pH impact. Unfortunately, most of the ideal properties can't be achieved simultaneously, since some are the opposite of others: for instance, giving strength to membranes is difficult without increasing their electrical resistivity [85], [87], [89].

Membrane features and their impact on MFC performance

Membranes are the major contributors to the MFC's internal resistance. The relationship between its characteristics and the electrolyte impact the power production profile.

The membrane resistance to the flow of protons is dependent on its internal charge, pore size, thickness and surface area. Negatively charged membranes, or CEMs, can have limited proton flow due to competition between cations (Na^+, K^+, Ca^{2+} and so forth) on the anolyte: the cations bind to the negative charges on the membrane surface and block the transport channels for protons. For double chamber reactors, this proton block leads to a decrease of the anolyte pH and an increase in the catholyte pH (pH splitting). Anaerobic bacteria thrive on alkaline to neutral pH solutions and an acidic environment is not favorable for their metabolism, which results in decreased MFC performance. Positively charged membranes, or AEMs, transport protons through proton carriers like hydroxide or carbonate ions and are more effective. However, to transport these ions, these membranes have bigger pores and allow substrate crossover, which in turn leads to cathode depolarization and the development of bacterial aerobic films (cathode biofouling). The biofouling phenomenon is most frequent, however, at the anode facing membrane side: in non-treated membranes, a biofilm of bacteria and organic substrates builds up at the membrane surface, and progressively changes the membrane composition, stops proton flow and consumes oxygen from the cathode facing side of the membrane, leading to pH splitting and reduced oxidation capabilities of the anaerobic bacteria on the anode. Biofouling can be reduced by treating the membrane with anti-microbial or anti-adhesion surface treatments, provided that these treatments don't end dissolved in the electrolyte and affecting the bacterial community composition. Another issue limited by the use of separators is oxygen diffusion: there are no known separators capable of completely stop oxygen from diffusing from the cathode to the anode chamber. With oxygen at the anode, the bacterial community stops from using the anode as the final electron acceptor and by using oxygen start converting their metabolism to aerobic respiration. This change can, however, be reversed, provided that oxygen is removed from the anode chamber. Thicker membranes are better at stopping oxygen diffusion, but their resistive contribution is higher. Thinner membranes present lower internal resistances but are less efficient on stopping oxygen and fuel crossover [78], [86], [89], [90]. Figure 2.5 presents an overview of the influence that each feature increased expression has on power.

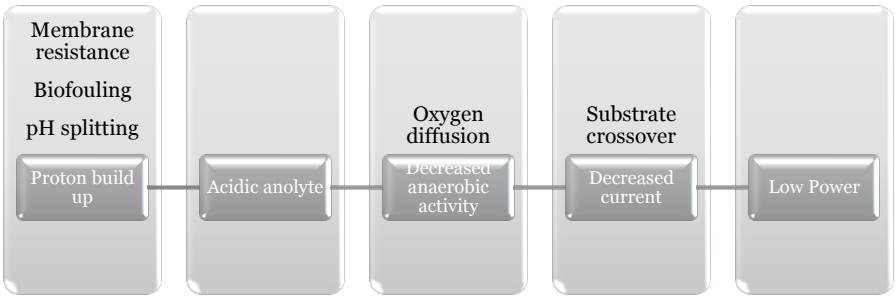

Figure 2.5 – Interdependence on membrane features and power impact.

Membrane types and their use on MFCs

Material choices for membranes and separators are very diverse and produce different results when applied to MFCs: choices can range from commercially available membranes (like Nafion, Ultrex, Hyflon, Zirflon ultrafiltration membranes, sulphonated polyether ether ketone membranes, CEMs and AEMs, bipolar membranes, forward osmosis membranes), polymer/composite membranes, j-cloths, nylon fibers, glass fibers, ceramics and biodegradable shopping bags, natural rubber to laboratory gloves. Cation exchange membranes, which pores are proton sized, are most frequently referred to as proton exchange membranes, or PEMs. Nafion and Ultrex are the two top brands of exchange membranes (EM): while Nafion membranes are prone to biofouling by ammonium they also have the lowest resistance of the two and have excellent proton conductivity. Ultrex is cheaper and a typical choice for studies where ferricyanide is used as a catholyte. Nafion membranes are extremely expensive and suffer from pH splitting, oxygen diffusion and consequent substrate loss (oxygen at the anode makes substrate consumption not power-useful) and biofouling. Although having being used before [91], AEMs aren't a suitable choice for MFC membranes, as previously discussed, due to its large pore sizes and ensuing fuel crossover [17], [28], [30], [70], [84], [86], [87], [89], [92], [93].

Although useful, membranes or separators are not mandatory on MFCs if the cathode is adapted from aqueous to air. For this to happen, reactors are converted to single-chamber and the cathode is coated with a layer of a hydrophobic material to stop the electrolyte from flowing out of the reactor. These membrane-less single-chamber air-cathode reactors present higher power densities, increased proton flow and cathode potential and reduced internal resistance and costs. Because there is no filtration barrier between the anode and the cathode, they also show reduced coulombic efficiency, oxygen diffusion and biofilm formation on the cathode's surface. Membrane electrode assemblies, or MEAs, appeared as a solution to the previous issues. MEAs have a polymeric membrane, acting as the ionic conductor, pressed on to the electrode surface. The MEA may join together the anode, the membrane and the cathode, although this strategy leads to decreased power levels since the anode will quickly be exposed to oxygen. MEAs where the membrane is pressed together with the air-cathode and catalyst present the best results. This concept has been further explored in studies that report membrane-less microbial fuel cells or MFCs with j-cloth as separators (cloth electrode assemblies). Such reports state that MFCs can

produce high power levels due to a decrease in the reactor's internal resistance. The use of Nafion as the membrane for MEAs suffers from the same issues than before, on double chamber reactors. Therefore, instead of applying membranes, air-cathodes are improved with diffusion layers, like layers of polytetrafluoroethylene (PTFE) or poly(vinylidene fluoride) (PVDF). These separator based assemblies (separator electrode assemblies, SEAs) are useful to reduce electrode spacing while limiting oxygen diffusion [8], [17], [94]–[97], [31], [77], [78], [81], [86], [87], [89], [90].

Decisions on whether to use MEA, SEA or membrane-less designs result from cost and performance goals.

Electrodes

Aiming for the MFC's highest power production implies making the right choices for materials and geometry. These choices must be made after careful studying each material's cost-performance relationship. Long term durability must also be accounted for, to improve the lifetime of each fuel cell. It is on the electrode's surface that oxidation-reduction reactions occur and, therefore, electrode material and geometry choices play a major role on power production.

In spite of assisting different reactions, both the anode and the cathode should be conductive and chemically stable, particularly in contact with the electrolyte:

1. Non-or mildly-conductive materials will limit electron transfer efficiency;
2. If either the anode or the cathode has a corrosive nature in the presence of the substrate, then the decomposition by-products can be toxic, therefore changing the electrolyte characteristics, impacting the MFC working profile and ultimately killing the microorganisms sustaining the MFC.

The anode should also be biocompatible, have a low resistance, appropriate mechanical strength and toughness and a large surface area (in order to improve the reaction surface). The cathode should have a high redox potential and easily capture protons [17], [18], [98].

Graphite and carbon are usually the first choices for either electrode. Their cost-efficiency relationship is one of the best, they can be easily shaped, and they are durable. There are even reports of high-school students using them as off the shelf materials to build MFCs' electrodes for science fairs [29].

The anode

The anode's interaction with the substrate is critical for the MFC power development. The bacterial species must be able to interface with the anode material, either by forming a biofilm or by developing nanowires, or other types of electron transfer mechanisms, on its surface. A weak bacterial-anode interface is a sure miss on power development.

The most adequate anode materials are non-fouling, need to have high-specific surface area (area per volume), high porosity, good electrical conductivity, strong biocompatibility and appropriate mechanical strength and toughness. Conductivity wise, copper is the best choice, followed by graphite, carbon and conductive polymer sheets. Copper, however corrodes very easily and will not withstand meaningful operating times [29], [98], [99].

Early research work on the electrode's material and geometry begun by using platinum electrodes, both as anode and as a cathode [44]. Rao and his team, in 1976, continued by pursuing the use of inorganic electrodes made of platinum/nickel combined with polyacrylic acid/polyvinyl alcohol. Even though these managed to achieve remarkable power output levels (at the time), they were also extremely sensitive to the negative influence of amino acids [23].

From 1993 onwards, the research on anode materials become more diverse, although most studies were developed with carbon or metallic materials, influenced by conventional fuel cell topologies.

Allen and Bennetto started publishing with graphite felt and reticulated vitreous carbon (RVC) [100]. By 1996, Cooeny et al used an activated charcoal anode [101]. Again, RVC and, anew, carbon felt were used between 1999 and 2000 by Kim et al [102]. Early in the 21st century, in 2000, 2002 and 2003, graphite has been the choice for several researchers: Chaudhuri and Lovley, Park and Zeikus, Rabaey et al, and Schroder et al [103]–[106]. Other BES fuel cells, specifically enzymatic fuel cells, have used graphite as well, platinum and platinum black, carbon paper and carbon cloth [22]. Carbon cloth is expensive, more so when the electrode needs to be bigger [107]. More recent work, firstly briefly described by Logan on his book [29], was developed using conductive polymers as the anode material. Early results pointed to concerns with the stability of these materials and their erratic and inconsistent performance but recent updates showed that, with adequate surface modification, this anode material allowed for higher conductivities than other materials [108]. The use of metal or metal-based coatings was also researched, with results very far-off, regarding expectations and needs. Bounding mediators to graphite electrodes and treating carbon cloth with ammonium gas preparations are a few examples of other non-conventional studies [29]. The immobilization of cells directly at the anode for improved power production is also feasible, although there are few research records of these endeavors. The immobilized cells, usually, are grown on composite foams, before being subjected to wastewater, in order to stimulate extracellular anaerobic respiration metabolism [108]–[111].

With technological advancements, geometry manipulation became cheaper and more easily addressed in several studies. Since carbon-based materials gather most of the preferred characteristics for the anode – and are usually cheaper, readily available and simpler to produce – a way was found to improve the anode surface area.

Graphite materials seem to have a better behavior for fiber and brushes configurations, resulting in the highest specific surface areas and porosities. They can also be shaped into rods (low internal

porosity), sheets (not porous), felts and granules. Felts and rods result in approximately the same current production (normalized to the surface area) and granules need to be in contact with each other to guarantee a high conductivity [22], [28]–[30], [70], [107]. It was found that granular activated carbon materials, albeit having higher surface areas, negatively impact the internal resistance while being prone to clogging and difficult to interface with wires or other electron collection methodology. Carbon nanotubes have also been explored but some material doping is needed to limit their toxicity. On top of that, they are expensive and also present some clogging issues [98]. Graphite, or carbon, fiber brushes were developed as a way to increase the surface area and maintaining the electrode resistance at its minimum: they have large porous surface areas, low resistance, good electrical conductivity, they are not prone to biofouling and are cheap. It was also found that, contrary to what happens with foams, the biofilm development doesn't take a toll on MFC performance. They are usually wound around titanium wires for their resistance to corrosion and high conductivity [98], [107].

Table 2.1 summarizes the advantages and disadvantages of several anode materials.

Table 2.1 - Comparison between different carbon composed anode materials.

Anode materials	***Advantages***	***Disadvantages***
Graphite rod	Good electrical conductivity and chemical stability; cheap	Difficult to increase surface area
Graphite fiber brush	Higher specific surface areas, easy to produce	Clogging
Carbon cloth	Large relative porosity	Expensive
Carbon paper	Easy to connect wiring	Lack of durability, fragile
Carbon felt	Large aperture	High resistance
Reticulated Vitreous Carbon	Good electrical conductivity and plasticity	High resistance, fragile

Carbon fiber brush anodes, heat treated at 450 ºC for 30 minutes [112], [113], are currently the standard material, and best performing, for MFC studies with air-cathode reactors. However, since their first study, in 2007 [107], further analysis of the appropriate size and spacing has been in place, particularly because of scalability concerns. Studies have also addressed the number of brushes that should be used for a particular reactor. It was found, for a single chamber air-cathode reactor, that multi-brush anodes have no meaningful impact on performance. For large reactors, however, this is not true. And changes also happen with the feeding mode of the electrolyte: for a 175 mL reactor, 3 brushes of a 25 mm diameter are the winning combination for batch studies and 8 brushes of 8 mm diameter are better in continuous feeding mode (considering artificial wastewater). Results of using these strategies with real wastewater showed that additional studies with raw electrolyte should be conducted before drawing any conclusions on reactor scale-up [74], [75].

The cathode

For cathodes, materials aren't very different. The cathode should be able to facilitate a reaction between the electrons it receives and an electron acceptor, hence presenting a high redox potential [98]. The electron acceptor can be on the cathode itself or dissolved or spurged on the catholyte. Hexacyanoferrate (IV) and permanganate are two examples of dissolved electron acceptors: they have high redox potentials and fast reduction reactions, producing large currents. Although there are several publications on the use of these compounds as reduction mediators ([64], [106], [114] serve as an example), oxygen, in spite of having slower reaction kinetics, has a high standard potential, is more readily available, less toxic, cheaper and, in air-cathodes, doesn't need continuous replacement [17], [92], [115], [116].

The electron final acceptor is, therefore, the starting point for the choice of cathode materials. A typical cathode is composed of a catalyst layer and a layer of supporting material, acting as the current collector [117]. Choosing a suitable combination between the supporting material and the catalyst is of the greatest importance and difficulty in an MFC.

With oxygen as the electron acceptor, research started with platinized carbon paper (PCP) cathodes in Allen and Bennetto's team by 1993 [100]. 6 years later, Kim et al applied a RVC cathode [102] and by the year 2000, platinum and graphite cathodes were used by Kim as well as by Park and Zeikus [104], [118]. From then onwards, between 2002 and 2004, graphite became a natural choice for several researchers [29], [30]. The most popular and effective supporting materials were found to be carbon based, which, eventually, led to choices for the cathode supporting material mimicking the material choices for anodes. These materials proved to be cheap, highly conductive, very durable and with a high mechanical strength and surface area [117].

After several studies pointing to the cathode as the power limiting element on MFCs [30], [32]–[34], in 2011, Cheng and Logan found that the cathode specific area was a key point factor for improving maximum power density [119]. The oxygen reduction reaction (ORR) happening at the cathode surface ($2O_2 + 8H^+ + 8e^- \rightarrow 4H_2O$, Figure 2.1) is currently the main technological bottleneck on power production with MFCs, due to high over-potentials and low kinetics. In fact, the energy needed to overcome the activation barrier to convert the oxidant to a reduced form is responsible for a significant potential drop. The catalyst choice – the utmost player on improving reaction kinetics – is made between platinum-group-metal (PGM) free materials, platinum based compounds, carbon-based mixtures and biocatalysts [17], [86], [115]–[117], [120]. PGM free catalysts are created by merging a transition metal (which, by decreasing performance order, can be iron, cobalt, nickel or manganese) with carbon and nitrogen (provided by the use of organic compounds like guanosine, sulfadiazine, pyrazinamide, niclosamide, sulfacetamide, ricobendazole, quinine or succinylsulfathiazole). PGM free catalysts perform worse than platinum on acidic media and better than platinum on alkaline media. Platinum, a noble metal, is an excellent catalyst, being highly oxidant, but is very expensive and not very durable. The ORR with a platinum catalyst favors an acidic pathway with a production of 4 electrons per oxygen molecule,

while the ORR with a carbon-based catalyst follows more easily an alkaline path with the production of 2 electrons per oxygen molecule. Carbon based catalysts, like carbon nanotubes, graphene, carbon black and activated carbon, are less oxidant but cheaper and their application is more straightforward on scaled up designs [17], [98], [116], [117], [120], [121]. With adequate loadings, they can even be more durable than platinum catalysts [122].

Biocatalysts (biocathodes) were firstly studied in 1966 but without any applicable results. They work by making use of bacteria to receive the electrons on the cathode and became a study subject after researchers saw biofilm formation on the cathode on some studies. Instead of trying to limit its unavoidable development, some researchers tried to condition its development to improve the MFCs' performance. Enzymes can be used as biocatalysts as well: enzyme-based catalysts have a short lifetime, although having a high-power output, and are more useful on disposable devices. For cyclic operation, bacterial catalysts are better suited. The construction and development of biocathodes can be achieved by polarizing a biocompatible cathode in an organic rich environment with bacteria having an electrogenic profile. The biofilm formation, which is a common acclimation step on the anode as well, can also be achieved by leaving the electrodes on the electrolyte in open circuit or connected with a high-value (around 1kΩ) resistor. However, for single-chamber reactors, the biofilm development in these conditions undercuts the anode's purpose: the cathode surface is highly aerobic (due to the needed cathode oxygen permeability) and specific bacteria can adhere to the cathode and use oxygen directly, bypassing the anode usefulness. This phenomenon has a slow onset, but once started it can only be limited by appropriate cleaning of the cathode or, as a last resource, stopped by applying a new cathode [123]–[126].

Biocathodes can be applied to double-chamber MFCs and are cheap (compared to platinum based catalysts) to construct and operate and take advantage of evolutionary adaptations [86], [92], [115], [116], [120]. A biocathode was used for nitrate removal and simultaneous electricity production, by applying carbon cathode electrodes and *Bacillus Subtilis* bacteria on a glucose and nitrate rich medium, proving that biocatalysts can also be used to clean the electrolyte from unwanted products – for instance, in denitrification processes - or even to stimulate the production of useful compounds [76], [116].

Cathode topologies have also changed in time. Early studies were conducted with double chamber reactors and aqueous cathodes. Due to significant power losses in double chamber reactors, research pointed to the use of single-chamber MFCs, with or without the use of a membrane or separator. In single-chamber reactors, cathodes (as well as the supporting material and the catalyst layer) are merged with a diffusion layer (which allows air exchanges but no liquid leaks).

These air-cathodes have a submerged side and an air exposed surface. They are responsible for higher power densities than their aqueous cathode equivalent since oxygen is more soluble in air than in water [32], [96], [97]. The use of a physical barrier between the anode and the cathode prevents oxygen diffusion to the anode (if the anode biofilm receives oxygen, the bacteria will progressively stop to exhibit exoelectrogenesis) but reduces power by increasing the reactor's total internal resistance [81], [116]. The most efficient material combination for an air-cathode corresponds to having a stainless steel supporting material (current collector) and a carbon black and activated carbon catalyst, as pictured in Figure 2.6 [112], [117].

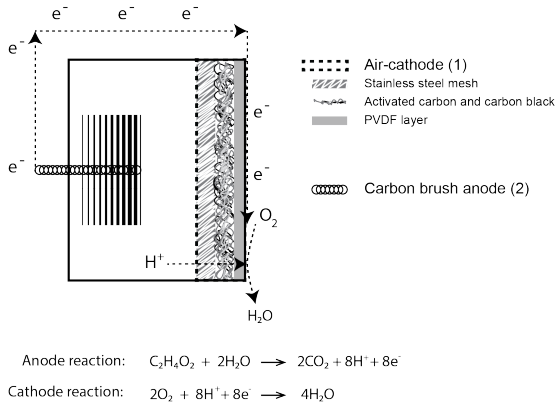

Figure 2.6 – Schematic representation of a stainless steel, activated carbon air-cathode. Adapted from [112].

The production method of these cathodes also impacts their performance and the machine rolling method with poly(vinylidene fluoride), acting both as the binder and the diffusion layer, seems to present better results [17], [112], [115]. Amidst binder choices, mixing polytetrafluoroethylene (PTFE) with Nafion, although decreasing costs of using a membrane, also decreases power performance. Poly(vinylidene fluoride) (PVDF) presents low cost and larger power densities, withstanding high water pressures. As with other cathodes, biofilm development is inevitable. Although helping to limit oxygen crossover to the anode, it also limits proton flow and energy production. Studies have successfully proved that the cathode surface can be doped with an antibiotic substance to limit biofouling of the air-cathode [115]. More recently, in 2016, increased power levels were also achieved by increasing the number of catalyst layers on an air-cathode, rather than increasing the catalyst loading, and integrating a polytetrafluoroethylene (PDVF) diffusion layer to improve oxygen permeability and waterproofing [77].

Substrate and media

The fuel used in MFCs, as in other fuel cells, is decisive for power production. MFC's fuel can be separated in two major constituents: the medium or substrate, which usually contains the carbon source, and the inoculum, or starting culture.

The starting culture can be sampled from real wastewater or from sediments on streams, rivers or lakes. Bacteria will behave better if collected from oxygen deprived environments, like the ones aforementioned or food leftovers stuck on the kitchen sink piping.

The medium gathers the needed conditions for the inoculum or bacteria to grow, usually consisting of a buffer solution, a mineral and vitamin mixture and the carbon source (bacteria energy source). The medium can either be artificially produced, converted from real wastewater or used directly as pure wastewater, with no altered composition. The medium is not electrochemically active but has great energy stored in the connections between their different compounds. The characteristics of the carbon source have been found to have significant impact on the fuel cell's electricity generation process. Several studies have been conducted to clarify the latter relationship: according to their findings, a complex carbon source builds a diverse and electrochemically active microbial community and the use of a simple substrate results in a faster and easier decomposition process, improving the electric output of the system [22], [24], [29], [127].

Early studies began by using simple substrates to evaluate MFCs so as to have the fewest variables as possible. Acetate and glucose were the first choices. Acetate is the immediate energy source for the citric acid cycle (more commonly referred to as Krebs cycle) and leaves, at room temperature, no possibility for other microbial respiratory process to occur. It is also the final product for several other metabolic pathways. When compared to the use of protein-rich wastewater, acetate-based MFCs achieved more than two times the maximum electrical power than with the mentioned wastewater. Glucose does not achieve results as impressive: comparing acetate and glucose energy conversion efficiency, it was found that acetate had a 42% conversion efficiency rate and glucose only 3% [127]. These results seem to be justified by the fact that glucose is a substrate usable by other metabolic energy retrieving processes, like fermentation and methanogenesis. These processes do not help power development on MFCs. Glucose was responsible, however, for the development of a more diverse microbial culture. The use of lignocellulosic biomass is an example of complex medium or substrates. It cannot be directly used by the bacterial colonies unless converted to monosaccharides or other simpler compounds. It has been proven that basic cellulosic components, monosaccharides, are good starting points for electricity generation in MFCs [70], [127].

The microbial community working with this raw material has, however, to have cellulolytic and exoelectrogenic characteristics. Comparatively with glucose, this fuel type seems to, conversely, have a lower power output and no microorganisms have been found to be capable of digesting

pentoses, one of the main sugar types resulting from cellulose breakdown. Lignocellulosic biomass is a result of residual plant material and MFCs using this substrate are not very effective. Other wastewater types have been evaluated: brewery wastewater, with high organic matter content (almost ten times above domestic wastewater) - low strength, low concentration of inhibitory substances - starch processing wastewater (also with a high organic content), dye wastewater (a choice driven by the importance of their removal from water resources), paper recycling wastewater, biorefineries wastewater and swine wastewater. Non-conventional substrates, like cellulose and chitin have also been studied. These compounds are considered non-conventional because of their particulate nature. It was found that for solid, or particulate, substrates like these, a low hydrolysis (cleavage of chemical bounds by the addition of water) rate limits power production. Landfill leachates were scoped by some studies in 2009 but no power output was reported. The concept was validated but further studies are needed to understand their full potential [127].

Synthetic wastewater has a well-defined composition and is an emblematic choice to check the influence of its composition on the performance of an MFC. Rodrigo et al found that, for wastewater with the same pollutants (organic glucose and peptone), the slower the MFC's feeding rate, the higher was the electrical output, most likely because of the pilling up of intermediates [128]. Artificial wastewater is still the default choice for isolating variables and studying their influence on power production [74], [107], [112], [121], [129], [130].

Pure, unaltered domestic wastewater still lags in power output levels but its use is increasing to determine what optimizations need implementation [8], [75], [112], [129]–[134].

Feeding strategies

The operation mode of microbial fuel cells can be classified according to the type of substrate flow. Microbial fuel cells can be fueled through:

1. Continuous flow: an uninterrupted flow of substrate is provided by using pumps that push/pull the reactor liquid. Such a methodology leads to low hydraulic retention times (HRT), and, therefore, low concentration of metabolic byproducts.
2. Semi-continuous flow: At a regular interval, a set volume of the reactor's fuel is refreshed. The attainable HRTs are higher.
3. Batch or fed-batch flow: a parameter is chosen that determines the complete replacement of the reactor's fuel. That parameter can be physical (voltage, current) or biochemical, like oxidation-reduction level, pH, dissolved oxygen, biochemical oxygen demand or others. This mode assures the highest HRTs.

The operation mode of the MFC will eventually determine the biofilm conditions, impacting on the power profile [135]–[138]. It is however important to distinguish the operation mode from the method of acquiring a polarization curve for reactor characterization (further details on the

polarization subject ahead). An MFC can be operated in batch mode but the polarization data can be retrieved by varying the external resistor in the same batch or only at substrate replacement.

Bacteria and biofilm

The bacterial population on an MFC is also a critical factor determining its power output. The basic structural, functional and biological unit of all living organisms is the cell. They are usually called the "building blocks of life" and can either be eukaryotic or prokaryotic, according to their elements. A eukaryotic cell has a nuclear membrane (delimiting the nucleus, where the genetic material is), its ultimate characteristic; a prokaryotic cell does not – in fact, its genetic material (DNA) is unbound in the cytoplasm of the cells. A bacterial organism is made of prokaryotic cells.

Prokaryotic organisms, as well as eukaryotic, have different processes from which they can obtain energy and nutrients. The overall set of reactions that occur in living organisms, and that are required for energy generation and its use to synthesize cell material from small molecules in the environment, is called metabolism – from the Greek word "change" (μεταβολή). If the metabolism has an energy-generating final balance, it is called catabolism; if it has an energy-consuming, biosynthesis stage, it is called anabolism.

Because prokaryotic organisms have been around for longer that eukaryotic ones, their metabolic pathways are incredibly adaptive: according to their living conditions so is their metabolism. So, the same prokaryotic organism, living in two different environments, can exhibit different metabolic pathways.

There are two major metabolic pathways: *Heterotrophy* and *Autotrophy*.

The separation between both lies in the use of an organic compound as a source of carbon and energy – *Heterotrophy*; or carbon dioxide's direct fixation – *Autotrophy* (the fixation is made by a compound known as Ribulose 1,5-bisphosphate (RUBP) Carboxylase). A further categorization of these two major catabolic pathways is presented.

For *Heterotrophy*, Fermentation and Respiration are two energy producing alternatives: Fermentation occurs when energy is derived from the partial oxidation of an organic compound using organic intermediates as electron donors and electron acceptors. No outside electron acceptors are involved and no membrane or electron transportation system is required; for Respiration, there is a complete oxidation of the substrates by an outside electron acceptor.

As *Autotrophy* is concerned, there are also two major catabolic alternatives: Lithotrophy implies the use of an inorganic compound (no carbon and no hydrogen in its constitution) as a source of energy and can be used by hydrogenic bacteria, methanogens (which transfer electrons from H_2 to CO_2 while reducing it to methane, CH_4), carboxydobacteria ($CO \rightarrow CO_2$), nitrifying bacteria ($NH_3 \rightarrow NO_3$), sulfur oxidizers and iron bacteria; Phototrophic organisms take advantage of light and use it as a source of energy for growth. Phototrophic metabolisms can also be divided into

three major types: oxygenic photosynthesis, anoxygenic photosynthesis and nonphotosynthetic photophosphorylation.

All these metabolism types can be grouped into three major categories, according to the final electron acceptor: aerobic for using molecular oxygen; anoxic for using non-molecular oxygen; and anaerobic when there is no use of oxygen (single or molecular) [139]. Figure 2.7 synthesizes all these concepts.

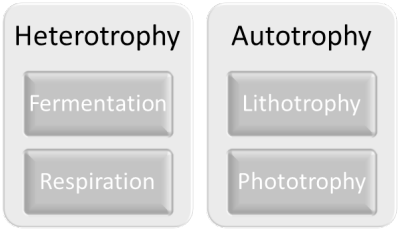

Figure 2.7 - Major metabolic pathways. Heterotrophic organisms obtain carbon from organic compounds; Autotrophic organisms make direct carbon fixation.

For an MFC to work, bacteria, while processing the substrate, should be able to transfer the electrons produced by their catabolic reactions to the anode. Exoelectrogens, electricigens, electrochemically active or anode respiring bacteria are all common terms applied to describe bacteria that are capable of doing just that. They can do so resorting to outer membrane components (cytochromes: inner-membrane, periplasmic and outer-membrane redox proteins), excreted mediators (also known as electron shuttles) or synthesizing appendages capable of transferring electrical current (nanowires or pili). Figure 2.8 makes a clearer explanation of how these processes affect electron production and transfer.

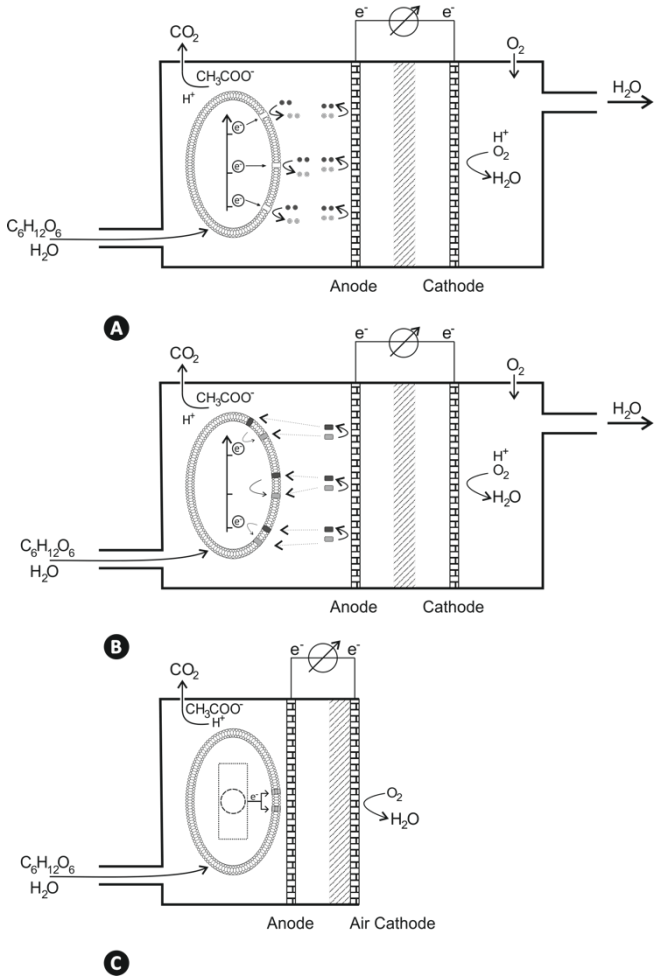

Figure 2.8 - Different types of electron transfer methods. Glucose has been used as an example substrate. In (A), an example of an indirect microbial fuel cell, with hydrogen (metabolic end product) used for electron production at the anode; In (B), a mediator-driven microbial fuel cell is shown: it will be the mediator, converted from its reduced to oxidized form, to transport the electrons resulting from the bacterial metabolism to the anode; Finally, in (C), the schematic displays an air-cathode MFC with electron transport proteins making the electron transfers (Adapted from [24]).

Having this ability doesn't necessarily mean that it'll be used. And that's where the metabolism choice takes part. For an MFC, the best achievable results will appear when the electron output is at its highest; different catabolic reactions give rise to different net electron production. Choosing conditions that favor an aerobic metabolic path (or a bacterial strain) will be of no use: if the final electron acceptor is molecular oxygen, and that is available at the biofilm development site, than the electrode will not be used (no power output); also, if organic substrates are considered, the bacterial strains that end up developing in an MFC anode can be conditioned by the carbon source choice: acetate, for instance, can force bacteria to exhibit an anaerobic heterotrophic metabolism, namely anaerobic respiration [10], [24], [29], [32].

Potter's early investigations used living cultures of *Escherichia Coli* and *Saccharomyces*. The first problems encountered with these species had to do with the low power output because no electron mediators had been used. Since then, several studies have been conducted and presented, shedding light on exoelectrogens choices and their relationship with the cell's power output [28].

For *Escherichia Coli*, *Pseudomonas*, *Proteus* and *Bacillus* species, the use of artificial mediators cannot be ignored. If it weren't for them, the power output of MFCs with these bacterial populations would be neglectable since these strains cannot effectively transfer electrons at key metabolic points. Typical electron shuttles include thionine, benzylviologen, 2,6-dichorophenolindophenol, 2-hydroxy-1,4-naph-thoquinone and various phenazines, phenothiazines, phenoxoazines, iron chelates and neutral red [24], [26].

The use of artificial shuttles, or mediators, has several shortcomings: firstly, even though some electrons are captured by the shuttles, others remain with unbroken chemical connections and continue to be processed in parallel metabolic paths (fermentation); secondly, the use of artificial shuttles will increase the difficulties of maintaining a MFC, since many of the electron shuttles used are pollutants [24].

There are also other species that do not require artificial mediators, capable of biosynthesizing them. This has energetic costs and is usually not a good alternative as it reduces the net electron production of the MFC. The *Pseudomonas aeruginosa* strain, and the *Lactobacillus* and *Enterococcus* species are examples of bacteria capable of producing its own mediators. Experiments with similar bacterial strains for a one-time replacement of the substrate resulted in a decreased power output of about 50 %, which seems to point that species with these characteristics will not be a popular choice.

For whichever form of bacteria previously mentioned, studies report that they also do not fully oxidize the substrate they are in.

Only one type of exoelectrogens remains: bacteria which are able to "directly" transfer electrons to the electrode. *Shewanella putrefaciens* have outer-membrane components, named cytochromes, which are vital in this process. These cytochromes make the catabolic electrons available at the cell's membrane and they end up reacting with other substrate components which can directly be oxidized by the anode. Other strains, like *Aeromonas hydrophila* and some *Clostridium* and *Geobacter* species have also been reported to have the ability to directly interact with the electrode. However, they seem to do so using some biosynthesized conductive appendages - nanowires or pili – and forming a biofilm in the anodes surface.

Other than considering the bacteria-electrode interface, other studies have been developed so as to gain an understanding of how power production depends on single or multi strain/species of bacteria at the anode [22], [24], [25], [27]–[29], [32].

Biofilm development on MFCs

As previously presented, bacteria are living organisms. Their lifecycle is mostly dependent upon environmental conditions, and, in an uncontrolled environment, is not patterned. However, the lifecycle observed in controlled settings can help understand the overall steps of this process. Furthermore, and when considering the biofilm development in a Microbial Fuel Cell, a controlled setting is imposed.

The typical lab grown culture of bacteria has 4 lifecycle stages: the lag phase, the log (or exponential) phase, the stationary phase and the death phase. The lag phase comprehends the period of time when bacteria don't reproduce and can last anywhere between 1 hour to several days. The number of bacteria doesn't diminish, and, in most cases, bacteria are adapting to new conditions. The log phase ensues, where bacteria reproduce by binary fission and their replication rate is higher than that of bacterial death. When going through binary fission, the cell's DNA replicates concomitantly with cell elongation. The final step of bacteria replication is the formation of a septum in the middle of the cell: the septum will be the new cell wall and a bacterium has now produced two. This phase can run indefinitely if the medium is not depleted and environmental conditions aren't adverse. Bacteria cells in this phase are larger than on any other phase.

The stationary phase happens when the growth and death rate are equal. Cells on this phase are slow growing and small. For each cell death, a new cell is produced, maximizing the carrying capacity of the environment. The last phase on the lifecycle of a bacteria is the death phase. In this phase, appearing as a consequence of nutrient depletion and/or adverse changes to the environmental condition, more bacteria die than those being produced [140], [141]. Figure 2.9 is a graphical representation of the lifecycle stages and cell size in time.

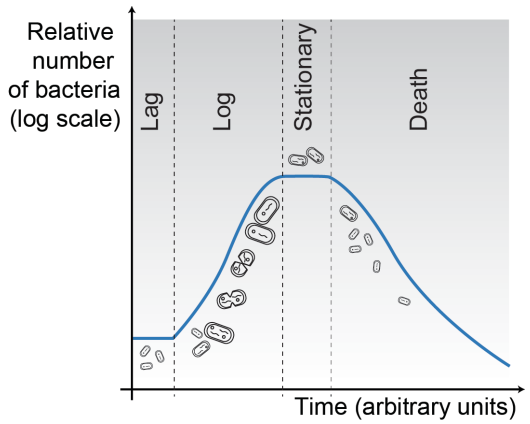

Figure 2.9 – Relative number of bacteria according to the lifecycle phase in a controlled experiment. The image also shows how bacteria cell size change according to the lifecycle stage.

Biofilm inoculation and transfer

The development of a microbial biofilm on the anode surface of an MFC is an obligatory requirement for power production. The primary inoculation of a bacterial biofilm can happen through:

1. The use of wastewater or other anaerobic organic water samples (e.g., from standing water, ponds);
2. By promoting biofilm transfer from a previously colonized surface.

The primary inoculation through the use of a wastewater sample is slow: the bacterial population present in the anaerobic water sample is diverse and not fully adapted to anaerobic conditions, since they aren't fully deprived of oxygen. As such, the first days of MFC biofilm development are used for exoelectrogen selection and anaerobic respiration imposition, by connecting the electrodes through a 1 kΩ load. For 3 days, the anaerobic water source in the reactor is replaced by half at 24-hour periods. At the fourth day, the reactor volume is emptied until half and an artificial wastewater solution with a carbon source is used to refill it. Voltage is then monitored, and the reactor's contents are fully replaced whenever the voltage reads under 50 mV. When stable voltage readings are achieved, the biofilm attachment is considered successful, but no conclusion can be drawn for the biofilm maturation, since steady power densities can be verified although the biofilm is not fully adapted. Thus, a polarization trial is conducted to check the biofilm maturation stage. A mature biofilm presents a polarization curve without power overshoot [29], [72], [130].

Biofilm transfer is quicker, although subject to lower success rates when compared to the biofilm development through wastewater samples. In fact, this procedure consists of placing a colonized surface in contact with a non-colonized surface while guaranteeing adequate conditions for biofilm extension. In an MFC, one of the methods for this transfer consists in placing a previously colonized anode ("old" anode) in direct contact with a fresh anode ("new" anode). The anode set (old and new anodes) is electrically connected and the anode-cathode connection is forced to short-circuit conditions until stable power densities are verified. When that condition is met, the "new" anode is placed in a fresh reactor and the aforementioned acclimation procedure is applied. The biofilm transfer can be achieved by using other methodologies, but usually imply damaging or sacrificing the "old" anode (biofilm scrapping and potential control through the use of a potentiostat) [142]. Both these procedures will be further discussed with application examples.

Although undesirable, a biofilm also develops on the cathode surface: as an oxygen permeable surface, bacteria start growing on this surface (both in the inside and outside of the reactor), bypassing the anode usefulness. This colony has a major impact on the power generation of MFCs, by increasing the MFC's internal resistance and the pH at the cathode vicinity, decreasing the cathode potential and activity. As such, cathode cleaning must happen regularly, whenever biofilm development is detected. The cleaning procedure is usually done by scrapping the inner

cathode surface. When the need to clean the cathode is recurrent, cathode replacement is obligatory to guarantee adequate MFC operation [123], [143], [144].

Electrobiochemical characteristics of electroactive biofilms

Although the term biofilm has been used to refer to a group of bacteria, further details are needed to discuss how electrons flow between the bacteria in that biofilm and the electrodes. A biofilm, aside from the bacteria, is a bacteria self-secreted polymeric matrix (extracellular polymeric substance, EPS) attached to a biotic or abiotic surface, which thickness can vary. At MFCs, this influences power production, since biofilms that are too thin have low current densities and those too thick have hindered electron flow [145], [146].

Extracellular electron transfer (EET) from the biofilm to the electrode can happen by two major mechanisms: directly, through cytochromes (outer-membrane or periplasmatic, in the cell interior), and indirectly, through mediators or conductive pili (nanowires). The way that EET happens is intrinsically related with how the MFC's electrodes are connected. The biofilm can be treated as having 3 different charge storing zones, where zone 1 is closer to the anode and zone 3 is furthest, as picture in Figure 2.10.

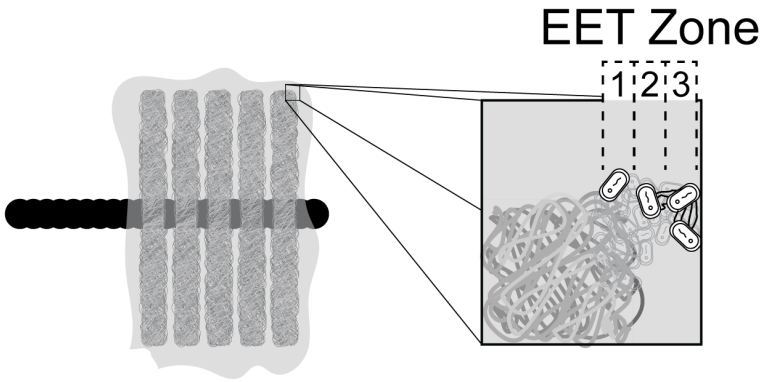

Figure 2.10 – Detailed image of the biofilm, where three different extracellular electron transfer (EET) mechanisms are exposed. Bacteria in zone 1 transfer electrons to the electrode directly, whereas zone 2 and zone 3 bacteria use indirect transfer mechanisms, with nanowires or mediators, or even to neighboring bacteria.

In zone 1, charge is stored in the cytochromes and is transferred either directly or by nanowires to the anode; in zone 2, electrons are transferred between bacteria until reaching the electrode; zone 3 charge corresponds to the exoelectrogenic bacteria itself [147]–[150]. As mentioned, the electrode connection condition influences from what zone researchers think electrons flow from: highest external loads (open circuit voltage being the highest possible load) force bacteria to migrate to the outside layer of the biofilm, increasing the distance to the electrode and leading to zone 3 EET, where bacteria change electrons between each other. When the outside load decreases, bacteria begin closing in on the anode and zone 3 and zone 2 EET are considered to happen, which is coherent with decreased voltage and increase current readings. When the external load is lowest (short-circuit being the lowest possible load) electrons flow freely from

zone 3, zone 2 and zone 1. At these conditions, power production is conditioned by the metabolic rate of electron production [147], [149]–[151].

Irrespective of the EET zone, the biofilm exhibits a charge storing behavior. As such, each zone can be seen as a separate capacitor, where its discharge time is dependent on the electrode connection conditions. In fact, and for open circuit conditions, electron flow is retarded and becomes backed-up in the biofilm, causing respiratory shutdown to prevent oxidative damage to the bacteria. If these conditions are maintained for over 30 minutes, death ensues. When the anode-cathode connection is restored, a transient behavior with an overcurrent is observed: current from the discharge of the capacitor-like behavior of zone 1, zone 2 and zone 3 (decreasing in an exponential way) adds up to the current due to metabolic activity, which has a steady-state performance. The magnitude of the external load applied, and the open circuit time determine the overcurrent discharge time and size [147], [148], [152].

References

[1] V. G. Gude, “Wastewater treatment in microbial fuel cells - An overview,” *J. Clean. Prod.*, vol. 122, pp. 287–307, 2016.

[2] L. T. Angenent, K. Karim, M. H. Al-Dahhan, B. A. Wrenn, and R. Domíguez-Espinosa, “Production of bioenergy and biochemicals from industrial and agricultural wastewater.,” *Trends Biotechnol.*, vol. 22, no. 9, pp. 477–85, Sep. 2004.

[3] P. Aelterman, K. Rabaey, P. Clauwaert, and W. Verstraete, “Microbial fuel cells for wastewater treatment.,” *Water Sci. Technol.*, vol. 54, no. 8, pp. 9–15, Jan. 2006.

[4] Sic Notícias, “Território nacional em seca severa e extrema.” [Online]. Available: http://sicnoticias.sapo.pt/pais/2017-11-17-Territorio-nacional-em-seca-severa-e-extrema-1. [Accessed: 22-Nov-2017].

[5] Observador, “Seca extrema no sul da Europa: nascente do rio Douro sem água,” 2017. [Online]. Available: http://observador.pt/2017/11/06/seca-extrema-no-sul-da-europa-nascente-do-rio-douro-sem-agua/. [Accessed: 18-Nov-2017].

[6] H. Liu, R. Ramnarayanan, and B. E. Logan, “Production of Electricity during Wastewater Treatment Using a Single Chamber Microbial Fuel Cell,” *Environ. Sci. Technol.*, vol. 38, no. 7, pp. 2281–2285, Apr. 2004.

[7] Z. He, S. Minteer, and L. Angenent, “Electricity generation from artificial wastewater using an upflow microbial fuel cell,” *Environ. Sci. …*, 2005.

[8] H. Liu, B. E. Logan, and L. E. B. Liu Hong, “Electricity Generation Using an Air-Cathode Single Chamber Microbial Fuel Cell in the Presence and Absence of a Proton Exchange Membrane,” *Environ. Sci. Technol.*, vol. 38, no. 14, pp. 4040–4046, 2004.

[9] A. S. Mathuriya, “Novel microbial fuel cell design to operate with different wastewaters simultaneously,” *J. Environ. Sci. (China)*, vol. 42, pp. 105–111, 2016.

[10] R. A. Rozendal, H. V. M. Hamelers, K. Rabaey, J. Keller, and C. J. N. Buisman, “Towards practical implementation of bioelectrochemical wastewater treatment.,” *Trends Biotechnol.*, vol. 26, no. 8, pp. 450–9, Aug. 2008.

[11] L. Zhuang, Y. Zheng, S. Zhou, Y. Yuan, H. Yuan, and Y. Chen, “Scalable microbial fuel cell (MFC) stack for continuous real wastewater treatment.,” *Bioresour. Technol.*, vol. 106, pp. 82–8, Feb. 2012.

[12] Y. R. J. Thomas, M. Picot, A. Carer, O. Berder, O. Sentieys, and F. Barrière, “A single sediment-microbial fuel cell powering a wireless telecommunication system,” *J. Power Sources*, vol. 241, pp. 703–708, 2013.

[13] D. Sartori and D. Brunelli, “A smart sensor for precision agriculture powered by microbial fuel cells,” *2016 IEEE Sensors Appl. Symp.*, pp. 1–6, 2016.

[14] F. Yang, K.-C. Wang, and Y. Huang, “Energy-neutral communication protocol for based wireless sensor network,” *IEEE Sens. J.*, vol. 15, no. 4, pp. 2306–2315, 2015.

[15] D. Brunelli, P. Tosato, and M. Rossi, “Microbial fuel cell as a biosensor and a power source for flora health monitoring,” *Proc. IEEE Sensors*, no. 2, 2017.

[16] F. Zhang, L. Tian, and Z. He, “Powering a wireless temperature sensor using sediment microbial fuel cells with vertical arrangement of electrodes,” *J. Power Sources*, vol. 196, no. 22, pp. 9568–9573, 2011.

[17] C. Santoro, C. Arbizzani, B. Erable, and I. Ieropoulos, “Microbial fuel cells: From fundamentals to applications. A review,” *J. Power Sources*, vol. 356, pp. 225–244, 2017.

[18] M. Rahimnejad, A. Adhami, S. Darvari, A. Zirepour, and S. E. Oh, “Microbial fuel cell as new technology for bioelectricity generation: A review,” *Alexandria Eng. J.*, vol. 54, no. 3, pp. 745–756, 2015.

[19] T. H. Pham *et al.*, “Microbial fuel cells in relation to conventional anaerobic digestion technology,” *Eng. Life Sci.*, vol. 6, no. 3, pp. 285–292, 2006.

[20] H. Wang and Z. J. Ren, “A comprehensive review of microbial electrochemical systems as a platform technology.,” *Biotechnol. Adv.*, vol. 31, no. 8, pp. 1796–807, Dec. 2013.

[21] J. B. A. Arends and W. Verstraete, “100 years of microbial electricity production: three concepts for the future.,” *Microb. Biotechnol.*, vol. 5, no. 3, pp. 333–46, May 2012.

[22] R. A. Bullen, T. C. Arnot, J. B. Lakeman, and F. C. Walsh, “Biofuel cells and their development,” *Biosens. Bioelectron.*, vol. 21, no. 11, pp. 2015–2045, May 2006.

[23] F. Davis and S. P. J. Higson, “Biofuel cells - recent advances and applications.,” *Biosens. Bioelectron.*, vol. 22, no. 7, pp. 1224–35, Feb. 2007.

[24] D. R. Lovley, “Bug juice: harvesting electricity with microorganisms.,” *Nat. Rev. Microbiol.*, vol. 4, no. 7, pp. 497–508, Jul. 2006.

[25] K. Rabaey *et al.*, “Microbial ecology meets electrochemistry: electricity-driven and driving communities,” *ISME J.*, vol. 1, no. 1, pp. 9–18, May 2007.

[26] S. Karmakar, K. Kundu, and S. Kundu, “Design and Development of Microbial Fuel cells,” *Technol. Educ. Top.* ..., 2010.

[27] V. G. Debabov, “Electricity from microorganisms,” *Microbiology*, vol. 77, no. 2, pp. 123–131, May 2008.

[28] Z. Du, H. Li, and T. Gu, “A state of the art review on microbial fuel cells: A promising technology for wastewater treatment and bioenergy.,” *Biotechnol. Adv.*, vol. 25, no. 5, pp. 464–82, 2007.

[29] B. E. Logan, *Microbial Fuel Cells*. Hoboken, NJ, USA: John Wiley & Sons, Inc., 2007.

[30] B. E. Logan *et al.*, “Microbial Fuel Cells: Methodology and Technology †,” *Environ. Sci. Technol.*, vol. 40, no. 17, pp. 5181–5192, Sep. 2006.

[31] S. E. Oh and B. E. Logan, “Proton exchange membrane and electrode surface areas as factors that affect power generation in microbial fuel cells,” *Appl. Microbiol. Biotechnol.*, vol. 70, no. 2, pp. 162–169, 2006.

[32] B. E. Logan, “Exoelectrogenic bacteria that power microbial fuel cells.,” *Nat. Rev. Microbiol.*, vol. 7, no. 5, pp. 375–81, May 2009.

[33] S. Oh, B. Min, and B. E. Logan, “Cathode performance as a factor in electricity generation in microbial fuel cells,” *Environ. Sci. Technol.*, vol. 38, no. 18, pp. 4900–4904, 2004.

[34] B. E. Logan, “Essential data and techniques for conducting microbial fuel cell and other types of bioelectrochemical system experiments.,” *ChemSusChem*, vol. 5, no. 6, pp. 988–94, Jun. 2012.

[35] K. Scott *et al.*, *Microbial Electrochemical and Fuel Cells: Fundamentals and applications*, vol. 88. 2016.

[36] B. E. Logan, M. J. Wallack, K. Y. Kim, W. He, Y. Feng, and P. E. Saikaly, “Assessment of Microbial Fuel Cell Configurations and Power Densities,” *Environ. Sci. Technol. Lett.*, vol. 2, no. 8, pp. 206–214, 2015.

[37] H. Wang, J. Park, and Z. J. Ren, “Practical Energy Harvesting for Microbial Fuel Cells: A Review.,” *Environ. Sci. Technol.*, vol. 49, pp. 3267–3277, 2015.

[38] L. Galvani, *Aloysii Galvani De viribus electricitatis in motu musculari commentarius*. 1791.

[39] A. des Sciences (Paris), *Comptes rendus hebdomadaires des séances de l'Académie des Sciences*, no. vol. 8. Gauthier-Villars, 1839.

[40] HAAKE and O., "Uber die Ursachen electrischer Strome in Pflanzen," *Flora*, vol. 75, pp. 455–487, 1892.

[41] B. Klein, "Zur Frage über die elektrischen Ströme in Pflanzen," *Ber. Dtsch. Bot. Ges.*, vol. 16, no. 10, pp. 335–346, Jan. 1898.

[42] A. D. Waller, "An attempt to estimate the vitality of seeds by an electrical method," *Annals of Botany*. 1901.

[43] A. D. Waller, "On skin currents.—Part I. The frog's skin," *Proc. R. Soc. London*, vol. 68, pp. 480–494, 1901.

[44] M. Potter, "Electrical effects accompanying the decomposition of organic compounds," *Proc. R. Soc. London. Ser. B, ...*, 1911.

[45] S. Rachinski, A. Carubelli, A. P. Mangoni, and A. S. Mangrich, "Pilhas de combustíveis microbianas utilizadas na produção de eletricidade a partir de rejeitos orgânicos: Uma perspectiva de futuro," *Quim. Nova*, vol. 33, no. 8, pp. 1773–1778, 2010.

[46] B. Cohen, "The Bacterial Culture as an Electrical Half-Cell," *J. Bacteriol.*, vol. 21, no. 1, pp. 18–19, 1931.

[47] U. S. Canfield, J. H. (Magna Corp., Anaheim, CA, U. S. Goldner, B. H. (Magna Corp., Anaheim, CA, and U. S. Lutwack, R. (Magna Corp., Anaheim, CA, "Research on applied bioelectrochemistry First quarterly progress report, 14 Mar. - 30 Jun. 1963," California, 1963.

[48] Wired UK, "NASA Wants to Power Robots With Microbes," 2012.

[49] G. Rohrback, W. Scott, and J. Canfield, "Proceedings of the 15th Annual Power Sources Conference," *J. Electrochem. Soc.*, vol. 109, no. 2, p. 42C, 1962.

[50] M. DelDuca, J. Friscoe, and R. Zurilla, "Developments in Industrial Microbiology," *AIBS Bull.*, vol. 10, no. 6, p. 36, Dec. 1960.

[51] K. R. Williams and R. Koslow, "An Introduction to Fuel Cells," *J. Electrochem. Soc.*, vol. 113, no. 6, p. 139C, 1966.

[52] L. B. Wingard, C. H. Shaw, and J. F. Castner, “Bioelectrochemical fuel cells,” *Enzyme and Microbial Technology*. 1982.

[53] G. Davis, H. A. O. Hill, W. J. Aston, I. John Higgins, and A. P. F. Turner, “Bioelectrochemical fuel cell and sensor based on a quinoprotein, alcohol dehydrogenase,” *Enzyme Microb. Technol.*, 1983.

[54] A. P. F. Turner, W. J. Aston, and I. J. Higgins, “Applied aspects of bioelectrochemistry: Fuel cells, sensors, and bioorganic synthesis,” in *Biotechnology Bioengineering Symposium*, 1982.

[55] H. P. Bennetto and J. L. Stirling, “Reduction of ‘redox’ mediators by NADH and electron transduction in bioelectrochemical systems,” *Chem. Ind.*, 1985.

[56] H. P. Bennetto, G. M. Delaney, J. R. Mason, S. D. Roller, J. L. Stirling, and C. F. Thurston, “The sucrose fuel cell: Efficient biomass conversion using a microbial catalyst,” *Biotechnol. Lett.*, 1985.

[57] C. F. Thurston, H. P. Bennetto, and G. M. Delaney, “Glucose metabolism in a microbial fuel cell. Stoichiometry of product formation in a thionine-mediated Proteus vulgaris fuel cell and its relation to coulombic yields,” *J. Gen. Microbiol.*, 1985.

[58] I. Karube, T. Matsunaga, S. Tsuru, and S. Suzuki, “Biochemical fuel cell utilizing immobilized cells of clostridium butyricum,” *Biotechnol. Bioeng.*, vol. 19, no. 11, pp. 1727–1733, Nov. 1977.

[59] B. H. Kim and E. Al, “Patent: Mediator-less biofuel cell,” 1999.

[60] I. A. Ieropoulos, J. Greenman, C. Melhuish, and J. Hart, “Comparative study of three types of microbial fuel cell,” *Enzyme Microb. Technol.*, vol. 37, no. 2, pp. 238–245, Jul. 2005.

[61] B. Min, S. Cheng, and B. E. Logan, “Electricity generation using membrane and salt bridge microbial fuel cells,” *Water Res.*, 2005.

[62] B. Min and B. E. Logan, “Continuous electricity generation from domestic wastewater and organic substrates in a flat plate microbial fuel cell.,” *Environ. Sci. Technol.*, vol. 38, no. 21, pp. 5809–14, Nov. 2004.

[63] J. K. Jang *et al.*, “Construction and operation of a novel mediator- and membrane-less microbial fuel cell,” *Process Biochem.*, vol. 39, no. 8, pp. 1007–1012, Apr. 2004.

[64] P. Aelterman, K. Rabaey, and W. Verstraete, “Continuous Electricity Generation at High Voltages and Currents Using Stacked Microbial Fuel Cells,” vol. 40, no. 10, pp. 3388–3394, 2006.

[65] A. Fraiwan, S. Mukherjee, S. Sundermier, and S. Choi, “A microfabricated paper-based microbial fuel cell,” *Proc. IEEE Int. Conf. Micro Electro Mech. Syst.*, no. i, pp. 809–812, 2013.

[66] H. Bennetto, “Electricity generation by microorganisms,” *Biotechnol. Educ.*, 1990.

[67] D. Sell, P. Kramer, and G. Kreysa, “Use of an oxygen gas diffusion cathode and a three-dimensional packed bed anode in a bioelectrochemical fuel cell,” *Appl. Microbiol. Biotechnol.*, vol. 31, no. 2, pp. 211–213, Aug. 1989.

[68] S. You, Q. Zhao, J. Zhang, J. Jiang, and S. Zhao, “A microbial fuel cell using permanganate as the cathodic electron acceptor,” *J. Power Sources*, 2006.

[69] K. Rabaey, P. Clauwaert, P. Aelterman, and W. Verstraete, “Tubular microbial fuel cells for efficient electricity generation,” *Environ. Sci. Technol.*, 2005.

[70] B. E. Logan and J. M. Regan, “Microbial fuel cells-challenges and applications.,” *Environ. Sci. Technol.*, vol. 40, no. 17, pp. 5172–80, Sep. 2006.

[71] B. R. Ringeisen *et al.*, “High power density from a miniature microbial fuel cell using Shewanella oneidensis DSP10,” *Environ. Sci. Technol.*, 2006.

[72] P. M. D. Serra, A. Espírito-Santo, and M. Magrinho, “A steady-state electrical model of a microbial fuel cell through multiple-cycle polarization curves,” *Renew. Sustain. Energy Rev.*, 2020.

[73] S. Wu, W. He, W. Yang, Y. Ye, X. Huang, and B. E. Logan, “Combined carbon mesh and small graphite fiber brush anodes to enhance and stabilize power generation in microbial fuel cells treating domestic wastewater,” *J. Power Sources*, vol. 356, pp. 348–355, 2017.

[74] V. Lanas, Y. Ahn, and B. E. Logan, “Effects of carbon brush anode size and loading on microbial fuel cell performance in batch and continuous mode,” *J. Power Sources*, vol. 247, pp. 228–234, 2014.

[75] V. Lanas and B. E. Logan, “Evaluation of multi-brush anode systems in microbial fuel cells.,” *Bioresour. Technol.*, vol. 148, pp. 379–85, Nov. 2013.

[76] V. R. Nimje *et al.*, “A single-chamber microbial fuel cell without an air cathode,” *Int. J. Mol. Sci.*, vol. 13, no. 3, pp. 3933–3948, 2012.

[77] W. Yang and B. E. Logan, “Engineering a membrane based air cathode for microbial fuel cells via hot pressing and using multi-catalyst layer stacking,” *Environ. Sci. Water Res. Technol.*, vol. 2, no. 5, pp. 858–863, 2016.

[78] S. Kazemi, M. Mohseni, and K. Fatih, “A systematic study of separators in air-breathing flat-plate microbial fuel cells-Part 1: Structure, properties, and performance correlations,” *Energies*, vol. 9, no. 2, pp. 1–18, 2016.

[79] M. Di Lorenzo, A. R. Thomson, K. Schneider, P. J. Cameron, and I. Ieropoulos, “A small-scale air-cathode microbial fuel cell for on-line monitoring of water quality,” *Biosens. Bioelectron.*, vol. 62, pp. 182–188, 2014.

[80] I. Ieropoulos, J. Greenman, C. Melhuish, and I. Horsfield, “EcoBot-III: a robot with guts,” in *Artificial Life XII: Proceedings of the 12th International Conference on the Synthesis and Simulation of Living Systems, ALIFE 2010*, 2010, pp. 733–740.

[81] Y. Ahn and B. E. Logan, “A multi-electrode continuous flow microbial fuel cell with separator electrode assembly design,” *Appl. Microbiol. Biotechnol.*, vol. 93, no. 5, pp. 2241–2248, 2012.

[82] W. He, X. Zhang, J. Liu, X. Zhu, Y. Feng, and B. E. Logan, “Microbial fuel cells with an integrated spacer and separate anode and cathode modules,” *Environ. Sci. Water Res. Technol.*, vol. 2, no. 1, pp. 186–195, 2016.

[83] W. He *et al.*, “Pressurized air cathodes for enhanced stability and power generation by microbial fuel cells,” *J. Power Sources*, vol. 332, no. 73, pp. 447–453, 2016.

[84] K. Rabaey and W. Verstraete, “Microbial fuel cells: novel biotechnology for energy generation,” *TRENDS Biotechnol.*, 2005.

[85] J. J. Krol, “Monopolar and bipolar ion exchange membranes,” *Membr. Technol. Gr.*, p. 165, 1997.

[86] H. Rismani-Yazdi, S. M. Carver, A. D. Christy, and O. H. Tuovinen, “Cathodic limitations in microbial fuel cells: An overview,” *J. Power Sources*, vol. 180, no. 2, pp. 683–694, 2008.

[87] G. Hernández-Flores *et al.*, “Characteristics of a single chamber microbial fuel cell equipped with a low cost membrane,” *Int. J. Hydrogen Energy*, vol. 40, no. 48, pp. 17380–17387, 2015.

[88] F. Zhao, R. C. T. Slade, and J. R. Varcoe, “Techniques for the study and development of microbial fuel cells: an electrochemical perspective,” *Chem. Soc. Rev.*, vol. 38, no. 7, p. 1926, Jul. 2009.

[89] J. X. Leong, W. R. W. Daud, M. Ghasemi, K. Ben Liew, and M. Ismail, “Ion exchange membranes as separators in microbial fuel cells for bioenergy conversion: A comprehensive review,” *Renew. Sustain. Energy Rev.*, vol. 28, pp. 575–587, Dec. 2013.

[90] O. Rubaba *et al.*, "Performance comparison of microbial fuel cells equipped with different membrane electrode assemblies," *J. Phys. Conf. Ser.*, vol. 433, no. 1, p. 012022, Apr. 2013.

[91] J. R. Kim, S. Cheng, S.-E. Oh, and B. E. Logan, "Power Generation Using Different Cation, Anion, and Ultrafiltration Membranes in Microbial Fuel Cells," *Environ. Sci. Technol.*, vol. 41, no. 3, pp. 1004–1009, Feb. 2007.

[92] G. Zhang, Q. Zhao, Y. Jiao, K. Wang, D. Lee, and N. Ren, "Efficient electricity generation from sewage sludge using biocathode microbial fuel cell," *Water Res.*, vol. 46, no. 1, pp. 43–52, 2011.

[93] S. J. Peighambardoust, S. Rowshanzamir, and M. Amjadi, "Review of the proton exchange membranes for fuel cell applications," *Int. J. Hydrogen Energy*, vol. 35, no. 17, pp. 9349–9384, Sep. 2010.

[94] S. Yao, Y.-L. He, Y.-S. Li, and H. Xi, "Effect of the Membrane Electrode Assemble Design on the Performance of Single Chamber Microbial Fuel Cells," *Energy Procedia*, vol. 61, pp. 1947–1951, 2014.

[95] G. K. S. Prakash, F. A. Viva, O. Bretschger, B. Yang, M. El-Naggar, and K. Nealson, "Inoculation procedures and characterization of membrane electrode assemblies for microbial fuel cells," *J. Power Sources*, vol. 195, no. 1, pp. 111–117, 2010.

[96] J. Wei, P. Liang, and X. Huang, "Recent progress in electrodes for microbial fuel cells," *Bioresour. Technol.*, vol. 102, no. 20, pp. 9335–9344, Oct. 2011.

[97] Y. Fan, H. Hu, and H. Liu, "Enhanced Coulombic efficiency and power density of air-cathode microbial fuel cells with an improved cell configuration," *J. Power Sources*, vol. 171, no. 2, pp. 348–354, 2007.

[98] M. Zhou, M. Chi, J. Luo, H. He, and T. Jin, "An overview of electrode materials in microbial fuel cells," *J. Power Sources*, vol. 196, no. 10, pp. 4427–4435, 2011.

[99] Y. Zhang *et al.*, "A graphene modified anode to improve the performance of microbial fuel cells," *J. Power Sources*, vol. 196, no. 13, pp. 5402–5407, 2011.

[100] R. M. Allen and H. P. Bennetto, "Microbial fuel-cells," *Appl. Biochem. Biotechnol.*, vol. 39–40, no. 1, pp. 27–40, Sep. 1993.

[101] M. J. Cooney, E. Roschi, I. W. Marison, C. Comninellis, and U. Von Stockar, "Physiologic studies with the sulfate-reducing bacterium Desulfovibrio desulfuricans: Evaluation for use in a biofuel cell," *Enzyme Microb. Technol.*, vol. 18, no. 5, pp. 358–365, Apr. 1996.

[102] N. Kim, Y. Choi, S. Jung, and S. Kim, “Development of microbial fuel cells using Proteus Vulgaris,” *Bull. Chem. Soc.*, vol. 21, no. 1, pp. 44–48, 2000.

[103] S. K. Chaudhuri and D. R. Lovley, “Electricity generation by direct oxidation of glucose in mediatorless microbial fuel cells,” *Nat. Biotechnol.*, vol. 21, p. 1229, Sep. 2003.

[104] D. H. Park and J. G. Zeikus, “Electricity generation in microbial fuel cells using neutral red as an electronophore.,” *Appl. Environ. Microbiol.*, vol. 66, no. 4, pp. 1292–7, Apr. 2000.

[105] K. Rabaey, G. Lissens, S. D. Siciliano, and W. Verstraete, “A microbial fuel cell capable of converting glucose to electricity at high rate and efficiency,” *Biotechnol. Lett.*, vol. 25, no. 18, pp. 1531–1535, 2003.

[106] U. Schröder, J. Nießen, F. Scholz, J. Niessen, and F. Scholz, “A Generation of Microbial Fuel Cells with Current Outputs Boosted by More Than One Order of Magnitude,” *Angew. Chem. Int. Ed. Engl.*, vol. 42, no. 25, pp. 2880–2883, Jun. 2003.

[107] V. Watson and G. Estadt, “Graphite Fiber Brush Anodes for Increased Power Production in Air-Cathode Microbial Fuel Cells,” vol. 41, no. 9, pp. 3341–3346, 2007.

[108] P. Pérez-Rodríguez, V. M. Ovando-Medina, S. Y. Martínez-Amador, and J. A. Rodríguez-de la Garza, “Bioanode of polyurethane/graphite/polypyrrole composite in microbial fuel cells,” *Biotechnol. Bioprocess Eng.*, vol. 21, no. 2, pp. 305–313, 2016.

[109] T. H. Pham, P. Aelterman, and W. Verstraete, “Bioanode performance in bioelectrochemical systems: recent improvements and prospects,” *Trends Biotechnol.*, vol. 27, no. 3, pp. 168–178, 2009.

[110] Y. Yuan and S.-H. Kim, “Improved performance of a microbial fuel cell with polypyrrole/carbon black composite coated carbon paper anodes,” *Bull. Korean Chem. Soc.*, vol. 29, no. 7, pp. 1344–1348, 2008.

[111] Y. Yuan, S. Zhou, Y. Liu, and J. Tang, “Nanostructured macroporous bioanode based on polyaniline-modified natural loofah sponge for high-performance microbial fuel cells,” *Environ. Sci. Technol.*, vol. 47, no. 24, pp. 14525–14532, 2013.

[112] W. Yang, W. He, F. Zhang, M. A. Hickner, and B. E. Logan, “Single-Step Fabrication Using a Phase Inversion Method of Poly(vinylidene fluoride) (PVDF) Activated Carbon Air Cathodes for Microbial Fuel Cells,” *Environ. Sci. Technol. Lett.*, vol. 1, no. 10, pp. 416–420, 2014.

[113] Q. Yang, S. Liang, J. Liu, J. Lv, and Y. Feng, “Analysis of Anodes of Microbial Fuel Cells When Carbon Brushes Are Preheated at Different Temperatures,” *Catalysts*, vol. 7, no. 11, p. 312, 2017.

[114] X. Zhang, H. Ren, S. Pyo, J.-I. Lee, J. Kim, and J. Chae, “A High-Efficiency DC-DC Boost Converter for a Miniaturized Microbial Fuel Cell,” *IEEE Trans. Power Electron.*, vol. 30, no. 4, pp. 2041–2049, 2015.

[115] Z. Wang, G. D. Mahadevan, Y. Wu, and F. Zhao, “Progress of air-breathing cathode in microbial fuel cells,” *J. Power Sources*, vol. 356, pp. 245–255, 2017.

[116] Z. He and L. T. Angenent, “Application of bacterial biocathodes in microbial fuel cells,” *Electroanalysis*, vol. 18, no. 19–20, pp. 2009–2015, 2006.

[117] I. Merino-Jimenez, C. Santoro, S. Rojas-Carbonell, J. Greenman, I. Ieropoulos, and P. Atanassov, “Carbon-Based Air-Breathing Cathodes for Microbial Fuel Cells,” *Catalysts*, vol. 6, no. 9, p. 127, 2016.

[118] N. Kim, Y. Choi, S. Jung, and S. Kim, “Effect of initial carbon sources on the performance of microbial fuel cells containing Proteus vulgaris,” *Biotechnol. Bioeng.*, vol. 70, no. 1, pp. 109–114, 2000.

[119] S. Cheng and B. E. Logan, “Increasing power generation for scaling up single-chamber air cathode microbial fuel cells,” *Bioresour. Technol.*, vol. 102, no. 6, pp. 4468–4473, 2011.

[120] B. Erable, D. Féron, and A. Bergel, “Microbial catalysis of the oxygen reduction reaction for microbial fuel cells: A review,” *ChemSusChem*, vol. 5, no. 6, pp. 975–987, 2012.

[121] X. Zhang *et al.*, “High-Performance Carbon Aerogel Air Cathodes for Microbial Fuel Cells,” *ChemSusChem*, vol. 9, no. 19, pp. 2788–2795, 2016.

[122] X. Zhang, X. Xia, I. Ivanov, X. Huang, and B. E. Logan, “Enhanced Activated Carbon Cathode Performance for Microbial Fuel Cell by Blending Carbon Black,” *Environ. Sci. Technol.*, vol. 48, no. 3, pp. 2075–2081, Feb. 2014.

[123] R. Rossi, W. Yang, E. Zikmund, D. Pant, and B. E. Logan, “In situ biofilm removal from air cathodes in microbial fuel cells treating domestic wastewater,” *Bioresour. Technol.*, vol. 265, no. May, pp. 200–206, 2018.

[124] G. Pasternak, J. Greenman, and I. Ieropoulos, “Regeneration of the power performance of cathodes affected by biofouling,” *Appl. Energy*, 2016.

[125] M. T. Noori, S. C. Jain, M. M. Ghangrekar, and C. K. Mukherjee, “Biofouling inhibition and enhancing performance of microbial fuel cell using silver nano-particles as fungicide and cathode catalyst,” *Bioresour. Technol.*, 2016.

[126] D. Li, J. Liu, Y. Qu, H. Wang, and Y. Feng, “Analysis of the effect of biofouling distribution on electricity output in microbial fuel cells,” *RSC Adv.*, 2016.

[127] D. Pant, G. Van Bogaert, L. Diels, and K. Vanbroekhoven, “A review of the substrates used in microbial fuel cells (MFCs) for sustainable energy production,” *Bioresour. Technol.*, vol. 101, no. 6, pp. 1533–1543, Mar. 2010.

[128] M. A. Rodrigo, P. Cañizares, H. García, J. J. Linares, and J. Lobato, “Study of the acclimation stage and of the effect of the biodegradability on the performance of a microbial fuel cell.,” *Bioresour. Technol.*, vol. 100, no. 20, pp. 4704–10, Oct. 2009.

[129] S. Cheng, H. Liu, and B. E. Logan, “Increased power generation in a continuous flow MFC with advective flow through the porous anode and reduced electrode spacing,” *Environ. Sci. Technol.*, vol. 40, no. 7, pp. 2426–2432, 2006.

[130] F. Vicari *et al.*, “Influence of the methodology of inoculation in the performance of air-breathing microbial fuel cells,” *J. Electroanal. Chem.*, vol. 803, no. September, pp. 81–88, 2017.

[131] S. Cheng and B. E. Logan, “Ammonia treatment of carbon cloth anodes to enhance power generation of microbial fuel cells,” *Electrochem. commun.*, vol. 9, no. 3, pp. 492–496, 2007.

[132] A. J. Hutchinson, J. C. Tokash, and B. E. Logan, “Analysis of carbon fiber brush loading in anodes on startup and performance of microbial fuel cells,” *J. Power Sources*, vol. 196, no. 22, pp. 9213–9219, 2011.

[133] Y. Ahn and B. E. Logan, “Domestic wastewater treatment using multi-electrode continuous flow MFCs with a separator electrode assembly design.,” *Appl. Microbiol. Biotechnol.*, vol. 97, no. 1, pp. 409–16, Jan. 2013.

[134] Y. Feng, X. Wang, B. E. Logan, and H. Lee, “Brewery wastewater treatment using air-cathode microbial fuel cells,” *Appl. Microbiol. Biotechnol.*, vol. 78, no. 5, pp. 873–880, 2008.

[135] F. Vicari, M. Albamonte, A. Galia, and O. Scialdone, “Effect of mode of operation, substrate and final electron acceptor on single-chamber membraneless microbial fuel cell operating with a mixed community,” *J. Electroanal. Chem.*, 2018.

[136] S. B. Pasupuleti, S. Srikanth, S. Venkata Mohan, and D. Pant, “Continuous mode operation of microbial fuel cell (MFC) stack with dual gas diffusion cathode design for the treatment of dark fermentation effluent,” *Int. J. Hydrogen Energy*, 2015.

[137] S. Sevda *et al.*, “Shift to continuous operation of an air-cathode microbial fuel cell long-running in fed-batch mode boosts power generation,” *Int. J. Green Energy*, 2016.

[138] L. Huang and B. E. Logan, “Electricity production from xylose in fed-batch and continuous-flow microbial fuel cells,” *Appl. Microbiol. Biotechnol.*, 2008.

[139] K. Todar, “Online Textbook of Bacteriology,” 2008. [Online]. Available: http://textbookofbacteriology.net/index.html. [Accessed: 01-Jan-2013].

[140] S. Cooper, “Bacterial Growth,” in *Bacterial Growth and Division*, Elsevier, 1991, pp. 7–17.

[141] R. E. Buchanan, “Life Phases in a Bacterial Culture,” *J. Infect. Dis.*, vol. 23, no. 2, pp. 109–125, Aug. 1918.

[142] A. Vogl, F. Bischof, and M. Wichern, “Surface-to-surface biofilm transfer: A quick and reliable startup strategy for mixed culture microbial fuel cells,” *Water Sci. Technol.*, vol. 73, no. 8, pp. 1769–1776, 2016.

[143] X. Zhang, D. Pant, F. Zhang, J. Liu, W. He, and B. E. Logan, “Long-Term Performance of Chemically and Physically Modified Activated Carbons in Air Cathodes of Microbial Fuel Cells,” *ChemElectroChem*, 2014.

[144] E. Zhang, F. Wang, Q. Yu, K. Scott, X. Wang, and G. Diao, “Durability and regeneration of activated carbon air-cathodes in long-term operated microbial fuel cells,” *J. Power Sources*, 2017.

[145] R. Kumar, L. Singh, and A. W. Zularisam, “Exoelectrogens: Recent advances in molecular drivers involved in extracellular electron transfer and strategies used to improve it for microbial fuel cell applications,” *Renew. Sustain. Energy Rev.*, vol. 56, no. May 2018, pp. 1322–1336, 2016.

[146] P. Bond, S. T. Read, P. Dutta, P. L. Bond, J. Keller, and K. Rabaey, “Initial development and structure of biofilms on microbial fuel cell anodes Initial development and structure of biofilms on microbial fuel cell anodes,” no. May 2014, 2018.

[147] J. Do Park, T. M. Roane, Z. J. Ren, and M. Alaraj, “Dynamic modeling of a microbial fuel cell considering anodic electron flow and electrical charge storage,” *Appl. Energy*, vol. 193, pp. 507–514, 2017.

[148] P. S. Bonanni, G. D. Schrott, L. Robuschi, and J. P. Busalmen, “Charge accumulation and electron transfer kinetics in Geobacter sulfurreducens biofilms,” *Energy Environ. Sci.*, vol. 5, no. 3, pp. 6188–6195, 2012.

[149] Y. Cao *et al.*, “Electricigens in the anode of microbial fuel cells: Pure cultures versus mixed communities,” *Microb. Cell Fact.*, vol. 18, no. 1, pp. 1–14, 2019.

[150] A. Kumar *et al.*, “The ins and outs of microorganism-electrode electron transfer reactions,” *Nat. Rev. Chem.*, vol. 1, pp. 1–13, 2017.

[151] B. Erable, M. A. Roncato, W. Achouak, and A. Bergel, “Sampling natural biofilms: A new route to build efficient microbial anodes,” *Environ. Sci. Technol.*, vol. 43, no. 9, pp. 3194–3199, 2009.

[152] G. D. Schrott, P. S. Bonanni, L. Robuschi, A. Esteve-Nuñez, and J. P. Busalmen, “Electrochemical insight into the mechanism of electron transport in biofilms of Geobacter sulfurreducens,” *Electrochim. Acta*, vol. 56, no. 28, pp. 10791–10795, 2011.

Chapter 3

Energy harvesting and power management

Energy supply and environmental concerns have steered scientific research into fields of innovation and resource maximization. Efficiency is the word of the century. To optimize processes, materials and methods, process monitoring is of the greatest importance. The instrumentation field plays a major role in this objective since it allows the observation of intrinsic phenomena otherwise unmeasurable. Aside from their use in laboratory experiments, instrumentation devices are also needed in real world applications: in health, industry, sports or even for domestic use. Instrumentation devices allow us to keep track of changes and analyze data. As with any other electric device, instrumentation modules require power. And power availability ultimately limits their real-world applications: a sensor's usefulness is very limited if it needs a connection to the main power grid or if it is powered by a battery, running only for a couple of hours. Versatility and reliability are among the main concerns while developing any electrical device, instrumentation included, irrespective of its application area. If power sources are as readily available as the physical or chemical properties that need measuring, then a high control degree is attainable. Harvesting energy from the environment can help overcome such a challenge, provided adequate transducers are used, by removing the need for wires and increasing the service life of a device. Even though wires are cheap and reliable, imposing near to none energy constraints and being quite shielded to interferences and being extremely fast and secure, they are also a weakness due to being susceptible to moisture and dust, limiting both the portability and versatility of devices [1]–[3]. By removing wires, physical constraints are dramatically reduced, becoming a key aspect only on environments with high interference noise and for circumstances where the technology limits (for instance, range) have been achieved. Besides this, wireless methods are extremely convenient, either financially either regarding their integrity and interoperability [1]–[3]. Wireless technologies tended to use significant power and specific equipment, hindering their mass use. Nowadays, the overall power consumption of circuits has had a sharp drop, making it possible to incorporate this technology in sensors for several areas [2], [3].

The energy requirements are, indeed, the reason why this technology still hasn't the same importance and reliability as its wired counterpart. The increased interest in the development of sensor networks is a significant motivation for advances in this technology, irrespective of their application.

Some bibliographic records point to 74% of all the consumed power of a sensor node being directed at the transceiver module [1]. Given this, one of three challenges can be tackled: to decrease the power consumption of this module; to increase the effective rate of transmitted data,

decreasing the time for which the module has to be turned on; or to come up with sustainable energy alternatives that can account for all the power needs of these circuits [3].

Energy harvesting can do just that. Energy harvesting, power harvesting or even energy scavenging, is a suitable solution for powering remote devices where no conventional power source is available. It has been around for centuries and windmills and watermills are the most evident examples. Though, at the time, the produced energy couldn't be measured, it was, nevertheless directly applied to milling. Nowadays, the most common examples for energy harvesting are wind turbines, hydro-electric generators and solar panels. For wireless instrumentation systems, power requirements aren't high. For most common remote sensors, power in the range of milliwatts is enough [4]. In fact, for ultralow-power sensors, power between 10 and 100 μW will suffice [5]. Though energy harvested from electrochemical (such as microbial fuel cells), mechanical (wind and hydroelectric energy), photovoltaic (solar cells), thermoelectric, electromechanical (piezoelectric energy) and electromagnetic (ambient radio frequency, RF) sources is virtually inexhaustible and with no or little adverse environmental effects, it is also unregulated, intermittent and small. So, strategies like the use of optimized switched power supplies and the usage of more than one power converter circuit are usually applied [4], [5]. These methods are implemented by the power management system (PMS): it manages the harvested energy, amasses it in a proper storage medium and, when requested, delivers the needed power to all the other system's components, efficiently controlling its distribution and usage [5]. In a sensor system, for instance, the typical elements of a PMS are [5]:

1. Power Management Controller: A low power microcontroller or microprocessor that manages and distributes the harvested energy;
2. POR-PG (Power-on-reset pulse generator): Does the initialization of the sensor node. Only works at startup and consumes virtually no power in any other circumstance;
3. Bandgap reference: Fed by the electric power converter, this element provides a reference for voltage and current that is independent of external conditions (like temperature). This way, the sensor node always has a stable reference to work with;
4. Oscillator and timer: together, this group is used for duty cycled operations, giving the power management controller unit tools to implement power management strategies (like selectively powering on or off specific system elements);
5. Sensor interface: Acquires the data needed to, besides the application objectives, activate and manage the watchdog (malfunction timer) and trigger group;
6. Current-Voltage-Power Conditioner (IVP): Implements the maximum power point tracking (MPPT, technology below summarily approached) algorithm by working together with the sensors, the power management controller and converters. Although not mandatory, it is most frequently found in photovoltaic systems;
7. Electric power converter: Energy converter circuit that can take a DC or AC unregulated source and convert it to a regulated, amplified or cut, DC or AC signal. More than one of these devices can be in a single system. Other examples are charge pumps;

8. Nonvolatile (NV) memory unit (like RAM) to store the information needed to configure the PMS and MPPT algorithms;
9. Communication port: uploads or downloads information.

Figure 3.1 represents each of these elements and their interconnectivity.

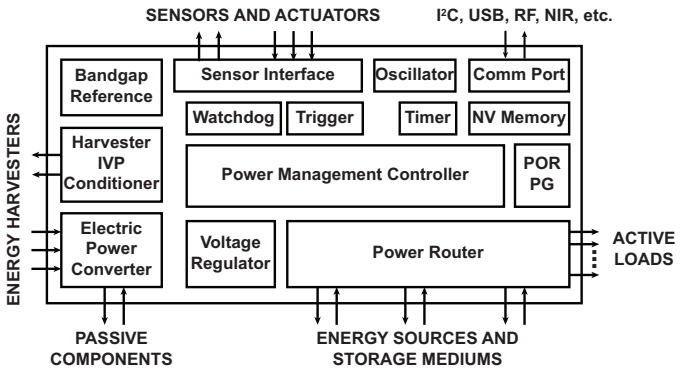

Figure 3.1 - Typical elements of a power management system (PMS) and their interconnectivity [5].

Making a smart management of energy resources is a key effort in efficiently using harvested energy. Configuring how the PMS works, after acquiring and regulating the harnessed power, is mandatory. Two main strategies are the usual choices for the PMS functioning: duty cycling or adaptive sensing. For duty cycling, the system wakes up in a periodic fashion, does its task and goes back to sleep mode. In adaptive sensing, conditions are dynamically monitored (watchdog and trigger) and the sensor wakes up when certain criteria are met. As described before, in duty cycling, the system does its task and goes back to sleep. The time for each task is managed by the oscillator and timer group.

Figure 3.2 shows the relationship of power consumption and time in a low power system [5].

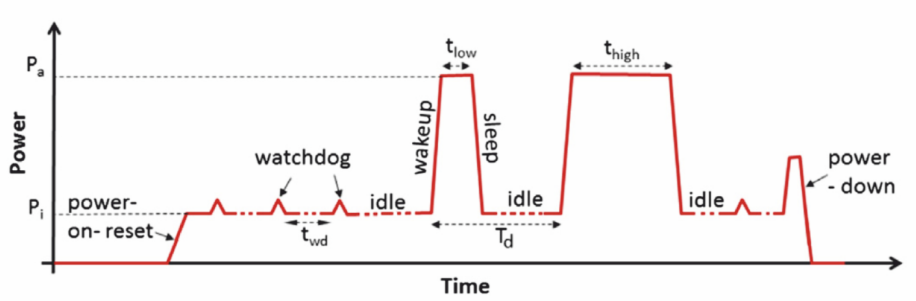

Figure 3.2 - Graphical representation of different power consumption cycles [5].

The system is initially off. When powered on, the POR-NG unit is activated and the power management unit (PMU) is initialized and set up (Power-on Reset). According to its configuration, the system can enter one of the two PMS strategies of duty cycling or adaptive sensing. If on adaptive sensing, then some power spikes will appear on the graph: these correspond to the moments when the watchdog is activated (increasing power consumption). If,

on the other hand, the sensor works with duty cycling, then no watchdog spikes will be noticeable (and, when design choices are previously made so as to make the system follow this approach, the watchdog element may even be discarded and the trigger component will suffice). The PMU will be spending enough power to not lose its configurations (P_i) but will only wake up when a specific amount of time has passed. After waking up, the PMU activates the sensor: if the task is complex, then the wake-up time, and power consumption (P_a) will be bigger (t_{high}); if not, then it'll be lower (t_{low}). The amount of time between the sensor wake up, task performance, sleep and next event is represented by T_d on the graph [5].

One last analysis is missing: the actual conditioning of the harvesting process. That process may, or may not, happen at the maximum energy production point. There are instances where harvesting energy at the maximum power point decreases the lifetime of the power source (in MFCs, for instance, this occurs due to substrate depletion) and cases where harvesting energy at operation points different of the maximum power lead to the same result of decreased time of operation or negligible power levels (microbial fuel cells operating in batch mode close to its short-circuit current also quickly deplete substrate but at low power). With photovoltaic systems, for example, operation at the maximum power point is desirable since the system's IV characteristic presents a clear maximum, irrespective of the operation conditions. Moreover, the solar energy is stored in large capacitors and its use can be required at any time, even when the device is offline. Bioelectrochemical systems, however, show a different electrical behavior for different operation conditions and may produce increased energy if operated outside of the maximum operation point, in a balanced setting between time and load (dynamic response).

The maximum power point approach is a traditional solution for photovoltaic systems and, in this work, will be used as the benchmark for determining the best approach to retrieve maximum energy from microbial fuel cells. In fact, the MFC maximum power production capability is a standard parameter for energy studies.

Maximum power point theorem

The efficiency of a system is a measure of how well the output reflects the input. Computed by the ratio between two equal parameters – one referring to the input, another to the output -, its value can be anywhere between 0 and 1 (or, more commonly, 0 and 100 %). Since there is still no way to remove every system losses', an efficiency of 100 % is still not realistic. So, in order to achieve higher efficiencies, every other parameter of the system has to be improved. Let's consider an electrical system, simplified to its Thévenin equivalent, as in Figure 3.3.

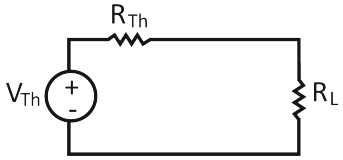

Figure 3.3 - Thévenin equivalent circuit with a resistive load (R_L).

Considering the system's losses have been optimized to the fullest, the efficiency of the system can be expressed by:

$$P_{eff} = \frac{P_{Out}}{P_{Total}} = \frac{i^2 R_L}{i^2 R_L + i^2 R_{Th}} = \frac{\left(\frac{V_{Th}}{R_{Th}+R_L}\right)^2 R_L}{\left(\frac{V_{Th}}{R_{Th}+R_L}\right)^2 R_L + \left(\frac{V_{Th}}{R_{Th}+R_L}\right)^2 R_{Th}} = \frac{R_L}{R_L + R_{Th}} \quad (3.1)$$

According to the ratio above, efficiency increases with the increase of R_L values relatively to those of R_{Th}. That difference would, however, limit the power actually delivered to the load. Proper dimensioning of the resistive load value will guarantee that P_{Out} is maximized:

$$P_{R_L} = i^2 R_L = \left(\frac{V_{Th}}{R_{Th}+R_L}\right) \cdot R_L \quad (3.2)$$

Since V_{Th} and R_{Th} are fixed, the power will ultimately be determined by R_L:

$$\frac{dP}{dR_L} = V_{Th}\left(\frac{(R_{Th}+R_L)^2 - 2 \cdot R_L(R_{Th}+R_L)}{(R_{Th}+R_L)^4}\right) \quad (3.3)$$

Power is maximized for:

$$\frac{dP}{dR_L} = 0 \Leftrightarrow (R_{Th}+R_L)^2 = 2 \cdot R_L(R_{Th}+R_L) \Leftrightarrow R_L = R_{Th} \xrightarrow[\left(\frac{V_{Th}}{R_{Th}+R_L}\right)\cdot R_L]{} P_{R_L} = \frac{V_{Th}^2}{4R_L} \quad (3.4)$$

With $R_L = R_{Th}$, $P_{eff} = 50$ %. So, in order to achieve the maximum power transfer between source and load, the efficiency of the system has to be of 50 % [6], [7], which corresponds to when the internal impedance of an energy harvesting device equals its load impedance. An IV curve of a photovoltaic system, in Figure 3.4, is presented to aid in this representation.

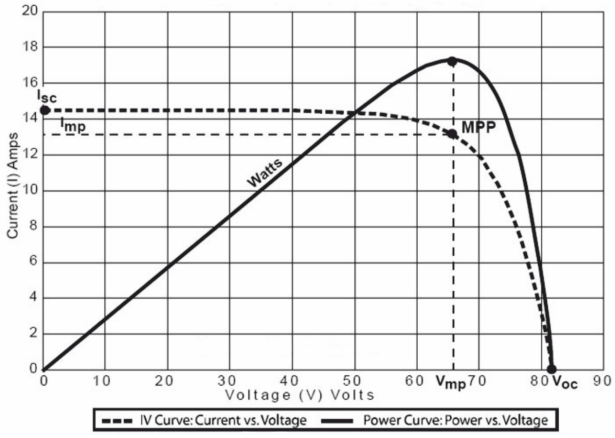

Figure 3.4 - Maximum power point (MPP). I_{SC} corresponds to the short circuit current, V_{OC} to the open circuit voltage and I_{mp} and V_{mp}, respectively, to the current and voltage on the maximum power point.

A starting point: photovoltaic systems

Photovoltaic systems are subjected to varying conditions throughout the day: from sunrise to sundown, the irradiance and temperature levels of the photovoltaic panels change, which contributes to operations outside the of MPP [8], [9]. Since PV systems have a limited lifespan and high initial cost (not only with the panel itself but also with the energy conditioning equipment), retrieving the maximum amount of power for as long as possible reduces the net cost of the system [10], [11]. For this, two solutions can be implemented: mechanical tracking of the sun and electrical tracking of the maximum power point. Mechanical tracking of the sun has a limited use because it is only useful for good irradiance conditions. For itself, this solution can't get the system to operate at the best possible efficiency. Electrical tracking, achievable with a power conditioning stage, can adapt to different environmental conditions, improving the system's versatility [10]. Electrical tracking corresponds to the application of maximum power point tracking algorithms.

To find the maximum power point (MPP) for a PV cell, without an algorithm, elaborate mathematical computations are needed and the solution has to be found with the help of numerical methods. If we start with a theoretical model of a PV cell, the IV behavior is given by [12]:

$$I = n_P \left[I_L - I_s \left(e^{q\left(\frac{V}{n_S} + \frac{IR_S}{n_P}\right)/A \cdot K \cdot T} - 1 \right) - \frac{\frac{V}{n_S} + \frac{I \cdot R_S}{n_P}}{R_P} \right] \tag{3.5}$$

And power by:

$$P = V \cdot n_P \left[I_L - I_s \left(e^{q\left(\frac{V}{n_S} + \frac{IR_S}{n_P}\right)/A \cdot K \cdot T} - 1 \right) - \frac{\frac{V}{n_S} + \frac{P \cdot R_S}{V \cdot n_P}}{R_P} \right] \tag{3.6}$$

If we intend to maximize the above parameter:

$$\frac{dP}{dV} = 0 \tag{3.7}$$

Just by direct observation, the complexity of the above equations becomes clear. So, and in order to have a way to effectively apply the theorem to real systems, simplified models have been developed. To date, three models have been presented: a generic model, with a single diode, and two resistors (one in series and the other a shunt); the two diodes model, more accurate than the generic model but needing more parameters to compute; and the simplified model, which is in fact the two diodes model but with fewer parameters to compute [11], [13]–[16].

According to the simplified model, pictured in Figure 3.5, the IV characteristic of a PV cell can be described by:

$$I_{PV} = I_{Ph} - I_0\left(e^{V_{PV}/V_{TA}} - 1\right) : \; I_{Ph} = \lambda \cdot \left(I_{SC} + K_1(T - T_{Ref})\right) \tag{3.8}$$

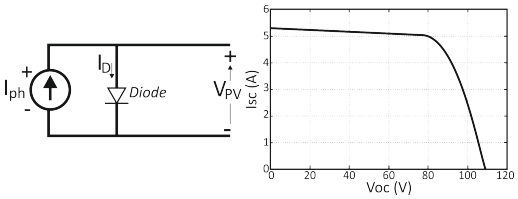

Figure 3.5 - At left: the simplified model of a PV cell; at right: characteristic I-V curve.

Where:

I_0 ≡ cell's saturation of dark current;

T ≡ temperature of the p-n junction in Kelvin;

I_{SC} ≡ cell's short-circuit current at standard test condition (1000 W/m^2 and 25 $ºC$);

K_1 ≡ coefficient of the cell's short-circuit current;

T_{Ref} ≡ cell's reference temperature;

λ ≡ solar irradiance in W/m^2.

With these simplifications, applying maximum power point tracking (MPPT) algorithms is faster and more efficient [11].

Maximum power point tracking algorithms for PV systems

Generally, MPPT algorithms can be grouped into three categories: offline, online and hybrid methods. Offline methods – model based – need a control signal like an open circuit voltage (OCV) or a short circuit current (ISC) to drive the operation to its maximum power point. Examples of these methods are: open circuit voltage (OCV), short circuit current (SCC) and artificial intelligence. The control signal of online methods – model-free – is an instantaneous value read from the device's operation. This control signal is applied with a small and predicted perturbation and the operation of the device is modified with it: if the perturbation leads to a positive power increase, then perturbations in the same directions are applied. If not, then those perturbations will be made in the opposite direction. The online methods involve small variations around the optimum value and can be: perturbation and observe methods (P&O), extremum seeking control methods (ESC) or incremental conductance methods (IncCon). Hybrid methods, as the name implies, use both offline and online strategies in two steps: firstly, offline methods are used to place the operating point of the energy harvesting device near its MPP. Then, the fine-tuning step is made using online methods [1, 2].

The energy levels produced by PV cells or arrays are not constant and have a fluctuant nature. Even though applying MPPT algorithms makes the system work at maximum power, that point changes with environmental conditions. In order for a battery to be charged, or to deliver the power to the power grid, power conditioning stages are essential [17]. They are responsible for stepping voltage up or down (boost or buck converter), creating AC or DC signals as the final application requires. It is also through them that MPPT algorithms are applied.

DC/DC converters are the main element in the power conditioning stage. They may be followed by DC/AC converters if power is to be delivered to the grid. For MPPT applications, a MPPT controller is applied to the converter. It's inputs are collected from the PV cell/array and the controller acts on the converter which influences the cell's/array's operating point (Figure 3.6) [12], [17]–[25].

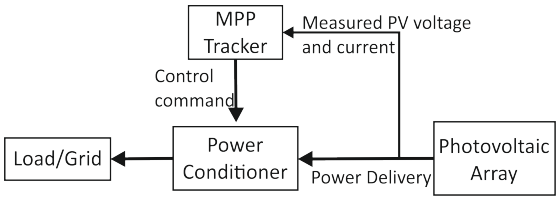

Figure 3.6 - Block diagram for a typical topology in PV systems.

DC/DC converters take a fluctuating, non-periodical, PV output voltage and, due to the relationship between its conducting (ON) and non-conducting (OFF) regimes – duty ratio – output an averaged voltage. This technique is called pulse width modulation (PWM). Duty ratio, D, is set by the commutation frequency of the transistor in the converter and ultimately leads to new operating points of the system. The DC/DC converter duty ratio is responsible for impedance matching and, therefore, working in the MPP [6], [12], [18], [21], [26]–[31].

There are three major DC/DC converter configurations: the buck converter, the boost converter and the buck-boost converter. All three configurations are shown in Figure 3.7.

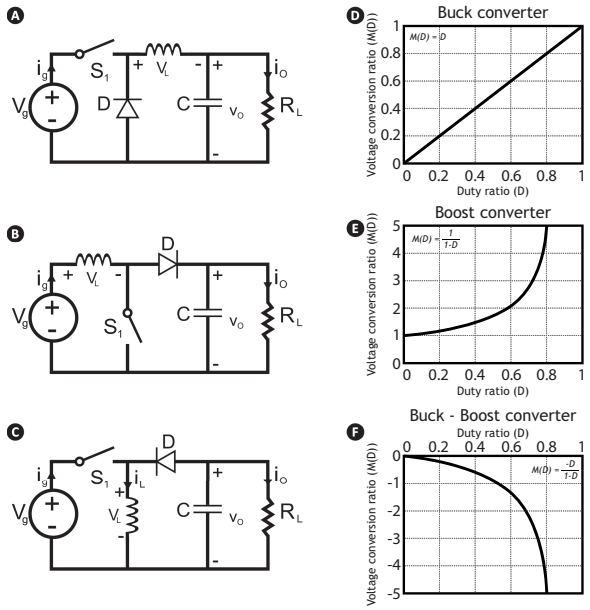

Figure 3.7 - DC/DC converter topologies: a) buck converter; b) boost converter; c) buck-boost converter. Each plot (from d) to f)) represents the voltage conversion ratio (M(D)) vs duty ratio (D).

The buck converter, voltage step-down or current step-up converter, is more efficient than linear regulators since it does not dissipate energy as heat. Its output voltage can be between 0 and its

input voltage, V_i. The boost converter, voltage step-up or current step-down converter, can output voltages between V_i and ∞. The buck-boost converter is the more versatile configuration, being able to output voltages between 0 and ∞. Therefore, they are suitable choices for PV energy harvesting with MPP tracking [12].

There are over 10 different MPP tracking algorithms. Their classification can be made according to several parameters and differs from researcher to researcher. Table 3.1 sums up different classifications created by different researchers regarding the same algorithms. There are 18 major algorithm groups. Each group is represented on Table 3.1 with the following correspondences:

1. Uniform irradiance condition [11];
2. Partial shading condition[11];
3. Low-power methods [9];
4. Analogue [29];
5. Digital [29];
6. Fast and continuous tracking [29];
7. Minimum cost [29];
8. Easy implementations [29];
9. Periodic tunning [29];
10. Heuristic search [25];
11. Extreme value search [25];
12. Linear aprox. [25];
13. Intelligent control [25];
14. Linear control [25];
15. Two variable methods [17], [29];
16. One variable method [17], [29];
17. Direct [17], [29];
18. Indirect [17], [29].

Table 3.1 – Classification of the currently available MPPT algorithms.

	1	2	3	4	5	6	7	8	9	10	11	12	13	14	15	16	17	18
Perturb and Observe	x		x			x				x					x		x	
Incremental Conductance	x					x	x			x					x		x	
Fractional V_{OC}	x		x	x				x	x		x				x		x	
Fractional I_{SC}	x			x				x	x			x				x		x
Ripple Correlation Control	x			x		x						x				x		x
Current Sweep	x						x		x									
Load Current or Load Voltage Max.	x			x		x												
dP/dV or dP/dI Feedback control	x				x									x	x		x	
Particle swarm optimization		x																
Genetic algorithm		x																
Differential evolution		x																
Artificial Neural Network		x			x	x			x				x					
Fuzzy Logic		x			x	x			x				x					

Hill climbing techniques

Two of the most referenced MPPT algorithms are hill climbing techniques: the perturb and observe algorithm and the incremental conductance algorithm. The technique's name derives from the shape of the PV curve.

The perturb and observe (P&O) algorithms can be further classified according to its perturbation step or perturbation parameter [32].

The perturbation step can be:

- Fixed – Classical Perturb and Observe;
- Adaptive:

    1. Size wise - Adaptive P&O;
    2. Direction and size wise - Three Point Weight Comparison.

As for the perturbation parameter, options are:

- Reference voltage perturbation;
- Reference current perturbation;
- Duty ratio perturbation.

The classical P&O algorithm is further explored. Two initial measurements of voltage and current are taken for two separate time instants. Instant values taken afterwards result from a perturbation. The power is calculated and compared for each pair, by subtracting one another. If the difference is positive, that means power in the second instant is higher than for the first and the systems is further perturbed with the parameters of the first perturbation. If the difference is negative, then the perturbation direction is changed. The algorithm imposes a cyclic perturbation operation that ensures the operating point is at the MPP region. Its flow chart is presented on Figure 3.8 [11], [29], [32], [33].

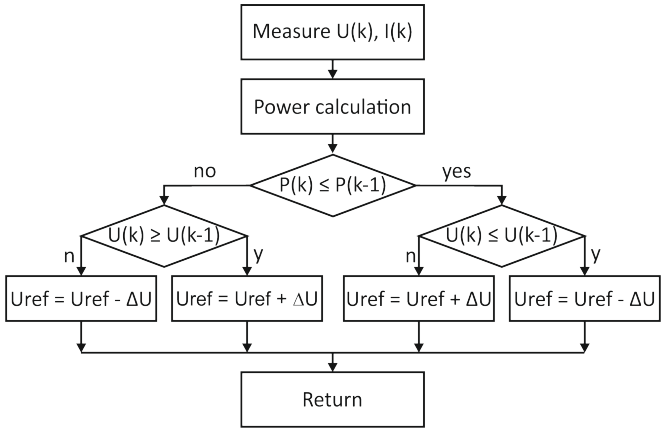

Figure 3.8 - Flowchart for the classical Perturb and Observe method.

P&O algorithms have been studied and improved according to several considerations. In [26], researchers have adapted the algorithm to better answer sudden changes in irradiance levels by perturbing current and using a boost converter. The team on [22] also studied the application of the P&O algorithm to variable irradiance conditions and current perturbations. The size and frequency of the P&O perturbations is studied on [18]. The three-point P&O algorithm is addressed with [34].

As far as the incremental conductance algorithm goes, according to [29], a voltage is imposed on the PV module at every iteration. After that, the incremental change on conductance is measured and compared to the instantaneous conductance for determining the relative position of the operating point regarding the MPP. The method is described as being more efficient than the P&O algorithm because it does not fluctuate over the MPP. Its flowchart is represented on Figure 3.9.

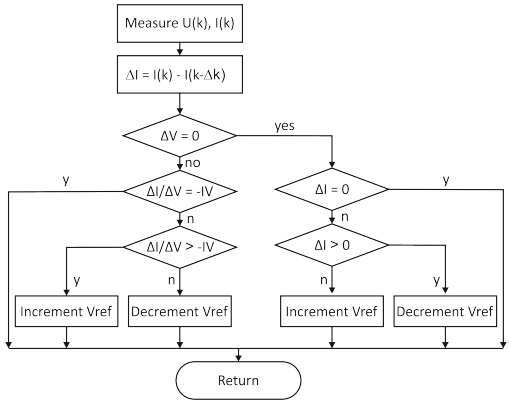

Figure 3.9 - Flowchart for the incremental conductance algorithm.

The incremental conductance method and the perturb and observe method are usually described as separate algorithms. A careful analysis of both, leads to the conclusion that they are, in fact, equivalent. They are studied both from a mathematical stand-point and from an application perspective and results show a deviation of less than 0.15% for their efficiencies (0.13% for dynamic conditions and 0.02% for static operation) [35].

Fractional algorithms

These algorithms are based on the idea that the voltage or current at the MPP is a set fraction of the open circuit voltage or short circuit current at a given instant. As the name implies, the fractional voltage open circuit algorithm measures the open circuit voltage V_{OC} of the PV system and sets its voltage operating point V_{MPP} according to:

$$V_{MPP} = k \times V_{OC} \tag{3.9}$$

The variable k has a value between 0.71 and 0.78 and is dependent on the PV characteristics.

The fractional short circuit current algorithm measures the short circuit current I_{SC} of the PV system and sets its current operating point I_{MPP} according to:

$$I_{MPP} = k \times I_{SC} \tag{3.10}$$

As it was with the proportionality constant on the open circuit voltage algorithm, here k is also attributed according to the PV characteristics, usually resting between 0.78 and 0.92.

The use of the V_{OC} algorithm is simpler and cheaper than the use of the I_{SC} variant, although not so accurate. Both methods work at the MPP region rather than on the MPP itself. A pilot cell can be used with these systems so as to periodically measure the unloaded voltage and current values of the system. Otherwise, load shedding on the measuring process leads to power losses [9], [11], [29], [33].

Load current or load voltage maximization

A PV system connected to a power converter and subjected to an MPP algorithm makes the converter load work at its maximum power. The reverse, considering a lossless system and according to the maximum power transfer theorem previously approached, is also true: a load working at its maximum power will make the power converter induce an MPP working regime for the PV system. Since there are only three types of loads – voltage-source type, current-source type and mixed types – and considering non-negative impedance types, either voltage or current can be used to drive the system to its MPP, considering appropriate matching between load type and stimulus [11], [17], [29], [36].

Current sweep

This algorithm usually takes up to 50 milliseconds to run: it applies a sweep waveform to the PV system, gathers the data for building an IV characteristic curve and finds the MPP with it. Then the system is biased and its operating point is positioned at the MPP. Due to the time the algorithm needs to reposition its operating point, the MPP may shift and the repositioning may not be successful. Besides, and because of its stepped-up energy requirements, it is only useful if the power consumption it takes is lower than the retrieved power from the system. This method is particularly useful for circumstances where multiple local maximum points are present. In this circumstance, other algorithms, like those from the hill climbing techniques, are not so accurate [11], [17], [29].

Ripple Correlation Control

The ON/OFF behavior of the power converter device leads to ripples on the retrieved power. The ripple correlation control algorithm, or RCC, makes use of these ripples to achieve the MPP. With the time derivatives of power related with voltage or current derivatives, the operating point position is found relative to the MPP. Its repositioning is achieved by changing the duty ratio of the converter and getting the power gradient equal to zero. The RCC algorithm is quick and accurate, even in varying irradiance levels. Since it does not require any previous information or

knowledge about the PV characteristics, its implementation is easier. The algorithm has analogue implementation and is considered a two variable method [11], [17], [29].

Stochastic algorithms

The irregularity and unpredictability of environmental conditions are behind the need to develop and adapt probabilistic and artificial intelligent methods. Fuzzy logic controllers [30], [31], neural networks [11], [17], [21], [29], [33], particle swarm optimization [28], differential evolution or genetic algorithms [11], [17], [21], [29], [33] are some examples of stochastic MPPT algorithms.

These methods are of digital nature and implementation and mostly inspired on the behavior of biological organisms. They are usually applied in systems where irradiance and temperature values may change rapidly. Apart from fuzzy logic controllers, a training period is needed for the accurate operation of these methods. This training is usually conducted with the actual PV system so that the algorithm can adapt itself to its particular conditions. Due to this, these methods have a higher cost and are less common in large scale applications [11], [25], [29].

The problem at hand: energy harvesting from MFCs

Harnessing energy from renewable sources presents several challenges, particularly related with efficiency and energy levels. Microbial fuel cells are no exception, presenting longer response times than PV systems and other renewable energy sources. This characteristic is of paramount importance when designing power management systems, due to the relationship between energy availability and requirements.

The relationship between the MFC's internal resistance and the external load is another major player for efficient energy harvesting. As formerly stated, only when the external load equals the internal resistance of the MFC can maximum power be achieved [37]–[39]. Since the MFC's internal resistance has a dynamic behavior, exhibiting significant changes according to inlet concentration, a time-fixed resistive-load between each electrode will not guarantee the highest power generation. Still, a time-fixed resistive-load can be of use.

MFC power production

An MFC produces energy if the electrolyte consumption leads to a current flow between the anode and cathode. As with other fuel cells, this will only happen if the reaction between the cell's electrodes is thermodynamically favorable, which means that no energy input is needed for the reaction to happen. The maximum voltage level that can be produced by any fuel cell corresponds to its electromotive force, or E_{emf}, derived with the Nernst equation:

$$E_{emf} = E_{cat} - E_{an} \tag{3.11}$$

where E_{cat} represents the cathode potential and E_{an} the anode potential. These potentials can be determined if the reaction equation, the concentration of each oxidizing and reducing agent and the specific temperature is known:

$$E_{cat} = E_{cat}^{0} - \frac{RT}{nF}\ln(\prod) \tag{3.12}$$

and

$$E_{an} = E_{an}^{0} - \frac{RT}{nF}\ln(\prod) \tag{3.13}$$

where, E_{cat}^{0} and E_{an}^{0} represent the electrode potential in standard conditions (298.15 K, 1 bar pressure, 1 M for all species), R corresponds to the universal gas constant, T is the temperature in Kelvin and $\prod$ is the reaction quotient. The reaction quotient is a chemical measure of the relative amounts of the reactants and the products according to time.

For a neutral pH of 7, acetate oxidation at the anode, and oxygen as the electron acceptor at the cathode, the theoretical E_{emf} is of 1.1 V.

The E_{emf}, however, cannot be achieved since fuel cells have inherent internal energy losses. These losses will be discussed in the appropriate section. A rough estimate of the energy losses can be found by applying the following relationship:

$$V_{cell} = OCV + IR_{int} \tag{3.14}$$

where OCV stands for the Open Circuit Voltage (the voltage measured with no current flow), I stands for the cell's current and R_{int} for the internal resistance of the system. The IR_{int} term accounts for all the internal losses of the cell. These losses have three contributors: ohmic losses – correspond to the resistance to electron and proton flow; activation losses or charge overpotentials – sum the energy lost to initiate the oxidation/reduction reactions; and mass transport losses - which are linked to the unbalanced flow of reactants and/or products. Details on each loss and their impact on the cell's power production capability will be discussed.

The electrode spacing, the substrate temperature and pH, and the electrode surface area and geometry also have a sizable impact on the MFC performance. For instance, power output is higher if the electrode spacing is smaller – for air-cathode reactors, the most efficient anode bristles' distance (when in a brush format) from the cathode is around 4 mm [40]; however, when the anode and the cathode are perpendicular, the anode tip must be around 1 cm away from the cathode [41] – if the electrodes are too close, oxygen and substrate diffusion increase, biofouling onsets quicker and power decreases. A substracte pH lower than 6 or higher than 9.5 makes the bacterial community change its metabolic profile and decreases power output, which highlights the usefulness of an adequate proton exchange membrane. The anode surface should also foster biofilm development, though if too good conditions are provided, the electrode will quickly suffer

from biofouling: in such conditions, the biofilm grows to the point where exchanging electrons between bacteria is more energy efficient than between the biofilm and the electrode [42]–[48].

This delicate equilibrium between all these conditions is very difficult to achieve and control, since bacteria are living organisms genetically engineered to adapt and survive, irrespective of the conditions they encounter.

Techniques for measuring parameters and characterizing an MFC

In order to maximize the energy production of an MFC, all the energy losses need to be reduced. To do so, they first need to be identified and measured. This step is crucial if efficient adjustments are to be applied. Measurements of the cell's voltage and current with respect to external resistance and electrode's potential as a function of time are keystone for such studies. Polarization reports are the most fundamental studies that can be conducted on an MFC. The cell can be analyzed all altogether or studies can be made independently to each electrode. For probing the cell, using a potentiometer and a voltmeter, though simple and extremely accessible, produces low detailed data and can be a cumbersome process, whether due to the lack of precision in the magnitude of changes in the external load, or due to the lack of time precision of those changes. A digital potentiometer and a DAC can help improve the reliability of such a method, but the retrieved data will lack resolution, particularly if the analysis of bacterial changes are of interest. The use of a potentiostat answers to all the above shortcomings, being the most used instrument for characterizing an MFC. A potentiostat can also be used to explore each electrode independently. All and all, a potentiostat can retrieve the electrochemical activity of microbial strains, determine the standard redox potentials of redox active components, test the performance of cathode materials, acquire polarization curves, and quantify the overpotentials and ohmic losses of an MFC. The results of using this measuring instrument go well beyond the electrical characterization of a MFC and can also contribute to the electrochemical study of the cell's electrode and microbial communities [49]–[51]. A potentiostat allows for building polarization curves, current interrupt techniques, electrochemical impedance spectroscopy, linear, differential pulse and cyclic voltammetry and chrono studies, namely chronoamperometry and chronopotentiometry.

Polarization studies for MFC

There are three categories of polarization studies that can be conducted with a potentiostat. These discharge curves result from: (i) applying different external loads to the MFC's terminals and measuring the output currents and voltages; (ii) stepwise measuring the current after applying a small DC voltage signal; (iii) applying small DC current increments or decrements to the cell and measuring the output voltages. Nonetheless the potentiostat usefulness, the following discussion will consider polarization studies conducted with a potentiometer and a voltmeter due to their accessibility and ease of use.

The scientific community is still debating the time needed for an MFC to adjust to a change in its operating conditions. This means that no steady-state time has been determined, uniformly, for an MFC – particularly due to different reactor geometries and electrode arrangments. Even though control MFCs can be used to estimate this parameter, a single small variation on the substrate concentration or on the electrode surface (just as an example) may greatly vary the time constant for two similar, in principle, MFCs. Therefore, a control MFC is usually used to outline the steady-state time which is then extended to guarantee the operation in that same regime [51].

A typical type (i) polarization curve is shown in Figure 3.10:

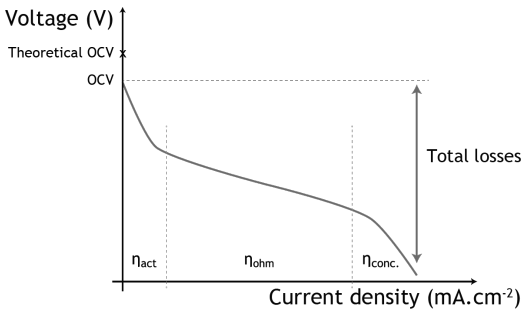

Figure 3.10 – An example of a polarization curve.

This curve can be built by applying a single-cycle or multiple-cycle method. A single-cycle method is used when several resistance changes are made during on batch of wastewater, or if the cell is operated in continuous flow. Multiple-cycle methods are applied in fed batch reactors and imply a resistance change per batch, where the number of batches will be dependent on the resolution needed for the polarization curve. A common occurrence found in polarization curves is power overshoot. Power overshoot is the phenomenon found at high current densities after the maximum power point, where the cell's voltage and current drops to lower values, producing lower power values than those achieved before. Simply put, a decline in voltage results in a decline in the current and leads to a bending on the polarization curve. It is usually associated with the anode and immature biofilms – the anodic community is unable to maintain the increasing electron demand; or inadequate measurement procedures with resistance changes too quick that don't allow the biofilm to adjust. This can happen for any reactor type, geometry or even for reactors operated as a stack. To bypass such event, multiple-cycle methods are the best choice, since, provided the adequate readiness of the biofilm, full acclimation to the external load on the reactor is guaranteed [50], [52]–[57].

In this curve, three regions can be identified. Each of them is associated with an overpotential. Charge overpotentials (η_{act}), or activation losses, occur at low currents. They result from the energy needed for the reactions to happen at the electrode's surface. The Tafel equation models these losses accurately:

$$\eta_{act} = b \times \ln\left(i_c / i_0\right) \tag{3.15}$$

where b is related with the cell's characteristics: the higher the value, the slower the reactions; i_c represents the MFC's current density and i_0 the exchange current density. The exchange current density characterizes the catalytic ability of the electrode's surface: higher i_0 values are related with faster reactions. In MFC's, current densities are usually expressed in mA/cm2. This equation is only applicable when $i_c > i_0$, since there are no circumstances were there are no activation losses ($i_c = i_0$) or where they add up to the outputted voltage ($i_c < i_0$). As previously mentioned, the analysis will be applied to the steady-state behavior, which means that the variables i_c and i_0 have a constant relationship. As such:

$$\eta_{act} = b \times \ln(i_c/i_0) = b \times \ln(i) \tag{3.16}$$

This approximation is valid for currents over 1 mA/cm^2, since $\ln(1) = 0$. For $i < 1$ mA/cm^2:

$$\eta_{act} = b \times \ln(i) = b \times \ln\left(\frac{i}{b_1} + 1\right) \tag{3.17}$$

The ohmic losses (η_{ohm}) exhibit a linear behavior and can be modeled by the ohm's law:

$$\eta_{ohm} = i \times \mathrm{R}_{ohm} \tag{3.18}$$

Concentration losses can be modeled by:

$$\eta_{conc} = c \times \ln(1 - \frac{i}{i_1}) \tag{3.19}$$

The c parameter is a constant that depends on the fuel cell and its operating state. i_1 is used to represent the limiting current at which the fuel is used up at a rate equal to its maximum supply speed. This equation, however, has severe limitations when applied to describe air exposed, batch-fueled, fuel cells, rather than fuel cells exposed to pure oxygen. Low temperature fuel cells are also not adequately described by this equation. Applying these considerations and the same principle as for equation 16, equation 20 outputs a curve that better fits experimental data:

$$\eta_{conc} = c \times e^{d \times i} \tag{3.20}$$

The contribution of each of the losses accounts for the overall voltage and current measured at an MFC terminal by the equation:

$$V_{OUT} = A_{theory} - b \times \ln\left(\frac{i}{b_1} + 1\right) - i \times R_{ohm} - c \times e^{d \times i} \tag{3.21}$$

Where A_{theory} represents the theoretical open circuit voltage. Considering that during the experimental procedures, the same cathode area and reactor volume was preserved, current densities can be converted to absolute current values, in mA. The open circuit voltage measured will also be different than the theoretical value and equation 21 yields:

$$V_{OUT} = A - B \times \ln(\frac{I}{B_1} + 1) - I \times R_{ohm} - C \times e^{D \times I} \tag{3.22}$$

With equation 22 and suitable methods for quantification of each of the losses, the cell's static behavior can be modeled.

MFC and energy harvesting studies: a state-of-the-art review

Microbial Fuel Cells (MFCs) have been explored from different approaches, with researches in electrode materials [58], reactor geometry and configuration (single chamber [40], double chamber [59], flat plate [60], membrane-less [61], up-flow [62], stacked [63], nested [64] or in-plane [65] are just some examples), fuel cell types (besides the classical microbial fuel cell, other biofuel cell typologies like benthic microbial fuel cells (BMFC), also called sediment MFCs (SMFC) [66]–[71] and photosynthetic microbial fuel cells [72]) have been explored), substrate composition [73], bacteriological profiling [74]–[76], biochemical parameter determination [77] (biochemical oxygen demand [78]–[80], electronic nose [81], flora health [82]) and other applications apart from energy production, like bioremediation [83]–[86].

There is, however, a separate field of investigation, well framed and mostly associated with low power energy harvesting research, specifically aimed at understanding, maximizing and managing the produced power. This research path rose from the need to apply MFCs as power sources for instrumentation and communication devices, such as the previously mentioned biochemical sensors, temperature [87] and humidity sensors [88] and other wireless sensors and wireless sensors networks [89]–[94].

To build a clear picture of each research line tracked in the field of microbial fuel cells and energy harvesting strategies, data will be presented in a systematic and theme-oriented manner, according to the energy harvesting solution complexity. After pinpointing the highlights of MFC and energy harvesting research, power harnessing from benthic microbial fuel cells is discussed. Some of those concepts were also applied to microbial fuel cells, and that state-of-the-art review ensues, with particular interest in passive components, energy converters and mixed topologies.

Ecobots and biological energy harvesting roadmap

In MFC history, perhaps the most famous use of MFC power is the application to autonomous robots. This concept, firstly discussed by Stuart Wilkinson [95], was afterwards explored by Ieropolous et al in 2003 with Ecobot-I [96]–[98], in 2005 and 2006 with Ecobot-II [99], [100] and in 2010 with Ecobot-III [101]. The Ecobot is generally defined as an energetically independent robot, powered by MFCs, capable of autonomous actions as motion, sensing and computation. Each generation is pictured in Figure 3.11.

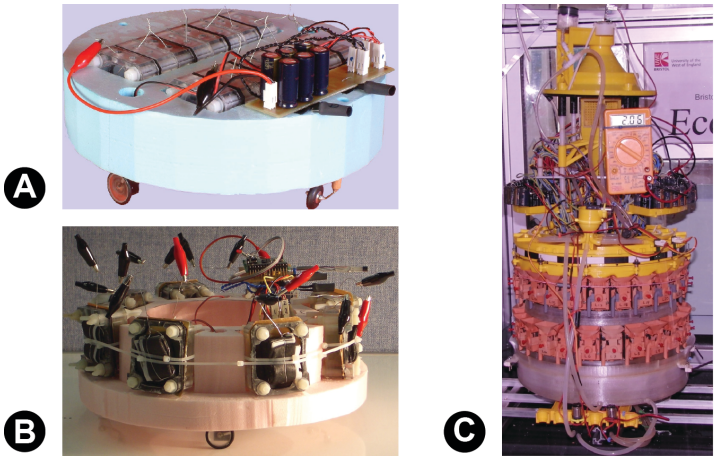

Figure 3.11 – Ecobot family overview. Ecobot-I is represented in (A), Ecobot-II in (B) and Ecobot-III in (C). Images courtesy of the Bristol BioEnergy Centre, BRL, University of the West of England, UK.

The work in Ecobot-I is mostly related with the optimization of the MFC power source. In the Ecobot-II generation, also moving with pulsed behavior as Ecobot-I, the robot was already equipped with sensing capabilities. Its main task was to reach a light source and measure temperature while moving. The robot remained idle while energy was below the required minimum and the carbon source for the MFCs was an innovative mixture of flies and water (experiments were conducted, in order, with refined sugar, rotten peach portions and dead flies; the team chose to present only data with dead flies, as they are representative of the work innovation). With Ecobot-III, robot feeding was converted to an autonomous task, by additionally preparing the device with ingestion and egestion capabilities. The device was presented as a proof of concept for the "symbot" concept, where real life organisms and machine operated in a symbiotic manner. Further Ecobot works were resumed in 2013, although not presented under the same name.

The Ecobot-IV research, in Figure 3.12, has been focusing on improving individual cell power output and performance, while decreasing the total cell number (from 48 MFCs on Ecobot-III to 24 in Ecobot-IV). Research is also being directed at wireless data transfer related, mostly, with individual MFC status [102]–[104].

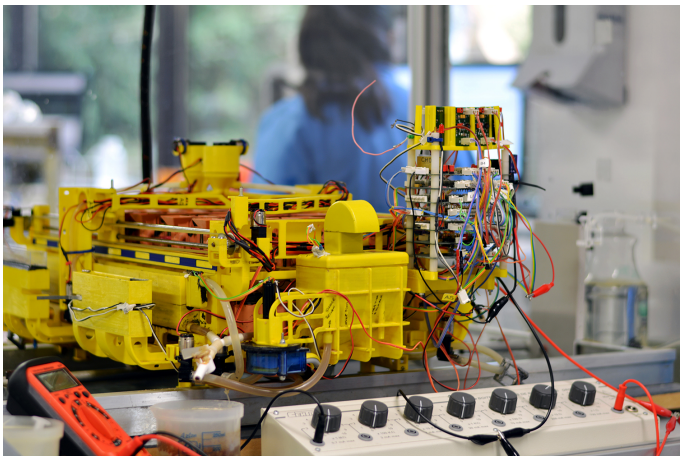

Figure 3.12 – Ecobot-IV, a work published only on H2FC Supergen Hydrogen Research Conference in 2013. Images courtesy of the Bristol BioEnergy Centre, BRL, University of the West of England, UK.

Figure 3.13 presents a cluster of researchers and research lines, on the subject of MFC and energy harvesting, organized by year, which can be used as a highlight's overview from 2000 to 2019.

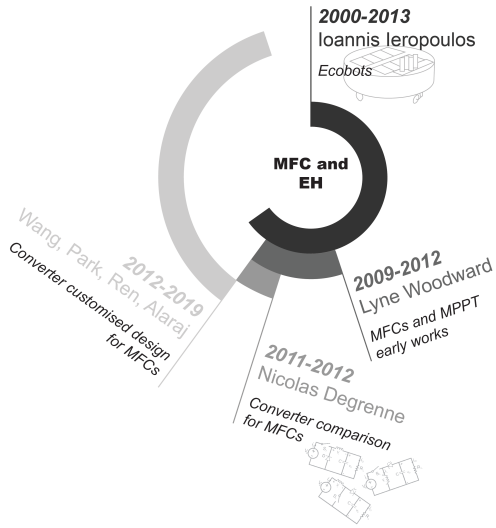

Figure 3.13 – Microbial fuel cell and energy harvesting research highlights from 2000 until 2019.

Benthic fuel cells and energy harvesting strategies

The first study to be published addressing the power management of the energy harnessed from MFCs was conducted by Shantaram et al, in 2005 [93]. Their work consisted on using a benthic microbial fuel cell (BMFC, where the cathode is afloat and the anode is buried in sediment of the water bed), deployed in a fresh water creek with a magnesium alloy based sacrificial anode, together with a capacitor and a DC/DC converter to power a commercially available thermocouple/transmitter/receiver kit. The lifetime of the system was estimated to be, approximately, 7 years, or the time imposed by the corrosion rate of the sacrificial anode.

This benthic MFC was capable of achieving a maximum of 2.1 V but poses significant concerns with the manganese oxides forming on the cathode surface from the sacrificial anode reactions. Promoting the magnesium oxidation in an aquatic environment may increase manganese oxides concentration, which have been found to be toxic for aquatic environments [105].

Donovan's team, in 2008, continued to explore the use of BMFCs as power sources, this time for wireless sensors. The BMFC consisted of a graphite anode, buried in the sediment of a river, and a stainless-steel cathode. Due to the electrode nature, the attainable voltage of the BMFC was lower than that of Shantaram et al. [93], under 500 mV. As such, the team developed a power management system (PMS) working between 320 and 52 mV of the BMFC. The PMS consisted of a super capacitor, a voltage comparator to determine when the PMS should start and stop, and a charge pump and a DC/DC boost converter to provide the voltage boost to 3.3 V, allowing the sensor operation. The temperature sensor chosen was ready for wireless communication. The team set the measurement frequency to one sample for every 30 seconds, which limited the duration of each cycle of operation to only 3 measurements before the supercapacitor was discharged, and around 20 minutes were needed before a new measurement cycle could be started. Although larger capacitors could have allowed for more measurements per cycle, that would also increase the system's charging time.

In the same year, Tender et al [106] took a bold step and explored the application of the BMFC power to a commercial device, proving BMFC's could be used as independent power sources. In their work intitled "The first demonstration of a microbial fuel cell as a viable power supply: Powering a meteorological buoy" they report on the use of a BMFC to power an 18-mW meteorological buoy, on a salt marsh, that could measure temperature, pressure and relative humidity. Power production on a salt water environment was more successful than on freshwater due to the easier ionic balance of the system. Information on the power conditioning of the system is very scarce, as the use of a voltage conditioner and a capacitor is only briefly mentioned.

Less than a year later, in 2009, Meehan (first in [107] and then in 2011 in [108]) continued the work by Tender and explored the use of 2 serially connected, double chamber, BMFCs, where, because they were subjected to the same water body, the overall voltage of the device was the voltage measured between the two most outer electrodes of the system.

Figure 3.14 clarifies the series association of BMFCs, while additionally picturing how a parallel association works.

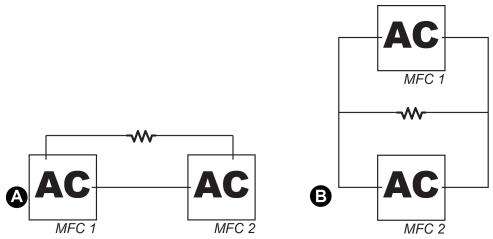

Figure 3.14 – Series (A) and parallel (B) connection of 2 microbial fuel cells. The electrode connection follows the same pairing for whichever number of microbial fuel cells. "A" stands for the anode, the negative electrode, and "C" for the cathode, the positive electrode.

The harvested energy was firstly boosted with a charge pump (Seiko S-882Z), stored in a supercapacitor and then, at 1.8 V, delivered to a boost converter (ST L6920DB) for voltage boosting to 3.3 V. A hydrophone was then powered from this microbial source. The PMS was modified so that the charge pump's internal MOSFET was bypassed when routing power to the boost converter: the aforementioned MOSFET had an internal resistance of around 100 ohms that would absorb a large portion of the harvested power. The system had a low end-to-end efficiency, mostly due to the charge pump.

The use and improvement of power management systems and the application of the harvested energy for instrumentation was also addressed, in 2011, by Donovan et al [109] and Zhang et al [87]. While Donovan's strategy was to prove a large capacitor – 350 F – could be charged by a BMFC, Zhang's attention was directed towards the relationship between cathode placement and power production: their findings suggest that floating cathodes perform better than bottom cathodes. Nevertheless, both researches were validated by applying the harvested energy to wireless temperature sensors, powered by an arrangement of supercapacitors, charge pumps and commercially available DC/DC converters. The DC/DC converter parameters' impact on the power development was researched by Gardel et at [110]. The anode connection and disconnection conditioned the converter's duty cycle.

By 2013 the work initiated by Donovan et al in 2011 [109] was resumed and carefully updated in [111], while Thomas et al [70] proved that the same fuel cell typology could be applied to power an independently developed platform, capable of autonomous communication. That platform was customized to include a radio board (CC2420EM from Texas Instruments), a low power microprocessor (16-bit low-power MSP430 from Texas Instruments) and an energy harvesting stage (LTC3108 step-up converter from Linear Technology, accompanied by a 20:1 transformer). Voltage measurements were chosen as the data to transmit with the platform. The system operation was ultimately determined by the BMFC power availability, relinquishing whichever external control to prove the platform's autonomy.

While improving the harnessed power from BMFC's, by 2015, efforts were also made to decrease the power conditioning stage's start-up voltage. Lin et al [112] proposed a 4 stages Dickson charge-pump alternative achieving that goal, by lowering the start-up voltage to 300 mV. The proposed charge-pump alternative was applied to a BMFC to power two wireless sensors. Figure 3.15 presents an exemplary Dickson charge-pump of only 2 stages.

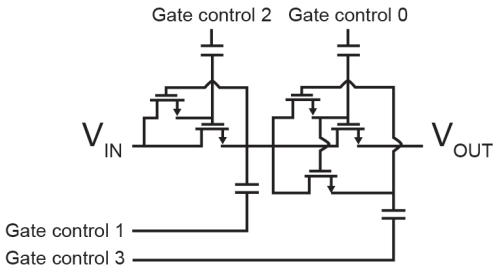

Figure 3.15 – Two stage Dickson charge-pump topology example.

The maximum BMFC power production was also investigated by using several fuel cells with one PMS while not connecting them to each other. Tang et al [68] suggested a source-load isolation is necessary to work with different BMFCs independently and, therefore, improve the amount of harvested energy. The idea came when comparing the power from 4 smaller BMFCs with the power from 1 large BMFC, where the area of the latter was 4 times the area of the smaller reactors. The referred isolation can be achieved by using diodes or transformers: diodes present significative voltage losses and transformers used in DC systems imply sharing the same ground for the primary and secondary windings. As such, Tang et al advocate the load connection when energy transfer is needed, not sooner. The investigation found that the charge-pump and boost converter were responsible for dissipating more than half of the power of the system.

To prove the affordability of BMFC use as power sources, in 2016, Chailloux et al [113] developed a PMS, not self-sustainable, built from off-the-shelf components and proved the legitimacy of the concept by powering a wireless temperature sensor.

In the same year, PMS and BMFCs were also used to power a single-hop wireless sensor network by Zhang et al [114]. The work was sourced from the 2012 research with a single-chamber air cathode microbial fuel cell [115].

Benthic MFCs with innovative designs or applications were also investigated. Sudirjo et al [116] focused on a BMFC with an innovative design. The MFC was a silicon tube which is installed in a rice paddy field. The tube design is proposed to overcome the need to excavate the soil for the BMFC installation. The study was conducted to determine if the BMFC installation was detrimental to the culture development and if power generation was affected by the dry and wet seasons. Continuous power monitoring was achieved by using LoRa technology with a separate power source. Results have shown that little to no impact was found on the rice culture and that power development was uninterrupted for, at least, four crop seasons.

Single MFCs as independent energy sources: energy harvesting with passive components

Research specifically related with energy harvesting optimization from MFCs was initiated by Dewan et al [117], in 2009. His work investigated the power delivering capabilities of MFCs when the energy harvesting profile changed from continuous to interrupted: a comparison was in place between having the MFC continuously connected to an external load or to have it charging a capacitor, forcing its discharge to a 1 Ω load when a set voltage was achieved. For the particular conditions of their trials, 111% more energy was delivered with the interrupted method. A year later, the team tackled the challenge of adequately testing MFC powering capabilities without connecting the actual load, but rather a testing platform, pictured in Figure 3.16 [118]. Such a device allowed to determine the MFC charge period, the current limiting electrode and the best fitting capacitance for maximum energy storage.

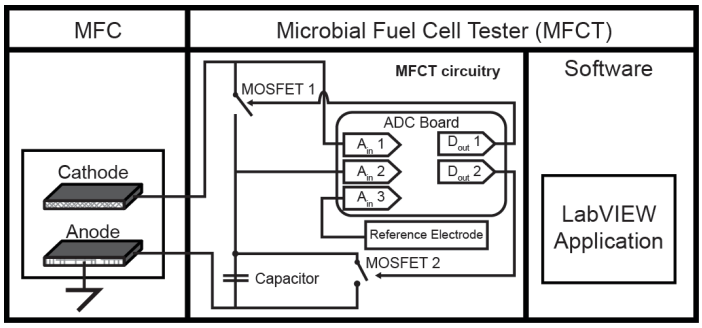

Figure 3.16 – Microbial Fuel Cell Tester platform proposed by Dewan et al [118]. Figure adapted from figure 3 and figure 4 of [118]*.

The year of 2011 registered yet another study conducted to find if the external device connected between the MFC electrodes had any effect in the extracted power. Liang et al [119] replaced the external resistance by a capacitor and studied if current production was affected by alternatively charging and discharging the capacitor from (microbial fuel cell) and to the system (microbial electrolysis cell). Comparing with the use of an external load, discharging the capacitor back to the cell produced higher currents, although converting the cell to the electrolysis equivalent, which is adequate for bioremediation instead of energy production.

It was only in 2013, by Ren et al [120], that an investigation was conducted to determine whether the capacitor switching time influenced the MFC power profile. The team found that, when dealing specifically with just capacitors and MFCs, without any other regulation or storage strategies, the capacitor switching time must be optimized to guarantee an appropriate charge recovery efficiency and, therefore, that the MFC is outputting power at its best rate.

*Journal of Power Sources, Vol. 195 Issue 1, Alim Dewan, Conrad Donovan, Deukhyoun Heo, Haluk Beyenal, Evaluating the performance of microbial fuel cells powering electronic devices, Pages No. 90-96, Copyright (2010), with permission from Elsevier, License Number 4753010828685.

In the same year and research line, and revisiting the work of Dewan et al [117], in 2009, Coronado et al [121] also investigated if modulating the load connected to the MFC terminals affected the maximum power retrieved from this power source. A noticeable improvement of over 20% was found for switched connection at frequencies above 100 Hz.

These works have determined that, in order to achieve maximum power, the switching time of passive components should be conformed to the MFC characteristics.

Single MFCs as independent energy sources: maximum power point tracking

Research on maximum power point tracking started after determining that a load continuously connected to and MFC is not adequate for harvesting the cell's maximum power. The problem was firstly addressed as in Photovoltaic (PV) systems.

It was in 2009 that Woodward et al [122] reported on the use of 2 continuous flow air-cathode MFCs for maximum power production with a multiunit optimization algorithm. At least two MFCs are needed to apply this maximum power point method because the algorithm is based on the comparison of the outputs between multiple units with inputs offset by a design parameter. For this study, the design parameter chosen was temperature, which resulted in a faster maximum convergence than would have been achieved with a perturb and observe algorithm (50 min vs 7 hours for an optimization from 140 Ω to 40 Ω). Nevertheless, the stock solution used as a carbon source of each MFC had 40 g/L of acetate, which is uncommon for common wastewater.

A similarly composed team, still led by Lyne Woodward, in 2010 [123], further related the performance of different maximum power point methods by comparing their performance in photovoltaic (PV) systems and microbial fuel cells: PV MPPT algorithms are mostly online, depending on the PV math model to match the system and the load's impedance; in MFCs, microbial kinetics are an added difficulty for developing the cell's math model, which, in turn, limits the how the PV studies can be applied to MFCs. The methods in comparison were perturb and observe (P&O), gradient and multiunit (MU) optimization. They were applied to the same MFCs as in the work by this team in 2009. They found that the P&O method took longer than the MU method to converge. This time can be decreased, although being always higher than that of the MU, with increased perturbation frequency but the oscillations around the maximum power point increase, leading to maximum power point over estimation and power overshoot. The same increased perturbation frequency did not affect the MU convergence time. Although quicker, the MU, as previously mentioned, requires more than one unit and previous knowledge on the MFC behavior.

The path was cleared for further studies related with MPPT strategies. One year later, Premier et al [124], along with the findings by Lyon et al [125] and Pinto et al [126], implemented a dynamic control of the external load imposed to a double-chambered H-type MFC in a way that was

determined by the sign of the gradient on the power-current curve, with 10 Ω steps. The external load variation was achieved with a digitally controlled potentiometer with a 40 Ω minimum resistance. When comparing the MFCs in this study, one with the dynamic control strategy and the other submitted to a fixed load, it was found that the control method resulted in higher maximum power and coulombic efficiency than the non-controlled MFC.

In 2012, Degrenne et al compared two different MPPT algorithms, the perturb and observe and the fractional open voltage [127]. Although the P&O method was found to be more efficient than the fractional open voltage, the low implementation cost of this second algorithm highlighted it as a promising compromise for MFC energy harvesting.

In 2013, MPPT research was continued by the team of [124], with Hitesh Boghani instead of Iain Michie [55]. The investigation was centered on how the power control affects the MFC behavior, specifically how the application of a hill climbing MPPT algorithm affected the start-up time of an MFC. With the use of a digitally controlled potentiometer, they found that the MPPT algorithm, either with or without anode poised potentials, improved the start-up time by 45%. Molognoni et al, in 2014 [39], referring specifically to this [55] and to the research of Degrenne et al [127], proved that the aforesaid MPPT strategy for MFC start-up improvement was also valid for continuous flow real wastewater, namely, swine effluent.

After 2013, MPPT studies became more diverse and were approached from other perspectives, apart from simply studying the algorithm's impact on power figures.

Song et al [128], in 2016, compared the power development profile of flate-plate MFCs when connected to a fixed load resistance and to a MPPT algorithm for different organic loading rates, hydraulic retention time and sampling interval, proving that, even for this reactor geometry, MPPT algorithms are successful in increasing the power producing capabilities.

In 2017, Alaraj et al [129] looked on the side effects of the extremum seeking (ES) algorithm, which applies a sinusoidal perturbation while finding the MPP. Their work clearly exposed the main problem with energy extraction for MFCs at currents near the MPP: in such conditions, voltage overshoot may happen, which induces a voltage switch on the anode (from negative to more positive) and concomitantly reduces the overall voltage of the cell. P&O algorithms in this condition usually increase the current extracted from the cell, leading to a further decrease of the voltage and the MFC's power. Instead of focusing on how to eliminate this voltage overshoot, the team tried a voltage overshoot avoidance algorithm to correct the MFC operation when voltage overshoot happens. The algorithm is capable of detecting the voltage overshoot condition and, when that happens, the ES is stopped, the MFC is led to open circuit operation and the system waits for the nominal OCV to be reached. At that point, the MFC is closed again and the ES algorithm is set to work at the last duty ratio before the onset of the overshoot condition, successfully eliminating the voltage overshoot phenomena.

Although other studies have been conducted in this theme, research specifically centered on MPPT algorithms and its application to MFC energy harvesting shows that: when dealing with MFC start-up, the hill climbing algorithm helps to decrease the setup time; when focusing on power maximization, the fractional open voltage is the best compromise between cost and efficiency: the P&O method suffers from overestimation and power overshoot and the gradient method advantages are short compared to any other MPPT algorithm applied to MFCs.

Single MFCs as independent energy sources: power converters and management systems

To further address energy harvesting maximization, other studies were conducted with DC/DC converters and related categories, while BMFC and MPPT research were being developed at the same time, a consideration of the uttermost importance.

To successfully connect MFCs directly to DC/DC converters, and produce a useful amount of energy, some technical challenges need to be overcome. Adami et al [130], in 2011, tried to increase the PMS efficiency by decreasing the power losses and implementing a cold start-up. This task was tackled by using a step-up converter based on the Armstrong oscillator, in the topology presented in Figure 3.17. With such topology, a single-chamber air-cathode MFC with 600 Ω internal resistance produced close to 100 μW.

The French researcher Nicolas Degrenne was also closely following the works of adapting DC/DC converters to bioelectrical fuel cells. Him and his team began by adapting and comparing the 3 most common DC/DC converter topologies, pictured in Figure 3.7, when applied to MFCs [131], [132]. By 2011/2012, most silicon components were not capable of switching at gate voltages below 0.5 V, which in some cases, were voltages higher than those of MFCs. The strategy to make those converters adequate for MFC use could rely on charge pumps or specifically designed devices, built upon, for instance, transformer-based oscillating devices.

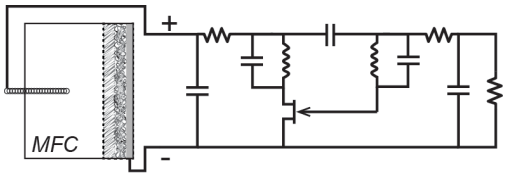

Figure 3.17 – Armstrong topology and its connection to a generic single-chamber air-cathode microbial fuel cell.

This last option was chosen by Degrenne et al, who adapted a boost, a flyback and an oscillator voltage-lifted topology with self-oscillating circuits. The oscillator voltage-lifter topology proposed was composed of a transformer based high step-up oscillator, a Greinacher voltage-lift and a starting aid circuit. All and all, the best performing topology was the boost, since the flyback suffered with current discontinuities and was very sensitive to transformer leakage inductances, while the oscillator voltage-lifter had the lowest efficiency.

Still searching for a solution to power the energy harvesting stages directly from an MFC, Yang et al [115], early in January 2012, presented a power management system based on a transformer topology with two extra capacitors: one immediately after the MFC and another just before the external load. The first capacitor can be analytically optimized to maximize the harvested power, while the second is dimensioned by the load requirements. The transformer topology was chosen, instead of a charge pump, to allow a lower voltage start-up, around 0.2 V. The energy was then boosted by a commercially available boost converter, the LTC3108 from Linear Technology, and applied, as a proof of concept, to a, also commercially available, sensor board which communicated through the IEEE 802.15.4 standard. Its end-to-end efficiency was low, as seen in Table 3.3, under 5%.

Heming Wang and Jae-Do Park continued the line investigating energy extraction and regulation to improve the overall energy production from an MFC. Their first work dates to 2011 and was presented on the 2011 IEEE Energy Conversion Congress and Exposition [133]. It is a simple application of a two-layer DC/DC converter with a voltage booster to an MFC. Next, on January 2012 [37] they went on to compare the use of a maximum power point circuit, with a capacitor replacing the external load – as described in [133]- with the use of a charge pump. For the same period, the proposed strategy of MPPT with a capacitor allowed 76 times more energy than that retrieved solely with a charge pump. They also determined that the diode was the element with the highest energy expenditure, and followed that topic, in February, by suggesting the use of a MOSFET in its place [38]. By adequately dimensioning the appropriate turn-off time, the efficiency of the converter was increased by 73%. By June 2012 [134], the team, equipping the same DC/DC converter as the one studied in [37], sought to find the influence of the duty ratio and switching frequency of the MOSFET and the effects of the inductance on the achievable power. It was found that: generally, and for a given MFC voltage, inductance is inversely proportional to the MFC current increase; high switching frequencies will request MFC energy more frequently but have no influence over the extraction period, which is determined by the duty ratio; higher duty ratios lead to smaller recovery times and increased energy extractions, which affects the MFC energy availability.

A similar investigation on the MFC duty ratio, by Grondin et al [135], was conducted in late 2011, published only in 2012, by controlling the connection and disconnection rate of the external load. The control was in place by monitoring the MFC voltage: whenever V_{MFC} reached a set V_{on}, the external load was connected; if V_{MFC} was below V_{on}, then the load was disconnected. This strategy guaranteed that the MFC energy extraction respected the MFC energy availability, although not working in the maximum power vicinity.

In the same month of [134], Zhang et al presented a comparison between the application of two PMS strategies to MFCs and load powering: the charge pump-capacitor-converter (like in [107], herein “CCC”) and the capacitor-transformer-converter (as in [115], herein “CFC”) [136]. The PMS input voltage, PMS charging/discharging cycle time and the PMS power efficiency were up for

comparison: the input voltage was determined by the charge-pump requirements (CCC) and by the transformer threshold voltage (CFC), which presented a lower input voltage; the cycle time was shorter for the CFC PMS, and the CCC PMS had a higher power efficiency. The study also supports the need of a customized PMS for MFC, while BMFC have fewer restrictions.

By 2014, the diode remained as the element with the highest voltage losses on DC/DC converters. Alaraj et al [137] presented a solution for addressing this topic, specifically for boost converters. Although MOSFETs can be used to solve major voltage losses, they are also controlled by independent power sources, adding to the system's complexity. Alaraj's team introduced the use of synchronous flyback converters with MFCs, advocating the use of transformers as a solution for increased performance and simpler configuration. When compared to boost converters operated with diodes, they achieved a 37.6% increase in harvesting efficiency.

The charge pump first stage for MFC voltage boosting was, however, not completely forgotten. Zheng et al present in [88] a PMS developed to power a set of two sensors (temperature and humidity) based on a charge pump, a supercapacitor and a boost converter. The PMS' 3 F capacitor limited the number of samples to two in 23 hour, 30 samples in 5 seconds intervals.

Efforts to decrease the start-up voltage of the DC/DC converters in the boosting stage of the PMS were not hindered. In 2014, Erbay et al [138], and Carreon-Bautista et al in 2015 [139], proposed a boost converter-transformer topology capable of continuous impedance matching and cold start-up from the MFC, with no need for a charge pump. The converter operation was based on the fractional open voltage algorithm, with the assumption that the MPP is half of the open circuit voltage. Although the work advertises that the PMS power converter was operated by the MFC itself, most of the impedance matching process was dependent on an external power source. The research was however very clear on the importance of the MFC time constant: this variable is fundamental for accurately reaching the nominal open circuit voltage of the MFC. With inadequate time, this value can be underestimated and, therefore, prevent the system from reaching the MPP. This consideration was not applied by Ayaz et al, in their simulation of a two-staged DC/DC low power converter [140].

A state of the art review, with a detailed description of the most important developments regarding the energy harvesting systems (capacitor-based, charge-pump, boost converter and MPPT and active harvesting), is presented by Wang et at [141].

Converter study was resumed from the research by Park and Wang, in 2012, by Zhang et al [142] in 2015. The investigation was aimed at the specific characteristics of switched inductor boost converters applied to μW power MFCs. To decrease the power requirements of the system, the team chose to follow an analogue approach with voltage conditioning (since digital conditioning of the control loop requires more power and area for implementation). Pulse frequency modulation (PFM) was chosen for voltage conditioning because pulse width modulation (PWM)

is more efficient for higher loads. The converter efficiency was determined to reach 85% but presented a high start-up voltage of over 0.6 V.

One year later, Dallago et al [143] put forth a low power PMS capable of running with 300 mV and, at least, 8 μA. The PMS consisted in a voltage supervisor and two supply regulation stages: a flyback step-up converter that guarantees an initial boosting of the voltage to drive the boost converter, which, after a minimum voltage is achieved, then works independently. The voltage supervisor was customized from a commercially available template. Application tests were conducted on PV cells and MFCs, with a charge transfer efficiency around 55%. The discussed solution requires additional power, besides that of the power source, to power the Armstrong oscillator of the flyback converter and the oscillator of the boost converter.

This two stage division on the PMS was even more discussed by Capitaine et al [144], with meticulous interest in the losses of the flyback converter in discontinuous conduction mode. This work clarifies the role of each of the stages of the converter, as the first does the impedance matching and the second the voltage boosting, being the major responsible for the limited efficiency of the system.

At this point in time, in 2017, Lobo et al [145] made a comparison of the power output and coulombic efficiency for 5 types of active and passive energy harvesting solutions: maximum power point with active energy harvesting (MPP-H), maximum current with active energy harvesting (MCP-H), maximum power point with passive resistor (MPP-R), maximum current point with passive resistor (MCP-R) and maximum voltage point with passive resistor (MVP-R). Texas Instruments' BQ25505 was used to apply the active harvesting solutions. The passive studies were developed by using a fixed value resistance, determined through the linear sweep voltammetry studies prior to this investigation. A set of 2 reactors was subjected to each EH solution. Results showed that the highest power output was achieved with the MPP-H and that MCP-H allowed the highest coulombic efficiency. Table 3.2 summarizes the investigation on this work.

Table 3.2 – Highlights of the research in [145].

	Active Energy Harvesting (H)	**Passive Resistor (R)**
Maximum Power Point (MPP)	MAX. Power Output	19% of Maximum Power Output
Maximum Current Point (MCP)	MAX. Coulombic Efficiency	Cathode Failure
Maximum Voltage Point (MVP)	Undesirable Operation: *slow organic removal, low energy*	MIN. Power Output

Works related with the converter efficiency were resumed also in 2017 led by Capitaine et al [146] and Wanderoild et al. [147]. Wanderoild et al [147], with Armande Capitaine, studied the flyback converter losses and using the knowledge from [144], focused on the magnetic losses of the inductor's magnetic core. The team proposes the use of coreless transformers because, in spite of their size, they are able to decrease the magnetic losses and are independent of the switching frequency. The experimental studies are not applied to real MFCs, and the research team advises that the magnetic interactions with water and bacteria need to be carefully documented. Additionally, the conduction losses are also higher than those of the classical transformer.

Armande Capitaine's team led an interesting study that also addressed the MFC dynamic losses induced by the operation of the flyback converter, building upon the knowledge from [144] and [147]. It was found that, at MPP, optimizing the inductance leads to no decrease of the power losses; increasing the duty cycle, decreases the dynamic losses but the converter efficiency as well; and that using a capacitor at the converter input (decoupling capacitor) of over 10 μF reduces the dynamic losses to 0.1% of the extracted MPP.

As Lobo et al, Alaraj et al [148], also explored the use of a Texas Instruments low power boost converter, the BQ25504. The work reports on a self-powered PMS where voltage is monitored, by an ultra-low power microcontroller, for MPPT control. The proposed MPPT algorithm considers the MFC transient behavior to better follow the maximum power operating point. The team advocates that ignoring the MFC transient behavior implies not operating the MFC at the MPP, since this is firstly calculated as a fraction of the open circuit voltage, which may not be fully achieved if the time constant is not accounted for. An equivalent circuit is used for dimensioning the transient behavior as well as the MFC output power. The use of a shunt resistor is typical in other fuel cells but, due to the small value of the MFC power, that would require the addition of an amplifier which would increase the power losses. With the reactor model, a trustworthy power estimate can be indirectly determined. The MPPT algorithm, a variation on perturb and observe, relies on the power estimate, by comparing two consecutive samples and determining the direction of the perturbation. Texas' BQ25504 boost converter was chosen to step-up the MFC voltage, supported by two rechargeable batteries of 1.25 V each. The batteries are used to start the converter but are dismissed after the conversion begins. The low power microprocessor was MSP430L092, which features low power and voltage consumption, a built-in analogue-to-digital converter (essential for voltage measurement) and PWM and sampling time control. A 59.4% overall efficiency was achieved for a 60 mL reactor, producing about 119 μW at maximum power point. The platform efficiency increases from 20 to roughly 60% when the input voltage increased from 50 to 350 mV; after 350 mV, the efficiency sharply drops to about 40%.

Besides this work, Jae Do Park was also close to the self-starting issue with PMS in [149]. The work addresses energy harvesting topologies capable of cold-start and resume after voltage drops. Specifically, the researchers propose a two-stage converter adequate for under 1 V power sources. This challenge is overcome by forcing the PMS to work in the unstable region with an approach

using a ringing-choke similar converter and corresponding to a variation of the flyback converter. The suggested system is capable of boosting voltages over 440 mV with a 25% efficiency rate, although not supporting heavy loads (for instance, 10 mW) [150].

Bond et al [151] also addressed self-starting, electrically isolated, energy harvesters for MFCs. The system follows the common configuration of double converters, a first stage boost converter and a second stage flyback in discontinuous conduction mode. The team chose not to implement MPPT algorithms to remove the need for continuous voltage or current monitoring and to decrease the space needed to accommodate every PCB component. This decision was also supported by the reliable MFC OCV value. An 80% efficiency for a 10-mW load was measured, while an increased load of 20 mW decreased the efficiency to 70%.

As work with anaerobic MFCs began producing more interesting figures for power production, Yamachita et al [152] studied ultra-low power energy harvesters for MFCs (UPEM), by comparing it with transformer-boost and MPPT-boost converter PMSs. The comparison was made by connecting the MFC with the UPEM and load module. The load modules were a temperature and humidity kit, a Bluetooth low-power transmission module and a carbon dioxide sensor. An evaluation of the UPEM and the MFC for transmitting data in short and long range (10 cm and 5.1 km) was also studied. The team justified the need for customizing the UPEM due to the excessive current extracted by commercially available boost converters, which do not take into account the negative correspondence between voltage and current in MFCs. The starting point is the use of a switching IC to manage the extracted current according to the available voltage: lower voltages lead to lower extracted currents and vice-versa. The research was directed at minimizing the consumption of the system and allowing for cold startp-up, which would not be possible with MPPT circuitry. The system can work from a 2.09 μW power source (starting at 0.2 V) with a single-step boosting of the input voltage to 3.55 V. The UPEM was found to surpass the performance of the transformer and MPPT PMSs', due to an accurate control of the extracted current. The use of the air-cathode single-chambered MFC (AS-MFC) allowed for data acquisition (temperature, humidity and carbon dioxide) as well as data transmission, both for short and for long range. BMFCs were also used as power sources, although having a lower performance than AS-MFCs. They could, however, be used for data acquisition and transmission, although with lower frequencies.

Table 3.3 is an organized dataset summarizing single MFC power management system custom developed topologies, with no simulations, stacks or BMFCs.

Table 3.3 – Table for single MFC power management system custom developed topologies. No simulations, stacks or BMFCs included.

		Power Management System Topology					Input Voltage (V)	Output Voltage (V)	Output Power (mW)	Effic. (%)	Ext. power (Y/N)	MPPT
Reference	Year	*Converter*	*Charge-pump Converter*	*Capacitor Converter*	*Transformer Converter*	*Other*						
[61]	2009					Capacitor only	0	0.5	0.152	100[i]	Y	N
[64]	2013					Capacitor only	0	≅ 0.35	≅ 0.25	100[i]	Y	N
[102]	2011					Capacitor only	0.7	2.5	0.73-0.78	100[i]	Y	N
[125]	2013					Capacitor only	0.3	0.48		90[i]	Y	N
[126]	2014					Capacitor only	0	0.45	0.76	63.6	Y	N
[80]	2012	Boost					0.34	2.5	5.20	42.1	Y	Y
[80]	2012					CP only	0.63	1	1.20	4.3[ii]	N	N
[76]	2011				T-Boost[iii]		0.475	2-7.5	0.1	58[ii]	N	N
[59]	2012				T-Boost		0.18	3.3	95	4.29[ii]	N	N
[84]	2012		CP-Boost[iv]				0.3	3.3	95	5.33[ii]	N	N
[82]	2012	Boost					0			<67.7[i]	Y	N
[85]	2014	S[v]-Flyback					0.3	2.2	22.37	46.1[i]	Y	Y
[81]	2012	S[v]-Boost					0.3	2.5		75.9[i]	Y	Y
[103,104]	2012	Boost					N/A	N/A	N/A	N/A	Y	Y
[86]	2014	Boost					0.36	2.5	85	17[ii]	Y	Y
[90]	2015	Boost					0.6-0.7	0.9-1.2	0.01	85[ii]	N	N
[87]	2015	Boost					0.3-0.72	2.5	0.25	58[ii]	Y	Y
[108]	2015		CP-Flyback[vi]				0.320	>3	0.538	71.2	N	Y
[91]	2016					Capacitor-flyback-boost	0	3	<1	55	Y	N
[97]	2019					Flyback-boost converter	0.44	5	No data	26	Y	N

[i] Circuit efficiency only, the external power not included in the efficiency determination.

[ii] Circuit efficiency and overall system efficiency, the external power is included in the efficiency determination or is nonexistent.

[iii] Transformer-boost converter

[iv] Charge-pump and boost converter

[v] Synchronous converter

[vi] Charge-pump and flyback converter

Microbial Fuel Cell groups for increased power availability

Single MFCs produce an average low voltage at their maximum power point. A way to overcome this challenge is to connect several reactors and create a larger fuel cell, built of smaller units. The series connection of several reactors helps to increase the maximum output voltage; a parallel connection improves current output.

The aforementioned connections, however, make the reactors vulnerable to voltage reversal [153]. This phenomenon is usually related with anode potential unbalances, a circumstance happening when substrate concentration is very low. Kim et al [154], in 2011, presented a solution which included the charging of several parallel connected supercapacitors and their serial discharge to an external generic load. The goal of the team was to prove that voltage reversal could be prevented and that the harvested power was adequate for application on boost converters. The voltage produced by the capacitor circuit was 340% higher than that produced by the circuit without capacitors, although the maximum current was cut to half with every capacitor.

The impact of power converter parameters was also a topic explored. Jae-Do Park teamed up with Zhiyong Ren, in [155] and [156], and proposed a system with a 2 layer DC/DC converter and an hysteresis controller, not self-sustainable, for controlling the switching frequency and the duty cycle when applied to a set of parallel connected MFCs. They found that low inductances and frequencies lead to high currents and low voltages; low duty cycles induce low currents and higher

voltages. Changes on the 3 parameters affect cathode potentials, while the anode potential remains stable.

Khaled et al, in 2013, proposed a voltage balancing circuit to prevent voltage reversal, either for series or parallel association of MFCs [157]. The suggested circuit is generally described in Figure 3.18, building upon the research in the Degrenne team [127]. The system determined the lowest power MFC and managed its connection to the serial/parallel association so that voltage reversal was prevented.

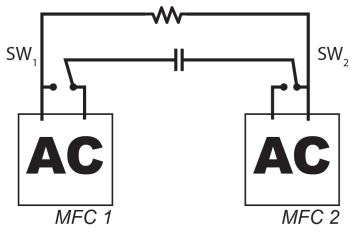

Figure 3.18 – Voltage balancing topology investigated in "Voltage Balancing Circuit for Energy Harvesting from a Stack of Serially-Connected Microbial Fuel Cells". "A" stands for the anode, the negative electrode, and "C" for the cathode, the positive electrode.

The cell reversal phenomena was also explored in 2014 by Boghani et al [158]: the starting point was to find if controlling the current sourced from a set/individual MFCs affected the onset of voltage reversal. The team investigated 3 topologies of connection, of which 2 were successful: individually connecting each MFC to a load forcing the cell to work at maximum power point (previously determined) and then, connecting the cells in series; and applying a hill climbing algorithm for current sourcing each MFC which are also connected in series. The latter was the most successful.

In 2015, Khaled et al [159], continuing the investigation on [157], determined that cells with different constructions and power points could be connected and fully explored for power production by using voltage balancing circuits together with an impedance matching MPPT algorithm. Although commercially available converters were capable of starting from the low output MFC voltage, the corresponding low currents were a burden. To overcome this challenge, the team tested a flyback topology in discontinuous conduction mode (DCM), so that the converter impedance could be independently controlled from the load conditions. The flyback topology in DCM was firstly presented by the team in [160].

Carreon-Bautista et al proceeded with the investigation of simultaneous energy harvesting from separate MFCs, proposing a time-multiplexing solution and an inductorless DC/DC converter to limit the system's power losses [161].

The system is not self-sustainable, outputs low voltages and is only capable of powering loads over 10 mW. As Zhang et al [142], this research also used a frequency modulation scheme, although associated with higher noise and electromagnetic interference; to limit this negative impact, a

large storage capacitor was used at the converter output. The power of each MFC was monitored individually [139] so that the highest power producing MFC was connected to a fractional open voltage MPPT stage. The stability of the DC/DC converter, which outputs low voltages, was discussed since not using an inductor increases the chances of input impedance mismatching. The research team argued that determining the system's efficiency without the power detection algorithm influence was acceptable because discrete clock switches were used.

Khaled et al [162], thinking about the high power requirements of sensors, the low power availability of a single MFC and the voltage reversal phenomena detected when using series connected MFC, explored the use of two MFC reactors by alternating the connection of one MFC to the MPPT algorithm while the other remained in open circuit. When the connected MFC voltage dropped below a defined value, that MFC is set to open circuit and the other is connected to the MPPT algorithm. The work also researched the functioning by using a batch of artificial wastewater (battery mode) and a continuous flow of artificial wastewater: both modes presented similar results.

The stack operation of MFCs and their improved was also addressed in 2017.

Boghani and Premier [163], with other researchers, teamed up to investigate sampled-time digital control applied to series connected MFC stacks, basing the voltage reversal prevention on the work in [158]. Even though successful, this work did not address the efficiency of the method, as the control mechanism was powered independently from the MFC stack. It cleared, however, that the measurement period of the OCV value for MFCs with Texas BQ25504 (256 ms) produced underestimated values.

The most relevant work related with the association of several MFCs for increased power production levels was developed by Nguyen et al [164] and is briefly summed with Figure 3.19. Also on the team was Lyne Woodward. The work reports the use of a switched capacitor-based converter to, using the fractional open voltage algorithm, achieve online MPP for each MFC individually. The PMS is then followed by a boost converter. An overall efficiency of 85% is reported, with voltage reversal prevention by disconnecting the lower voltage MFC whenever a threshold minimum voltage is achieved. The team identifies as future work the improvement on the number of MFCs participating in each cycle and the decrease of the time needed for capacitor charging.

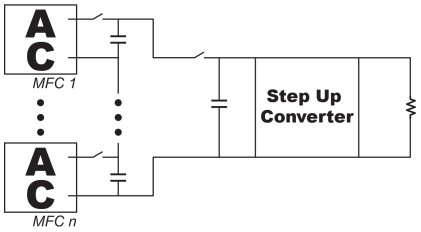

Figure 3.19 – Parallel association of multiple MFCs as proposed by Nguyen et al in [164].

Other research lines and real-world applications

The mainstream research topics gathered awareness for other investigations, not specifically related with power development but that could impact it. One such example is the influence of the substrate concentration on the performance of MPPT algorithms, namely on the multi-unit optimization method. This was addressed by Attarsharghi et al [165] (with Lyne Woodward cooperation), from a numerical analysis standpoint and strictly by simulation. It was found that a previous knowledge of the substrate concentration variation can limit the impact of this parameter on the power losses of an MFC.

Following the technological advances, some teams tried to present MFC technology as a viable solution for energy harvesting and water treatment at municipal wastewater treatment stations. Ge et al, first in 2015 [166] and then in 2016 [167], investigated the performance of a 200 L reactor (composed of 96 small double-chamber reactors) and a commercially available energy harvester from Texas Instruments, the BQ 25504 with municipal wastewater. The MFC energy was used to drive catholyte recirculation and the production cost of this experiment was compared to the cost of a small wastewater treatment facility.

Santoro et al [168] explored a different concept, where the MFC is conceptualized as the capacitor itself: specific cathode materials are used and a third electrode is added to decrease the equivalent series resistance. Figure 3.20 clearly depicts this approach. The MFC is then used by commuting between open circuit and a short discharge, with enough time for the MFC to return to its nominal OC voltage value. Nevertheless the validity of the work, further testing is necessary, since no information is provided regarding how long can such a methodology by applied and what is the behavior of the power profile.

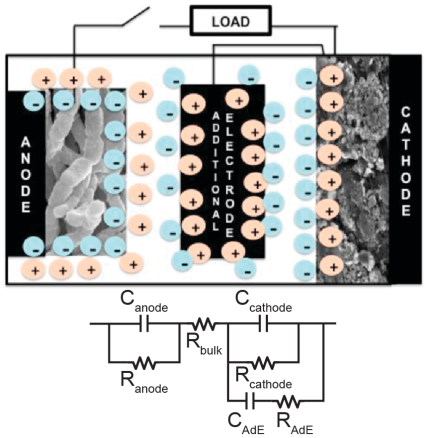

Figure 3.20 – MFC as a capacitor. Image rebuilt from figure 1 of [168] [†].

[†]Biosensors and Bioelectronics, Vol. 78, Carlo Santoro, Francesca Soavi, Alexey Serov, Catia Arbizzani, Plamen Atanassov, Self-powered supercapacitive microbial fuel cell: The ultimate way of boosting and harvesting power, Pages No. 229-235, Copyright (2015), with permission from Elsevier, License Number 4758160182827.

By 2017, the Alaraj team of [129] investigated how, in MFCs, power and other biochemical parameters develop when connecting the reactor to a resistor (continuous power extraction), to a resistor and a transistor (square-wave extraction) or to 2 resistors, one inductor and a transistor (triangular-wave extraction) [169]. Care was taken to keep the average current the same, irrespective of the extraction wave applied, so that power and energy could be compared between trials. The duty ratio and switching frequency were controlled by pulse width modulation and the MFC was operated in fed-batch mode, with an extraction wave kept for a full batch cycle and each experiment repeated twice. Results showed that the MFC lifespan, output power, energy extraction or chemical parameters were not dependent on the shape of extraction wave.

Later, in 2018, Wanderloid and Capitaine joined Morel and Pillonnet [170] to investigate coreless flyback transformers applied to microbial fuel cell reactors. The published research presents the work in [146], [147] with more detail, but referring to simulations and a generator mimicking a biological fuel cells.

On the matter of energy harvesters, Martinez et al [171] targeted the research on cold-starting a low power energy harvesting converter, although not aiming specifically for Microbial Fuel Cells. Cold starting an energy harvester is desirable to improve the autonomy of renewable power sources. By 2018, the low start-up voltage converters could follow one of three strategies: to focus on lowering the threshold voltage of transistors, to change the fabrication process to also lower the previous parameter or to explore forward body biasing of the transistors. Body biasing a transistor is achieved by using a fourth terminal on the transistor that is directly connected to its body (substrate). Changing the source to body voltage difference allows lowering the threshold voltage (increasing the leakage current) or lowering the leakage current (increasing the threshold voltage). Although not exploring this concept, the team proposes the use of an inductorless converter using an armstrong oscillator with a piezoelectric transformer and a normally ON depletion mode MOSFET. Exploring the body biasing of transistors may be of particular interest for MFCs, but piezoelectric transformers may have limited applicability as there is no mechanical stimulus to drive it.

Xu et al [172] presented a concept validation by proposing a constructed wetland-microbial fuel cell (CW-MFC), where the MFC is assembled as a benthic fuel cell, as the anode is buried in gravel and the cathode is left afloat on the surface of the reactor. In this work, the team recommends that the energy extraction process happens with capacitor engaged duty cycling (CDC) to decrease the energy losses associated with the large internal resistance of this devices. The CDC strategy consists of charging and discharging capacitors alternately, similarly to [119], [120], to improve the charge transfer from the fuel cell. The concept validation is achieved with reactors of around 2 L volume. Initial results show this as a valid strategy for energy harvesting in constructed wetland, as the maximum power density achieved was of 1.3 W/m^3, 40 times higher than the results in previous works [173].

14 years after the first works with MFCs and power management, a patent was submitted [174] in the United States for a power management system to be used with a low power input source, which, among others, can also be a microbial fuel cell. The patent was submitted, in the U.S.A., by 2019, by Asahi Kasei Microdevices Corporation, from Japan. The same patent had already been submitted in Japan, in 2010. The patent can be simplified to a boosting block and a control unit: the boosting block has an oscillation circuit, a boosting unit and a drive unit; the control section has two hysteresis comparators. Most of the technological developments so far researched are covered by this patent.

On the exclusive simulation domain, Umaz [150] presents a study of a PMS using the Texas Instruments low power boots converter, the BQ25505, two Ablic Inc. charge pumps, S-8880A20, and another boost converter from STMicroeletronics, the L6920DB. Tests of the proposed system's applicability were not conducted on actual MFCs, rather on their equivalent static model (a power source and a resistor in series). By using this commercially available options, Umaz achieved an estimated end-to-end efficiency of 53%.

In 2019, the use of MFCs with real wastewater were tackled by Su et al [175] and Santoro et al [176].

Double chamber MFCs, fed with piggery wastewater and colonized from anaerobic sludge were Su's responsibility. They were connected to a charge capacitor and studied regarding current decomposition in the frequency domain, by using Fast Fourier Transform (FFT). The retrieved results showed that the MFC current has AC and DC contributions, which can be associated with the exoelectrogen community behavior.

Santoro, on the other hand proposed a self-stratified microbial fuel cell operating with urine substrate. Compared with mixed composition wastewater, urine presents higher conductivities and concentration of dissolved ions, making it a more suitable candidate for MFC power production from naturally occurring substrates. The research presented with this paper treats the microbial reactor as a capacitor: the reactor design creates natural conditions for the development of a lower anaerobic region (the negative electrode, the anode equivalent in an MFC) and a more superficial aerobic section (positive electrode, the cathode equivalent in an MFC), partially exposed to oxygen. Such settings make urine ions effortlessly migrate, differently charging each of the electrodes. The capacitor was capable of recovering to its polarized state after a discharge was forced, although smaller discharging times produced higher power levels, around 1.20 mW per 0.01 seconds versus 0.65 mW per 5 seconds. Long term operation tests were also completed but the respective findings show that the recharge time between discharges needs careful planning to prevent decreased performance.

References

[1] L. Huang *et al.*, "Ultra low power wireless and energy harvesting technologies — An ideal combination," in *2010 IEEE International Conference on Communication Systems*, 2010, pp. 295–300.

[2] P. Smith, "Comparing Low-Power Wireless Technologies | DigiKey," 2011. [Online]. Available: http://www.digikey.com/en/articles/techzone/2011/aug/comparing-low-power-wireless-technologies. [Accessed: 03-Dec-2014].

[3] "Ultra low power wireless connectivity technology backgrounder." [Online]. Available: http://www.nordicsemi.com/eng/News/Press-Center/Press-Backgrounders/ULP-wireless-connectivity-backgrounder. [Accessed: 18-Oct-2014].

[4] M. Raju and M. Grazier, "ULP meets energy harvesting: a game-changing combination for design engineers," *TI, http//focus. ti. com/lit/wp/slyy018/slyy018. pdf*, 2008.

[5] A. Dewan, S. U. Ay, M. N. Karim, and H. Beyenal, "Alternative power sources for remote sensors: A review," *J. Power Sources*, vol. 245, pp. 129–143, Jan. 2014.

[6] Q. Mei, M. Shan, L. Liu, and J. M. Guerrero, "A Novel Improved Variable Step-Size Incremental-Resistance MPPT Method for PV Systems," *IEEE Trans. Ind. Electron.*, vol. 58, no. 6, pp. 2427–2434, 2011.

[7] J. W. Nilsson and S. A. Riedel, *Electric Circuits*. 2001.

[8] M. A. Taghikhani and I. Soltani, "A new maximum power point tracking control method of proton exchange membrane fuel cell's system," pp. 1–7.

[9] O. Lopez-Lapena, M. T. Penella, and M. Gasulla, "A New MPPT Method for Low-Power Solar Energy Harvesting," *IEEE Trans. Ind. Electron.*, vol. 57, no. 9, pp. 3129–3138, Sep. 2010.

[10] S. Jain and V. Agarwal, "Comparison of the performance of maximum power point tracking schemes applied to single-stage grid-connected photovoltaic systems," *IET Electr. Power Appl.*, no. Ccm, pp. 753–763, 2007.

[11] N. A. Kamarzaman and C. W. Tan, "A comprehensive review of maximum power point tracking algorithms for photovoltaic systems," *Renew. Sustain. Energy Rev.*, vol. 37, pp. 585–598, Sep. 2014.

[12] J. M. Enrique, E. Durán, M. Sidrach-de-Cardona, and J. M. Andújar, "Theoretical assessment of the maximum power point tracking efficiency of photovoltaic facilities with different converter topologies," *Sol. Energy*, vol. 81, no. 1, pp. 31–38, Jan. 2007.

[13] E. Rodrigues and R. Melício, “Simulation of a solar cell considering single-diode equivalent circuit model,” *... Renew. energies ...*, 2011.

[14] D. S. H. Chan and J. C. H. Phang, “Analytical methods for the extraction of solar-cell single- and double-diode model parameters from I-V characteristics,” *IEEE Trans. Electron Devices*, vol. 34, no. 2, pp. 286–293, Feb. 1987.

[15] H. Tsai, C. Tu, and Y. Su, “Development of generalized photovoltaic model using MATLAB/SIMULINK,” *Proc. world Congr. ...*, 2008.

[16] K. Ishaque, Z. Salam, and H. Taheri, “Simple, fast and accurate two-diode model for photovoltaic modules,” *Sol. Energy Mater. Sol. Cells*, vol. 95, no. 2, pp. 586–594, Feb. 2011.

[17] V. Salas, E. Olías, a. Barrado, and a. Lázaro, “Review of the maximum power point tracking algorithms for stand-alone photovoltaic systems,” *Sol. Energy Mater. Sol. Cells*, vol. 90, no. 11, pp. 1555–1578, Jul. 2006.

[18] Y. Jiang, “Adaptive step size with adaptive-perturbation-frequency digital MPPT controller for a single-sensor photovoltaic solar system,” *Power Electron. IEEE ...*, vol. 28, no. 7, pp. 3195–3205, 2013.

[19] G. Petrone, G. Spagnuolo, and M. Vitelli, “An analog technique for distributed MPPT PV applications,” *Ind. Electron. IEEE ...*, vol. 59, no. 12, pp. 4713–4722, 2012.

[20] M. Balato and M. Vitelli, “A new control strategy for the optimization of Distributed MPPT in PV applications,” *Int. J. Electr. Power Energy Syst.*, vol. 62, pp. 763–773, Nov. 2014.

[21] M. Muthuramalingam and P. S. Manoharan, “Comparative analysis of distributed MPPT controllers for partially shaded stand alone photovoltaic systems,” *Energy Convers. Manag.*, vol. 86, pp. 286–299, Oct. 2014.

[22] G. Carannante, C. Fraddanno, M. Pagano, and L. Piegari, “Experimental Performance of MPPT Algorithm for Photovoltaic Sources Subject to Inhomogeneous Insolation,” *IEEE Trans. Ind. Electron.*, vol. 56, no. 11, pp. 4374–4380, Nov. 2009.

[23] Z. Zhou, P. M. Holland, and P. Igic, “MPPT algorithm test on a photovoltaic emulating system constructed by a DC power supply and an indoor solar panel,” *Energy Convers. Manag.*, vol. 85, pp. 460–469, Sep. 2014.

[24] W. Xu, C. Mu, and J. Jin, “Novel Linear Iteration Maximum Power Point Tracking Algorithm for Photovoltaic Power Generation,” *IEEE Trans. Appl. Supercond.*, vol. 24, no. 5, pp. 1–6, Oct. 2014.

[25] W. Xiao and A. Elnosh, “Overview of maximum power point tracking technologies for photovoltaic power systems,” *IECON 2011-37th …*, pp. 3900–3905, 2011.

[26] S. K. Kollimalla and M. K. Mishra, “A Novel Adaptive P&O MPPT Algorithm Considering Sudden Changes in the Irradiance,” *IEEE Trans. Energy Convers.*, vol. 29, no. 3, pp. 602–610, Sep. 2014.

[27] L. Zhang, W. Hurley, and W. Wölfle, “A new approach to achieve maximum power point tracking for PV system with a variable inductor,” *Power Electron. IEEE …*, vol. 1, pp. 948–952, 2011.

[28] K.-H. Chao, “An extension theory-based maximum power tracker using a particle swarm optimization algorithm,” *Energy Convers. Manag.*, vol. 86, pp. 435–442, Oct. 2014.

[29] T. Esram and P. L. Chapman, “Comparison of Photovoltaic Array Maximum Power Point Tracking Techniques,” *IEEE Trans. Energy Convers.*, vol. 22, no. 2, pp. 439–449, Jun. 2007.

[30] B. N. Alajmi, K. H. Ahmed, S. J. Finney, and B. W. Williams, “Fuzzy-Logic-Control Approach of a Modified Hill-Climbing Method for Maximum Power Point in Microgrid Standalone Photovoltaic System,” *IEEE Trans. Power Electron.*, vol. 26, no. 4, pp. 1022–1030, Apr. 2011.

[31] R. Rahmani and M. Seyedmahmoudian, “Implementation of Fuzzy Logic Maximum Power Point Tracking Controller for Photovoltaic System,” *Am. J. Appl. Sci.*, vol. 10, no. 3, pp. 209–218, Mar. 2013.

[32] R. Rawat and S. S. Chandel, “Hill climbing techniques for tracking maximum power point in solar photovoltaic systems - a review,” *Spec. Issue Int. J. Sustain. Dev. Green Econ.*, vol. 2, no. 1–1, pp. 90–95, 2013.

[33] Y. Liu, M. Li, X. Ji, X. Luo, M. Wang, and Y. Zhang, “A comparative study of the maximum power point tracking methods for PV systems,” *Energy Convers. Manag.*, vol. 85, pp. 809–816, Sep. 2014.

[34] S.-T. Kim, T.-H. Bang, S.-C. Lee, and J.-W. Park, “Real-Time Maximum Power Point Tracking Method Based on Three Points Approximation by Digital Controller for PV System,” *J. Electr. Eng. Technol.*, vol. 9, no. 5, pp. 1447–1453, Sep. 2014.

[35] D. Sera, L. Mathe, and T. Kerekes, “On the perturb-and-observe and incremental conductance MPPT methods for PV systems,” *… , IEEE J.*, vol. 3, no. 3, pp. 1070–1078, 2013.

[36] D. Shmilovitz, “On the control of photovoltaic maximum power point tracker via output parameters,” *IEE Proc. - Electr. Power Appl.*, vol. 152, no. 2, p. 239, Mar. 2005.

[37] H. Wang, J. Park, and Z. Ren, “Active energy harvesting from microbial fuel cells at the maximum power point without using resistors.,” *Environ. Sci. Technol.*, vol. 46, no. 9, pp. 5247–52, May 2012.

[38] J.-D. Park and Z. Ren, “High efficiency energy harvesting from microbial fuel cells using a synchronous boost converter,” *J. Power Sources*, vol. 208, pp. 322–327, Jun. 2012.

[39] D. Molognoni *et al.*, “Reducing start-up time and minimizing energy losses of Microbial Fuel Cells using Maximum Power Point Tracking strategy,” *J. Power Sources*, vol. 269, pp. 403–411, Dec. 2014.

[40] H. Liu, B. E. Logan, and L. E. B. Liu Hong, “Electricity Generation Using an Air-Cathode Single Chamber Microbial Fuel Cell in the Presence and Absence of a Proton Exchange Membrane,” *Environ. Sci. Technol.*, vol. 38, no. 14, pp. 4040–4046, 2004.

[41] V. Watson and G. Estadt, “Graphite Fiber Brush Anodes for Increased Power Production in Air-Cathode Microbial Fuel Cells,” vol. 41, no. 9, pp. 3341–3346, 2007.

[42] B. E. Logan, *Microbial Fuel Cells*. Hoboken, NJ, USA: John Wiley & Sons, Inc., 2007.

[43] K. Scott *et al.*, *Microbial Electrochemical and Fuel Cells: Fundamentals and applications*, vol. 88. 2016.

[44] B. E. Logan, M. J. Wallack, K. Y. Kim, W. He, Y. Feng, and P. E. Saikaly, “Assessment of Microbial Fuel Cell Configurations and Power Densities,” *Environ. Sci. Technol. Lett.*, vol. 2, no. 8, pp. 206–214, 2015.

[45] S. Kazemi, M. Mohseni, and K. Fatih, “A systematic study of separators in air-breathing flat-plate microbial fuel cells-Part 1: Structure, properties, and performance correlations,” *Energies*, vol. 9, no. 2, pp. 1–18, 2016.

[46] Y. Ahn and B. E. Logan, “A multi-electrode continuous flow microbial fuel cell with separator electrode assembly design,” *Appl. Microbiol. Biotechnol.*, vol. 93, no. 5, pp. 2241–2248, 2012.

[47] S. Wu, W. He, W. Yang, Y. Ye, X. Huang, and B. E. Logan, “Combined carbon mesh and small graphite fiber brush anodes to enhance and stabilize power generation in microbial fuel cells treating domestic wastewater,” *J. Power Sources*, vol. 356, pp. 348–355, 2017.

[48] V. Lanas, Y. Ahn, and B. E. Logan, “Effects of carbon brush anode size and loading on microbial fuel cell performance in batch and continuous mode,” *J. Power Sources*, vol. 247, pp. 228–234, 2014.

[49] B. E. Logan *et al.*, “Microbial Fuel Cells: Methodology and Technology †,” *Environ. Sci. Technol.*, vol. 40, no. 17, pp. 5181–5192, Sep. 2006.

[50] B. E. Logan, “Essential data and techniques for conducting microbial fuel cell and other types of bioelectrochemical system experiments.,” *ChemSusChem*, vol. 5, no. 6, pp. 988–94, Jun. 2012.

[51] F. Zhao, R. C. T. Slade, and J. R. Varcoe, “Techniques for the study and development of microbial fuel cells: an electrochemical perspective,” *Chem. Soc. Rev.*, vol. 38, no. 7, p. 1926, Jul. 2009.

[52] G. K. S. Prakash, F. A. Viva, O. Bretschger, B. Yang, M. El-Naggar, and K. Nealson, “Inoculation procedures and characterization of membrane electrode assemblies for microbial fuel cells,” *J. Power Sources*, vol. 195, no. 1, pp. 111–117, 2010.

[53] F. Vicari *et al.*, “Influence of the methodology of inoculation in the performance of air-breathing microbial fuel cells,” *J. Electroanal. Chem.*, vol. 803, no. September, pp. 81–88, 2017.

[54] V. J. Watson and B. E. Logan, “Analysis of polarization methods for elimination of power overshoot in microbial fuel cells,” *Electrochem. commun.*, vol. 13, no. 1, pp. 54–56, 2011.

[55] H. C. Boghani, J. R. Kim, R. M. Dinsdale, A. J. Guwy, and G. C. Premier, “Control of power sourced from a microbial fuel cell reduces its start-up time and increases bioelectrochemical activity.,” *Bioresour. Technol.*, vol. 140, pp. 277–85, Jul. 2013.

[56] J. Winfield, I. Ieropoulos, J. Greenman, and J. Dennis, “The overshoot phenomenon as a function of internal resistance in microbial fuel cells,” *Bioelectrochemistry*, vol. 81, no. 1, pp. 22–27, 2011.

[57] Y. Hong, D. F. Call, C. M. Werner, and B. E. Logan, “Adaptation to high current using low external resistances eliminates power overshoot in microbial fuel cells,” *Biosens. Bioelectron.*, vol. 28, no. 1, pp. 71–76, 2011.

[58] M. Zhou, M. Chi, J. Luo, H. He, and T. Jin, “An overview of electrode materials in microbial fuel cells,” *J. Power Sources*, vol. 196, no. 10, pp. 4427–4435, 2011.

[59] B. Min, S. Cheng, and B. E. Logan, “Electricity generation using membrane and salt bridge microbial fuel cells,” *Water Res.*, 2005.

[60] B. Min and B. E. Logan, “Continuous electricity generation from domestic wastewater and organic substrates in a flat plate microbial fuel cell.,” *Environ. Sci. Technol.*, vol. 38, no. 21, pp. 5809–14, Nov. 2004.

[61] J. K. Jang *et al.*, “Construction and operation of a novel mediator- and membrane-less microbial fuel cell,” *Process Biochem.*, vol. 39, no. 8, pp. 1007–1012, Apr. 2004.

[62] Z. He, S. Minteer, and L. Angenent, “Electricity generation from artificial wastewater using an upflow microbial fuel cell,” *Environ. Sci. ...*, 2005.

[63] P. Aelterman, K. Rabaey, and W. Verstraete, “Continuous Electricity Generation at High Voltages and Currents Using Stacked Microbial Fuel Cells,” vol. 40, no. 10, pp. 3388–3394, 2006.

[64] H. Liu, R. Ramnarayanan, and B. E. Logan, “Production of Electricity during Wastewater Treatment Using a Single Chamber Microbial Fuel Cell,” *Environ. Sci. Technol.*, vol. 38, no. 7, pp. 2281–2285, Apr. 2004.

[65] A. Fraiwan, S. Mukherjee, S. Sundermier, and S. Choi, “A microfabricated paper-based microbial fuel cell,” *Proc. IEEE Int. Conf. Micro Electro Mech. Syst.*, no. i, pp. 809–812, 2013.

[66] C. Dumas, A. Mollica, D. Féron, R. Basséguy, L. Etcheverry, and A. Bergel, “Marine microbial fuel cell: Use of stainless steel electrodes as anode and cathode materials,” *Electrochim. Acta*, vol. 53, no. 2, pp. 468–473, 2007.

[67] P. Namour, M. Picot, L. Lapinsonnière, F. Barrière, and N. Jaffrezic-Renault, “Energy harvesting from river sediment using a microbial fuel cell: preliminary results.,” *Sensors & Transducers*, vol. 27, no. SI, pp. 290–294, 2014.

[68] N. Tang, W. Hong, T. Ewing, H. Beyenal, J. H. Kim, and D. Heo, “A self-sustainable power management system for reliable power scaling up of sediment microbial fuel cells,” *IEEE Trans. Power Electron.*, vol. 30, no. 9, pp. 4626–4632, 2015.

[69] G. Martins, L. Peixoto, D. C. Ribeiro, P. Parpot, A. G. Brito, and R. Nogueira, “Towards implementation of a benthic microbial fuel cell in lake Furnas (Azores): phylogenetic affiliation and electrochemical activity of sediment bacteria.,” *Bioelectrochemistry*, vol. 78, no. 1, pp. 67–71, Apr. 2010.

[70] Y. R. J. Thomas, M. Picot, A. Carer, O. Berder, O. Sentieys, and F. Barrière, “A single sediment-microbial fuel cell powering a wireless telecommunication system,” *J. Power Sources*, vol. 241, pp. 703–708, 2013.

[71] I. Bardarov, Y. Hubenova, and M. Mitov, “Sediment microbial fuel cells as power sources for small electrical consumers,” *Chemistry (Easton).*, vol. 24, no. 3, pp. 433–440, 2015.

[72] M. Rosenbaum, Z. He, and L. T. Angenent, “Light energy to bioelectricity: photosynthetic microbial fuel cells.,” *Curr. Opin. Biotechnol.*, vol. 21, no. 3, pp. 259–64, Jun. 2010.

[73] D. Pant, G. Van Bogaert, L. Diels, and K. Vanbroekhoven, “A review of the substrates used in microbial fuel cells (MFCs) for sustainable energy production,” *Bioresour. Technol.*, vol. 101, no. 6, pp. 1533–1543, Mar. 2010.

[74] B. H. Kim *et al.*, “Enrichment of microbial community generating electricity using a fuel-cell-type electrochemical cell,” *Appl. Microbiol. Biotechnol.*, vol. 63, no. 6, pp. 672–681, 2004.

[75] B. E. Logan, “Exoelectrogenic bacteria that power microbial fuel cells.,” *Nat. Rev. Microbiol.*, vol. 7, no. 5, pp. 375–81, May 2009.

[76] G. Pasternak, J. Greenman, and I. Ieropoulos, “Regeneration of the power performance of cathodes affected by biofouling,” *Appl. Energy*, 2016.

[77] H. Yang, M. Zhou, M. Liu, W. Yang, and T. Gu, “Microbial fuel cells for biosensor applications,” *Biotechnol. Lett.*, vol. 37, no. 12, pp. 2357–2364, 2015.

[78] I. S. Chang *et al.*, “Continuous determination of biochemical oxygen demand using microbial fuel cell type biosensor,” *Biosens. Bioelectron.*, vol. 19, no. 6, pp. 607–613, 2004.

[79] B. H. Kim, I. S. Chang, G. C. Gil, H. S. Park, and H. J. Kim, “Novel BOD (Biochemical Oxygen Demand) sensor using mediator-less microbial fuel cell,” *Biotechnol. Lett.*, vol. 25, no. 7, pp. 541–545, 2003.

[80] B. H. Kim, I. S. Chang, and H. Moon, “Microbial Fuel Cell-Type Biochemical Oxygen Demand Sensor,” *Encycl. Sensors*, vol. X, pp. 1–12, 2006.

[81] R. Palasuek, T. Seesa-Ard, C. Kunarak, and T. Kerdcharoen, “Electronic nose for water monitoring: The relationship between wastewater quality indicators and odor,” *ECTI-CON 2015 - 2015 12th Int. Conf. Electr. Eng. Comput. Telecommun. Inf. Technol.*, 2015.

[82] D. Brunelli, P. Tosato, and M. Rossi, “Microbial fuel cell as a biosensor and a power source for flora health monitoring,” *Proc. IEEE Sensors*, no. 2, 2017.

[83] I. Gajda *et al.*, “Water formation at the cathode and sodium recovery using Microbial Fuel Cells (MFCs),” *Sustain. Energy Technol. Assessments*, vol. 7, pp. 187–194, 2014.

[84] K. Agrawal, N. Bhardwaj, B. Kumar, and V. Chaturvedi, *Bioremediation of Wastes*. Elsevier Inc., 2019.

[85] S.-H. Liu, C.-Y. Lai, P.-H. Chang, C.-W. Lin, and Y.-H. Chen, “Enhancing copper recovery and electricity generation from wastewater using low-cost membrane-less microbial fuel cell with a carbonized clay cup as cathode,” *J. Clean. Prod.*, no. xxxx, p. 119118, 2019.

[86] S. Das, *Microbial Biodegradation and Bioremediation*. 2014.

[87] F. Zhang, L. Tian, and Z. He, "Powering a wireless temperature sensor using sediment microbial fuel cells with vertical arrangement of electrodes," *J. Power Sources*, vol. 196, no. 22, pp. 9568–9573, 2011.

[88] Q. Zheng, L. Xiong, B. Mo, W. Lu, S. Kim, and Z. Wang, "Temperature and Humidity Sensor Powered by an Individual Microbial Fuel Cell in a Power Management System," *Sensors*, vol. 15, no. 9, pp. 23126–23144, 2015.

[89] F. Yang, K.-C. Wang, and Y. Huang, "Energy-neutral communication protocol for based wireless sensor network," *IEEE Sens. J.*, vol. 15, no. 4, pp. 2306–2315, 2015.

[90] P. Serra and A. V. Espirito-Santo, "Harvesting Energy from Microbial Fuel Cells: Powering Wireless Sensor Networks Operating in Wastewater Treatment Plants," in *Biologically-Inspired Energy Harvesting through Wireless Sensor Technologies*, Hershey, PA, USA: IGI Global, 2016, pp. 121–171.

[91] A. Espírito-Santo, P. Sérra, S. Albuquerque, B. Ribeiro, F. Santos, and J. Páscoa, "Low-power smart sensing in energy and water systems integration," in *2017 IEEE International Workshop on Measurement and Networking, M and N 2017 - Proceedings*, 2017.

[92] A. Pietrelli, V. Ferrara, A. Micangeli, and L. Ube, "Efficient Energy Harvesting for Microbial Fuel Cell dedicated to Wireless Sensor Network," *2015 XVIII AISEM Annu. Conf. Effic.*, pp. 1–4, 2015.

[93] A. Shantaram, H. Beyenal, R. Raajan, A. Veluchamy, and Z. Lewandowski, "Wireless sensors powered by microbial fuel cells.," *Environ. Sci. Technol.*, vol. 39, no. 13, pp. 5037–5042, 2005.

[94] V. Raghunathan and P. P. H. Chou, "Design and power management of energy harvesting embedded systems," *Proc. 2006 Int. Symp. Low power Electron. Des. - ISLPED '06*, p. 369, 2006.

[95] S. Wilkinson, "`Gastrobots' - benefits and challenges of microbial fuel cells in food powered robot applications," *Auton. Robots*, 2000.

[96] I. . Ieropoulos, J. Greenman, and C. Melhuish, "Imitation metabolism: energy autonomy in biologically inspired robots.," *Proc. 2nd Int. Symp. imitation Anim. artifacts*, 2003.

[97] I. Ieropoulos, I. Ieropoulos, C. Melhuish, and J. Greenman, "Energetically Autonomous Robots," *Proc. 8TH Intell. Auton. Syst. Conf. (IAS8*, pp. 128--135, 2004.

[98] I. Ieropoulos, C. Melhuish, and J. Greenman, “Artificial metabolism: Towards true energetic autonomy in artificial life,” in *Lecture Notes in Artificial Intelligence (Subseries of Lecture Notes in Computer Science)*, 2003.

[99] I. Ieropoulos, C. Melhuish, J. Greenman, and I. Horsfield, “EcoBot-II: An artificial agent with a natural metabolism,” in *International Journal of Advanced Robotic Systems*, 2005.

[100] C. Melhuish, I. Ieropoulos, J. Greenman, and I. Horsfield, “Energetically autonomous robots: Food for thought,” *Auton. Robots*, vol. 21, no. 3, pp. 187–198, Nov. 2006.

[101] I. Ieropoulos, J. Greenman, C. Melhuish, and I. Horsfield, “EcoBot-III: a robot with guts,” in *Artificial Life XII: Proceedings of the 12th International Conference on the Synthesis and Simulation of Living Systems, ALIFE 2010*, 2010, pp. 733–740.

[102] G. Papaharalabos *et al.*, “Increased power output from micro porous layer (MPL) cathode microbial fuel cells (MFC),” in *International Journal of Hydrogen Energy*, 2013.

[103] I. A. Ieropoulos, J. Greenman, and C. Melhuish, “Miniature microbial fuel cells and stacks for urine utilisation,” *Int. J. Hydrogen Energy*, 2013.

[104] H. C. Boghani, J. R. Kim, I. Michie, R. M. Dinsdale, A. J. Guwy, and G. C. Premier, “Maximum power point tracking on microbial fuel cells can halve the start-up time, increase their performance and avoid voltage reversal,” *H2FC SUPERGEN Researcher Conference*. 2013.

[105] M. P. D. Howe, H. M. Malcolm, and D. S. Dobson, “MANGANESE AND ITS COMPOUNDS: ENVIRONMENTAL ASPECTS First draft prepared.”

[106] L. M. Tender *et al.*, “The first demonstration of a microbial fuel cell as a viable power supply: Powering a meteorological buoy,” *J. Power Sources*, 2008.

[107] A. Meehan, H. Gao, and Z. Lewandowski, “Energy harvest with microbial fuel cell and power management system,” *2009 IEEE Energy Convers. Congr. Expo. ECCE 2009*, pp. 3558–3563, 2009.

[108] A. Meehan, H. Gao, and Z. Lewandowski, “Energy Harvesting With Microbial Fuel Cell and Power Management System,” *IEEE Trans. Power Electron.*, vol. 26, no. 1, pp. 176–181, Jan. 2011.

[109] C. Donovan, A. Dewan, H. Peng, D. Heo, and H. Beyenal, “Power management system for a 2.5 W remote sensor powered by a sediment microbial fuel cell,” *J. Power Sources*, 2011.

[110] E. J. Gardel, M. E. Nielsen, P. T. Grisdela, and P. R. Girguis, “Duty cycling influences current generation in multi-anode environmental microbial fuel cells,” *Environ. Sci. Technol.*, 2012.

[111] C. Donovan, A. Dewan, D. Heo, Z. Lewandowski, and H. Beyenal, “Sediment microbial fuel cell powering a submersible ultrasonic receiver: New approach to remote monitoring,” *J. Power Sources*, 2013.

[112] F. T. Lin, Y. C. Kuo, J. C. Hsieh, H. Y. Tsai, Y. Te Liao, and H. C. Lee, “A Self-Powering Wireless Environment Monitoring System Using Soil Energy,” *IEEE Sens. J.*, vol. 15, no. 7, pp. 3751–3758, 2015.

[113] T. Chailloux, A. Capitaine, B. Erable, and G. Pillonnet, “Autonomous Sensor Node Powered by CM-Scale Benthic Microbial Fuel Cell and Low-Cost and Off-the-Shelf Components,” *Energy Harvest. Syst.*, vol. 3, no. 3, pp. 205–212, 2016.

[114] D. Zhang, Y. Zhu, W. Pedrycz, and Y. Guo, “A terrestrial microbial fuel cell for powering a single-hop wireless sensor network,” *Int. J. Mol. Sci.*, vol. 17, no. 5, pp. 1–13, 2016.

[115] F. Yang, D. Zhang, T. Shimotori, K.-C. Wang, and Y. Huang, “Study of transformer-based power management system and its performance optimization for microbial fuel cells,” *J. Power Sources*, vol. 205, pp. 86–92, May 2012.

[116] E. Sudirjo, P. De Jager, C. J. N. Buisman, and D. P. B. T. B. Strik, “Performance and long distance data acquisition via LoRa technology of a tubular plant microbial fuel cell located in a paddy field in West Kalimantan, Indonesia,” *Sensors (Switzerland)*, vol. 19, no. 21, 2019.

[117] A. Dewan, H. Beyenal, and Z. Lewandowski, “Intermittent Energy Harvesting Improves the Performance of Microbial Fuel Cells,” *Environ. Sci. Technol.*, vol. 43, no. 12, pp. 4600–4605, Jun. 2009.

[118] A. Dewan, C. Donovan, D. Heo, and H. Beyenal, “Evaluating the performance of microbial fuel cells powering electronic devices,” *J. Power Sources*, vol. 195, no. 1, pp. 90–96, 2010.

[119] P. Liang, W. Wu, J. Wei, L. Yuan, X. Xia, and X. Huang, “Alternate charging and discharging of capacitor to enhance the electron production of bioelectrochemical systems.,” *Environ. Sci. Technol.*, vol. 45, no. 15, pp. 6647–53, Aug. 2011.

[120] S. Ren, X. Xia, L. Yuan, P. Liang, and X. Huang, “Enhancing charge harvest from microbial fuel cells by controlling the charging and discharging frequency of capacitors.,” *Bioresour. Technol.*, vol. 146, pp. 812–815, Oct. 2013.

[121] J. Coronado, M. Perrier, and B. Tartakovsky, “Pulse-width modulated external resistance increases the microbial fuel cell power output,” *Bioresour. Technol.*, vol. 147, pp. 65–70, 2013.

[122] L. Woodward and B. Tartakovsky, “Maximizing power production in a stack of microbial fuel cells using multiunit optimization method,” *Biotechnol. …*, 2009.

[123] L. Woodward, M. Perrier, B. Srinivasan, R. P. Pinto, and B. Tartakovsky, “Comparison of real-time methods for maximizing power output in microbial fuel cells,” *AIChE J.*, vol. 56, no. 10, pp. 2742–2750, Oct. 2010.

[124] G. C. Premier, J. R. Kim, I. Michie, R. M. Dinsdale, and A. J. Guwy, “Automatic control of load increases power and efficiency in a microbial fuel cell,” *J. Power Sources*, vol. 196, no. 4, pp. 2013–2019, 2011.

[125] D. Y. Lyon, F. Buret, T. M. Vogel, and J. M. Monier, “Is resistance futile? Changing external resistance does not improve microbial fuel cell performance,” *Bioelectrochemistry*, 2010.

[126] R. P. Pinto, B. Srinivasan, S. R. Uiot, and B. Tartakovsky, “The effect of real-time external resistance optimization on microbial fuel cell performance,” *Water Res.*, 2011.

[127] N. Degrenne, F. Buret, B. Allard, and P. Bevilacqua, “Electrical energy generation from a large number of microbial fuel cells operating at maximum power point electrical load,” *J. Power Sources*, vol. 205, pp. 188–193, May 2012.

[128] Y. E. Song *et al.*, “Maximum Power Point Tracking to Increase the Power Production and Treatment Efficiency of a Continuously Operated Flat-Plate Microbial Fuel Cell,” *Energy Technol.*, 2016.

[129] M. Alaraj, M. Radenkovic, and J. Do Park, “Intelligent energy harvesting scheme for microbial fuel cells: Maximum power point tracking and voltage overshoot avoidance,” *J. Power Sources*, 2017.

[130] S. Adami, N. Degrenne, C. Vollaire, B. Allard, F. Buret, and F. Costa, “Autonomous Ultra-Low Power DC / DC Converter for Microbial Fuel Cells,” pp. 398–401, 2011.

[131] N. Degrenne, B. Allard, F. F. Buret, F. Morel, S.-E. Adami, and D. Labrousse, “Comparison of 3 self-starting step-up DC: DC converter topologies for harvesting energy from low-voltage and low-power microbial fuel cells,” *Proc. 2011 14th Eur. Conf. Power Electron. Appl.*, pp. 1–10, 2011.

[132] N. Degrenne *et al.*, "Self-Starting DC : DC Boost Converter for Low-Power and Low-Voltage Microbial Electric Generators To cite this version : Self-Starting DC : DC Boost Converter for Low-Power and Low-Voltage Microbial Electric Generators," *Ecce*, pp. 889–896, 2011.

[133] J.-D. Park and Z. Ren, "Efficient energy harvester for microbial fuel cells using DC/DC converters," *2011 IEEE Energy Convers. Congr. Expo.*, pp. 3852–3858, Sep. 2011.

[134] H. Wang, Z. Ren, and J.-D. Park, "Power electronic converters for microbial fuel cell energy extraction: Effects of inductance, duty ratio, and switching frequency," *J. Power Sources*, vol. 220, pp. 89–94, Dec. 2012.

[135] F. Grondin, M. Perrier, and B. Tartakovsky, "Microbial fuel cell operation with intermittent connection of the electrical load," *J. Power Sources*, vol. 208, pp. 18–23, 2012.

[136] D. Zhang, F. Yang, T. Shimotori, K. C. Wang, and Y. Huang, "Performance evaluation of power management systems in microbial fuel cell-based energy harvesting applications for driving small electronic devices," *J. Power Sources*, 2012.

[137] M. Alaraj, Z. J. Ren, and J. Do Park, "Microbial fuel cell energy harvesting using synchronous flyback converter," *J. Power Sources*, 2014.

[138] C. Erbay, S. Carreon-Bautista, E. Sanchez-Sinencio, and A. Han, "High Performance Monolithic Power Management System with Dynamic Maximum Power Point Tracking for Microbial Fuel Cells," *Environ. Sci. Technol.*, vol. 48, no. 23, pp. 13992–13999, Dec. 2014.

[139] S. Carreon-Bautista, C. Erbay, A. Han, and E. Sánchez-Sinencio, "Power Management System With Integrated Maximum Power Extraction Algorithm for Microbial Fuel Cells," *IEEE Trans. Energy Convers.*, vol. 15, no. 1, pp. 262-, 2015.

[140] M. Ayaz, E. Farjah, and T. Ghanbari, "A novel self-starting ultra low-power and low-voltage two-stage DC-DC boost converter for microbial energy harvesting," *6th Annu. Int. Power Electron. Drive Syst. Technol. Conf. PEDSTC 2015*, pp. 498–502, 2015.

[141] H. Wang, J. Park, and Z. J. Ren, "Practical Energy Harvesting for Microbial Fuel Cells: A Review.," *Environ. Sci. Technol.*, vol. 49, pp. 3267–3277, 2015.

[142] X. Zhang, H. Ren, S. Pyo, J.-I. Lee, J. Kim, and J. Chae, "A High-Efficiency DC-DC Boost Converter for a Miniaturized Microbial Fuel Cell," *IEEE Trans. Power Electron.*, vol. 30, no. 4, pp. 2041–2049, 2015.

[143] E. Dallago, A. L. Barnabei, A. Liberale, G. Torelli, and G. Venchi, "A 300-mV low-power management system for energy harvesting applications," *IEEE Trans. Power Electron.*, vol. 31, no. 3, pp. 2273–2281, 2016.

[144] A. Capitaine, G. Pillonnet, T. Chailloux, F. Khaled, O. Ondel, and B. Allard, “Loss analysis of flyback in discontinuous conduction mode for sub-mW harvesting systems,” *14th IEEE Int. NEWCAS Conf. NEWCAS 2016*, pp. 1–4, 2016.

[145] F. L. Lobo, X. Wang, and Z. J. Ren, “Energy harvesting influences electrochemical performance of microbial fuel cells,” *J. Power Sources*, vol. 356, pp. 356–364, 2017.

[146] A. Capitaine, G. Pillonnet, T. Chailloux, A. Morel, and B. Allard, “Impact of switching of the electrical harvesting interface on microbial fuel cell losses,” *Proc. IEEE Sensors*, vol. 2017-Decem, pp. 1–3, 2017.

[147] Y. Wanderoild, A. Capitaine, A. Morel, and G. Pillonnet, “100 Mw Coreless Flyback Converter for Microbial Fuel Cells Energy Harvesting,” *Proc. - 2017 1st New Gener. CAS, NGCAS 2017*, pp. 33–36, 2017.

[148] M. Alaraj and J. Do Park, “Net power positive maximum power point tracking energy harvesting system for microbial fuel cell,” *J. Power Sources*, vol. 418, no. February, pp. 225–232, 2019.

[149] J. Do Park and S. Lee, “Single-transistor sub-1-V self-startup voltage boost energy harvesting system for microbial fuel cells,” *J. Power Sources*, vol. 418, no. February, pp. 90–97, 2019.

[150] R. Umaz, “A Power Management System for Microbial Fuel Cells with 53.02% Peak End-to-end Efficiency,” *IEEE Trans. Circuits Syst. II Express Briefs*, vol. 7747, no. c, pp. 1–1, 2019.

[151] M. Bond, M. Kerber, M. Murphy, L. Hsu, D. B. Chadwick, and Y. M. Arias-Thode, “Electrically Isolated Energy Harvesting,” *Ocean. 2019 - Marseille*, pp. 1–8, 2019.

[152] T. Yamashita, T. Hayashi, H. Iwasaki, M. Awatsu, and H. Yokoyama, “Ultra-low-power energy harvester for microbial fuel cells and its application to environmental sensing and long-range wireless data transmission,” *J. Power Sources*, 2019.

[153] S. E. Oh and B. E. Logan, “Voltage reversal during microbial fuel cell stack operation,” *J. Power Sources*, 2007.

[154] Y. Kim, M. C. Hatzell, A. J. Hutchinson, and B. E. Logan, “Capturing power at higher voltages from arrays of microbial fuel cells without voltage reversal,” *Energy Environ. Sci.*, vol. 4, no. 11, p. 4662, 2011.

[155] J.-D. Do Park and Z. Ren, “Hysteresis-controller-based energy harvesting scheme for microbial fuel cells with parallel operation capability,” *IEEE Trans. Energy Convers.*, vol. 27, no. 3, pp. 715–724, May 2012.

[156] J.-D. Do Park and Z. Ren, “Hysteresis controller based maximum power point tracking energy harvesting system for microbial fuel cells,” *J. Power Sources*, vol. 27, no. 3, pp. 715–724, May 2012.

[157] F. Khaled, O. Ondel, B. Allard, and N. Degrenne, “Voltage balancing circuit for energy harvesting from a stack of serially-connected Microbial Fuel Cells,” *2013 IEEE ECCE Asia Downunder - 5th IEEE Annu. Int. Energy Convers. Congr. Exhib. IEEE ECCE Asia 2013*, pp. 392–397, 2013.

[158] H. C. Boghani *et al.*, “Controlling for peak power extraction from microbial fuel cells can increase stack voltage and avoid cell reversal,” *J. Power Sources*, vol. 269, pp. 363–369, Dec. 2014.

[159] F. Khaled, O. Ondel, and B. Allard, “Optimal energy harvesting from serially connected microbial fuel cells,” *IEEE Trans. Ind. Electron.*, vol. 62, no. 6, pp. 3508–3515, 2015.

[160] F. Khaled, B. Allard, O. Ondel, and C. Vollaire, “Autonomous Flyback Converter for Energy Harvesting from Microbial Fuel Cells,” *Energy Harvest. Syst.*, vol. 3, no. 2, 2015.

[161] S. Carreon-Bautista, S. Member, C. Erbay, S. Member, A. Han, and E. Sanchez-Sinencio, “An Inductorless DC-DC Converter for an Energy Aware Power Management Unit Aimed at Microbial Fuel Cell Arrays,” *IEEE J. Emerg. Sel. Top. Power Electron.*, vol. 3, no. 4, pp. 1109–1121, 2015.

[162] F. Khaled, O. Ondel, and B. Allard, “Microbial fuel cells as power supply of a low-power temperature sensor,” *J. Power Sources*, vol. 306, pp. 354–360, 2016.

[163] H. C. Boghani, R. M. Dinsdale, A. J. Guwy, and G. C. Premier, “Sampled-time control of a microbial fuel cell stack,” *J. Power Sources*, 2017.

[164] C. L. Nguyen, B. Tartakovsky, and L. Woodward, “Harvesting Energy from Multiple Microbial Fuel Cells with a High-Conversion Efficiency Power Management System,” *ACS Omega*, vol. 4, pp. 18978–18986, 2019.

[165] S. Attarsharghi, L. Woodward, and O. Akhrif, “An improved maximum power extraction scheme for microbial fuel cells,” in *IECON Proceedings (Industrial Electronics Conference)*, 2012.

[166] Z. Ge, L. Wu, F. Zhang, and Z. He, “Energy extraction from a large-scale microbial fuel cell system treating municipal wastewater,” *J. Power Sources*, vol. 297, no. AUGUST 2015, pp. 260–264, 2015.

[167] Z. Ge and Z. He, “Long-term performance of a 200 liter modularized microbial fuel cell system treating municipal wastewater: Treatment, energy, and cost,” *Environ. Sci. Water Res. Technol.*, 2016.

[168] C. Santoro, F. Soavi, A. Serov, C. Arbizzani, and P. Atanassov, “Self-powered supercapacitive microbial fuel cell: The ultimate way of boosting and harvesting power,” *Biosens. Bioelectron.*, vol. 78, pp. 229–235, 2016.

[169] M. Alaraj, S. Feng, T. M. Roane, and J. Do Park, “Effect of power shape on energy extraction from microbial fuel cell,” *J. Power Sources*, 2017.

[170] Y. Wanderoild, A. Morel, A. Capitaine, and G. Pillonnet, “A 50 μw microbial fuel cell isolated energy harvesting interface based on air coupled inductors,” *J. Low Power Electron.*, vol. 14, no. 1, pp. 170–178, 2018.

[171] T. Martinez, G. Pillonnet, and F. Costa, “A 15-mV Inductor-Less Start-up Converter Using a Piezoelectric Transformer for Energy Harvesting Applications,” *IEEE Trans. Power Electron.*, vol. 33, no. 3, pp. 2241–2253, 2018.

[172] L. Xu, B. Wang, X. Liu, W. Yu, and Y. Zhao, “Maximizing the energy harvest from a microbial fuel cell embedded in a constructed wetland,” *Appl. Energy*, 2018.

[173] P. Srivastava, S. Dwivedi, N. Kumar, R. Abbassi, V. Garaniya, and A. K. Yadav, “Performance assessment of aeration and radial oxygen loss assisted cathode based integrated constructed wetland-microbial fuel cell systems,” *Bioresour. Technol.*, 2017.

[174] K. Microdevices, “(19) United States (43),” 2019.

[175] J. C. Su, S. C. Tang, P. J. Su, and J. J. Su, “Real-time monitoring of micro-electricity generation through the voltage across a storage capacitor charged by a simple microbial fuel cell reactor with fast Fourier transform,” *Energies*, vol. 12, no. 13, 2019.

[176] C. Santoro, X. A. Walter, F. Soavi, J. Greenman, and I. Ieropoulos, “Self-stratified and self-powered micro-supercapacitor integrated into a microbial fuel cell operating in human urine,” *Electrochim. Acta*, vol. 307, pp. 241–252, 2019.

Chapter 4

Extracting power from Microbial Fuel Cells

General overview

A thorough review of the state-of-the-art on Microbial Fuel Cells has revealed significant advances in this technology.

The work here presented builds upon that review, adding a different point of view on the results. The main goal of this section is to provide experimental data substantiating that MFCs can be used as independent and autonomous power sources, albeit in laboratory-controlled conditions. Materials are presented and discussed, with methods and results being attended in each particular trial.

The experimented reactor constructions are the first topic, as they are common to every trial. They are also the building blocks of the studies, together with electrode materials and the substrate composition. Each reactor generation was evaluated regarding their leak-tightness (capability to withstand hydraulic pressure). Electrodes were updated in each generation according to the available materials and provisional state-of-the-art researches. Substrate composition was controlled only when the reactor design was finished, having tested three different compositions. The discussion of results begins by showing data related to exoelectrogenic biofilm development and biofilm transfer. Afterward, specific parameters are investigated so as to determine:

1. Influence of internal variables on power production:
    1.1. pH, ORP, DO and temperature;
    1.2. Biofilm age and cathode biofouling;
    1.3. Multi-cycle *vs.* single-cycle substrate feeding
2. Influence of external variables on power production:
    2.1. Continuous load;
    2.2. Steady state model development;
    2.3. Transient model development;
    2.4. Increasing the reactor size;
    2.5. Series and parallel association;
    2.6. Commuted load;
    2.7. Load and capacitor connection influence on MFC power

Complementary data will also be provided, namely data related to open-circuit voltage conditions. This chapter will be finished by presenting and discussing a two-stage power management system solution.

Reactor generations

Generation 1 – Double chamber reactors (Double MFCs)

Double chamber reactors were chosen to prove the concept of energy harvesting with microbial fuel cells. This choice of geometry was related with the ease of construction and the availability of the materials: the electrodes were made of carbon cloth, and the separation between chambers was achieved through a proton exchange membrane (Chemours Nafion® N115); the reaction chambers were constructed out of acrylic plastic, according to the geometry on Figure 4.1.

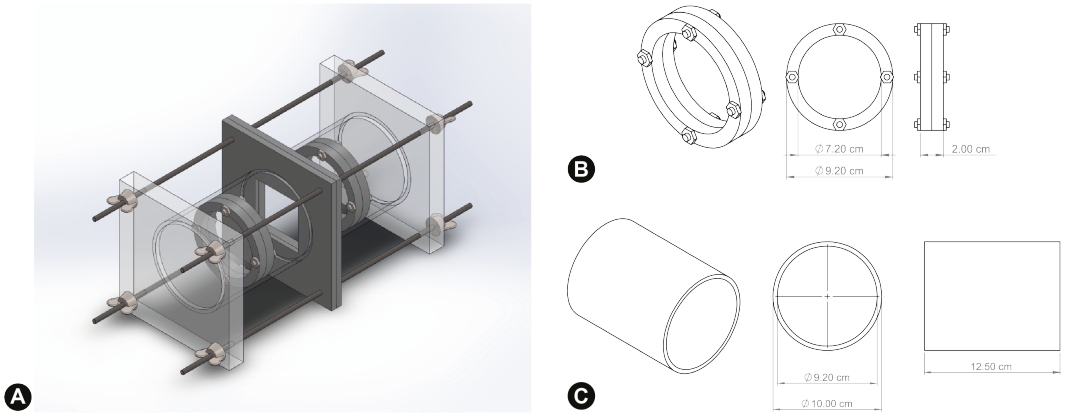

Figure 4.1 – Chosen geometry for the reactors and the overall microbial fuel cell. On A) the prototype built with a 3d CAD program; B) and C) highlight the crown and the tube dimensions respectively.

Each chamber, with a 1 L volume, was determined to have a cylindrical shape to limit any favorable deposition areas. The anolyte used was ill-characterized since it was retrieved from previous works related to wastewater decomposition analysis. However, it was safely assumed to be composed of an anaerobic bacterial culture, and a sodium acetate (CH_3COONa) solution. The catholyte was tap water, continuously aerated to guarantee oxygen saturation. The anode chamber was covered from direct light to prevent photobiodegradation, and the reactor was left undisturbed for two days, with the anode-cathode connection guaranteed through a 1 kΩ load, as shown in Figure 4.2.

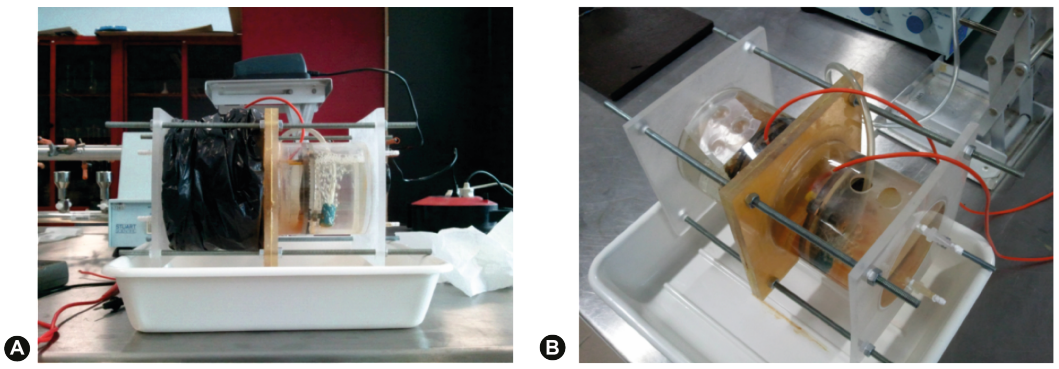

Figure 4.2 – Double chamber reactor. The anode is covered from direct sunlight, the cathode is aerated, and the electrodes are connected through a 1kΩ load. Both pictures have the cathode at right.

Generation 2 – 3D printed reactors (3D MFCs)

A research line in 3D printing double-chamber reactors was also explored. The goal was to develop a sustainable, economic and quick alternative for reactor development. The design brief was clear: the printed reactor should allow for substrate replacement, electrode maintenance, and chemical and physical parameter evaluation. The final proposal, displayed in Figure 4.3, was achieved after testing some designs.

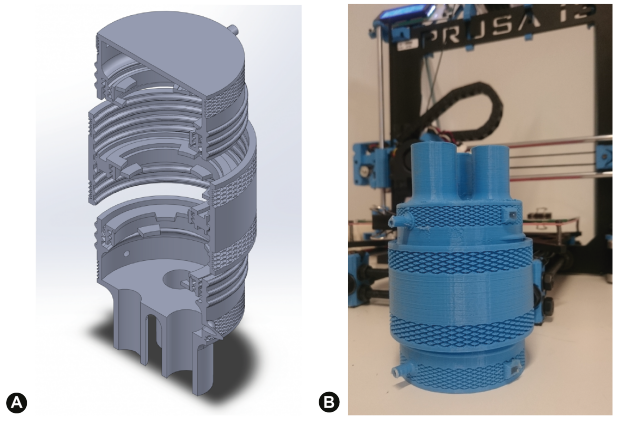

Figure 4.3 – 3D printed double chamber reactor: the project (A) and the actual printed design (B).

The design features SP-400 thread finishes like those applied to water bottles and caps. The reactors were printed in polylactic acid (PLA) in a custom-assembled Prusa i3 with a heated bed 3D printer. For leak-tightness, O-rings were also printed with flexible filament. The O-ring design followed the standards for O-rings ISO number 144. Three ring-like stoppers (similar to B in Figure 4.1) were used to allow the positioning of the electrodes and the membrane. The reactor's inner surface was fully threaded to allow studying the electrode and membrane distance impact in power development.

The cathode chamber was built with three cylindrical holes in order to fit three chemical sensors: pH, oxidation-reduction potential (ORP) and dissolved oxygen (DO). The use of this sensors was planned to evaluate the impact of varying the internal conditions.

A diamond knurling was also applied to the outside surface of each reactor element to ease the tightening of each part.

The reactor leak-tightness was not adequate, and the design was abandoned. Further investigation can follow this path by testing the outcome if changing the printing material to Acrylonitrile Butadiene Styrene (ABS), with post processing for improving the design impermeability.

Generation 3 – Double chamber reactors from domestic piping tubes (Double Domestic MFCs)

Further efforts were conducted pursuing the goal of developing reactors from easily obtained raw materials. Generation 3 reactors, pictured in Figure 4.4, were assembled from domestic piping tubes. As in previous generations, the reactors were also double-chambered. The electrodes and membrane used were the same as the ones in generation 1: carbon cloth and a Chemours Nafion® N115 PEM membrane. Each cathode chamber was aerated with a commercial air-pump and the anode was filled with wastewater collected after the primary treatment (without any solid particulates) in a wastewater treatment plant in a rural setting.

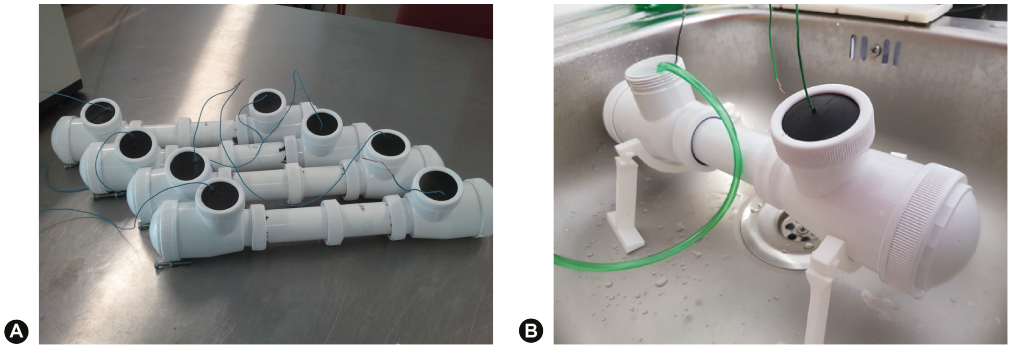

Figure 4.4 – Double chamber reactors built from domestic piping tubes. A set of four reactors is pictured in A); in B), a reactor in use.

Generation 4 – Single chamber reactors (Single MFCs)

As reviewed in Chapter 2, single-chamber cubic reactors provide a more adequate environment for MFC power production. As such, six small volume reactors (reactor 1 through reactor 6, R1 through R6) were built based on the work by [1]. The reactors, pictured in Figure 4.5, were made out of Poly(methyl methacrylate) (PMMA) and their inner cylindrical chamber is 4 cm long by 3 cm diameter, totalizing a volume of 28 mL. Each hole on the reactor was isolated with Teflon tape and custom, 3D-printed, O-rings.

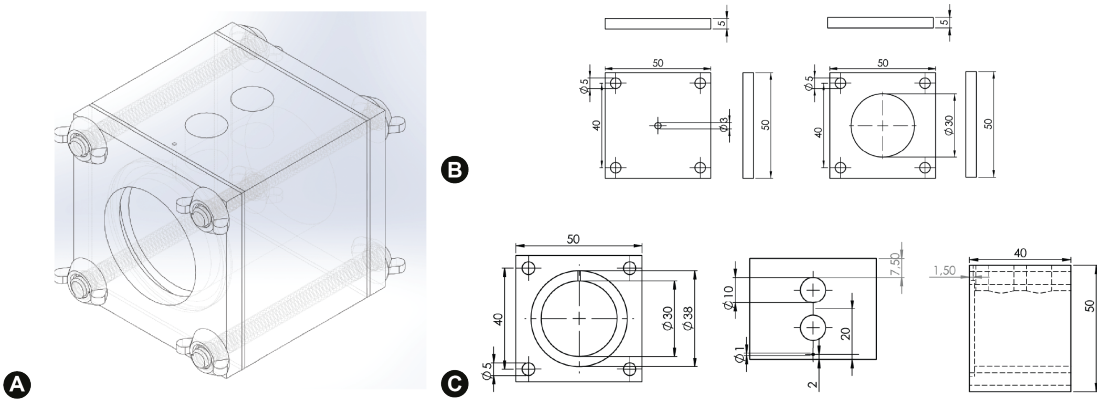

Figure 4.5 – Computer aided design of the Single MFCs. The full prototype is depicted on A), the lids for the electrodes (the anode on the left, the cathode on the right) are illustrated on B) and C) details the reactor's size. The measurement units have been omitted. Every measurement is in millimeters.

Both the electrodes, pictured in Figure 4.6, were carbon based: the anode was a graphite brush with a titanium rod (The Mill-Rose Company, Zoltek PX35), measuring 2.5 cm both in length and in radius, and heat treated (450 ºC for 30 minutes). The 7.07 cm^2 cathode is a layered deposition of carbon black and activated carbon suspended on Poly(vinylidene fluoride) (PVDF) through a phase inversion method.

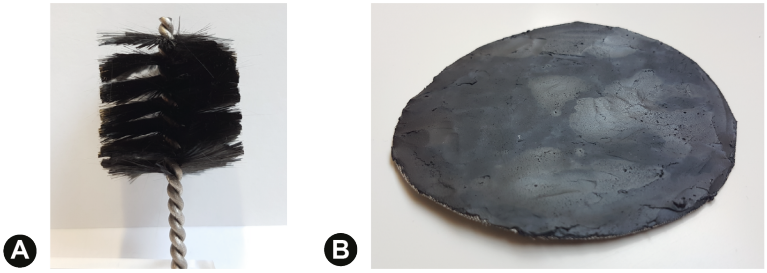

Figure 4.6 – The electrodes for single MFCs and single large MFCs: in A), the carbon brush anode and in B) the activated carbon air cathode.

The procedure for cathode production is reported on [2] and shown in Figure 4.7. The 10% PVDF solution was prepared by mixing 1 g of PVDF with 10 mL of N,N-Dimethylacetamide (DMAc). The proportion, in mL, between the activated carbon, the carbon black and the PVDF solution is wrongly stated on [2] as 30:3:10, respectively. After careful examination of other work [3], the experimentally applied proportion was corrected to 300:30:1. Mixing the PVDF solution with the carbonaceous compounds is a critical step, since the organic solvent evaporates quickly, drying the paste and greatly diminishing the paste adhesion to the stainless steel mesh. The cathode was submerged in deionized water for 30 minutes, with the stainless-steel side facing up. After that period, the cathode was left to dry in a fume hood for around 8 hours.

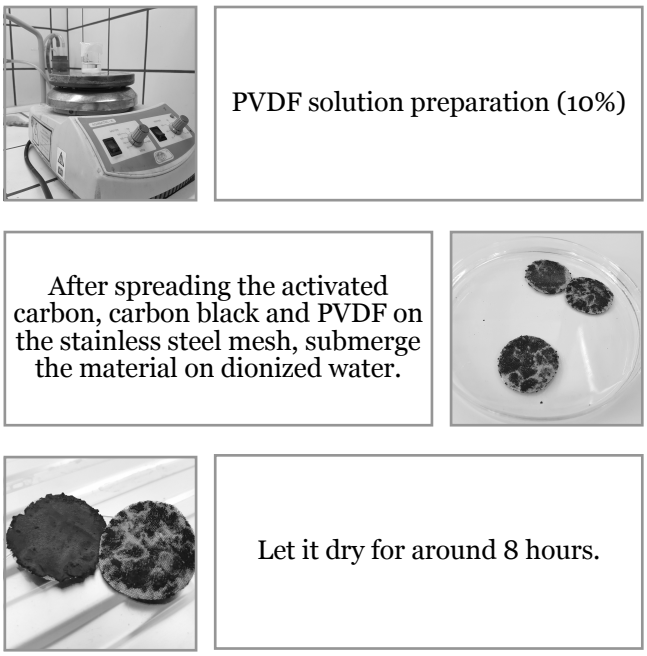

Figure 4.7 – Major steps of the air-cathode production.

Titanium wire was used to create a connection point between the cathode and the outside of the reactor. A fully assembled Single MFC is presented in Figure 4.8.

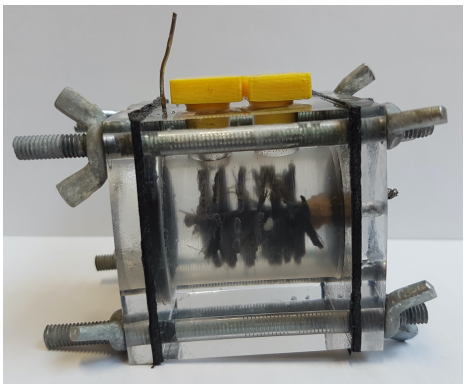

Figure 4.8 – A single MFC fully assembled. The cathode was fitted with an O-ring to promote water tightness and the anode titanium rod was covered with Teflon tape for the same end.

Three different substrates were developed to use with these reactors. Generally, this artificial wastewater, AW, is composed of a phosphate buffer solution (PBS), a sodium, potassium and ammonium source, and a carbon source. These elements guarantee adequate settings for the bacterial biofilm population activity in anaerobic conditions.

The first substrate developed, following the procedures in [4], did not suit the application: the prepared PBS did not dissolve, even when removing calcium chloride. A new medium solution was prepared according to [5]. Due, at the time, to the unavailability of the sodium phosphate compounds, the substrate was a 50 mM buffer solution at pH 7, prepared from potassium phosphates, with ammonium chloride at 0.31 g/L, and 1 g/L of sodium acetate (the carbon source). Sodium chloride was used instead of potassium chloride, as potassium was already present in the solution through the buffer solution. The mass of each reactant is determined below for 1 L of artificial wastewater.

Phosphate buffer solution

Acid: Potassium dihydrogen phosphate (KH_2PO_4)

$pKa(2)_{KH_2PO_4} = 7.21$

$Mw_{KH_2PO_4} = 136.09\ g/mol$

Base: Potassium phosphate dibasic (K_2HPO_4)

$Mw_{K_2HPO_4} = 174.20\ g/mol$

Determining the ratio of acid to base using the Henderson-Hasselbalch equation:

$$pH = pKa + log\frac{[Base]}{[Acid]} \xrightarrow[\substack{Base\ is\ K_2HPO_4 \\ pKa(2) = 7.21 \\ pH = 7}]{Acid\ is\ KH_2PO_4} [K_2HPO_4]/[KH_2PO_4] = 0.617$$

Determining the mass equivalents for the PBS solution:

$$\begin{cases} [K_2HPO_4] = 0.617[KH_2PO_4] \\ [K_2HPO_4] + [KH_2PO_4] = 0.05\ M \end{cases} \Leftrightarrow \begin{cases} [K_2HPO_4] = 0.03\ mol/l \\ [KH_2PO_4] = 0.02\ mol/l \end{cases} \xrightarrow[Using\ Mw]{} \begin{cases} m_{K_2HPO_4} = 4.08\ g \\ m_{KH_2PO_4} = 3.48\ g \end{cases}$$

Ammonium chloride mass

$Mw_{NH_4Cl} = 53.49\ g/mol$

$[NH_4Cl] = 5.80\ mM = 5.80 \times 10^{-3}\ mol/l$

$m_{NH_4Cl} = 5.80 \times 10^{-3} \times 53.49 = 0.31\ g$

Sodium chloride mass corresponding to the number of moles in potassium chloride

$[KCl] = 0.13\ g/L$

$Mw_{KCl} = 74.06\ g/mol$

$n_{KCl} = 0.13/74.06 = 1.74 \times 10^{-3}\ mol = n_{NaCl}$

$Mw_{NaCl} = 58.44\ g/mol$

$m_{NaCl} = 1.74 \times 10^{-3} \times 58.44 = 0.10\ g$

The third and last version of the substrate were developed when the sodium phosphate buffer compounds were available. The acid/base pair for the new phosphate buffer was sodium dihydrogen phosphate dihydrate/sodium phosphate dibasic ($NaH_2PO_4.2(H_2O)/Na_2HPO_4$). Since the acid source is dihydrated, some calculus was needed to meet the 50 mM brief for the buffer solution. The starting point will use the dehydrated compound. The other component concentrations remained unchanged.

Phosphate buffer solution

Acid: Sodium dihydrogen phosphate (NaH_2PO_4)

$pKa(2)_{NaH_2PO_4} = 6.82$

$Mw_{NaH_2PO_4} = 119.98\ g/mol$

Base: Sodium phosphate dibasic (Na_2HPO_4)

$Mw_{Na_2HPO_4} = 141.96\ g/mol$

Determining the ratio of acid to base using the Henderson-Hasselbalch equation:

$$pH = pKa + log\frac{[Base]}{[Acid]} \xrightarrow[\substack{Base\ is\ Na_2HPO_4 \\ pKa(2) = 6.82 \\ pH = 7}]{Acid\ is\ NaH_2PO_4} [Na_2HPO_4]/[NaH_2PO_4] = 1.51$$

Determining the mass equivalents for the PBS solution:

$$\begin{cases} [Na_2HPO_4] = 0.617[NaH_2PO_4] \\ [Na_2HPO_4] + [NaH_2PO_4] = 0.05\ M \end{cases} \Leftrightarrow \begin{cases} [Na_2HPO_4] = 0.03\ mol/l \\ [NaH_2PO_4] = 0.02\ mol/l \end{cases} \xrightarrow[Using\ Mw]{} \begin{cases} m_{Na_2HPO_4} = 4.26\ g \\ m_{NaH_2PO_4} = 2.40\ g \end{cases}$$

As previously stated, the sodium dihydrogen phosphate is used in its dehydrated form:

$Mw_{NaH_2PO_4.2(H_2o)} = 119.98 + 2 \times 18.02 = 156.01\ g/mol$

In a mole or a gram of $NaH_2PO_4.2(H_2o)$:

$H_2O\ percentage = ((2 \times 18.02)/156.01) \times 100 = 23.1\%$

$NaH_2PO_4\ percentage = 100 - 23.1 = 76.9\%$

As such:

2.40 $g\ of\ NaH_2PO_4.2(H_2o)$ have only 1.85 $g\ of\ NaH_2PO_4$ (76.9%). To have 2.40 $g\ of\ NaH_2PO_4$, we will need 3.12 $g\ of\ NaH_2PO_4.2(H_2o)$. Some water is already in the compound:

$m_{NaH_2PO_4.2H_2O} - m_{NaH_2PO_4} = 3.12 - 2.40 = 0.72\ g\ of\ H_2O \underset{\rho_{H_2O}=1\ g/L}{\Longleftrightarrow} 0.72\ mL\ of\ water$

Therefore, the solution should be prepared for a total volume of:

$1000\ mL - 0.72\ mL = 999.28\ mL$

In that case, the mass of Na_2HPO_4 also needs readjusting. The mass determined for 1 liter of solution was $m_{Na_2HPO_4} = 4.26\ g$. For 999.28 mL, the new mass should be $m_{Na_2HPO_4} = 4.257\ g$.

Since all mass changes happen at the thousandths, it was decided to round to the hundredths and keep the solution volume to 1 liter.

The final mass of the acid/base compounds is $m_{Na_2HPO_4} = 4.26\ g$ and $m_{NaH_2PO_4.2(H_2o)} = 3.12\ g$. This solution was used in all the trials herein discussed. A solution with such composition has around 9.8 joules of energy per mL (equation 2), which can be proved by using the organic source concentration, the equation describing the energy production process (equation 1) and the individual standard Gibbs free energy of formation, displayed in Table 4.1:

$$CH_3COO^-(aq) + 2O_2(g) \rightarrow 2HCO_3^-(aq) + H^+(aq) \quad (4.1)$$

Table 4.1 Summary of the standard Gibbs free energy of formation per compound of equation (1).

Compound	HCO_3^-	H^+	O_2	CH_3COO^-
ΔG_f^0 (kJ/mol)	-586.77	0	0	-369.31

$\Delta G_r^0 = 2 \times (-586.77) + 369.31 = -804.23\ kj/mol$ (4.2)

Using $C_{CH_3COONa} = 1\ g/L \wedge E = \Delta G_r^0 \times n_{H_3COONa} \therefore E = 9.8\ J$

This value will be used to accurately pinpoint the efficiency of each trial when comparing the influence of external variables on power production.

Generation 4a – Single chamber large reactors (Single Large MFCs)

To briefly study the influence of volume, reaction surface, chemical parameters and chamber size on power production, two large volume reactors were also assembled. One of those was developed to include four sensors: pH, dissolved oxygen, oxidation-reduction potential and temperature. Details of its dimensions can be found in Figure 4.9.

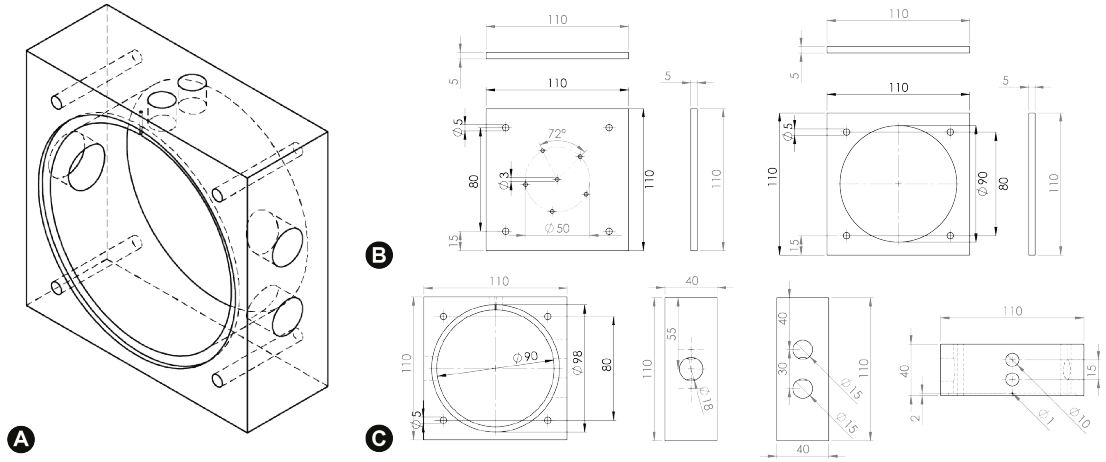

Figure 4.9 – Computer aided design of the large single-chamber reactor with sensor openings. The full prototype is depicted on A), the lids for the electrodes (the anode on the left, the cathode on the right) are illustrated on B) and C) details the size of the reactor. Every measurement is in millimeters.

The fully assembled, sensor rigged, MFC can be found in Figure 4.10.

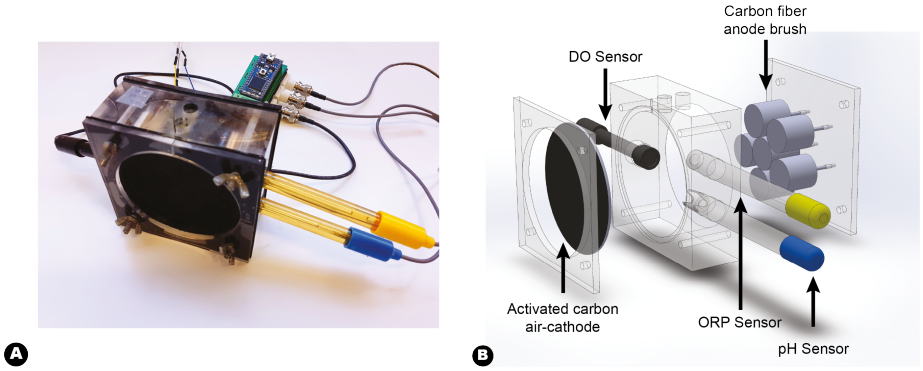

Figure 4.10 – The sensor equipped single large MFC fully assembled. In (B) a CAD simulation of the real assembly in (A). The figure at right also shows the microprocessor responsible for sensor management.

The other large reactor is similar, also presenting six anode brushes and a cathode with nine times the area in comparison with the cathode in the small reactors. It can be found in Figure 4.11.

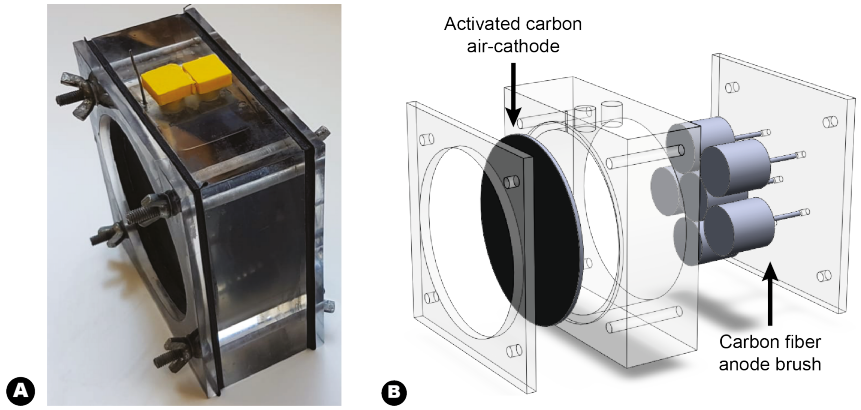

Figure 4.11 – The sensor-less single large MFC fully assembled. In (B) a CAD simulation of the real assembly in (A).

The total volume of each large reactor is approximately 0.25 L, also almost nine times the volume of the small reactors. Across all Generation 4 reactors, small or big, care was taken in order to leave the anode and the cathode with a 4 mm space between each other, as per reviewed.

The anode brush set was arranged in a concentric and circular fashion, which guaranteed the electrical contact between every brush and decreased its contribution to the internal resistance. The cathode was produced as previously described for the single small MFCs, but its total area amounted to 63.62 cm^2. As stated in [6], the cathode area and anode number increase were needed to maximize power production.

Power evaluation methodologies

To periodically evaluate the status of the Single and Single Large MFCs, polarization studies were applied. Each polarization study consisted in individually applying a set of 8 resistors to the reactor's electrodes in a multiple-cycle fashion. The multiple-cycle choice guarantees an adequate adap...ion of the biofilm to the external load of each batch.

The resistor values applied were 1000, 500, 200, 100, 68, 50 and 20 Ω. This choice of resistor values is capable of accurately describing the full electrical behavior of the reactors.

Data was retrieved and registered with the help of a microprocessor, the mbed NPC LPC1768, that will be discussed in its appropriate section. The polarization study plots will present voltage in Volts, current densities in mA/cm^2 and power densities in mW/m^2. The power density parameter relates to the ability of a system to supply power in relation to a cell size and cost. The area for reference is the cathode area, because, as already mentioned, this is the limiting electrode for power development. To determine the voltage achieved at each resistance load and to constrain the influence of artefacts and non-sustainable values, each reported value results from averaging the voltages for 1 hour. The maximum per load is than the maximum value found in that trial.

Biofilm inoculation and biofilm transfer

Inoculation procedure

In wastewater treatment stations, a high concentration of anaerobic bacteria can be found in the primary clarifier, before the aeration basin. A sample of the wastewater at this stage can, therefore, be used for developing the anaerobic exoelectrogenic biofilm needed for MFCs. The procedure applied consisted on filling the reactors with wastewater on the first day and then, on the second and third day, emptying the reactors to half and filing the remaining volume with the stored wastewater. A detailed description can be found in Figure 4.12.

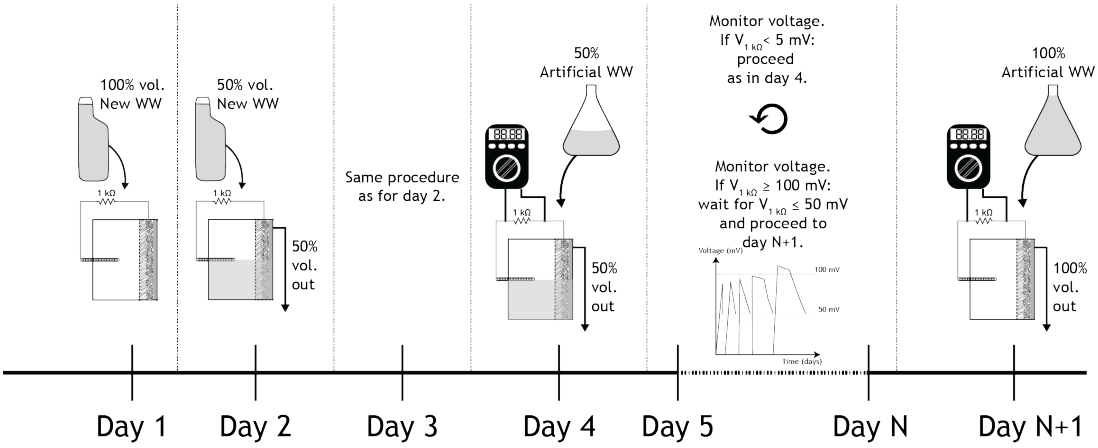

Figure 4.12 – Microbial fuel cell colonization procedure.

The first few days of inoculation do not present meaningful voltage values, since the bacterial population is not using anaerobic respiration for their metabolism, which means that the electrodes are being bypassed. The first step to force this metabolic choice is to limit the reactor's oxygen exposure. The solution applied was to completely fill the reactors. This procedure will help select bacteria exhibiting exoelectrogenic behavior, but with associated voltage decrease. At the fourth day, and by adding the artificial wastewater rich in sodium acetate, the selected bacteria begin to grow and multiply, which, in turn, increases the measured voltage levels.

Every Single MFC was colonized as previously discussed, being consecutively subjected to smaller loads in a multi cycle fashion: whenever the maximum voltage reading was close to the reading of the previous batch, the external resistance was lowered. When all the load values were applied to the reactor, with consistent readings – variations under 25% of the previous measure – a polarization trial was conducted.

For the Single Large MFCs, the biofilm was transferred from an old anode brush of a Single MFC, through a secondary colonization procedure. The method applied, summarily presented in Figure 4.13, consisted in replacing the middle brush (non-colonized) with a previously colonized brush (C brush). Having it in the middle guaranteed it had contact with the remaining non-colonized brushes (NC brushes). All the NC brushes rods were connected to each other and directly to the cathode, in short-circuit. The C brush was left in open circuit. These connections force the

migration of the biofilm to the NC brushes. To further promote this migration and bacteria selection process, the substrate added had 10 % of the substrate applied to a previously colonized MFC. According to Vogl *et al* [7], the research guideline for this method, this addition contributes with enzymes and other precursors capable of boosting the colonization. In order to determine the biofilm development stage, short circuit current was monitored. The substrate was changed whenever the measured current dropped below 50% of the maximum current measured. The biofilm was considered ready for a polarization study when the measured current, for successive trials, was consistent. At that stage, all brushes were connected to each other and a 1 kΩ external load was connected between the anode set and the cathode. Voltage was measured and a polarization trial was rerun after the retrieved voltage values were constant. After the biofilm presented repeatable results, the C brush was replaced by a NC brush and the reactor was considered fully acclimated after the above procedure produced the same results.

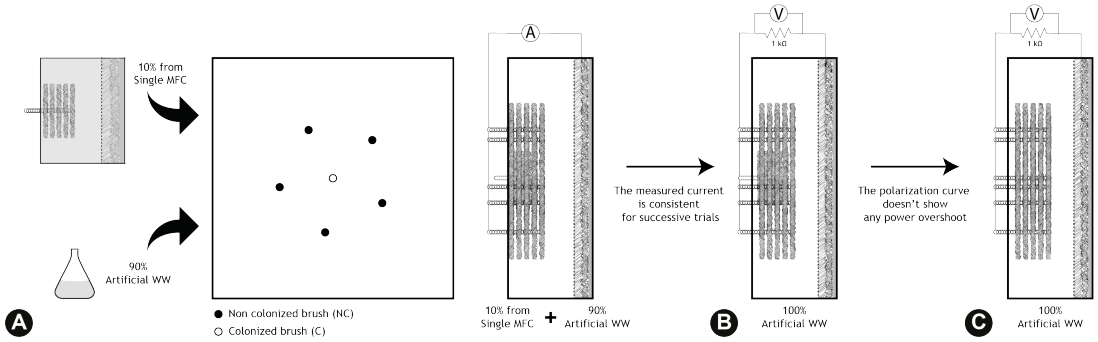

Figure 4.13 – Microbial fuel cell secondary colonization procedure. Initial acclimation procedure in (A), second acclimation step in (B) and NC anode replacement after successful polarization trials in (C).

Biofilm inoculation: voltage development

Voltage development was closely followed during reactor inoculation, for reactors 1 and 2 (Single MFCs). Figure 4.14 shows the averaged values for 202 inoculation days.

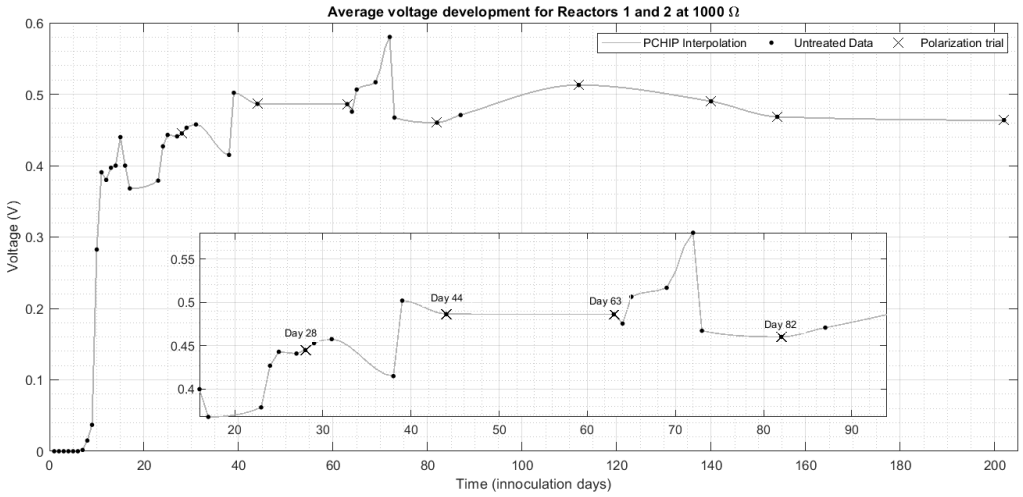

Figure 4.14 – Average voltage development for 1000 Ω load. Cross marks pinpoint the polarization runs and black dots the averaged voltage levels for reactor 1 and reactor 2. The interpolation method applied was Piecewise Cubic Hermite Interpolating Polynomial (PCHIP).

The unsteady development of the voltage profile in the first 15 days represent some issues with the reactors' watertightness. Still, the bacterial biofilm developed successfully, and the polarization trials started after 28 days of inoculation. The biofilm maturation stage can be determined by running polarization trials on the reactors. Figure 4.15 presents the averaged values for the first two polarization studies conducted with Single MFCs, particularly R1 and R2.

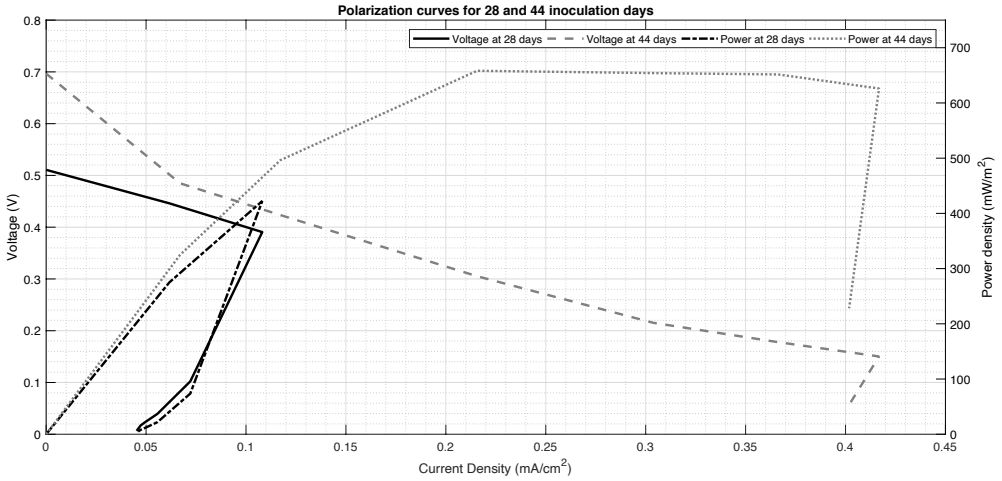

Figure 4.15 – Polarization curves built from averaged voltage values per external load at 28 and 44 inoculation days.

Data from both the polarization trials presents a clear example of power overshoot for the lowest load values. As referred in [8], this phenomenon is common in reactors acclimated to high external resistances and tends to disappear when the anodic biofilm matures and develops adequate redox enzymes for high current densities. Even so, the reactors averaged a maximum power of 658 mW/m2 (0.465 mW at approximately 305 mV and 200 Ω) at 44 inoculation days, after being subjected to lower loads.

Data on Figure 4.14 also shows that, after successful colonization, the maximum voltage at 1kΩ may be constant, hinting that the potential difference between the electrodes may not change in time. This hypothesis needs further validation due to aerobic biofilm growth on the cathode inner surface (cathode biofouling) and biofilm memory.

Biofilm memory can be found when loads are applied for 24 hours or more. In such cases, bacterial distribution on the biofilm is affected and that impacts the maximum voltage for a new load in a consecutive trial. Data from days 72 and 73 are a particular example of biofilm memory, since maximum voltage for 1kΩ decreased in successive batches at the same load. The absolute and relative maxima around 70 days derail from all other acquired values and suggest that open circuit conditions improve electrode potential difference. In fact, these values were acquired after leaving the reactors in open circuit voltage conditions for approximately 24 hours between load trials.

Biofilm transfer: voltage development

The biofilm development for both Single Large MFCs was accomplished by transference from previously colonized anodes, from Single MFCs. The original biofilm was approximately one year old. To adequately follow the biofilm development stages, short circuit current between the electrodes in both Single Large MFCs was monitored. Data in plot 1 of Figure 4.16 corresponds to the average short circuit current measurements.

Since five out of six anodes did not have an exoelectrogenic biofilm, the first four days present no meaningful values of short circuit current. At the fifth day, an improvement is noticeable, with a steady plateau being reached from the seventh day onwards. At that time, a polarization curve was conducted so as to ascertain the actual biofilm development. The polarization curve data for both reactors was averaged and is presented in plot 2 of Figure 4.16.

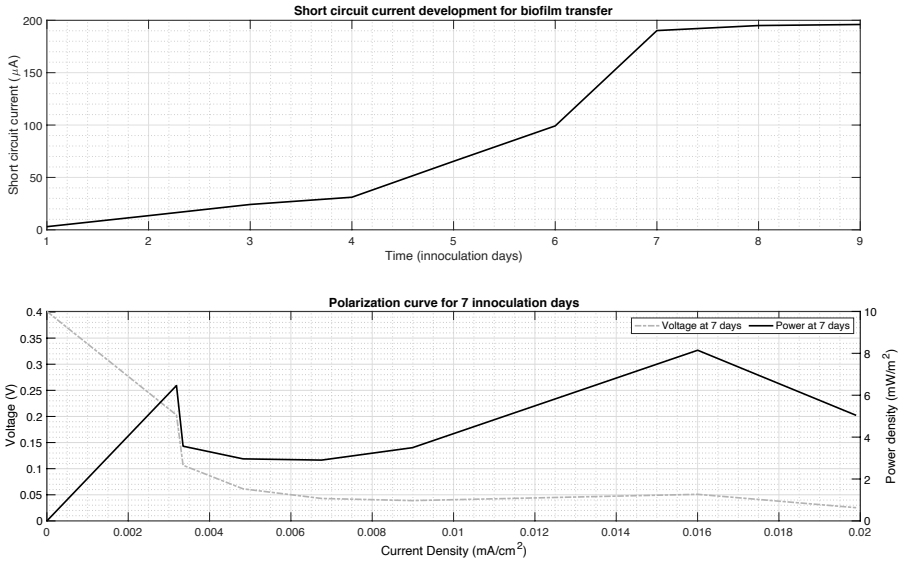

Figure 4.16 – The first plot, at top, displays the short circuit current for 9 inoculation days. The second plot, at bottom, presents the polarization curve at the ninth acclimation day.

The curve presents a maximum power density of 8.15 mW/m² (0.05 mW) for a load of 50 Ω. Power densities for other load values are well under this value and the curve does not present the expected shape. This is a clear indication that the biofilm isn't ready for polarization studies, as its actual power production capabilities are not fully developed.

To further promote the biofilm development, the reactors' electrodes were connected through a 1kΩ resistor, with concomitant maximum voltage monitoring. Data is displayed in Figure 4.17.

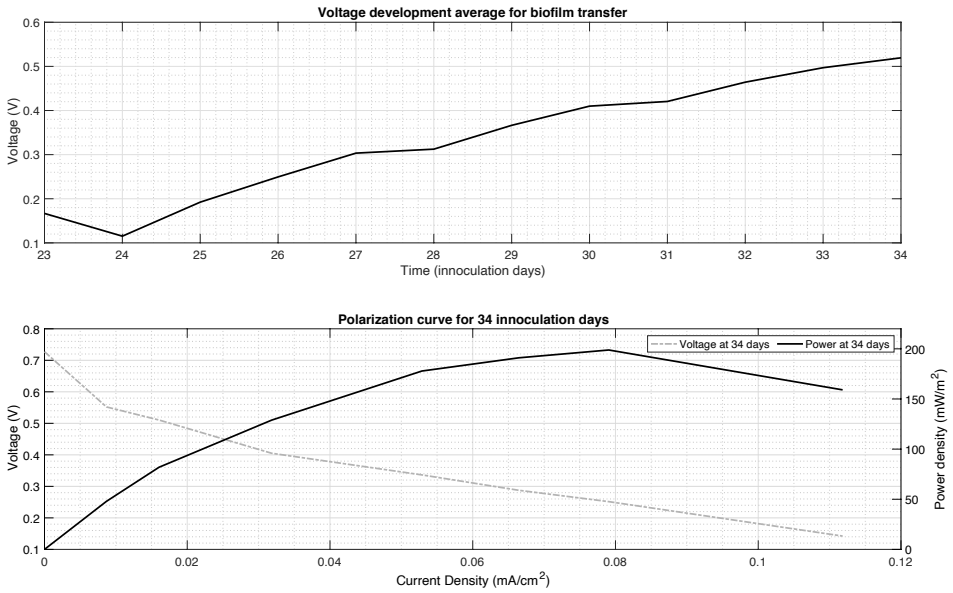

Figure 4.17 – Voltage development average for 1kΩ.

Subjecting the reactors to the 1kΩ load helped to promote the biofilm development in both reactors, allowing for approximately 68% improvement in the maximum voltage at 1kΩ. A new polarization trial, also plotted in Figure 4.17, was conducted to evaluate the extent of this improvement. This polarization curve presents a more balanced shape, with a maximum of 198 mW/m² (1.26 mW) around 50 Ω. A 96% maximum power improvement was achieved by ensuring adequate polarization of the electrodes.

The timeline for the maximum voltages at 1kΩ per biofilm day is presented in Figure 4.18.

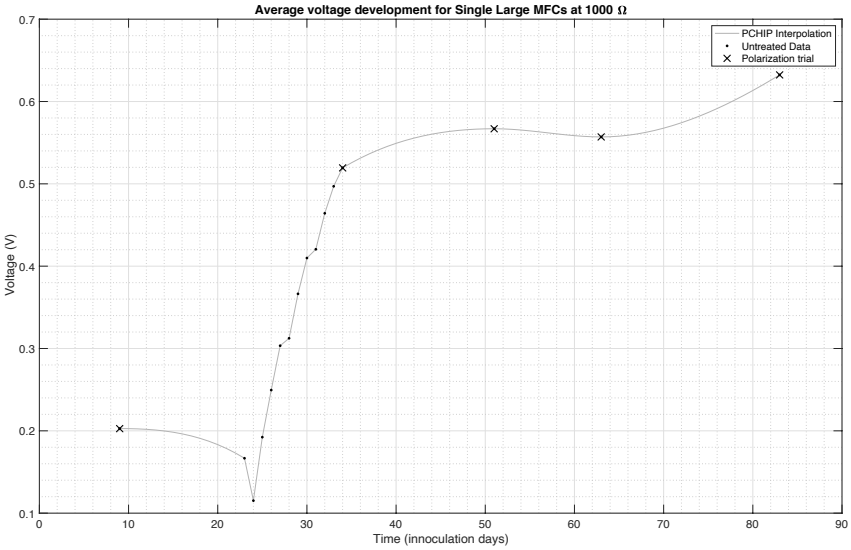

Figure 4.18 – Voltage development average for 1kΩ and 83 biofilm acclimation days.

Influence of internal variables on power production:

pH, ORP, DO and temperature

An instrumentation platform (IP) was designed to allow simultaneous measurements of different biochemical and physical parameters during polarization studies. It was designed to run automatic experiments supporting the study of MFCs, for extended periods of time, with minimal human intervention. A side goal was that it should be easy to replicate, using straightforwardly accessible off-the-shelf components. The low-cost instrumentation platform is capable of measuring pH, dissolved oxygen (DO), oxidation-reduction potential (ORP), temperature and voltage while modulating the connection and value of an external load (load varying assembly).

Measuring pH is a necessity due to the requirements of the biological population at the anode: suitable conditions of temperature, substrate and pH must be maintained in order to keep the oxidizing potential at its highest. pH is a measurement of how acidic a solution is: it is a logarithmic measure of hydrogen ions (H^+) concentration per liter of solution and can have values between 0 and 14 (corresponding to hydrogen ion concentrations from 1 to 10-14 mol/dm^3); an acidic solution has a pH value below 7 (a concentration of H^+ inferior to 10-7 mol/dm^3) and a basic solution a pH value above 7. If the measured pH value is 7, then the solution is said to be neutral. A pH sensor works with a pH probe, which has a measuring electrode, a reference electrode and a temperature sensor, and a conditioning circuit. The measuring circuit can be summed up as a battery where the positive terminal is the measuring electrode and the negative one the reference electrode. The circuit will compare the measuring electrode's potential (which has a direct relationship with the H^+ concentration) with the reference electrode's potential. As described before, this sensor works as an electrochemical battery and H^+ ions are spent on the measuring process.

The reference electrode, even when the pH sensor is submerged, is never in direct contact with the solution to be measured: its glass casing holds a buffer solution (usually potassium chloride) and, as such, the sensor hardly gets decalibrated. The other electrode, on the other hand, gets in contact with both the buffer solution and the solution to be measured: this last contact is maintained not directly but rather through a H^+-permeable glass (doped with Li^+). The acquired values vary according to the solution's temperature. As such, pH sensors are usually equipped with a temperature calibration circuit (by knowing the pH fluctuations on the buffer solution, an offset can be applied, and the values can be corrected). A preamplifier can also be found on the conditioning circuit: this element takes the electrodes' signal and processes it (lowering its impedance and increasing its strength and stability) so it no longer is easily affected by electrical noise [9]. Figure 4.19 makes a through representation of the measuring process.

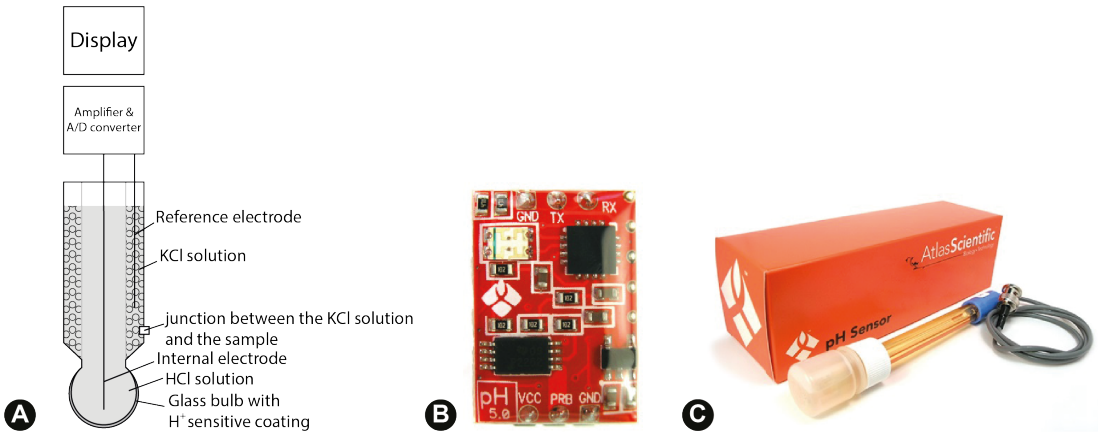

Figure 4.19 – In (A), a typical pH glass sensor probe; In (B) and (C), Atlas Scientific™ pH measuring equipment (respectively, integrated circuit and probe).

The Atlas Scientific™ available documentation isn't clear regarding the elements of the pH circuit. From the photos available on the datasheet, three integrated circuits are recognizable: a PIC16F1825 microcontroller, a TLC2262CPW operational amplifier and a TPS60400DBV voltage inverter.

The DO parameter is a regular experimental measurement when working with water derived substrates. DO sensor measurements can be expressed in mg/L or % of saturation and they translate the oxygen's concentration in water. This sensor guarantees a close monitoring of the oxygen values: low oxygen values at the cathode lead to a drop in the cell's electrical output, as the reduction reaction will be severely hindered. There are several types of dissolved oxygen (DO) sensors. They can be made to operate based on optical sensing methods or electrochemical sensing methods, quite similar to the pH sensor. Optical sensors measure luminescence either regarding its lifetime or its intensity. Clark electrochemical sensors or membrane-covered sensors are oxygen sensitive and their behavior is similar to that of a pH sensor. Atlas Scientific™ sells a galvanic DO sensor: in this electrochemical configuration, an anode (Zinc) and a cathode (Silver) are confined in an electrolyte solution delimited by an oxygen permeable membrane. When the probe containing these elements contacts with oxygen molecules, they diffuse through the membrane and get reduced at the cathode (Figure 4.20). The reduction rate creates an electric potential which is proportional to the oxygen diffusing through the membrane. The cycle keeps repeating because oxygen keeps being reduced at the cathode and new oxygen molecules are used for repeating measurements [10].

Circuit-wise, the Atlas Scientific™ DO embedded circuit shares the PIC16F1825 microcontroller of the pH sensor. The remaining conditioning circuit will be studied later on.

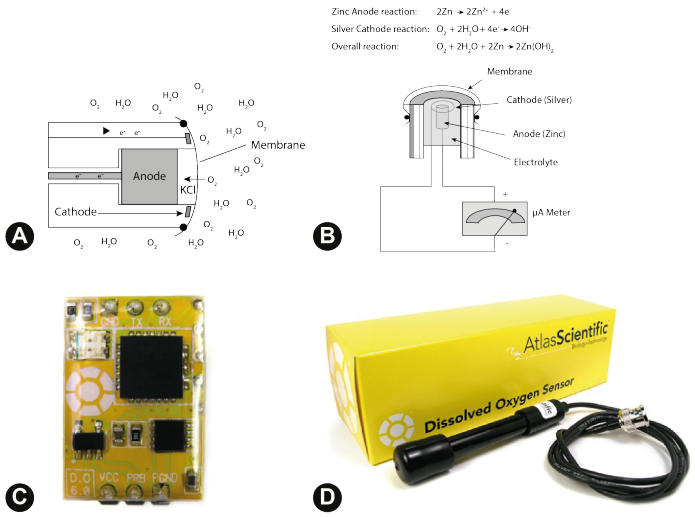

Figure 4.20 – Dissolved oxygen sensors: (A) oxygen diffusion; (B) electrode arrangement; (C) and (D): Atlas Scientific™ DO measuring equipment (respectively, integrated circuit and probe).

The ORP sensor will allow a continuous estimation of the MFC's power generation capabilities. As with any other fuel cell, the potential difference between electrodes is a major player in the cell's expected electrical output. The data retrieved by this sensor will also allow for the accurate pinpointing of when the fuel source (substrate) has to be replaced: a low absolute ORP value on the anode chamber means that the oxidation potential is low and the MFC's power production capabilities will be limited. The oxidation-reduction potential sensor, shown in Figure 4.21, has the same working principle has the other two previously mentioned sensors. The main difference is that the sensor's permeability is not as ion-selective. The sensor answers to the balance of oxidation-reduction reactions of where it is placed. The two electrodes on the system have two separate functions: the reference electrode provides a constant stable output value for comparison; the measuring electrode (made out of platinum) can act as an electron donor (reducing agent) or acceptor (oxidizing agent) [11,12].

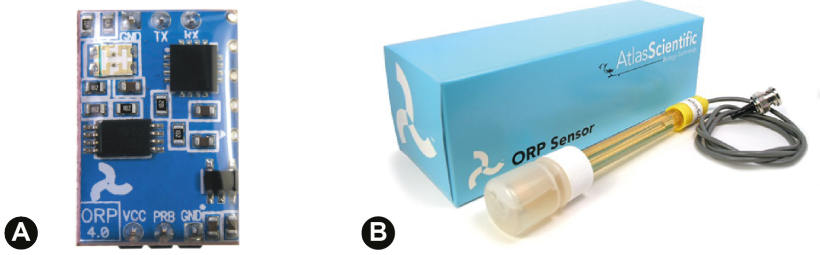

Figure 4.21 – Atlas Scientific™ ORP measuring equipment (respectively, integrated circuit, (A), and probe, (B).

The sensor will output values between -1023.99 [mV] and +1023.99 [mV] and the lower the outputted value, the more reductive character (incites the reduction of solution species, the gain

of electrons) is the solution where the sensor is used [13]. The ORP sensor at the cathode chamber of an MFC is expected to have negative values.

All biochemical sensors where acquired to Atlas Scientific™, after carefully considering the commercially available offerings. All three sensors have their working principle based on electrochemical batteries: they are composed of two electrodes (an anode and a cathode), with the reference electrode submerged on a known solution and separated by a permeable membrane.

The overall characteristics of these sensors are summarized in Table 4.2.

Table 4.2 - Biochemical Sensors Characteristics

Parameter	pH	DO	ORP
Full Range pH	.001 – 14.000	0.01 – 100+ mg/L	-1019.9mV – 1019.9mV
Response Time	1 reading per sec	1 reading per sec	1 reading per sec
Accuracy	+/– 0.002	+/– 0.05 mg/L	+/– 1mV
Calibration Points	1, 2, 3 points	1 or 2 points	Single point
Operating Voltage	3.3V – 5V	3.3V – 5V	3.3V – 5V
Reading Modes	Single / Continuous	Single / Continuous	Single / Continuous
Data Protocol	UART & I2C	UART & I2C	UART & I2C
Baud Rate	9600 Bps	9600 Bps	9600 Bps
Data Format	ASCII	ASCII	ASCII

A customized design was developed for the load varying assembly. The variation of the load applied to an MFC and the record of the output voltage allows studying the reactor's operation and the influence that the applied electric load, or the way it changes, has on its operation. For this, a resistor controlled by a digital input, MAX5451EUD+, was used as an electrical load. A digital switch, MAX4644EUT+, allows to temporarily disconnect the electrodes from the electrical load, supporting open circuit voltage measurements and load connection modulation. The customized design also integrates temperature recording using an LM35 sensor.

The IP management and control was designed around the Mbed rapid prototyping: a platform based on an ARM processor (Cortex M0 or Cortex M3) with a free remote compiler accessible with a web browser and internet connection (also being possible to have an offline toolchain like Code Red, GCC or IAR). Alongside this tool there are discussion forums, blogs and online documentation to use freely; all of which are neatly organized and appropriately detailed. There is also a vast library set (both for hardware and software) allowing for each user to quickly and efficiently implement some basic operations.

The selected microcontroller unit (MCU) was the NPC LPC1768, a 90 MHz processor, with an ARM cortex-M3 core, offering 32 KB RAM and 512 KB flash, with several peripherals around it: Ethernet, USB, CAN bus, four UART, two I2C, two SPI, 12-bit A/D and a single 10-bit D/A channel

converters, and a Realtime clock/calendar. The MCU's pinout is accessible from the exterior (see Figure 4.22), even though some digital output lines are connected to LEDs, and an input line to the reset button. It is worth mentioning that there is a USART communication port to establish a serial link with the PC through a USB port. This communication channel can also be used to upload new firmware into the Mbed, as it is recognized by the PC as a new disk. As such, firmware update is done by dragging and dropping the file into this memory space. After pressing the reset button, the last uploaded firmware starts to be executed. The mbed's memory space has a FAT filesystem that can be used to store files accessible through the computer.

The developed Mbed firmware was programmed in C/C++, built in the online environment, avoiding the installation and update of a programming IDE tool.

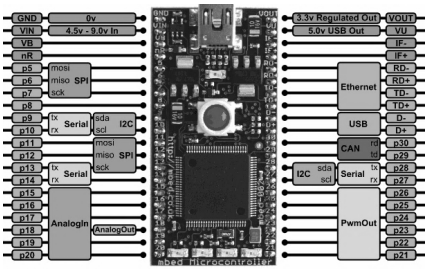

Considering the previously described characteristics of the platform, a printed circuit board (PCB) was developed. According to the Atlas Scientific™ sensors' manufacturer, the embedded circuits responsible for the biochemical data acquisition should be connected to a BNC plug: these plugs allow for better noise immunity, a safer and sturdier connection and impedance matching between peripherals. The PCB had to be able to integrate the embedded sensoring circuits, the BNC plugs and associated integrated circuits, the load varying assembly and the microprocessor in the smallest possible area (higher PCB area imply higher production costs). To accommodate all these devices, the PCB was idealized to have two layers: a top layer for the microprocessor and load varying assembly, and a bottom layer for the BNC plugs and the embedded sensoring circuits. The IP functional scheme is shown in Figure 4.23.

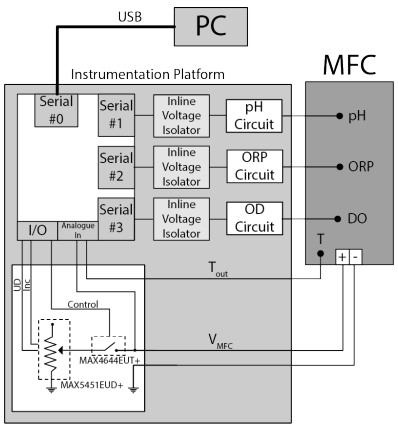

Figure 4.23 – Instrumentation platform functional scheme.

In order to manage, configure and display the retrieved data, an application programming interface was developed using Processing. The developed interface is displayed in Figure 4.24 and has two major sections: a programming console and a display window.

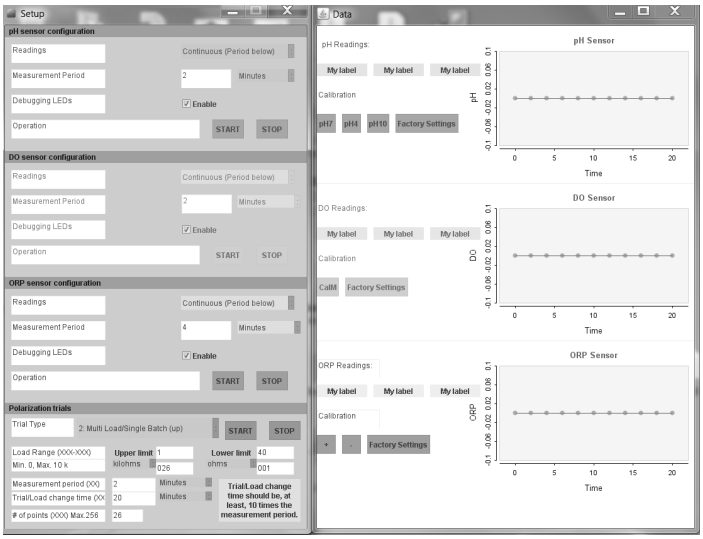

Figure 4.24 – Parametric UI's menus for each acquisition channel and respective graphical plot window.

The programming console allows for the configuration of each sensor parameters: the sensor identification, the use of the status LEDs and the acquisition type. The status LEDs inform the user about the working condition of the sensors. A red LED blinks if an unknown instruction has been received and a green LED blinks every time an instruction has been received or data has been sent. The acquisition can be of a single value or of periodic measurements, where the acquisition period is also configurable. It also supports the configuration of the load varying assembly. Its configuration parameters are presented in Table 4.3.

Table 4.3 – Load varying assembly configuration parameters

Byte Pos.	Abbrev.	Meaning
0	SOP	*Start of package*
1	ID	*Identification of the package*
2	SS	*Start/stop*
3	TrialT	*Type of trial (1, 2, 3, 4, 5)*
4-6	TapsUp	*Taps equivalent of the upper load*
7-9	TapsDo	*Taps equivalent of the lower load*
10-11	MP	*Time elapsed between voltage measurements*
12	MPUnits	*Time unit for MP (seconds 's' or minutes 'm')*
13-14	PolP	*Time elapsed between trials (applies only to TrialT #1, #4 and #5)*
15	PolUnits	*Time unit for PolP (seconds 's' or minutes 'm')*
16	EOP	*End of package*

Before starting the acquisition, a message package, with the structure shown in column “Byte Pos”, is sent from the UI to the mbed through the USB link channel. These parameters are entered into the UI through the bottom window shown in Figure 4.24. Load resistance upper and lower limits are defined by the user. These values are converted into the equivalent number of *TapsDo* and *TapsUp* taps, respectively, considering the origin at the minimum value. The variable resistance has 256-tap points accessible to the wiper along the resistor arrays between the minimum and maximum value of resistance. This means that each tap modifies load resistance value by 39 Ω, starting from the minimum measured value of 227 Ω. Five different test trial scenarios are supported. Successive V_{MFC} voltage values are acquired at trial #1 without changing the resistance value, where time between samples is defined by the *MP* parameter and the trial total time is defined by the parameter *PolP*. The number of obtained measurements, *NP*, is given by *PolP/MP*. In trial modes #2 and #3, after the acquisition of a new sequence of V_{MFC} voltage value, the resistance is incremented, or decremented, by one tap, respectively; the number of obtained measurements, *NP*, is given by *PolP/MP* and the number of measured sequences, *NS*, is equal to *TapsUp - TapsDo*.

In trial mode #4, successive V_{MFC} voltage values are acquired without applying a load (open circuit voltage); the number of obtained measurements, *NP*, is given by *PolP/MP*.

A switching test is performed by trial mode #5: the resistance load is switched on and off, with a resistive load increasing from *TapsDo* to open-circuit. Voltage V_{MFC} is continuously sampled, waiting for the steady-state regime, detected when, by successive samples, the variation of the signal voltage V_{MFC} is lower that a predefined value. Output circuit voltage is registered in four different situations: The open-circuit voltage; when the load *TapsDo* is applied; immediately after openning the switch; and Δt seconds after the switch opening, defined by *TapsUp*. The number of tests performed, *NP*, is given by *PolP/MP*. This procedure allows to identify equivalent circuit components values as it will be described when addressing the MFC dynamic behavior.

By pressing the Start button the test begins. Pressing the Stop button skips the running trial.

Time diagrams for the supported test scenarios are outlined in Figure 4.25.

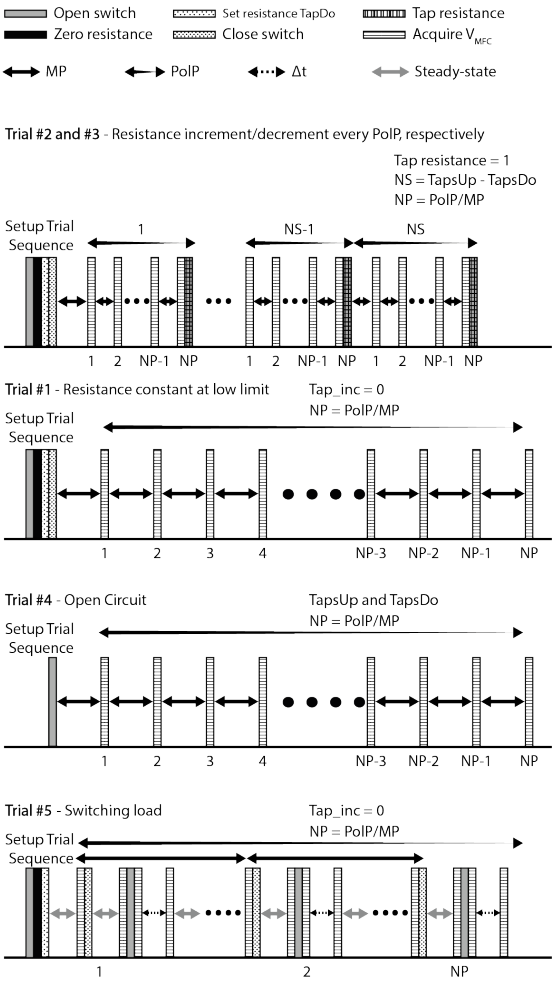

Figure 4.25 – Trial#1 - Single load/single batch; Trial #2 – Multi load/single batch (up); Trial #3 – Multi load/single batch (down); Trial #4 – Open circuit measurement; Trial #5 –Switching Load.

To guarantee an adequate understanding of the platform capabilities, this section will only address the study of simultaneous acquisition of biochemical measurements while at a continuous load, as plotted in Figure 4.26. The use of the IP for MFC electrical profiling will be addressed in the section "Influence of external variables on power production".

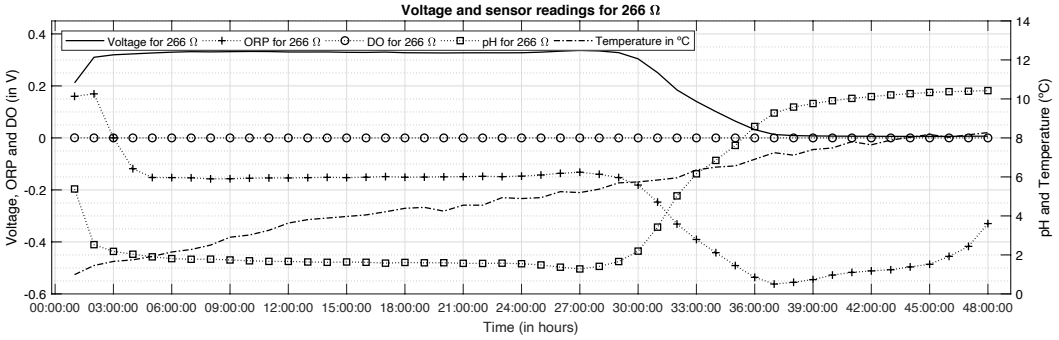

Figure 4.26 – Voltage, acidity (pH), oxidation-reduction potential (ORP), dissolved oxygen (DO) and temperature readings from a Single Load/Single Batch trial with a fixed load of 266 Ω (1 tap). The left vertical axis is used for the voltage, ORP and DO readings and the right vertical axis for the remaining measures, pH and temperature.

For the same artificial wastewater batch, data was retrieved for voltage development, oxidation reduction potential (ORP), dissolved oxygen (DO), acidity (pH) and temperature. The measurement period was of 2 minutes for voltage, DO, pH and ORP and 60 minutes for temperature. An hourly average was applied for every measurement besides temperature.

Voltage, ORP and DO were measured in millivolts and converted to volts for representation. All these variables are plotted against time on the left vertical axis. The pH and temperature measurements are also plotted against time but on the right vertical axis. Although the units for these two variables are different, their range is similar, which allowed for their simultaneous representation.

The voltage develops very quickly, reaching 90% of its final value in the first 3 hours. When the carbon source (acetate, CH_3COO^-) availability begins decreasing, voltage also starts dropping, at around 28 hours with the same artificial wastewater batch. When correlating the pH measurements and the voltage development, a relationship can be established: as long as the carbon source is aplenty, the pH remains acidic (under 7). This happens due to the increased concentration of H^+ and CO_2, both by-products of the anode reaction, where acetate is metabolized by the bacteria biofilm. It can be observed that when the acetate availability decreases, with a concomitant drop in the measured voltage, the pH increases due to the decreased production of H^+. The gas permeability of the cathode allows for a partial release of the carbon dioxide (CO_2) pressure, which is higher for acidic pH values [14]. When the pH begins increasing, the remaining CO_2 is more easily solved on the medium, converting to bicarbonate (HCO_3^-). This bicarbonate production, further contributes to the pH increase, alkalinizing the medium and leading to the precipitation of sodium salts (trona, $Na_3(CO_3)(HCO_3).2H_2O$) [15], that increase when the bicarbonate ion is saturated on the medium, at around 37 hours. At that time, the ORP reading also sees an increase, corroborating the oxidation action of the medium and the trona production. Due to the intense smell found when emptying the reactor after a batch trial, it is also suspected that some nitrogen oxidation is happening, leading to the production of nitrates (NO_3^-) and nitrogen dioxide (NO_2) [16]. Furthermore, the ORP results also justify the increased reducing strength of the medium when acetate is available and a further reducing boost when bicarbonate is produced. At that point, however, the bacteria can't metabolize it and the current production decreases, leading to the detected voltage drop. The DO reading, mostly equal to 0, represents the anaerobic conditions of the reactor, forced by covering the feeding inlets of the reactor. This action guarantees the anaerobic conditions but research presented on [15,17] indicates that trapping the carbon dioxide on the reactor leads to a quicker alkalization of the medium. The temperature variation observed is due to feeding the reactor with the artificial wastewater stored on a refrigerator and around 1ºC with an average ambient temperature of 14ºC.

Biofilm age and cathode biofouling

As the inoculation stage made clear, time has a significant impact on the MFC bacterial population. Due to the reactor conditions, the bacterial population on a single chamber MFC begins by developing at the anode. Nevertheless, the cathode oxygen permeability ends up playing a significant part on the reactor performance. The anodic biofilm age in discussion in this section is analyzed considering two major conditions for every trial: the same substrate composition and no cleaning or scrapping none of the reactor's components. The analysis will begin with Single MFCs and continue with the two Single Large MFCs.

As depicted with the timeline in Figure 4.14, six more polarization trials were conducted before applying any change to the reactor's elements. The plots on Figure 4.27 correspond to polarization trials three and four.

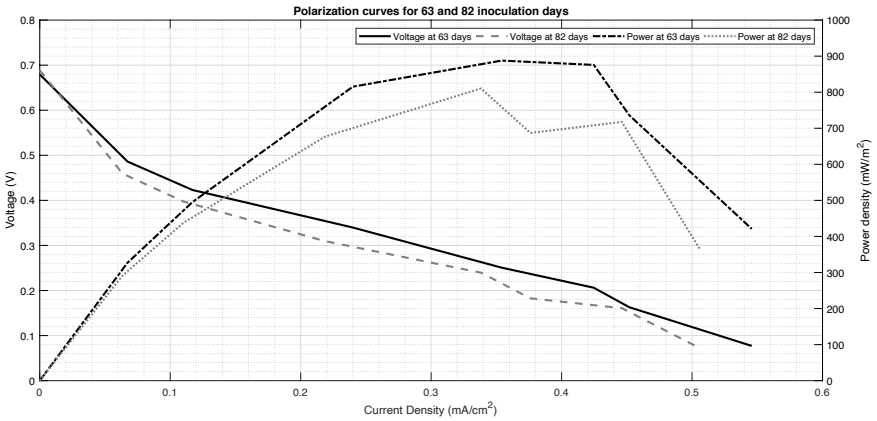

Figure 4.27 – Polarization curves built from averaged voltage values per external load at 63 and 82 inoculation days.

These plots are sharper representations of an adequate polarization curve than those of Figure 4.15. The voltage losses discussed in Chapter 3 are more easily identified in each of the different slopes of the IV curve. A maximum power of about 887 mW/m² (0.627 mW at approximately 250 mV and 100 Ω) was achieved at 63 inoculation days. The polarization trial conducted at 82 days shows signs of decreased reactor performance. In between polarization trials, the reactors were kept with fresh feedstock and the electrodes connected through an external resistance. Since the external resistance was the same, around 1 kΩ, the biofilm's ability to answer to low external resistances with high currents became hindered (the high current redox enzymes became less expressed).

A further proof of this event is clear with data on Figure 4.28.

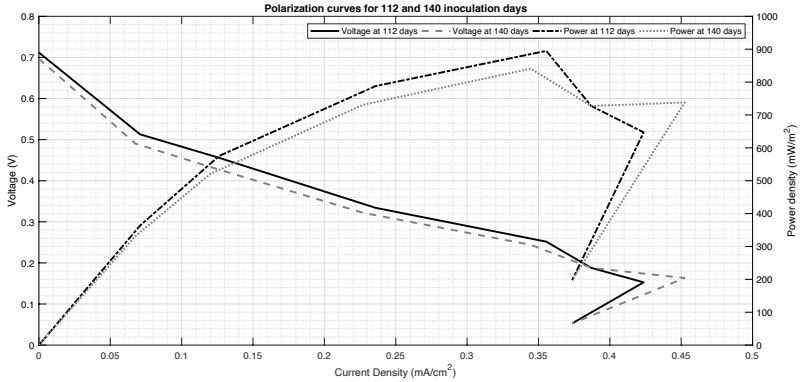

Figure 4.28 – Polarization curves built from averaged voltage values per external load at 63 and 82 inoculation days.

A power overshoot is again found, with a harsher drop on the plot for 112 days. This performance limitation is already being addressed at the trial on 140 inoculation days, since the external load between trials was lowered to 500 Ω. This is why a second peak is found around 0.45 mA/cm2: the biofilm is already more successful in answering to a higher current request, although not capable of a complete follow-up and doubling back at around 20 Ω. A maximum power of approximately 895 mW/m2 (0.632 mW at approximately 250 mV and 100 Ω) was achieved at 112 inoculation days. The biofilm was successfully re-adapted to higher current densities by varying loads in the complete polarization range, as proved by Figure 4.29.

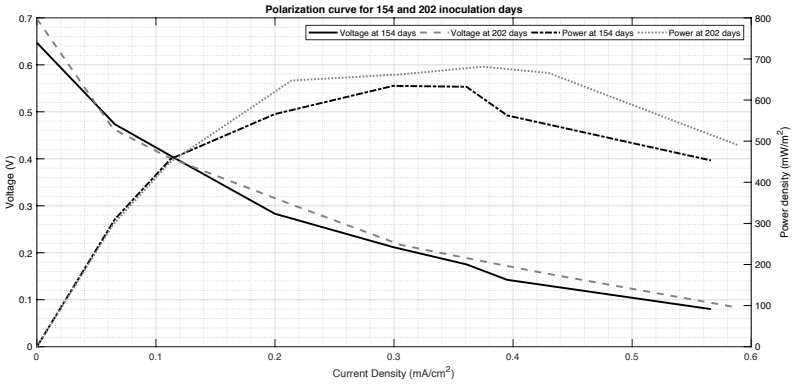

Figure 4.29 – Polarization curves built from averaged voltage values per external load at 154 and 202 inoculation days.

No power overshoot is found. However, the maximum power dropped, reaching values close to 680 mW/m2 (0.481 mW at approximately 180 mV and 68 Ω) at 202 inoculation days. This decreased power density is most likely due to biofilm build-up on the cathode: although anaerobic conditions are constantly being applied to the reactors, the cathode surface is highly aerobic, due to the needed cathode oxygen permeability. As such, specific bacteria can adhere to the cathode and use oxygen directly, bypassing the anode usefulness. This phenomenon has a slow onset, but once started it can only be stopped by appropriate cleaning of the cathode [18] and the reactor or, as a last resource, by applying a new cathode.

Figure 4.30 presents a comparison between both the electrodes in the begin and after 202 days of reactor operation.

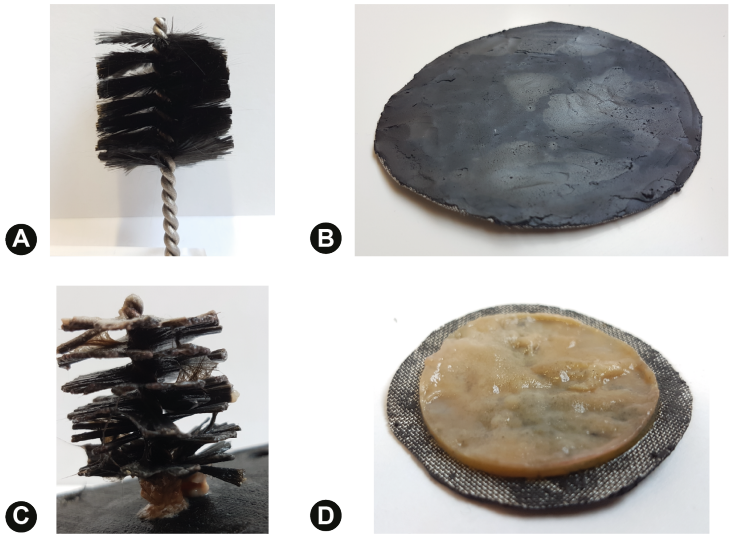

Figure 4.30 – Electrode comparison. In (A) and (B) the anode and cathode, respectively, before being assembled in a reactor. In (C) and (D) the same electrodes after 202 days of operation in an MFC. The cathode in (D) has its stainless-steel mesh side facing up: this is the side of the cathode in direct contact with the substrate.

As displayed, both reactors show clear signs of bacterial adhesion. Although that is desirable for the anode, the same cannot be said for the cathode. The biofilm on the cathode surface may be considered of aerobic nature, since these bacteria are using oxygen directly from its permeable surface. This assumption would need further confirmation by microbiology tests. Nevertheless, and according to the previous analysis, it is clear that cathode biofouling is non-desirable and cannot be prevented, only delayed. This discussion was started in chapter 2 and is now further explored by plotting the cathode age against the internal load evolution of a single MFC, as showed in Figure 4.31.

Figure 4.31 – Single MFC internal load tracking per cathode age.

For the first 200 days of biofilm development, the single MFC internal load shifted from 200 to 68 Ω. This change cannot be singled out to a specific factor, since the anode bacterial colony was still in development. However, tracking the reactor's internal load when a new cathode is applied can confirm the influence of cathode biofouling on the internal load evolution with time. To further guarantee that this influence can be traced to the cathode, the second period of time in Figure 4.31 happened for an anode colony time of over 300 days (359 days). It is noticeable that a 40-day period, changes the reactor's internal load. This new value was maintained for two consecutive polarization trials, indicating that parameters like electrode distance, temperature or AW composition cannot be held accountable. Therefore, this data indicates that cathode biofouling has a decremental effect on the reactor's internal load. The aerobic biofilm developing at the cathode's surface seems to be decreasing the resistance of electron and proton flow due to its contribution in substrate consumption. However, as previously seen, a concomitant power density decrease ensues.

A similar investigation of the anodic biofilm development with time was conducted on two Single Large MFCs. The polarization trials previously discussed, with Single MFCs, were always conducted with the loads being varied from the highest to the lowest load (from 1k to 20 Ω), in a downward direction. This time around, the investigation was aimed at determining if the load varying direction had any influence on the polarization curve. At this point, the Single Large MFC capable of fitting the biochemical sensors was trialed without them. As such, and to make a clearer distinction between both the reactors, the sensor equipped Single Large MFC will be referred to as R7 and the other Single Large MFC as R8. Three polarization trials were conducted to this aim. R7 was subjected to two consecutive downward polarization trials and a third in the upward direction. The load varying direction for MFC 8 was downward, upward and downward respectively for polarization trials one, two and three. Figure 4.32 displays the maximum voltages measured per applied load.

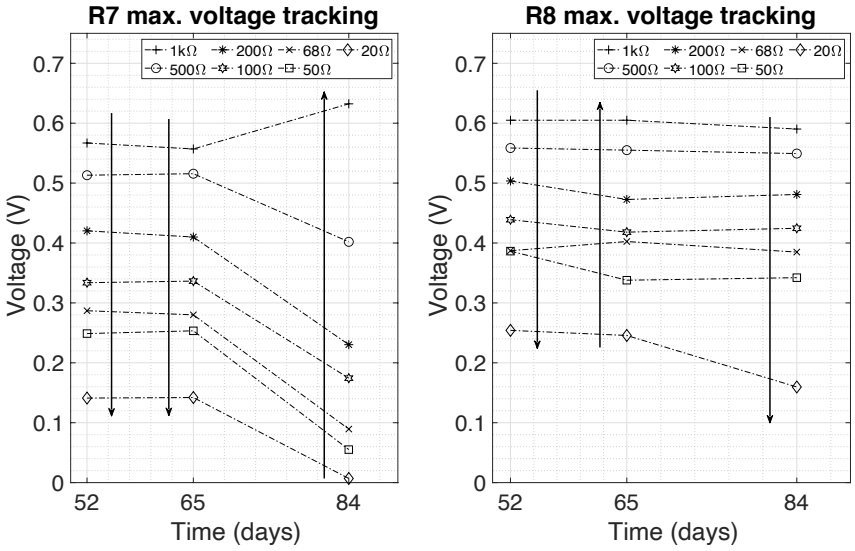

Figure 4.32 – Maximum voltages per reactor for each load value and for three consecutive polarization trials. The arrows represent the load varying direction.

This initial observation suggests that the third polarization curve for R 7 will have lower maximum voltages. It is also very clear that R7 lags in performance when compared with R8, since every load achieves lower maximum voltages than for R8.

Polarization trial data for each reactor and trial is pictured in Figure 4.33.

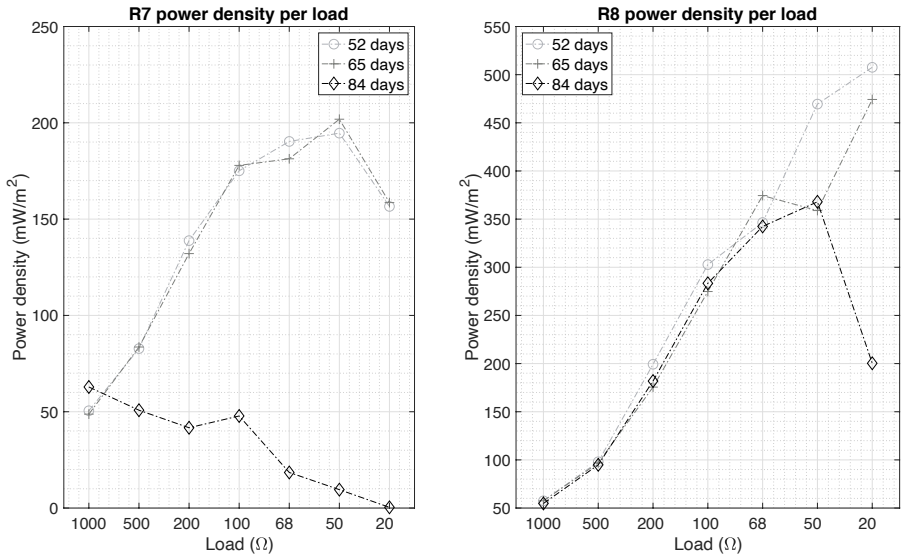

Figure 4.33 – Power density curves for R7 and R8 and polarization trials three, four and five.

The third and fourth polarization trials present a similar behavior per MFC, although with different power densities. Of particular interest is the shape of these curves for R8. In these trials, no maximum power density could be determined for a particular load, suggesting an internal load below 20 Ω. The same conclusion cannot be drawn from the results in the fifth polarization trial. For R7, a sharp decrease in all but one (1 kΩ) loads is noticeable, pointing to an overall biofilm inadaptation. Also, irrespective of the reactor, the power densities are lower than in previous trials, supporting the suspicion of cathode biofouling. As for R8, the fifth polarization trial presents a decrease for the last load value. This, together with lower power density values also corroborates the cathode biofouling possibility.

Multi-cycle vs. single-cycle substrate feeding

The MFC energy source is its substrate. A research on the impact of the substrate feeding type was conducted in one of the Single MFCs to determine its influence in the MFC power development profile. While in the multi-cycle method, loads were changed with each substrate change, for the single-cycle substrate feeding option, loads were updated after applied for a set duration. Table 4.4 presents a record of the applied loads in both operation modes, together with its application time.

Table 4.4 – Multi-cycle and single-cycle load magnitude and application time

Multi-cycle loads (Ω)	Time with the load (min.)	Single-cycle loads (Ω)	Time with the load (min.)
1021	Batch duration	1024	30
511.7		515	
202.1		261	
100.1		175.2	20
67.9		104.1	
51.2		64.5	
20		21.1	10

The criteria to determine the duration magnitude was the time needed for the MFC voltage to reach approximately 90% of its maximum value when operated in multi-cycle. The same load range was applied to both operation modes to allow an adequate comparison. A breadboard and a set of resistances was used for both operation modes. In the single cycle, the loads applied were changed by parallel association of others, so as to assure no disconnection of the electrodes. Irrespective of the operation mode, loads were changed from the highest to the lowest value. Figure 4.34 displays the polarization curves for single and multi-cycle polarization trials.

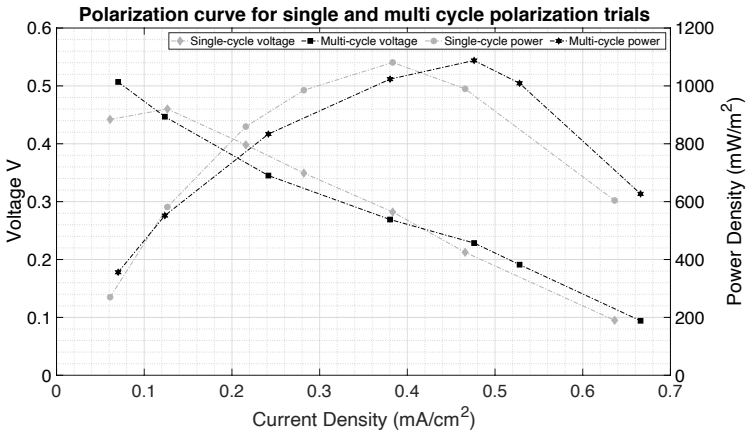

Figure 4.34 – Polarization curves for multi and single-cycle operation of a Single MFC.

The behavior between the curves is quite similar, with the maximum power happening for lower current densities at the multi-cycle trial. In fact, the difference between maximum power for both trials is 7 mW/m², 0.05 mW, about 0.6% of the absolute maximum power of both curves. The difference between current densities also amounts to a very low value, about 0.1 mA/cm². Figure 4.35 presents a box plot built from the average values per current density and voltage in each curve, with the grey whiskers representing the absolute deviation value for multi-cycle and the black whiskers the same values for single cycle.

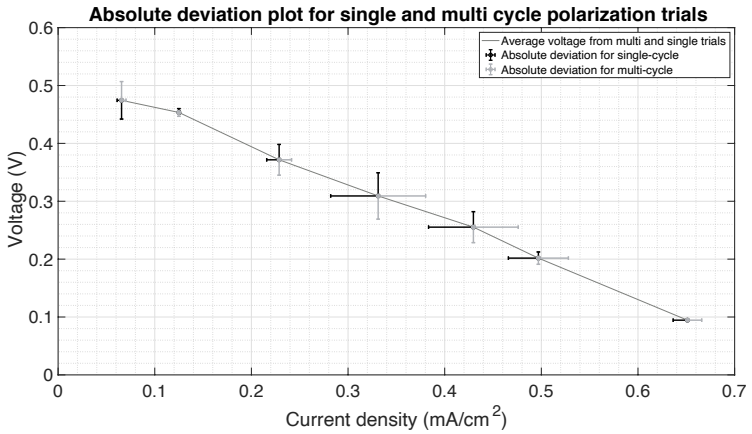

Figure 4.35 – Curve of the average voltage of each operation mode. The black whiskers represent the absolute deviation for the single cycle operation while the grey whiskers represent the same for multi cycle.

This representation shows that there are no significative differences between both operation modes. The highest current density difference was registered at around 0.33 mA/cm² for the 100 Ω range and amounts to approximately 0.049 mA/cm², 0.34 mA. As for the voltage values, the highest difference was found at the same point, with a magnitude of 0.04 V. A plot of the power density values with the difference between trials, as shown in Figure 4.36, will help further clarify if the operation mode is determinant for the maximum power extracted from a single MFC.

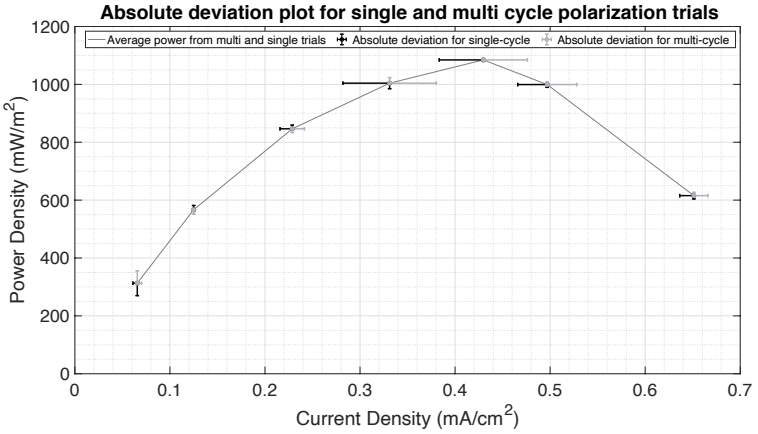

Figure 4.36 – Power density curve built from averaging the power densities for each operation mode. The black whiskers represent the absolute deviation for the single cycle operation while the grey whiskers represent the same for multi cycle.

This last plot suggests that single or multi-cycle operation of reactors following the single MFC topology will lead to the same power density values, since the highest deviations occur in the current density direction. This is particularly clear when considering there is a maximum power variation of 43 mW/m^2, or 0.03 mW in absolute power.

Although both trials were not conducted with the same load values, applying the density representations allows a direct comparison between plots. This investigation has proven that, for a fully developed biofilm, and provided enough time is guaranteed for each load, the same power levels can be achieved in single or multi cycle operation. Single cycle operation, however, decreases the time needed for conducting polarization studies. This is advantageous if a polarization study is needed, for, for instance, determining the reactor's internal load estimate quickly.

Influence of external variables on power production:

Continuous load

Data from two Single MFCs (reactor 1 and reactor 2) shows that, irrespective of the reactor, voltage profiles for the same loads exhibit the same behavior and very close final values, as showed in Figure 4.37. Having had the same wastewater and time for inoculation, it is safe to assume that the bacterial community composition must be very close, meaning that polarization trials for similar reactors with the same inoculation time return values with little discrepancy. Value fluctuations can be attributed to changes in the electrode's characteristics, namely cathode biofouling.

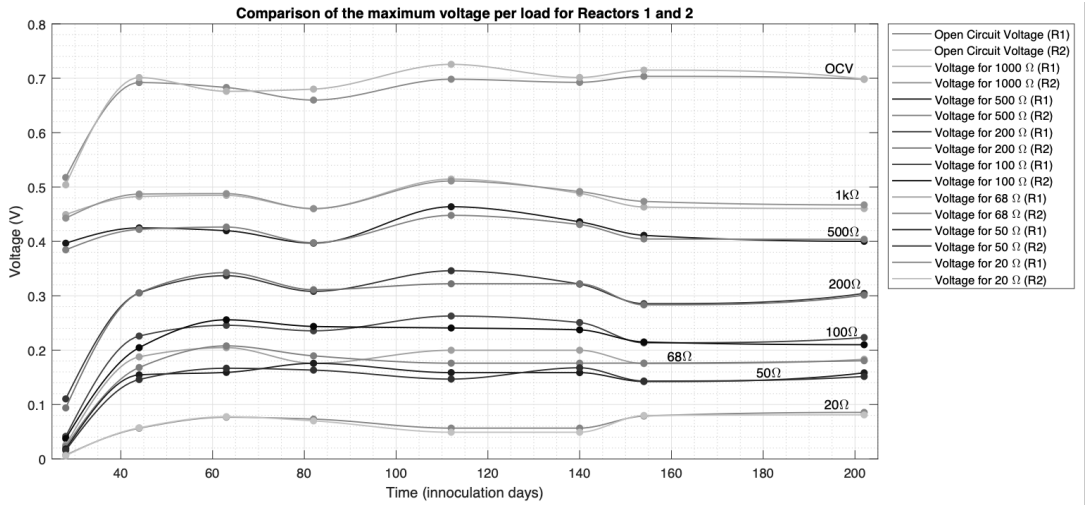

Figure 4.37 – Voltage development for different loads in reactor 1 and 2 for 202 days.

The voltage development for an MFC is neither linear with load nor with time, as can be seen by Figure 4.38. Data here represented was gathered by starting voltage monitoring as soon as a reactor was refilled with a new wastewater batch.

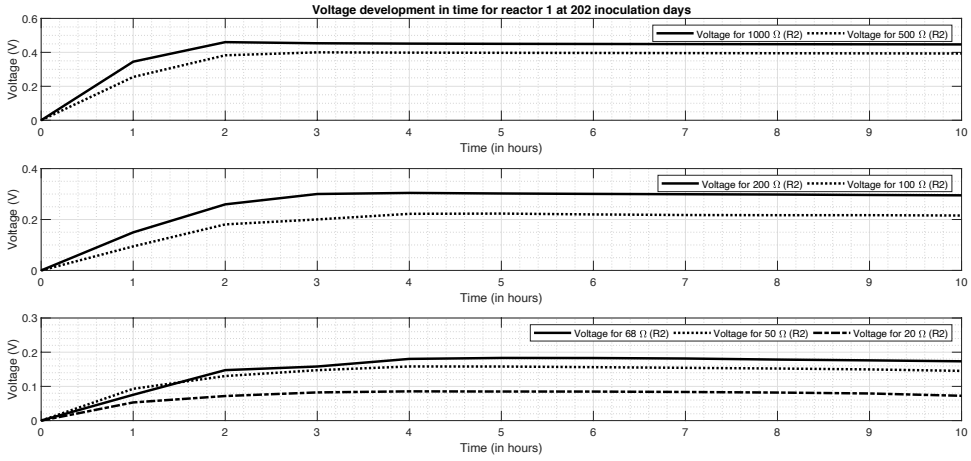

Figure 4.38 – Voltage development for different external loads at 202 inoculation days of R1.

The voltage development for an MFC exhibits properties that change according to the load value. The steady state voltage value is achieved after a specific time, which is dependent on the load and the biofilm complexity. To determine the real influence of the load on the transient response, a trial was conducted where voltage was monitored on the transition from open circuit to a load, applying the multi-cycle method, as showed in Figure 4.39.

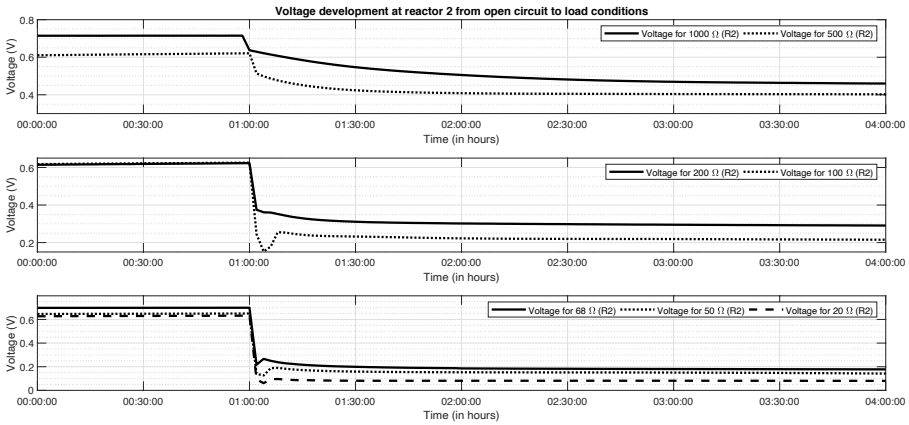

Figure 4.39 – Voltage profile from open circuit to load transition.

Such trial showed that 1 hour after the load application, the voltage value stabilizes to around 90% of the final value, irrespective of the load magnitude. It is noticeable, however, that loads of 1000 and 500 Ω need more time for voltage stabilization than loads under 200 Ω.

By knowing the response presents little no none oscillations after 1 hour, polarization trials can be conducted reliably and for shorter times, particularly using the single-cycle operation.

There is an elbow behavior on the open-circuit load transition, particularly noticeable for resistances under 200 Ω. The description of the electrobiochemical characteristics of electroactive biofilms in chapter 2 makes a reasoning of this event. This reasoning is further justified by Figure 4.40.

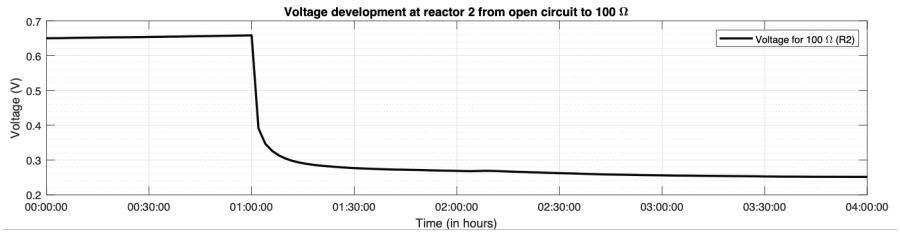

Figure 4.40 – Voltage profile from open circuit to 100 Ω transition.

The trial of open circuit to load transition for 100 Ω was repeated, after subjecting reactor 2 to 100 Ω during 2 consecutive wastewater batches, until substrate depletion. It can be concluded that successive open circuit to load trials have an impact on the voltage per load development, since the elbowing disappeared. This indicates that the exoelectrogenic bacteria may have become

closer to the anode surface and may be more readily available to promote electron transfer between the MFC's electrodes. The open circuit to load transition will be further discussed when addressing the commuted load MFC operation. These trials have further validated that, when dealing with continuous load operation, the cell exhibits a hysteretic behavior. As such, a steady-state model of the reactors can be developed.

Steady state model development

Contrary to what happens in other fuel cells without living species, the microbes on MFCs have numerous metabolic options for energy production. This has a major negative impact on the predictability of MFCs, conditioning the development of a unified model for MFC behavior. Therefore, several models are available, developed to different ends [19–22]. A unified proposal for a classification model is suggested in Figure 4.41.

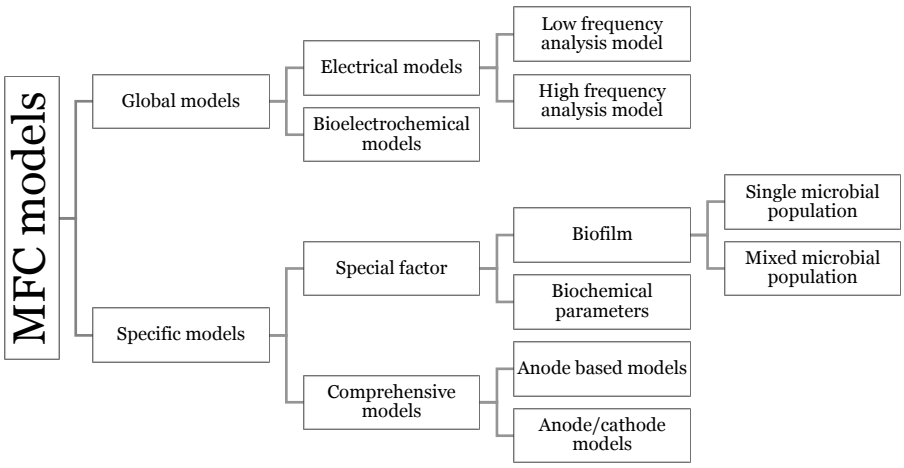

Figure 4.41 – Possible model categorization for microbial fuel cell studies.

Each model describes an MFC from a different perspective and should be applied carefully and according to its intended final use. For instance, an anode-based model should not be used to describe the MFC behavior regarding the biofilm growth and substrate consumption, since the latter is better characterized by a biochemical parameter model.

As already discussed in this chapter, the bacteria age and diversity on the anode biofilm, the substrate, the anode, the cathode and the reactor volume all differently impact a Microbial Fuel Cell's electrical behavior. This discussion will entail the development of a steady state model for Single MFCs and Single Large MFCs, estimating their internal power losses and respectively identifying their contribution on the overall polarization curve. Other studies have also been developed with similar reactors [2] and the developed algorithm will be tested against them, allowing for some data comparison. In spite of all the variability in play, a discussion of the results will show that the polarization curve typology is adequate for the electrical behavior description and that, additionally, the steady state response can be even be further simplified. Polarization

curves, particularly the voltage-current curve will support this study. Additionally, the analysis will be supported by the losses' description in Chapter 3. Data was processed in MATLAB 2018 and GraphPad Prism 7. The analysis on GraphPad Prism 7 consisted on importing the polarization data and applying two fits to the voltage-current curve: firstly a linear fit for estimating the internal resistance of the reactor, a parameter which rounds up all its direct and indirect contributions; secondly, a non-linear least square fit to estimate the parameters best describing the data. The linear regression is applied to a set of 3 values: one voltage-current pair under, one equal and one over the voltage-current pair corresponding to the maximum power. This approximation will allow estimating the internal resistance of the reactor – the slope on the linearization equation – according to the maximum power point theorem, where the maximum power is achieved when the internal and external load are equal. The non-linear regression, used for determining the full equation describing the polarization curve, outputs estimates for all the variables by setting the OCV value to the experimentally determined, the ohmic resistance to a value smaller than the internal resistance estimate from the linear regression, and all the other parameters to be positive.

Steady state model development for Single MFCs

The model was firstly applied to Single MFCs, after successful acclimation was guaranteed. The trial selected for the steady state model development was the trial at 63 days for Single MFC reactors 1 and 2. Figure 4.42 represents the linear regression for 200, 100 and 68 Ω built with GraphPad Prism 7 and equation (3.22) on chapter 3, also presented below.

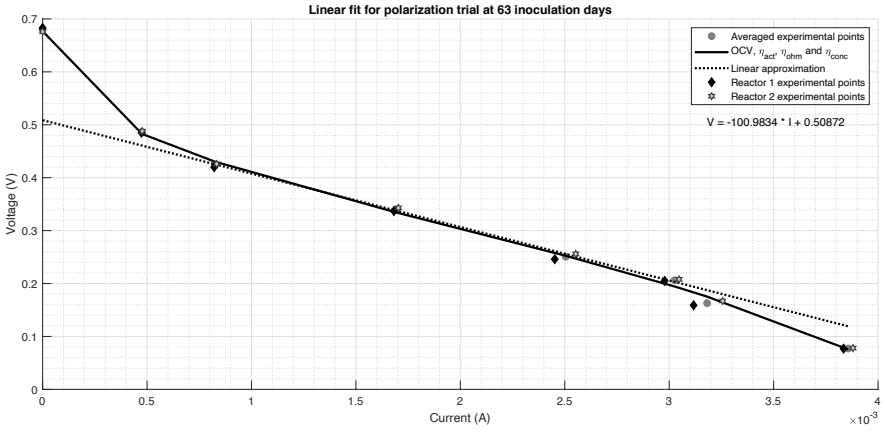

Figure 4.42 – Linear fit for loads between 200 and 68 Ω at 63 inoculation days. The plot also shows the relationship between the averaged experimental points, the actual points for each reactor and their proximity to the steady-state equation.

$$V_{OUT} = A - B \times \ln\left(\frac{I}{B_1} + 1\right) - I \times R_{ohm} - C \times e^{D \times I} \tag{4.3}$$

With both the OCV value (variable A) and an upper limit for the R parameter, an assessment for all the variables is now possible. The parameter estimation is summed up in Table 4.5.

Table 4.5 – Parameter estimation through GraphPad Prism 7 for non-linear regression and linear regression for internal resistance.

Parameter	Values for non-linear regression	Value for linear regression
A	Fixed at 679.5×10^{-3} V	
B	636.5×10^{-4}	
B1	3.628×10^{-5}	
R	50.51 Ω	≈ 100 Ω
C	2.671×10^{-3}	
D	967.4	

As can be seen by the data on Table 4.5, the internal resistance of an MFC reactor is more than the ohmic contribution [23]. Approximately half of the contributions to the internal resistance are related with activation and concentration losses. The value found for the total internal resistance is also consistent with the external resistance at which the maximum power was achieved, following the maximum power point theorem [24]. Figure 4.43 allows for a clearer representation of the influence and weight of each loss, with the plot in the lightest grey representing the sum of the losses, and, therefore, the full steady-state equation.

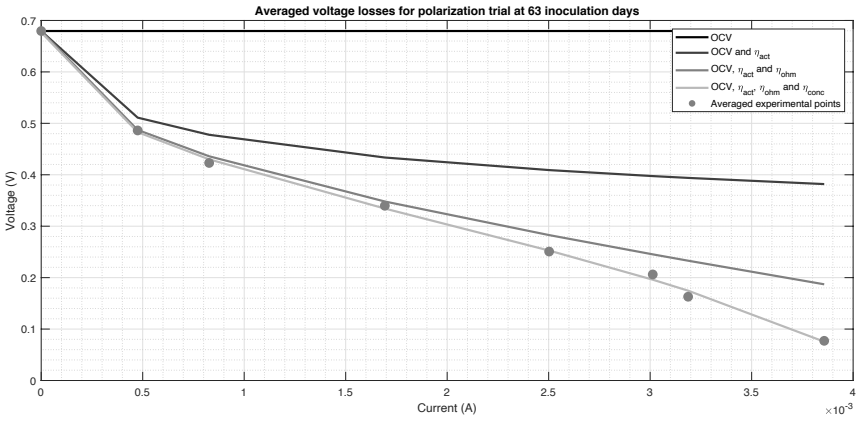

Figure 4.43 – Polarization curve built from averaged voltage and current values per external load at 63 inoculation days.

Single MFC reactors 3 through 6 were used to determine the validity of the steady-state equation previously determined. To clearly represent all the data points, voltage values belonging to the same polarization trials were averaged and used for comparison purposes.

The plots on Figure 4.44 clearly show that there were no power overshoot conditions in either trial and that the maximum power of about 880 mW/m2 (0.622 mW at 248 mV) was achieved at 43 days and around the same external load, approximately 100 Ω.

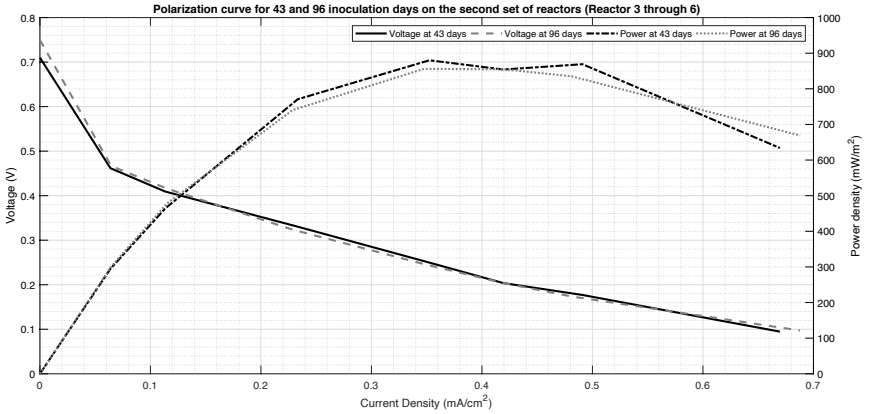

Figure 4.44 – Polarization curves built from averaged voltage values per external load at 43 and 96 inoculation days for reactors 3 through 6.

Having results so close to the ones used to determine the steady state equation is a clear indication that similar reactors exposed to similar conditions are expected to have close voltage current profiles, as proved on Figure 4.45.

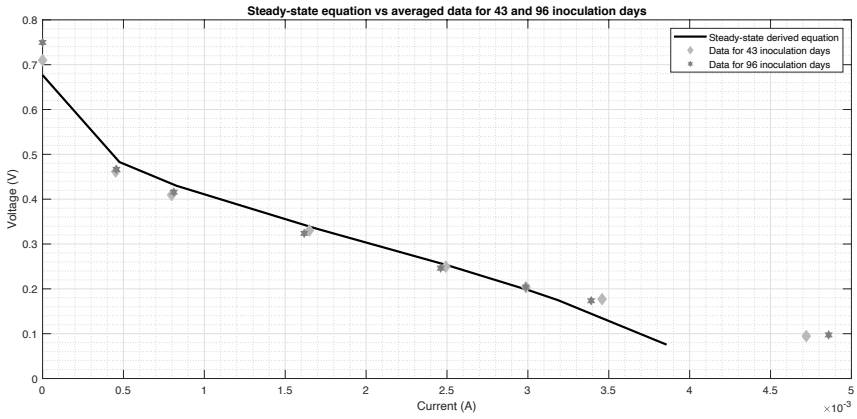

Figure 4.45 – Polarization curves built from averaged voltage values per external load at 43 and 96 inoculation days for reactors 3 through 6.

Supported by previous colonization procedures, reactors from the second colonization batch reached higher current densities, although similar voltage levels. Determining the absolute deviation from the steady state equation shows that this standard equation can be used to estimate the voltage current profile from 500 to 68 Ω, as shown by Figure 4.46.

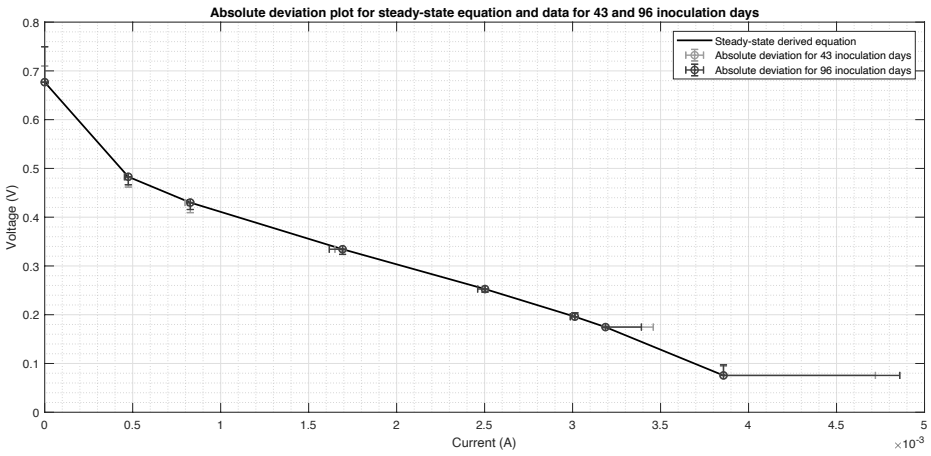

Figure 4.46 – Absolute deviation of the experimental data and the steady state equation for polarization trials at 43 and 96 inoculation days for reactors 3 through 6.

An accurate calculus of the relative deviation, presented in Table 4.6, further reinforces the applicability of the steady-state equation, and what range is safe to use for an electrical model development.

Table 4.6 – Relative error, in percentage, between the steady state curve and the averaged data from trials at 43 and 96 inoculation days.

Relative deviation from Steady State equation

Load (Ω)	43 inoculation days		96 inoculation days	
	Voltage deviation (%)	Current deviation (%)	Voltage deviation (%)	Current deviation (%)
OCV	4.30	0	9.34	0
1000	-4.59	-5.11	-3.50	-4.08
500	-5.05	-3.71	-3.43	-1.98
200	-1.20	-2.63	-3.26	-4.66
100	-1.20	-0.38	-2.60	-1.70
68	3.76	-0.83	3.80	-0.86
50	1.39	7.85	-0.60	6.02
20	20.23	18.29	22.35	20.62

Steady state model development for MFCs from another study

The work in [2] is a detailed description of the method applied for producing the activated carbon air-cathode. To validate such procedure and achievement, the research team subjected the electrode to application settings, using it on a 28 mL MFC with the same anode brush and substrate as the one described in this work. The polarization data of the reactor there presented, and here in Figure 4.47, was used to apply the described method.

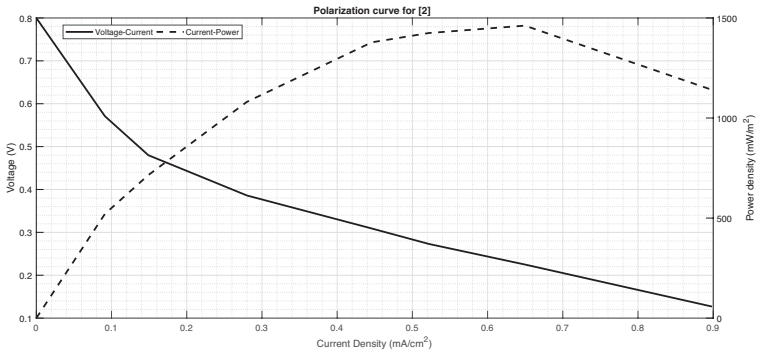

Figure 4.47 – Polarization curve reconstructed from the data on [2] and the trial with the PVDF cathode.

Since the maximum power was reached for 50 Ω, two other values in the ohmic region were chosen for the linearization procedure: the voltage-current pairs for 75 and 100 Ω.

The slope of the line in Figure 4.48 provides a rough estimate for the internal resistance of the aforementioned reactor.

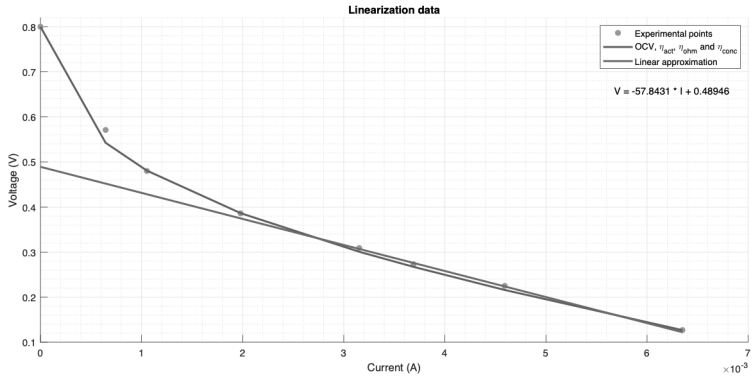

Figure 4.48 – Linearization procedure for polarization data on [2]. The slope of the linear regression, the internal resistance estimate, is between 50 and 75 Ω.

Although no information was retrieved on the open circuit voltage of the considered research, an estimate, based on the results for R1 through R6 of this study, of 0.8 V was made. Table 4.7 presents the result of the non-linear regression on all the equation variables, which is, as expected, over 50 Ω and under 75 Ω.

Table 4.7 – Parameter estimation through GraphPad Prism 7 for non-linear regression and linear regression for internal resistance.

Parameter	Values for non-linear regression	Value for linear regression
A	Fixed at 800×10^{-3} V	
B	1.107×10^{-1}	
B1	8.515×10^{-5}	
R	30.62 Ω	≈ 58 Ω
C	3.842×10^{-6}	
D	227.3	

The weight of each loss in this polarization trial is exposed with Figure 4.49. It can be observed that the ohmic and concentration losses are superimposed, meaning that the concentration losses are neglectable. This means that the flow between reactants (acetate) and products (water) happens without any unbalances, which, in turn, proofs that the biofilm is acclimated even for high currents. Typically, such polarization curves are common between biofilms with over 1 year.

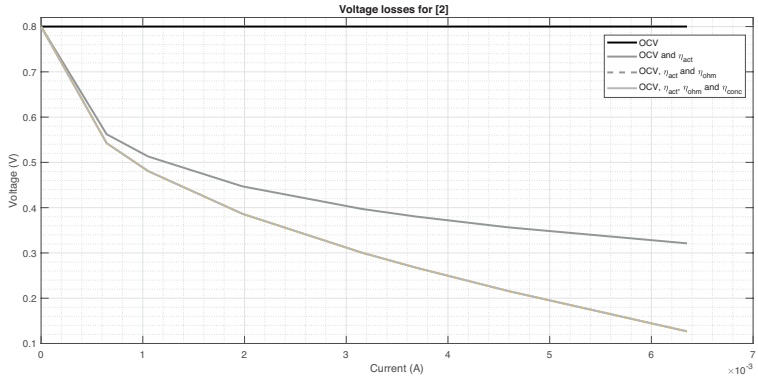

Figure 4.49 – Voltage losses plot for the polarization data on [2]. The ohmic losses are missing because they are superimposed on the activation losses, meaning they are irrelevant for the particular settings on this reactor.

Steady state model development for Single Large MFCs

The presented method for determining the polarization curve equation was applied to one of the Single Large MFCs, R8, as a further proof of the method feasibility. The data used for method validation was retrieved with a biofilm 84 days old. The polarization data is presented in Figure 4.50.

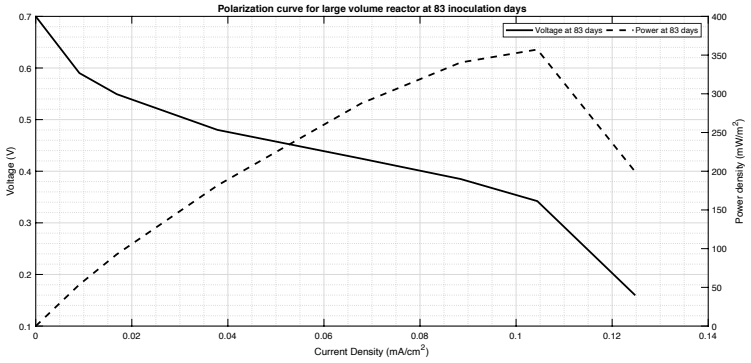

Figure 4.50 – Polarization curve built from averaged voltage values per hour and external load at 83 inoculation days for a large volume reactor.

The polarization curve shows a typical behavior, albeit the drop for higher currents. This drop shows that the biofilm still needs more time to develop and achieve full maturation, although ready for polarization trials as no power overshoot is pictured. The maximum power achieved was of 357 mW/m² (2.27 mW at approximately 342 mV for 51.5 Ω).

Applying the same method as for the Single MFCs, a linear regression, pictured in Figure 4.51 was applied to the vicinity of the maximum power point: the voltage-current relationship for 68 Ω and 100 Ω were selected as the most adequate data points to describe the ohmic region, apart from the pair for the maximum power (51.5 Ω). In this particular case, since data between 51.5 Ω and 20 Ω is missing (as depicted by the sharp drop after 0.10 mA/cm²), specific measures were needed to dimension the polarization equation.

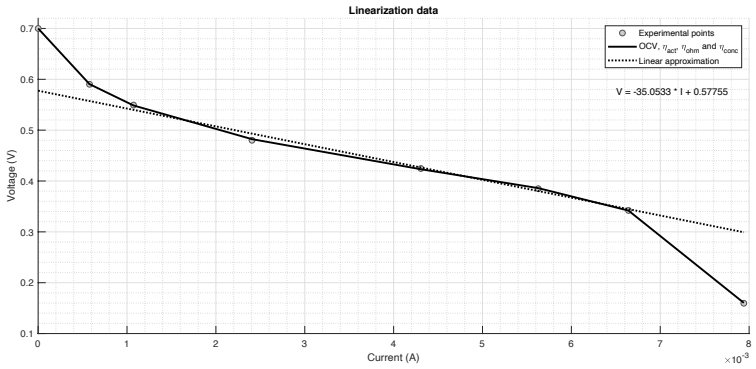

Figure 4.51 – Linear fit for a large 250 mL reactor and loads between 100 and 51.5 Ω at 84 inoculation days.

Table 4.8 presents the estimates for each of the polarization curve unknowns.

Table 4.8 – Parameter estimation for a larger volume equivalent of the small reactors.

Parameter	Values for non-linear regression	Value for linear regression
A	Fixed at 700×10^{-3} V	
B	7.65×10^{-2}	
B_1	1.98×10^{-4}	
R	8.49 Ω	≈ 35 Ω
C	2.906×10^{-6}	
D	1395	

By knowing each of the variables weight, a full description of the reactor's losses can be developed, as shown in Figure 4.52.

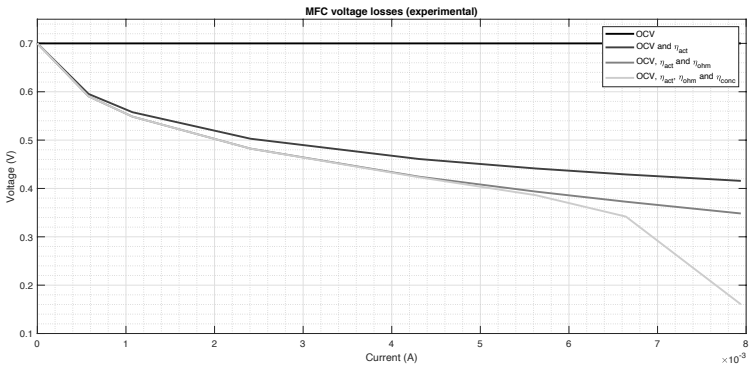

Figure 4.52 – Voltage losses discrimination according to the estimates for the polarization curve parameters.

A quick comparison of the internal resistance of the Single and Single Large MFCs hints that the internal resistance of the large reactor is smaller, allowing for the development of larger currents at similar loads. The proportion in volume, however, does not follow the same path: a large volume reactor exhibits smaller power densities although higher in absolute value.

Considering Table 4.6 and a generic 28 mL air-cathode, anode carbon brush, acetate substrate reactor, as represented by the Single MFCs, a steady state MFC electrical model can be developed to resistances between 500 and 68 ohms. In such range, the polarization curve is mostly described by a linear regression in the following form:

$$V_{mfc} = V_{OCV} - I \times R_{eq} \tag{4.4}$$

Where V_{OCV} represents the measured open circuit voltage and R_{eq} the total value of the internal resistance, as previously discussed. The model, therefore, has an equivalent electric circuit composed of a voltage source and a 100 Ω resistance connected in series. The model on Figure 4.53 is applied as describing only the steady state behavior of a specific, previously described, MFC.

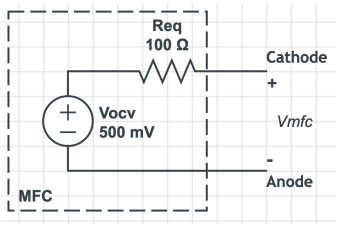

Figure 4.53 – Electrical model for describing the steady state behavior of a 28 mL single chamber air-cathode microbial fuel cell.

Transient model development

The transient model of the same reactor type has also been studied. The instrumentation platform (IP) previously described in the section “Influence of internal variables on power production” of the present chapter, was used to develop the transient model of Single MFCs. A transient model is proposed in [25] and consists of a DC voltage source, two resistors and a capacitor. This model is presented in Figure 4.54.

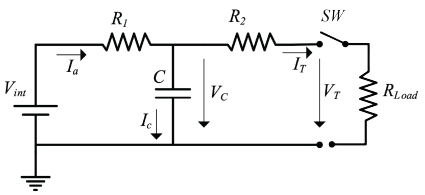

Figure 4.54 – MFC transient equivalent circuit.

The circuit parameters are determined by applying the methodology in [26]. The voltage V_{int} corresponds to the open-circuit voltage (no load applied) and is determined with the MFC in open circuit, for a time period guaranteeing that the terminal voltage, V_T, reaches the steady state. To that end, a resistive load, R_{load}, is applied to the MFC output, closing switch SW, for a period of time long enough so that the steady state is achieved. Voltage V_T^- is the voltage measured immediately before opening the switch SW, disconnecting the resistive load. The current I_T^- is determined by:

$$I_T^- = \frac{V_T^-}{R_{Load}} \tag{4.5}$$

At steady-state, current I_c is zero and the capacitor voltage is fixed (fully charged). Immediately after opening the switch SW, the current I_T goes to zero. Because the voltage V_c does not change instantaneously, the voltage V_T^+ acquired immediately after opening the switch SW, will be equal to the capacitor voltage, V_c, before switch SW opening.

Resistance R_2 can be determined by:

$$R_2 = \frac{V_T^+ - V_T^-}{I_T^-} \tag{4.6}$$

At the moment when the current I_T^- is determined, the capacitor C is fully charged and, therefore, it has no current, corresponding to an open circuit. For this reason, the current flowing trough R_1 is equal to I_T^-. The value of resistance $R_1$is determined by:

$$R_1 = \frac{V_{int} - V_T^+}{I_T^-} \tag{4.7}$$

The time sequence of the four successive acquisitions is shown in Figure 4.55.

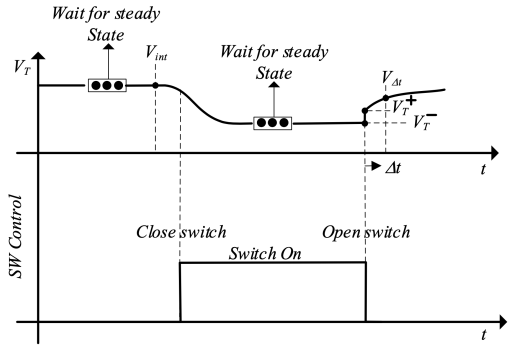

Figure 4.55 – Switching voltage acquisition.

A Single MFC reactor was tested with a resistive load of 227 Ω (*TapsDo* = 0), a waiting time, Δt, for sampling after switch opening of 30 seconds (using *TapsUp* as the configuration) a 60 minutes period between sampling sequence (*MP* = 60 min) and a total trial time of 1440 minutes (*PolP* = 1440 min). The experimental data presented in Table 4.9 is used to determine the values of R_1 and R_2.

Table 4.9 – Experimental data.

V_{int} (mV)	V_T^- (mV)	V_T^+ (mV)	R_{Load} (Ω)	R_1 (Ω)	R_2 (Ω)
650	448	480	227	86.1	16.2

The capacitor voltage $v_{c(t)}$ development after opening the switch is given by:

$$v_c(t) = V_{int} + V_T^+ e^{-\left(\frac{1}{CR_1}\right)t} - V_{int} e^{-\left(\frac{1}{CR_1}\right)t} \tag{4.8}$$

A time, Δt, after opening the circuit and measuring V_T^+, corresponds to a new open circuit voltage measurement, $V_{\Delta t}$. Solving (8) in order to the capacitance, C, equation (9) can be used with data from Table 4.9 and Table 4.10.

$$C = -\frac{\Delta t}{ln\left(\frac{V_{\Delta t} - V_{int}}{V_T^+ - V_{int}}\right) R_1} \tag{4.9}$$

The time constant associated with the variation of the output voltage is given by:

$$\tau = \frac{CR_1R_2}{R_1 + R_2} \tag{4.10}$$

Table 4.10 – Parameter estimation for the transient model.

$V_{\Delta t}$ (mV)	Δt (sec)	C (F)	τ (sec)
590	30	0.33	4.50

Increasing the reactor size

A performance comparison for Single and Single Large MFC is addressed in this section. In order to conduct a more precise comparison between the experimental data, a benchmark trial was conducted on a Single MFC, R6. The anodic biofilm had 674 days and the cathode applied was freshly produced, without any aerobic biofilm deposition. The polarization curve is displayed in Figure 4.56. This data will also serve as reference for the series and parallel association of reactors.

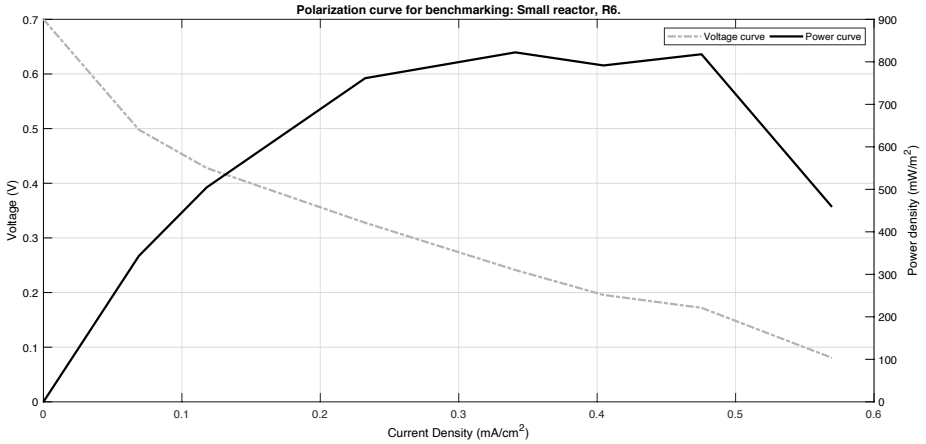

Figure 4.56 – Polarization curve for a small volume reactor, R6, with a fresh cathode and an anodic biofilm of 674 days (over 1 year and a half).

The analysis of the data on Figure 4.56 shows that a maximum power density of 822 mW/m² (0.58 mW) was produced at 0.34 mA/cm² or 100 Ω. By applying the maximum power transfer theory, this load value can be identified with the reactor's internal resistance [27]. A lower power density than the curve would anticipate is noticeable at about 0.4 mA/cm². This, however, is not corroborated by the total energy extracted, as shown in Figure 4.57.

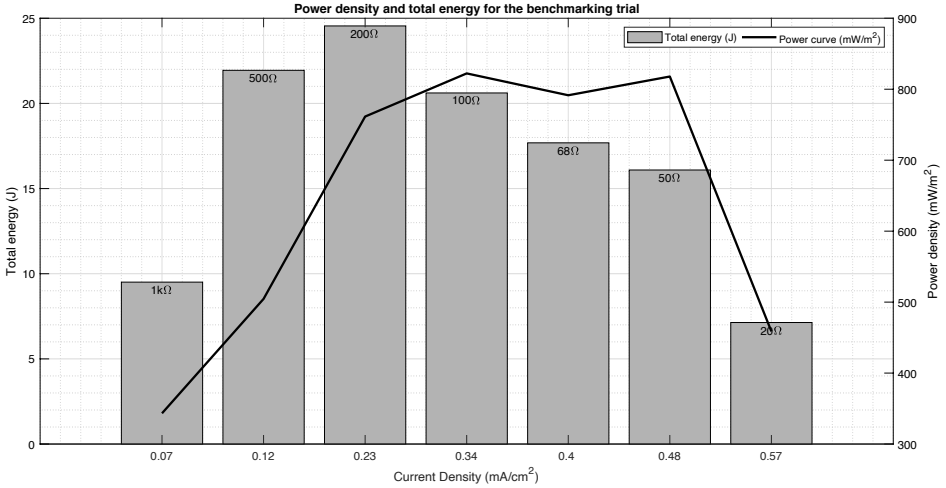

Figure 4.57 – Stacked view of the power curve and extracted energy values per load for a Single MFC, R6.

The analysis of the total extracted energy per load, considering trials run until substrate depletion, also shows that the maximum energy harvested does not occur at the load for maximum extracted power. In fact, between the two loads (200 and 100 Ω), more energy is extracted at the lowest current value. The difference corresponds to approximately 0.05 J/per hour, where the trial for 200 Ω run for 21 hours and the trial for 100 Ω for 17 hours, both until current values remained over 0.1 mA. The trial running for longer presents larger energy values. The maximum efficiency of the reactor was determined to be 8.9%, with 24.5 J extracted from 28 mL of the AW (274.4 J).

To determine if an increase in the reactor volume can be related with an increase in the produced power, a polarization trial was run on a Single Large MFC, R8, and is presented with Figure 4.58. As with the trial on R6, the load was uninterruptedly connected between the electrodes until substrate exhaustion.

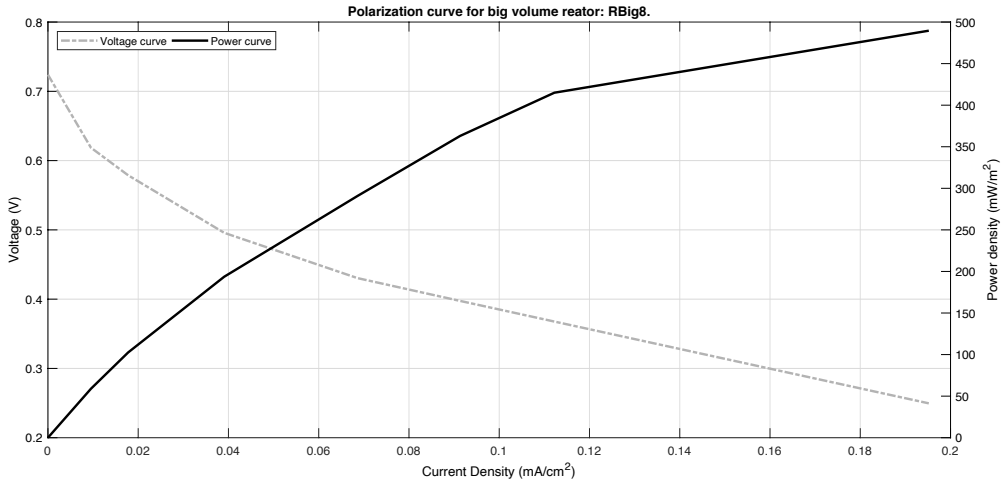

Figure 4.58 – Polarization curve for a big volume reactor, R8, with a fresh cathode and an anodic biofilm of 415 days (over 1 year).

In comparison with the small volume reactor, all the voltage values are higher, although current and power density figures are lower. As Table 4.11 shows, the same can't be said for absolute power and current values, which present higher values than the small volume reactor for loads under 100 Ω, inclusive. The curve shape hints that the polarization run load values were not adequate to find the reactor's internal resistance and, consequently, its maximum power production capabilities. The lowest load value on the set, 20 Ω, seems to be an overestimation of the reactor's internal resistance. Nevertheless, and for 20 Ω, the maximum power found for the trial was of 487 mW/m^2 (3.1 mW).

As Figure 4.59 clearly represents, the total extracted energy was higher for 68 Ω, 207 J, which also corroborates the conclusion for the trial with the Single MFC.

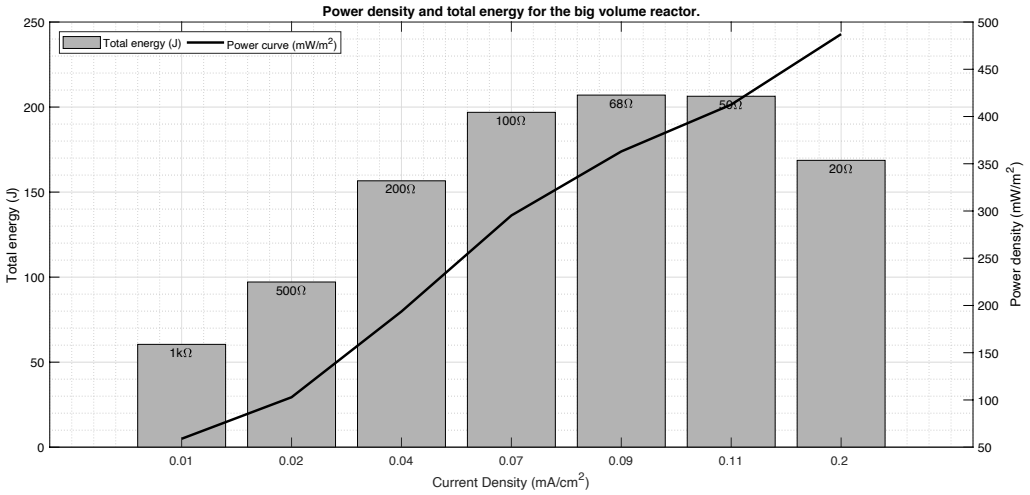

Figure 4.59 – Stacked view of the power curve and extracted energy values per load for the Single Large MFC, R8.

The volume relationship between the two reactor types is 9-fold. However, neither power nor extracted energy increased in that proportion. In fact, power density decreased and the reactor performance at the maximum energy extraction was 5.8% lower. At the maximum power production load, the difference was even 3.3% higher, at 9.1%. No 9-fold proportion was found between the reactor volume increase and any other energy production parameter, although the anode number and cathode surface were increased.

Table 4.11 – Summary of performance comparison between Single and Single Large MFCs.

Variable	Unit	Trial	
		Single MFC	Single Large MFC
Anodic biofilm time	Days	674	415
Cathode	Days	0	
Cathode area	cm^2	7.07	63.62
Voltage at max. power | max. energy	V | V	0.24 | 0.33	0.25 | 0.40
Current at max. power | max. energy	mA | mA	2.41 | 1.64	12.42 | 5.81
Power at max. power | max. energy	mW | mW	0.58 | 0.54	3.10 | 2.31
Current density at max. power | max. energy	mA/cm^2 | mA/cm^2	0.34 | 0.23	0.20 | 0.09
Power density at max. power | max. energy	mW/m^2 | mW/m^2	822 | 761	487 | 363
Max. total energy extracted | available	J | J	24.55 | 274	207 | 2450
Max. performance absolute | versus Single MFC	%	8.95 | -	8.45 | 8.95

Series and parallel association

Another strategy that can be used to improve the energy production levels from MFCs is the series or parallel association of two reactors. Theoretically, considering two reactors as two equal voltage sources, their series association will improve the total voltage of the set, while the parallel grouping will contribute to higher current levels. The choice of the best association will ultimately rely on the application. Nevertheless, and considering the 100 Ω internal resistance of the small reactors found with the benchmarking trial, the series association is expected to produce the highest power levels for 200 Ω and the parallel combination at 50 Ω. According to this expectation, series and parallel trials were conducted only for three load values: 200, 100 and 50 Ω. The biofilm for these trials has the same time, 674 days.

The series trial datapoints are superimposed on the Single MFC, R6, polarization curve in Figure 4.60.

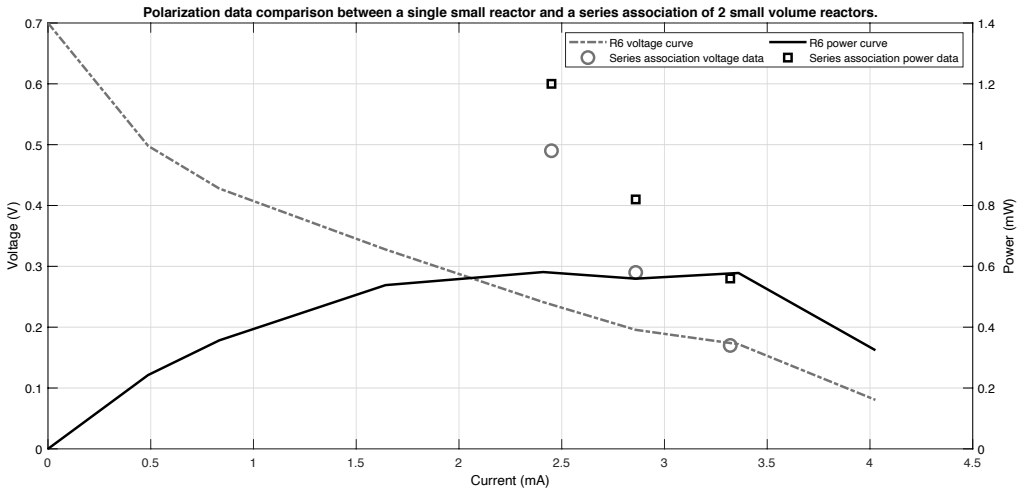

Figure 4.60 – Polarization curve of Single MFC (R6) and datapoints for series association of two Single MFCs (R5 and R6).

The polarization curve is presented with absolute values of power and current since no assumption can be made on the reference area for reaction: there are no guarantees that the reactors performed the same way and, therefore, the cathode area can't be doubled on that assumption.

Overall, the series association of two reactors produced higher voltage values, except for 50 Ω. As far as current is concerned, the values were approximately the same for a single reactor or two series connected MFCs. These datapoints seem to point that, for lower loads, the series behavior approaches the performance of a single MFC. As far as power is concerned, due to the higher voltages resulting from the series association, values are also higher for higher loads. In fact, for the 200 Ω load – corresponding to the series association of two reactors with an internal load of 100 Ω – the value is 52% higher than the one achieved with a single reactor (1.2 mW versus 0.58 mW). For 2 reactor series grouping, power seems to double when compared with power harvested

with a single reactor. When analyzing the extracted energy, the available energy considered for calculation was two times that of a single reactor. This has produced the plots on Figure 4.61.

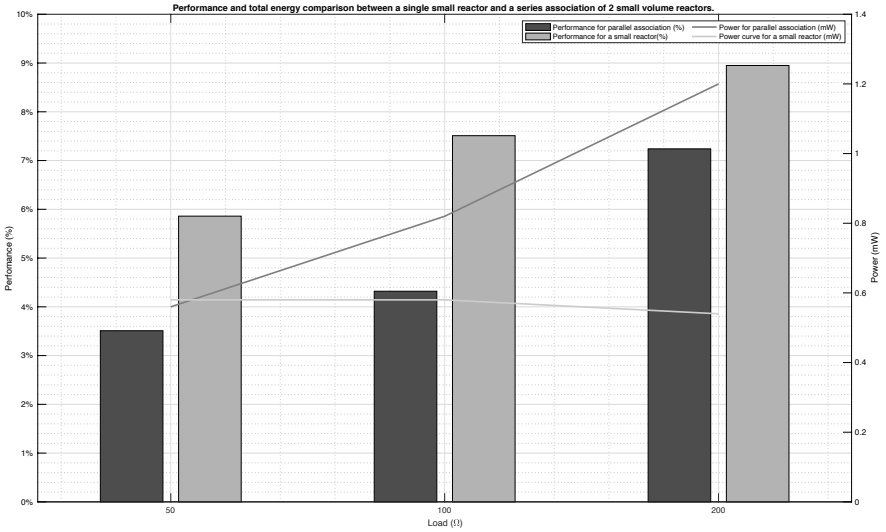

Figure 4.61 – Comparison of the power and extracted energy values, per load, for a single reactor and a series association.

Irrespective of the load value, the performance of this trial was always lower than the performance of a single reactor. The biggest performance difference was 73.7%, observed at 100 Ω. The maximum energy harvested was 39.7 J of a combined total of 548.8 J, for the same load as the maximum power (200 Ω).

On the parallel association of reactors, a power increase is also predictable due to increased currents. The same consideration for power and current presented for building the series curve is applied to Figure 4.62.

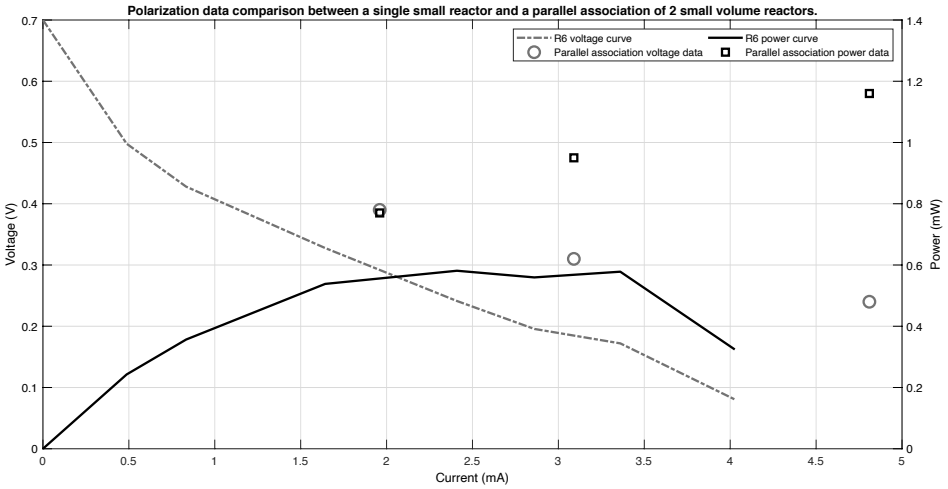

Figure 4.62 – Polarization curve of the Single MFC (R6) and datapoints for parallel association of two Single MFCs (R5 and R6).

In this mode of operation, both voltage and current figures have increased. The best performance is found at 50 Ω, substantiating the theoretical prediction. All datapoints present significative gains when compared to the single reactor, with absolute power improvements ranging from 29.75% at 200 Ω to 50.09% at 50 Ω.

Data on Table 4.12 provides precise values that authenticate the above data and plot. As with series grouping, also parallel merging of reactors leads to increased power, with simultaneous increases in voltage and current. A similar behavior can be found for the performance of the reactor, as showed by the plot on Figure 4.63.

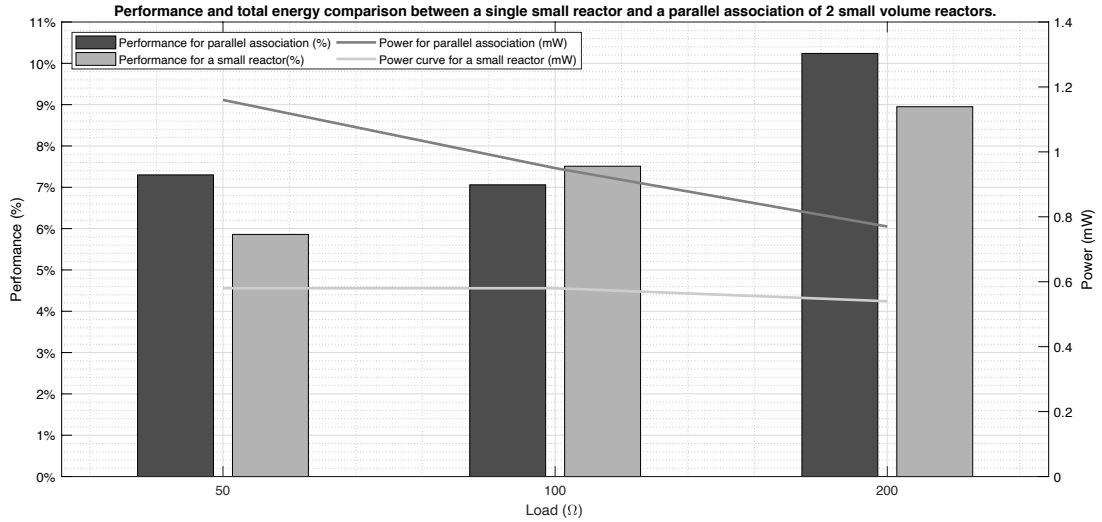

Figure 4.63 – Comparison of the power and extracted energy values, per load, for a single reactor and a parallel association.

The best performance of the trial was found at the load for maximum power, 50 Ω, and corresponds to a 19.7% improvement from the single reactor. At 200 Ω the improvement was smaller, around 12.6% whilst at 100 Ω the single reactor outperformed the parallel association of MFCs.

A power comparison between single reactor, series and parallel association is presented in Figure 4.64.

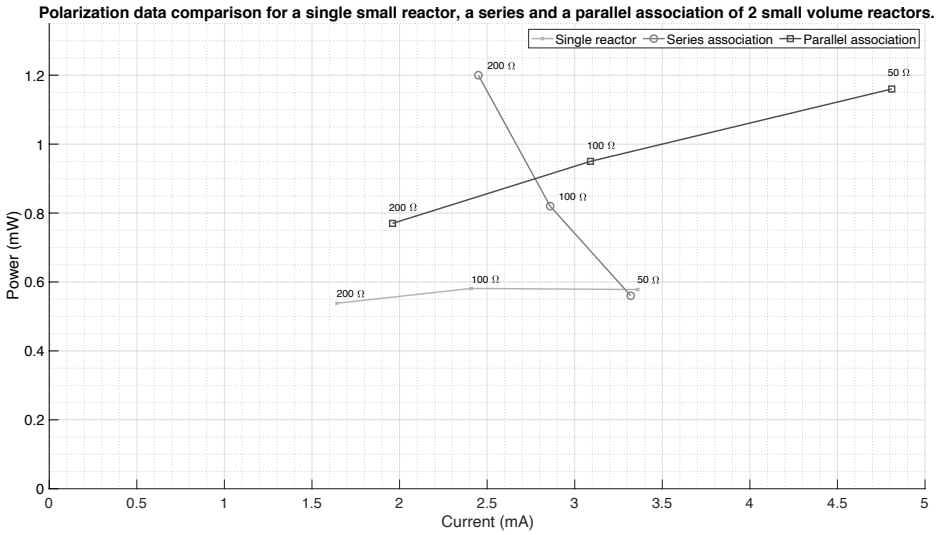

Figure 4.64 – Comparison between the power production capabilities of a single reactor, a series and a parallel association.

This complete representation highlights the clear dominance of the 50 Ω parallel trial, with increased power and current when compared to every other trial. It is also very noticeable that lower loads improve the produced current.

When comparing the performance of each trial, using Figure 4.65, it becomes clear that the 200 Ω load leads to greater energy extractions from the reactors, particularly for parallel associations. For 100 Ω, a single reactor has a better energy extraction than any other association and the parallel grouping is highlighted again at 50 Ω.

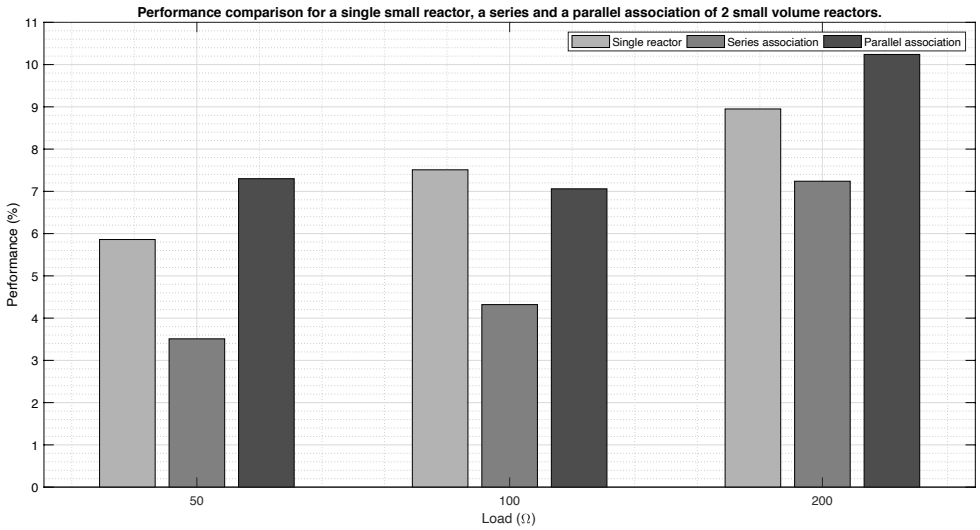

Figure 4.65 – Comparison of the extracted energy values, per load, for a single reactor, a series and a parallel association.

Considering both the power and performance studies, for small reactors, the best way to use two MFC reactors for energy production is to have them connected in parallel and subject to a load which value equals the parallel equivalent of their internal resistances. This work should be further investigated for associations of more than two reactors. Also, other studies have found that these associations are subjected to voltage reversal phenomenon, which limits their application capabilities [28,29]. Other studies have determined that an advantageous way to explore these associations is to have them done intermittently, rather than continuously [30–32]. Table 4.12 presents a summary of the results with series and parallel grouping compared with a Single MFC.

Table 4.12 – Summary of performance comparison between Single, Series and parallel grouping of Single MFCs.

Variable	Unit	Trial		
		Small volume	Series association	Parallel association
Anodic biofilm time	Days	674		
Cathode	Days	0		
Cathode area	cm^2	7.07		
Voltage at max. power | max. energy	V | V	0.24 | 0.33	0.49 | 0.49	0.24 | 0.39
Current at max. power | max. energy	mA | mA	2.41 | 1.64	2.45 | 2.45	4.81 | 1.96
Power at max. power | max. energy	mW | mW	0.58 | 0.54	1.20 | 1.20	1.15 | 0.77
Current density at max. power | max. energy	mA/cm^2 | mA/cm^2	0.34 | 0.23	0.35 | 0.35	0.68 | 0.28
Power density at max. power | max. energy	mW/m^2 | mW/m^2	822 | 761	1705 | 1705	1639 | 1084
Max. total energy extracted | available	J | J	24.55 | 274	39.71 | 548	56.19 | 548
Max. performance absolute vs Single MFC	%	8.95 | -	7.24 | 8.95	10.24 | 8.95

Interrupted and commuted operation

The last researched strategy for power optimization of MFC reactors was identified when open circuit voltage conditions were imposed, for the same AW batch, before load connection, as determined in the "Continuous load" discussion. The plot shape of Figure 4.39 suggests a capacitive behavior of the reactor, more evident when the external load applied was close to the cell's internal resistance value. The work on this subject is herein presented.

The initial trials were conducted for 50% duty cycles and ON times of 5, 10, 15 and 30 minutes.

A set of 4 reactors was chosen to conduct the trials. Reactor 1 was tested with a ON time of 5 minutes (1.67 mHz), reactor 2 with a ON time of 10 minutes (833.33 μHz), reactor 3 with a ON time of 15 minutes (555.56 μHz) and reactor 6 with 30 minutes (277.78 μHz). Reactors 4 and 5 were tested, respectively, with 20 and 25 minutes of ON time. This data was left out due to issues with the data acquisition instrumentation. The trials consisted in feeding the reactor with fresh AW and connecting a 100 Ω load for 30 minutes before starting the interrupted connection investigation. After 30 minutes, the load was connected and disconnected from the MFC for several times, with at least 3 OFF cycles. The load value was determined according to the reactor's internal load estimate, found through a polarization trial. The period for comparison was 4 hours and datapoints were acquired at 2 minutes intervals. The energy calculus was the cumulative sum of the 2 minutes differential energy for 30 minutes.

These interrupted load trials were compared against continuous operation trials in the same reactors: the reference data for interrupted load with 5 minutes ON time (reactor 1) was collected by applying the same load, continuously, to reactor 1 with a same age cathode.

The plots on Figure 4.66 begin the voltage comparison discussion.

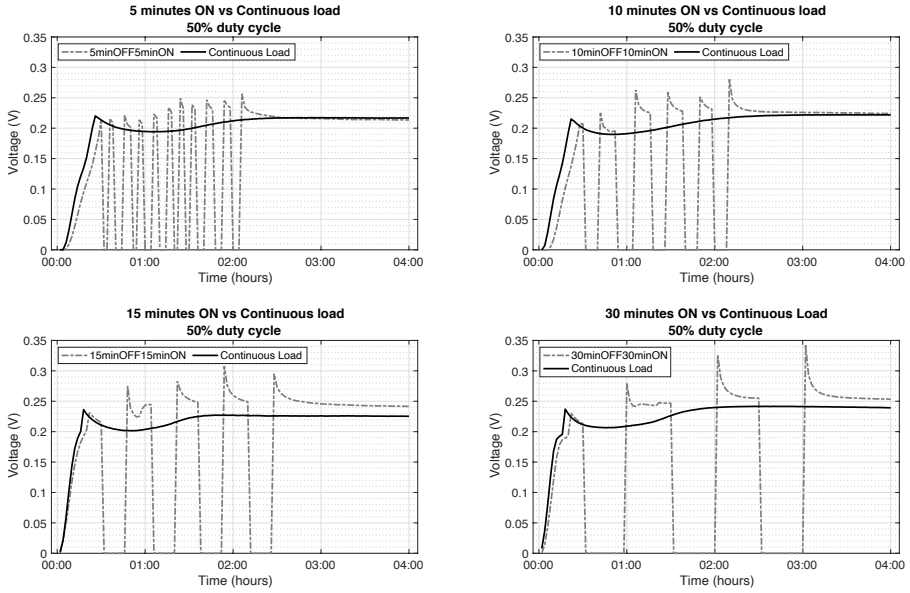

Figure 4.66 – Voltage datapoints acquired at 2 minutes intervals for 4 hours for continuous and interrupted load operation. The interrupted load operation was tested for ON times of 5 (top left), 10 (top right), 15 (bottom left) and 30 (bottom right) minutes, always with a 50% duty cycle.

The interrupted load connection seems to induce overvoltages, confirming that the biofilm is capable of storing charge. The 30 minutes initial time applied across the reactors also shows that not all the reactors reached the same operation regime before applying open circuit conditions. Reactors 1 and 2 had a slower voltage development than reactors 3 and 5. However, when the load conditions were not preceded by open circuit, all reactors followed the continuous operation behavior. When considering the OFF-time duration, periods of 15 minutes or greater seem to induce more profound changes on the biofilm performance. The continuous operation after interrupted load (approximately over 3 hours for all reactors) does not follow the continuous load trial as closely as for OFF times under 15 minutes.

There are some reading fluctuations derived from instrumentation issues. To determine the performance improvement between the trials above mentioned and the continuous load trial, a sample per ON time was selected. This sampled data is displayed in Figure 4.67. To guarantee the comparison happens for a stabilized operation, voltage, power and energy per ON time plots will be compared against the same ON periods of a continuous operation after 3 hours. This 3-hour value was selected because each continuous load plot shows a steadied operation after that operation time. The sample choice was based on the sample exhibiting the profile closest to all the remaining cycles.

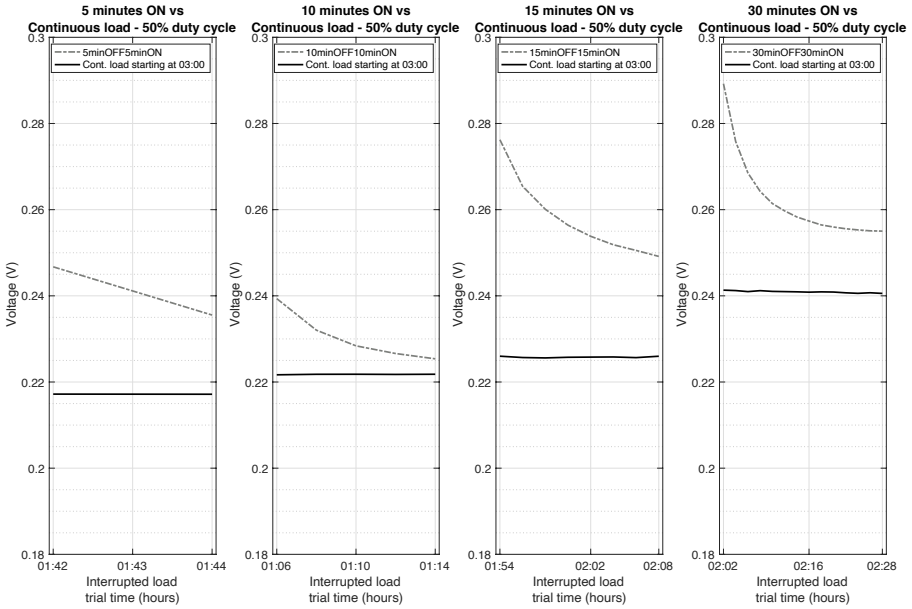

Figure 4.67 – Voltage sample per each ON time. The continuous data, represented with a black line, corresponds to the voltage values measured for the duration of each ON time, after operating each corresponding reactor for 3 hours. This separate trial happened with the same wastewater composition, the same cathode age and roughly the same temperature.

All the plots show that having the cell operating in open circuit conditions before connecting a load induces higher voltage levels than its continuous counterpart. It is noticeable that greater open circuit times (OFF) lead to greater differences between the voltages in both regimes of operation. The trial with 30 minutes of OFF time is, in fact, the trial with the highest voltage levels, although close to the trial with 15 minutes of OFF time.

Figure 4.68 displays the equivalent of the previous data in terms of power.

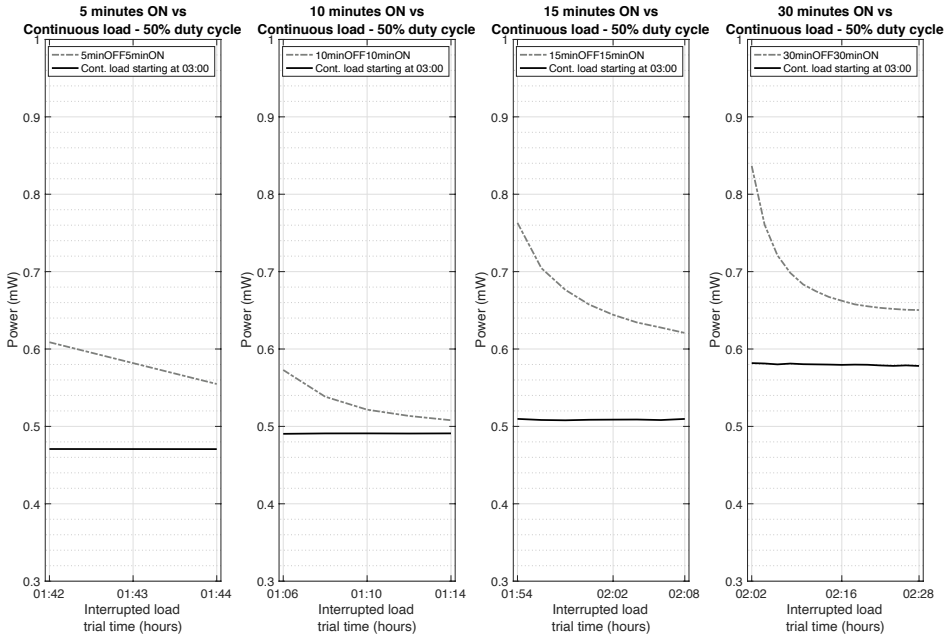

Figure 4.68 – Power sample per each ON time. The continuous data, represented with a black line, corresponds to the power values indirectly determined from the voltage measured for the duration of each ON time, after operating each corresponding reactor for 3 hours.

Increasing the ON duration has shown that the biofilm's improved response has a temporal limit, as can be seen by the smoothing of the power curve for 30 minutes of ON time. An accurate quantification of improvement can be determined by plotting the total energy equivalent for each ON time, as in Figure 4.69.

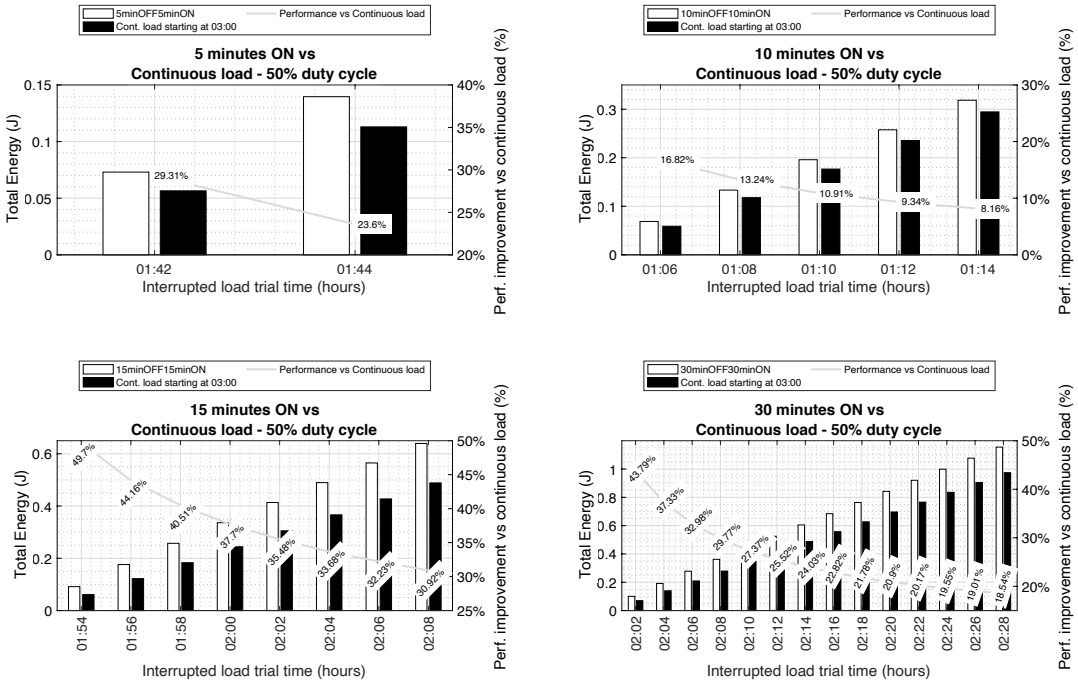

Figure 4.69 – Total energy per each ON time vs equivalent for continuous load. As before, the continuous equivalent corresponds to the total energy determined for the duration of each ON time, after operating each corresponding reactor for 3 hours. The total energy per trial is displayed with the left vertical axis. The performance improvement comparing with the continuous load is measured with the right vertical axis.

For the duration of each ON cycle, all periods present greater energy values than when the reactor is operated continuously. The general trend confirms that, for a maximum of 30 minutes, greater OFF times improve the performance of the interrupted operation. It is also clear that for a 50% duty cycle, 30 minutes of continuous load application allow for more energy extraction. Curiously, the trial with 5 minutes ON time also displays very interesting performance improvement values. Studies considering OFF times of 30 minutes or higher and commuted operation for periods of ON time of 30 minutes or less will reveal if the biofilm benefits from higher frequencies of commutation.

The global picture of how this operation affects the total energy harvested from a single reactor may only be determined by expanding the analysis window, as allowed by Figure 4.70.

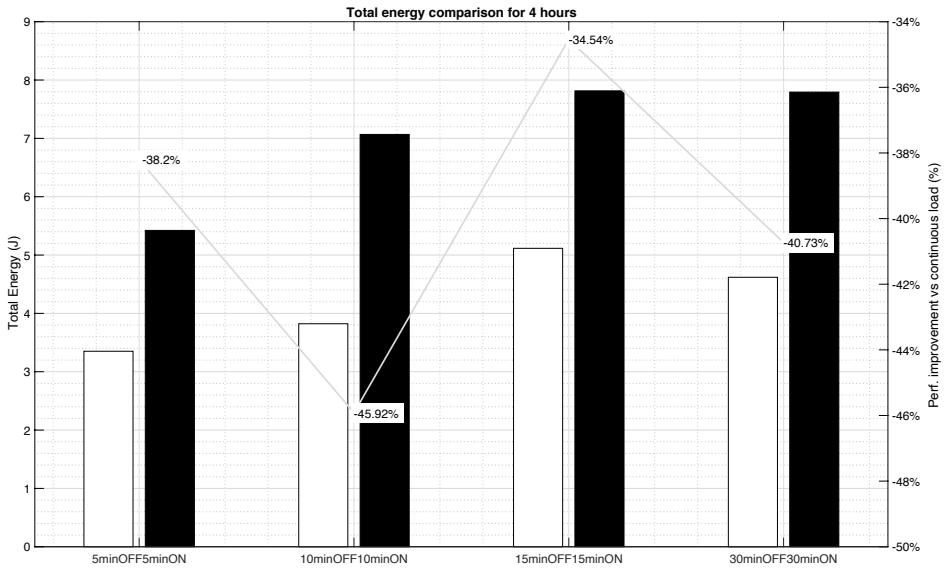

Figure 4.70 – Total energy per ON time vs equivalent for continuous load for 4 hours. Each white bar represents the 4-hour energy for a particular ON time. The black bar corresponds to the total energy calculated for a continuous load. In spite of considering the same period of operation, the continuous load reference changes because it is determined from data collected in different reactors: the 5minOFF5minON total energy for 4 hours was determined from the same reactor (reactor 1) as its continuous equivalent; this reactor, however equal to other small MFCs, is not the same as the reactor for other ON/OFF times.

As suspected, and because there are periods when no energy is extracted from the reactor, the interrupted load operation does not allow to extract more energy from the reactors than when connected to a load uninterruptedly. Again, the performance at 5 minutes ON time seems to indicate that an advantageous behavior may happen for smaller periods of load connection.

This initial research work with interrupted load connection has allowed to determine that the reactor performance is enhanced for OFF times over 15 minutes. It is not clear if the use of OFF times while operating an MFC allows it to function for longer periods of time with the same AW, which can ultimately be useful in wastewater treatment plants (WWTP) with conditioned access to organically enriched wastewater. Also, the ON time duration and mode (continuous or commuted) is yet to explore. This research line will be investigated by applying other duty cycles and operation frequencies.

To this end, an experimental procedure was devised, where the load varying assembly is used to apply a PWM and an oscilloscope is used for data acquisition. The trial consisted in, for an AW batch, varying the duty cycles for a set frequency, while guaranteeing a time in open circuit conditions to allow the MFC biofilm charging. The trial time was chosen according to the substrate exhaustion time at continuous load conditions. To more clearly identify the trial parameters, ON time will be used to refer to the duty cycle time and the OFF time to the OCV time between duty cycles. The term “Commuted” operation is, therefore, being reserved for commuted load operating in a specific ON time. According to the previous results, higher overvoltages were achieved for 30 minutes OFF times. The research in [33] reports higher average voltages for OFF

times of 1 hour, which was ultimately decided as the starting point for OFF times. The ON time was initially fixed at 20 minutes and the duty cycles chosen for each frequency test were 5, 20, 30, 40, 50, 60, 70, 80, 90 and 95%. Frequencies of 1 kHz, 500 Hz and 100 Hz were also fixed according to the works in [33]. The overviewed trial was applied to a single MFC (R5) and a 70 Ω load, with an aged cathode. This data cannot be directly compared with the data from previous interrupted load operation: the reactor characteristics, namely the cathode age, have changed between conducting both experiments.

Data is displayed in Figure 4.71. The load value choice was made after conducting a polarization trial for that single reactor and determining the load at which the maximum power was achieved. Waveform data from the oscilloscope was retrieved at 30 seconds intervals, with 4000 points per snapshot. The trials had a total duration of 13 hours and 20 minutes. After commuted load testing, the cell was set to continuous load operation. Voltage values on the plots in Figure 4.71 were retrieved by monitoring the cell's terminals. For reference, the mean voltage (load monitoring) for a continuous trial at 68 Ω is superimposed. The horizontal axis displays the sample number because the time between samples is not uniform: although every 4000 samples are 30 seconds apart, each sample is separated by the oscilloscope time base.

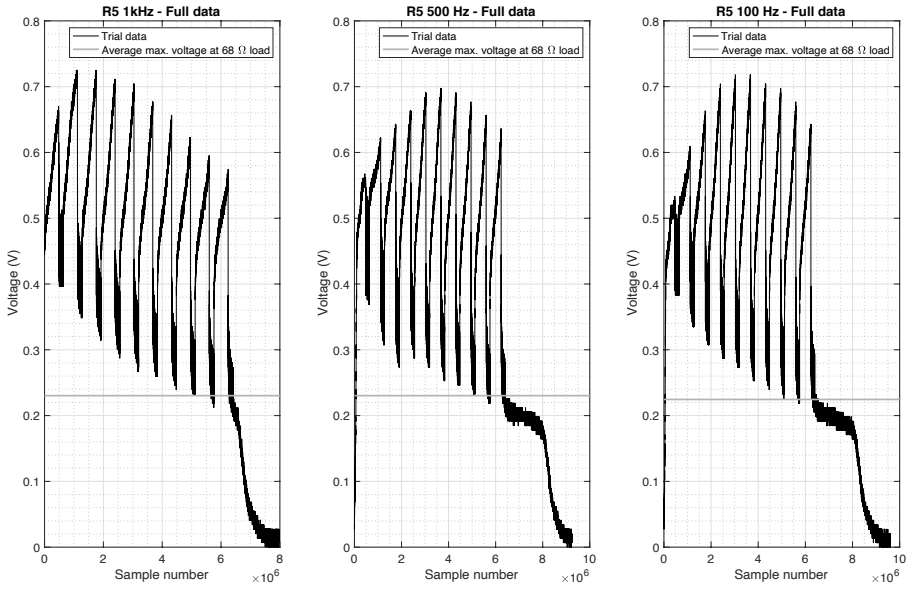

Figure 4.71 – Voltage profiles for commuted operation at 1 kHz, 500 Hz and 100 Hz. Each plot has the full duty cycle variation, from 5 to 95%. The average maximum voltage for a continuous load connection is displayed in grey.

The duty cycle variation direction was studied to ascertain the validity of these trials, as presented by Figure 4.72. As before, this trial was also conducted while monitoring the cell's electrodes.

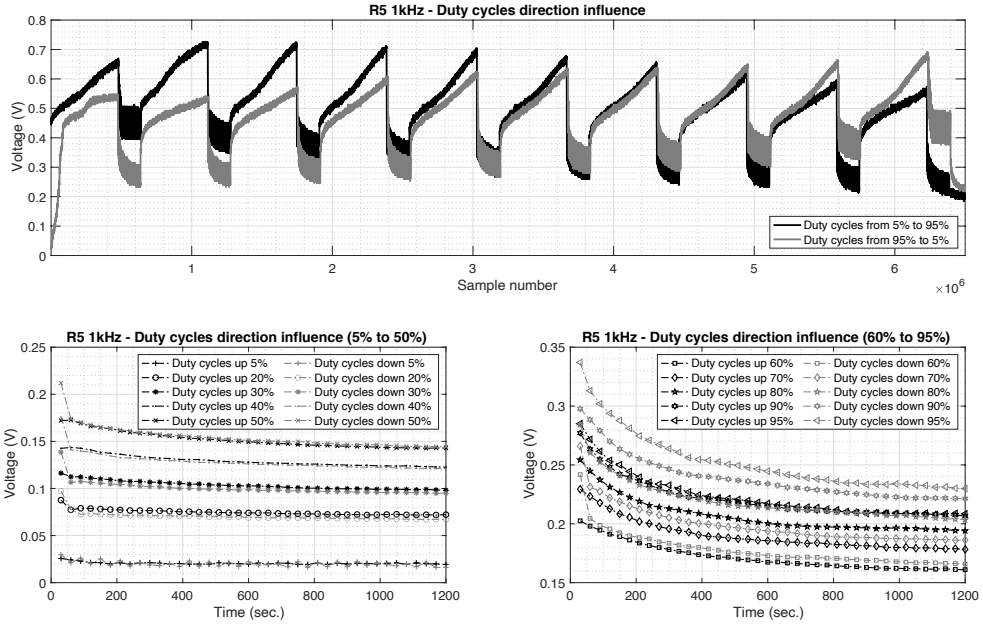

Figure 4.72 – Duty cycle direction influence on voltage profile. The test was conducted for 1 kHz and a set of 10 duty cycles. Data presented in black corresponds to increasing values of duty cycles while grey represents decreasing duty cycle values. Each voltage value corresponds to an average of 4000 measurements at that operation time.

As data shows, although the duty cycle variation direction changed, voltage values remained roughly the same. As such, the MFC voltage development profile is independent on the duty cycle variation direction. Also, voltage values are higher for higher duty cycles and decrease in time.

To expedite the performance evaluation of each trial, each duty cycle trial was isolated from the remaining trial. Each snapshot (4000 values) was reduced to its average value and plotted against the same average maximum voltage at 68 Ω, just as before. Since each duty cycle was applied for 20 minutes, the sample number is reduced to 40 (1 value per 30 seconds during 1200 seconds of ON time).

Figure 4.73 depicts this representation.

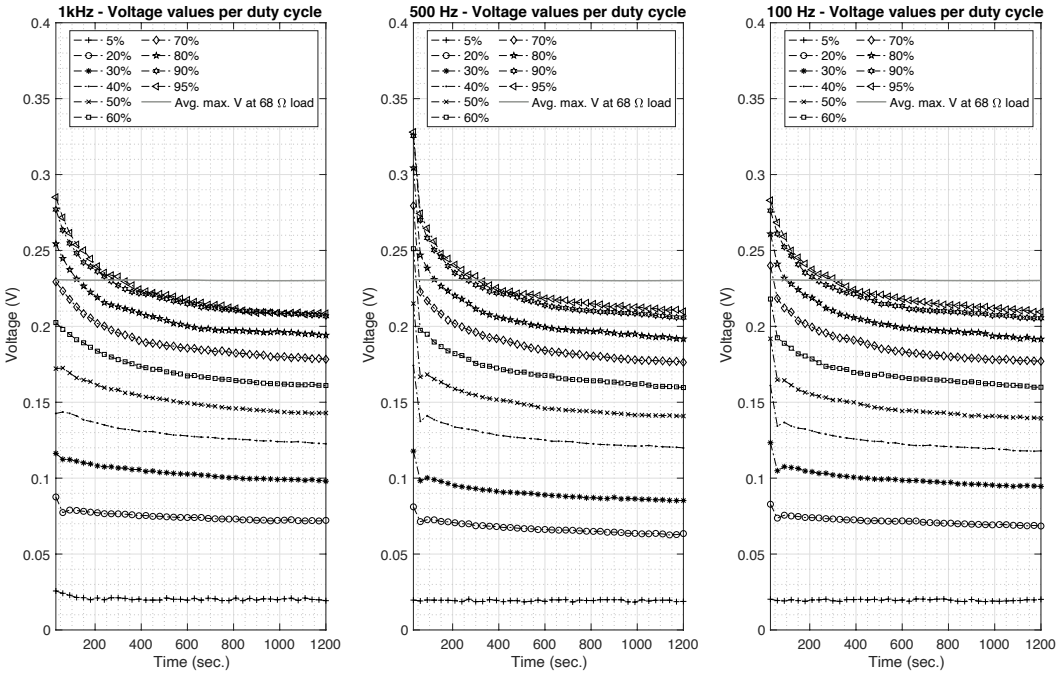

Figure 4.73 – Average voltage value per 30 seconds interval for every duty cycle at 3 different frequencies: 1 kHz, 500 Hz and 100 Hz. The average maximum voltage value for a continuous load trial is superimposed for reference. Each voltage value corresponds to an average of 4000 measurements at that operation time.

Across all frequencies, voltage values increase with increasing duty cycles. Noticeably, only duty cycles over 70% present voltages over the value achieved with a continuous load. The overvoltage found for the first 30 seconds is higher for higher duty cycles. Throughout the 20 minutes trial duration, voltage decreases continuously from that point. Moreover, voltages above the continuous load average are limited to durations of, approximately, 300 seconds. From that point onwards, it is assumed that the power production capabilities of this commuted operation are inferior. For that reason, the analysis of this data has been discarded.

The plots on Figure 4.74 make an accurate representation of the power differences per duty cycle and frequency for voltages over the continuous load equivalent.

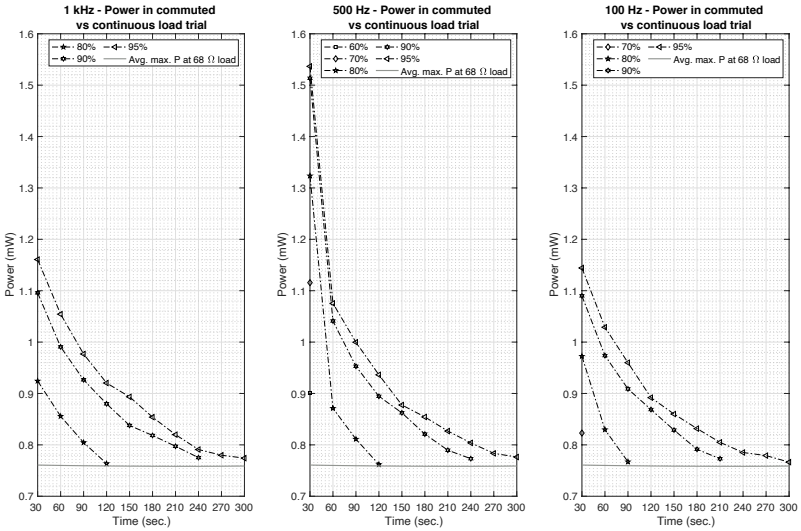

Figure 4.74 – Average power per 30 seconds interval for 3 different frequencies: 1 kHz, 500 Hz and 100 Hz. Only duty cycles producing voltages over the continuous reference (grey line) have been plotted. Each power value is indirectly determined from an average of 4000 voltage measurements at that operation time.

All frequencies present higher power production levels until 300 seconds of operation. The behavior for 500 Hz is significatively better than at any other frequency, particularly for the first sampling interval (at 30 operating seconds). For the remaining sampling points, the behavior converges, irrespective of the frequencies, for approximately the same power values. In fact, both 1 kHz and 100 Hz trials present very close values, pointing to the 500 Hz frequency as the best performing trial. Furthermore, the high-power value at 30 seconds and 500 Hz seems to indicate better biofilm energy extraction capabilities. A more in depth and detailed representation can be found in Figure 4.75.

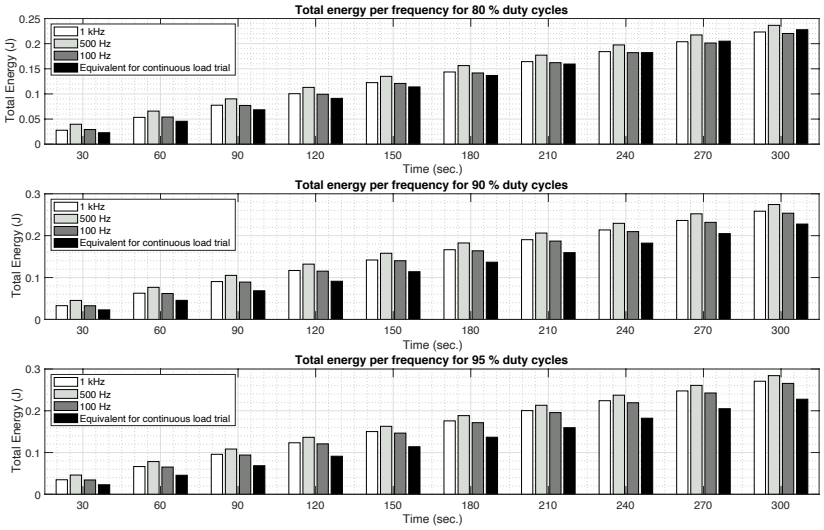

Figure 4.75 – Cumulative sum of energy values per operating time for 1 kHz, 500 Hz and 100 Hz and duty cycles of 80, 90 and 95%. The energy calculus was indirectly determined from the product between power and the time between sample acquisition, 30 seconds.

The cumulative sum of energy displayed in Figure 4.75 was retrieved by multiplying the power for that operating time with the time between acquisitions. The reference is represented in black and corresponds to the continuous load trial. Irrespective of the frequency, and for the considered duty cycles, the open circuit conditions imposed before commuted load connection improved the extracted energy from the reactor, further corroborating the charge storage characteristics of the electroactive biofilm. The best performing trial happened for a frequency of 500 Hz, across all time points and duty cycles. The time window was kept to 300 seconds as this was the limit for having power values above their continuous equivalent.

The relative comparison between the duty cycles at the same frequency is plotted in Figure 4.76.

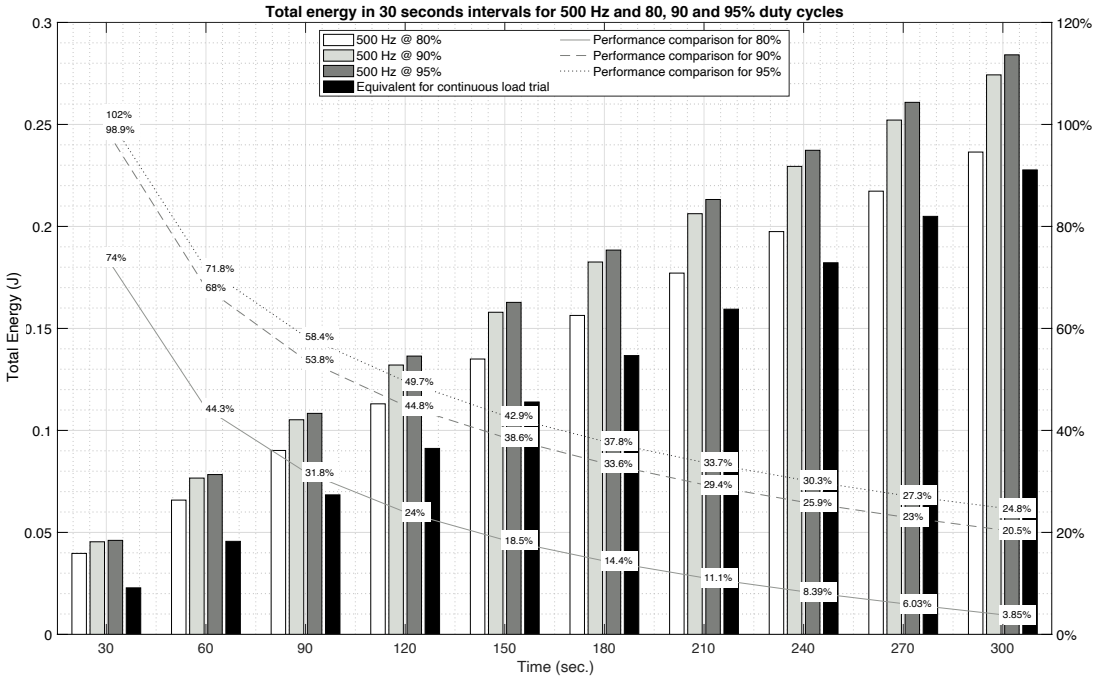

Figure 4.76 – Total energy for 500 Hz at 80, 90 and 95 % duty cycles. The right vertical axis displays the performance improvement of each trial when compared with the continuous load, represented by the solid and dashed lines. The bar plots magnitude is read on the left axis.

A 95% duty cycle presented the most significative improvements, particularly for the first 30 seconds. This corroborates the findings by [33]. For that same duty cycle, the improvement percentage remains close to 50% until 120 seconds. The performance improvement doesn't change linearly with time or duty cycle. In fact, the sharpest drop in performance improvement, around 30%, happens from 30 to 60 seconds of operation, indicating that the biofilm energy is more readily available. From that point until the 300 seconds mark, the performance improvement variation is reduced, showing signs that the biofilm has more difficulty than before to establish electron transfer between the bacteria and the electrode. This data set also highlights the quick adaptation capabilities of the biofilm.

The analysis so far seems to indicate that higher valued duty cycles produce more energy. To determine the relative positioning of these trials with the commuted load analysis done previously – corresponding to the application of open circuit conditions between load connection periods – a plot was developed with such data and is displayed in Figure 4.77.

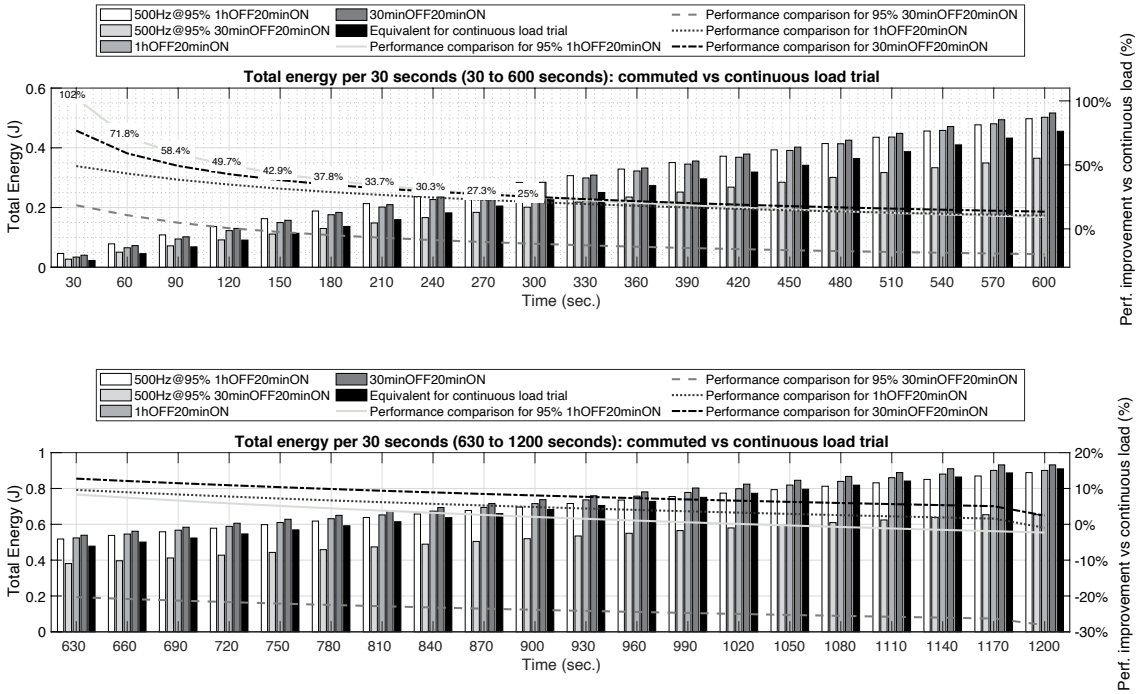

Figure 4.77 – Total energy for 5 different trial conditions, all with 20 minutes of load application: 500 Hz at 95 % duty cycle with 1 hour in open circuit conditions ("500Hz@95%1hOFF20minON"), 500 Hz at 95 % duty cycle with 30 minutes in open circuit conditions ("500Hz@95%30minOFF20minON"), 1 hour in open circuit conditions and 20 minutes of continuous load ("1hOFF20minON"), 30 minutes of open circuit conditions and 20 minutes of continuous load ("30minOFF20minON") and, finally, for a continuous load ("Equivalent for continuous load trial"). The load for all the trials is 70 Ω. The right vertical axis displays the performance improvement of each trial when compared with the continuous load, represented by the solid and dashed lines. The bar plots magnitude is read on the left axis.

The trials chosen for comparison were all conducted with a 70 Ω load: 500 Hz at 95 % duty cycle with 1 hour in open circuit conditions (Figure 4.77, "500Hz@95%1hOFF20minON"), 500 Hz at 95 % duty cycle with 30 minutes in open circuit conditions (Figure 4.77, "500Hz@95%30minOFF20minON"), 1 hour in open circuit conditions and 20 minutes of continuous load (Figure 4.77, "1hOFF20minON"), 30 minutes of open circuit conditions and 20 minutes of continuous load (Figure 4.77, "30minOFF20minON") and, finally, for a continuous load (Figure 4.77, "Equivalent for continuous load trial").

The analysis of Figure 4.77 assumes a freshly replenished reactor and an external load close to the MFC's internal load estimate. This data shows that all the trials, except for "500Hz@95%30minOFF20minON", present higher energy levels when compared to the continuous load connection, without any open circuit imposition. This confirms that the biofilm is capable of storing charge, and that its discharge can be modulated according to the load-imposed conditions. In fact, the trial "500Hz@95%30minOFF20minON" presents the lowest energy levels, indicating that the commuted operation at a high frequency may require the biofilm

to express specific characteristics, which may take more time to develop. The 1-hour counterpart of this trial, “500Hz@95%1hOFF20minON”, presents higher energy levels than any other trial, when considering a timeframe of approximately 300 seconds, or 5 minutes. From that point onwards, and for approximately 800 seconds, or 13 minutes, after, the reactor operation can be changed to continuous. The trials with continuous load application after an open circuit condition present very close energy levels, indicating that in these conditions, a 30-minute OCV window may suffice.

After confirming the improved behavior of these trials for 20 minutes, the relative positioning of this operation mode in an extended timeframe is needed. This will allow to clarify the sustainability of this operation mode. A comparison for 4 operation hours is displayed in Figure 4.78.

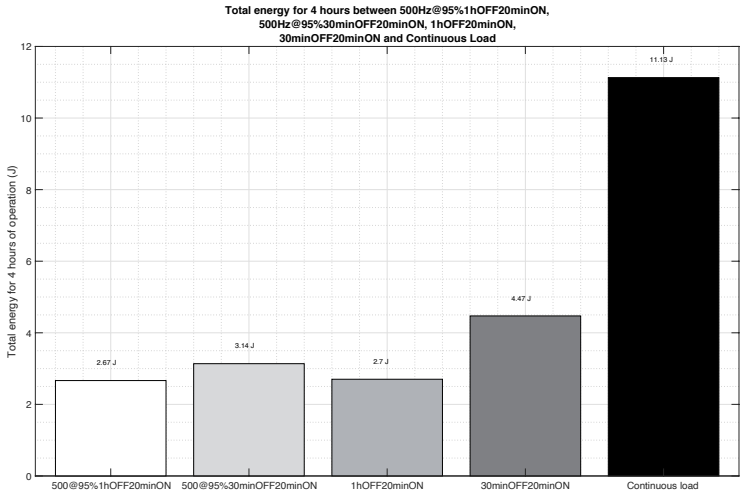

Figure 4.78 – Total energy for 4 hours and 5 different trial conditions, all with 20 minutes of load application: 500 Hz at 95 % duty cycle with 1 hour in open circuit conditions (“500Hz@95%1hOFF20minON”), 500 Hz at 95 % duty cycle with 30 minutes in open circuit conditions (“500Hz@95%30minOFF20minON”), 1 hour in open circuit conditions and 20 minutes of continuous load (“1hOFF20minON”), 30 minutes of open circuit conditions and 20 minutes of continuous load (“30minOFF20minON”) and, finally, for a continuous load (“Equivalent for continuous load trial”). The load for all the trials is 70 Ω.

As expected, the trials with less time in OCV conditions present higher energy levels, since the reactor spends less time disconnected from the load. Second to the performance of the continuous load is the trial “30minOFF20minON” with 4.47 J. The trials with 1 hour of OFF time behave similarly, although, the trial “500Hz@95%1hOFF20minON”, as previously discussed, is capable of increased energy production levels for a specific time. The usefulness of each trial becomes clearer when considering the substrate consumption rate when changing the OFF time, as pictured in Figure 4.79.

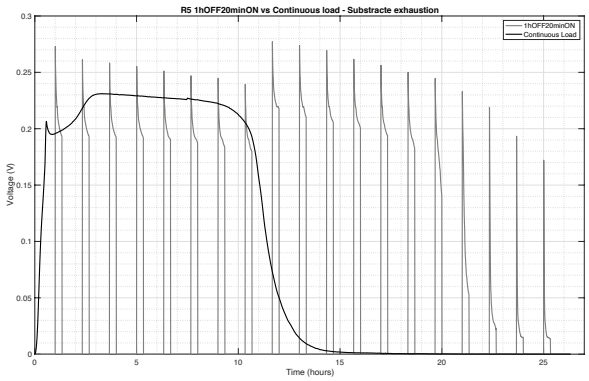

Figure 4.79 – Complete cycle of load application: from replenishment of the reactor until substrate exhaustion. The data for building this plot was acquired by monitoring the load terminals.

As presented, applying an open circuit condition to the reactor also leads to an increase of the MFC's useful lifetime. Although the data on the plot corresponds to a 1-hour OCV, the same conclusion can be made regarding other OFF times. It can be estimated that, whenever the reactor is disconnected from the load, the substrate consumption rate decreases. Care should be taken when dimensioning the OCV window: a too smaller window, as seen, may hinder the reactor operation; however an OFF time greater than 1 hour is suspected to impact the biofilm adhesion to the anode, leading the bacteria to choose other metabolic pathways that do not involve exoelectrogenesis and, as such, are not adequate for energy production with MFCs.

Table 4.13 summarizes the highlights for the commuted operation trials. The starting point for the interrupted and commuted load trial analysis is the initial conditions of the trial. Where the interrupted load was preceded of a 30 minutes continuous load application, the commuted load trials were preceded of 60 or 30 minutes of open circuit conditions. This accounts for the operation time differences for achieving maximum values. There seems to be no other influence on the reported values. Also, both trials were conducted at different times, which impacted the reactor's characteristics, particularly its internal load value. For all the researched ON and OFF times, the best combination for maximum power was an OFF time of 1 hour and a 500 Hz commutation at 95% duty cycle for as long as 5 minutes. A 30 minutes of open circuit conditions can also be applied for similar results, with no commutation happening during the ON time.

The commutation operation can be an adequate solution to apply if the MFC is used with a power converter, since voltage, current and power values are bigger than in any other tested condition. However, if energy extraction from the MFC is to continue after the converter start-up, a change to a continuous mode is more adequate, since more energy can be retrieved from the reactor.

The operation mode possibilities of an MFC make it an extremely versatile renewable low-power source. It can be operated in four different modes:

- Super: "500Hz@95%1hOFF20minON", useful for the start-up of a power converter;
- Stamina: "1hOFF20minON" (no commutation), adequate for improving the power source runtime;

- Balanced: “30minOFF20minON” (no commutation), where power figures are also interesting, and less energy is spent on modulating the power source functioning;
- Max. energy: continuous load connection and matching for maximum energy production.

Each mode can be achieved without having to change anything on the power source itself. Furthermore, operation changes may be applied during its runtime, without the need to change the substrate or environmental conditions. In fact, substrate and/or environmental changes may also be used as triggers for operation mode changes.

Load and capacitor connection influence on MFC power

As discussed, a load connection between the MFC terminals implies the biofilm discharge. The discharge rate can be adjusted by modulating the load connection and disconnection frequency. Furthermore, it was very clearly concluded that adequate open circuit condition times favor current charge, improving the energy extraction when compared with a continuous setting. This was considered for a resistive load connection. However, the voltage and current figures can’t safely guarantee a steady power source, needing further regulation by a boost converter. As such, a more adequate use for MFC power, as it can be enhanced when stored, is to have the MFC connected to a capacitor.

It is expected that having a capacitor directly and continuously connected to an MFC forces a quick biofilm discharge, unbalancing the current sinking and the biofilm electron availability and production rate. A higher capacitor value will lead to a higher voltage drop and biofilm perturbation, but a small-valued capacitor will prove of no use for a boost converter. However, a different behavior is expected if the capacitor has a commuted connection: by briefly connecting the capacitor, the cell answers in small bouts, allowing the biofilm to readjust and partially (or fully, if enough time is provided) replenish its charge. A single reactor was subject to the previously described conditions confirming the theoretical predictions. Results are displayed in Figure 4.80. This is thought to allow the development of a more resilient and durable biofilm, which is converted in a steady, regulated and predictable charge of a capacitor. Such a characteristic is fundamental to optimize the design and development of the boost converter, as it allows to adjust the connection periods in relation with the substrate availability.

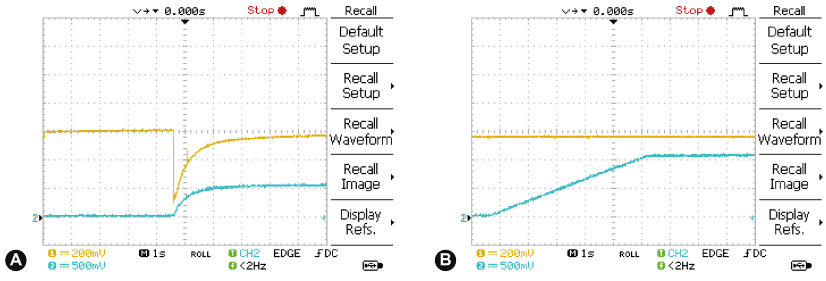

Figure 4.80 – The channel 1, yellow line, corresponds to voltage at the MFC’s terminals. The channel 2, blue line, represents the voltage at the capacitor. In A) a continuously connected capacitor; In B) a capacitor connected to a MFC at a 95% duty cycle. In the interrupted connection conditions, the MFC voltage is only marginally affected by the capacitor charging.

Table 4.13 – Summary of performance comparison between all the commuted operation trials with single MFCs.

Variable	Unit	Trial								
		Interrupted load								
		ON time	5 min.	10 min.	15 min.	30 min.	1.9 msec.	1.9 msec.	20 min.	20 min.
		OFF time	5 min.	10 min.	15 min.	30 min.	0.1 msec.	0.1 msec.	60 min.	30 min.
		Freq.	1.67 mHz	833.33 µHz	555.56 µHz	277.78 µHz	500 Hz	500 Hz	0.21 mHz	0.33 mHz
		Duty Cycle	50%	50%	50%	50%	60 min OFF, 95%	30 min OFF, 95%	25%	40%
Anodic biofilm time	Days		674				738			
Cathode	Days		0				77			
Cathode area	cm^2		7.07							
Load	Ω		100				70			
Max. voltage | operation time	V | min.		0.25 | 102	0.24 | 66	0.28 | 114	0.29 | 122	0.33 | 0.5	0.25 | 0.5	0.29 | 0.5	0.31 | 0.5
Max. current | operation time	mA | min.		2.47 | 102	2.39 | 66	2.76 | 114	2.89 | 122	4.69 | 0.5	3.59 | 0.5	4.08 | 0.5	4.39 | 0.5
Max. power | operation time	mW | min.		0.61 | 102	0.58 | 66	0.76 | 114	0.84 | 122	1.54 | 0.5	0.90 | 0.5	1.17 | 0.5	1.35 | 0.5
Total energy extracted per ON period | versus continuous operation for the same time	J | J		0.14 | 0.11	0.32 | 0.29	0.64 | 0.49	1.16 | 0.97	0.89 | 0.91 (20 minutes ON)	0.65 | 0.91 (20 minutes ON)	0.93 | 0.91 (20 minutes ON)	0.95 | 0.91 (20 minutes ON)
Best performance improvement | operation time	% | min.		29.3 | 102	16.8 | 66	49.7 | 114	43.8 | 112	102 | 0.5	18.4 | 0.5	49.1 | 0.5	76.8 | 0.5
Total energy extracted for 4 hours with interrupted operation| versus continuous operation for the same time	J | J		3.35 | 5.42	3.82 | 7.07	5.12 | 7.81	4.62 | 7.79	2.67 | 11.13	3.14 | 11.13	2.70 | 11.13	4.47 | 11.13
Performance improvement for 4 hours vs continuous load	%		-38.2	-45.9	-34.5	-40.7	-76	-71.8	-75.7	-59.8

A power management solution proposal

Before using the energy harvested from an MFC to power a smart sensor, two main problems need to be addressed. First, the voltage value is low and unregulated. Second, power output is not high enough to power a smart sensor in the operating mode continuously. The first issue is solved using a two-stage solution that, at first, raises the voltage level, to allow a DC/DC converter start operating. The second problem is solved by adopting low power operating modes, based in low-power deep sleeping mode, that optimize the use of the available energy.

The magnitude of the energy produced by an MFC is very low. It typically reaches 0.8 V when operating in open circuit, a condition where the internal impedance doesn't affect the cell's voltage output because no current is flowing between the electrodes. As described in the previous section, an increase in the cell's current leads to a drop in the corresponding output voltage, due to an increase in its internal impedance. This characteristic behavior usually makes the cell incapable of starting a DC/DC converter, which is needed to guarantee an adequate voltage regulation to adequate the cell to power a smart sensor. An answer to this issue is to use a second stage implementing a voltage raising mechanism capable of providing the necessary conditions for the start of the DC/DC converter. This second stage also helps to operate the converter in the most efficient way.

The proposed solution is based on the use of a two-stage converter, as previously described.

Since harvesting energy from an MFC, with this converter, is not a direct process, an operation control is required. The operation control is imposed by 4 switches: S_0, S_1, S_2 e S_3. Switches S_0 and S_1 are normally closed, while S_2 and S_3 are normally open. The commutation of these switches leads to 2 different operation conditions: a starting stage and a regular operation stage.

Starting stage

Initially, the smart sensor can't run because there is no power in the system. As such, all the switches are set to their default behavior. This forces the MFC's voltage to capacitor 1 (C1), which, when reaching the blocking oscillator's (BO) starting voltage (BOSV), charges capacitor 2 (C2). The voltage supervisor 2 (SV2) monitors C2's voltage: when it reaches SV2's high threshold value (SV2_H), the S2 switch closes. From that moment onwards, the DC/DC converter starts the voltage regulation from capacitor 3 (C3). The S2 switch remains closed as long as C2's voltage remains higher than the SV2's low threshold voltage (SV2_L). When the C3's voltage reaches the SV3_H, SV3 commutes the S3 switch, closing it. This cascade of events finally leads to the microcontroller unit (MCU) activation. This ends the starting stage and initiates the regular operation.

Regular operation stage

At this operation condition, the MCU controls the S_0 and S_1 switches, periodically commuting them. The capacitor C_1 is the first to charge, keeping the S_1 switch open. After C_1 is charged, S_0 is opened an S_1 closed, starting C_2 through the BO oscillator with the energy from C_1. The MCU is master of this process, using the JFET Driver controller lines and setting the commuting values of C_1's voltage.

The implemented control strategy is based on monitoring the voltage at C_1. The S_0 and S_1 switches are managed such as the C1's voltage varies between VC_{1_H} and VC_{1_L}. These boundary values are detected by the voltage comparator (VC), which compares them with the reference voltage (V_{REF}) output from filtering the pulse-width modulation, PWM (PWM_REF), signal generated by the MCU. In the charging period, with S_0 closed and S_1 open, the voltage comparator sees V_{REF_H}. When the higher value is achieved, the control line C_1_Status triggers a low to high transition. The MCU replies to this event by opening S_0 and closing S_1, starting the discharge period. The reference voltage is set to VC_{1_L}, a value resulting from filtering a MCU's PWM. When the capacitor reaches the discharge value, the control line C_1_Status triggers a high to low transition, generating a new interruption at the MCU that opens S_1 and closes S_0 to allow a new charging cycle for the C_1 capacitor.

As long as the energy stored at C_2 is enough to guarantee that the DC/DC converter is able to maintain the C_3 capacitor with a voltage higher than SV_{3_L}, the MCU continues to operate and control the S_1 and S_0 switches. If the C_2 voltage drops below SV_{2_L}, or if the C_3 voltage gets lower than SV_{3_L}, the MCU will enter in sleep mode, after being notified by the SV_2_Status and SV_3_Status lines.

A general overview of the energy module is presented in Figure 4.81. Each of its blocks is described, in more detail, in the following subsections.

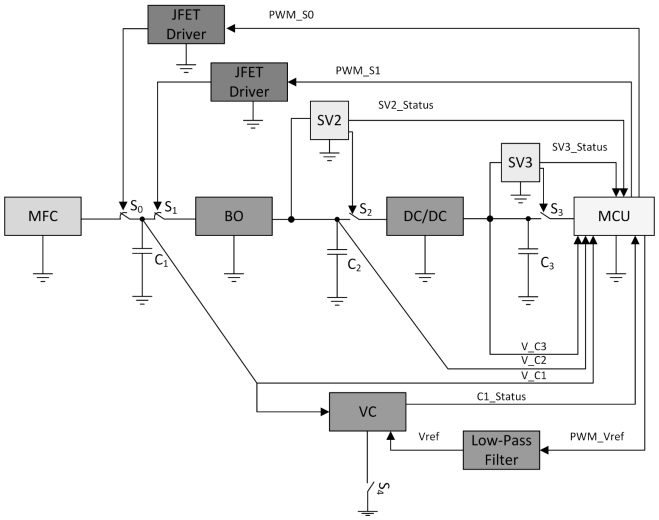

Figure 4.81 – Energy module structure diagram.

Oscillator

The blocking oscillator BO, pictured in Figure 4.82, is composed by a transformer, a resistance and a transistor working as an amplifier. The assembly places the transformer in a positive feedback. When the transistor is saturated, the second winding current will produce a voltage leading to a decrease in the transistor's base current, since the magnetic flow of the secondary winding of the transformer has an inverse signal of the primary winding. In this condition, the transistor immediately enters in cutoff, rapidly increasing the voltage at the transformer's secondary winding. The energy stored in the magnetic circuit of the transformer is transferred, through the diode, to the capacitor. When the voltage at the secondary winding of the transformer drops, the current in the primary circuit will increase again quickly, placing the transistor again in its saturation zone, conducting.

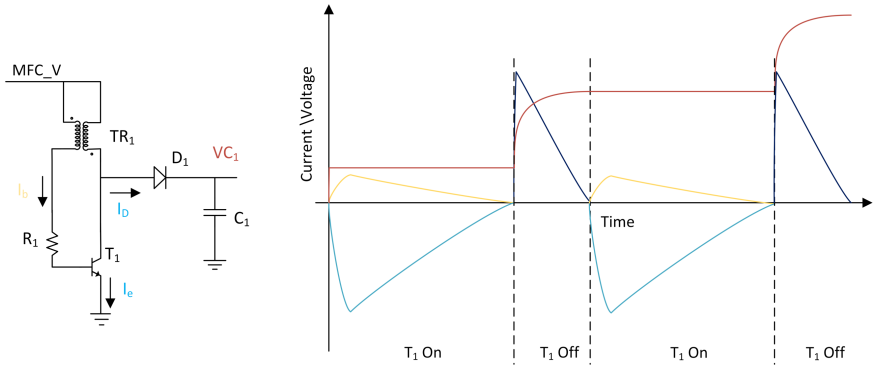

Figure 4.82 – The blocking oscillator.

Voltage comparator

The MFC operation efficiency is optimized by adjusting the charge and discharge times of the C_1 capacitor. The C_1's voltage is monitored by a comparator, displayed in Figure 4.83, that evaluates its value against the reference voltage V_{REF} supplied by the MCU. At any particular time when the capacitor voltage is higher than the reference value, the comparator output is set to high. At transitions, the MCU answers by commuting the S_0 and S_1 positions, according to the regulation strategy defined. The reference voltage level is set by a DAC, implemented by filtering a PWM signal, with 256 different levels, resulting in a 12-mV resolution. A low-pass filter is used to determine the PWM average value.

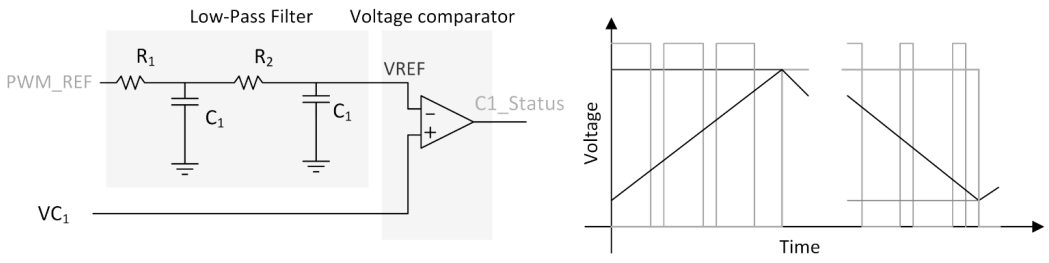

Figure 4.83 – The voltage comparator.

FET Driver

A JFET is capable of conducting current between drain and source when the terminal gate has no voltage. To turn off an N-channel JFET a high enough negative voltage has to be applied at the terminal gate. Due to this behavior, the JFET can be designated has a normally closed switch. A charge pump uses a PWM generated by the MCU to produce the negative voltage needed to place the JFET at cutoff, opening it. Figure 4.84 represents the FET Driver and its desired operation.

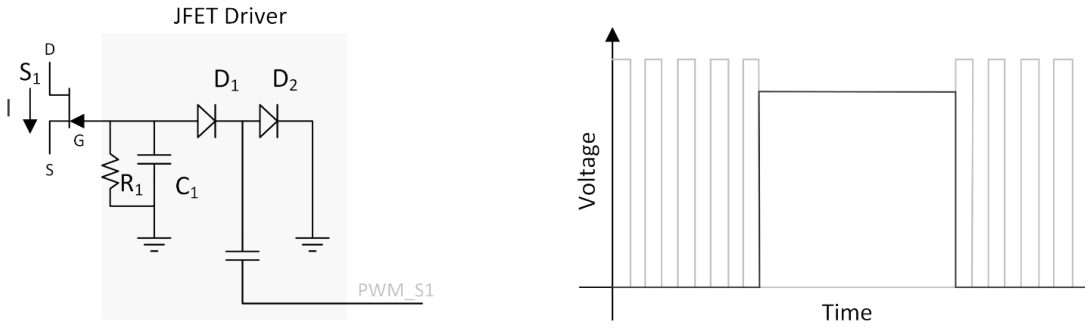

Figure 4.84 – The FET Driver.

Voltage supervisor

The charge status of capacitors C_2 and C_3 is monitored by voltage supervisors. Whenever the voltage value is higher than a preset value, the S_2 and S_3 switches status is updated, according to the variation direction. The LTC2935 device is responsible for this task, allowing to program the levels of commutation of the status line.

The supervising circuit monitors the input voltage and sets the RST line to low when the capacitor voltage drops below the preset threshold value. When the capacitor voltage increases, and surpasses the programmed high threshold voltage in 5%, an internal timer delays the RST line reset to high in 200 milliseconds. Several different commutation levels are configurable by using 3 configuration lines.

While the capacitor charges, and with the supervisor configured to detect the higher voltage level (S_2 = \RST (Low); S_1 = Low; S_0 = High), the RST line is low, which sets the limit value to 3.15 V. When the higher value is reached, the RST line is triggered to high and closes the switch S_1. The voltage supervisor is now configured to detect the lower limit (S_2 = \RST (High); S_1 = Low; S_0 = High), corresponding to 2.40 V. The DC/DC converter now begins its operation and the capacitor voltage decreases. When it reaches 2.40 V, the RST line is again triggered, this time to low. This forces a switch opening and the capacitor charge.

Using the PMS and the MFC as a smart sensor power source

The function of a smart transducer is to acquire information from the process where it is deployed, if it has a sensor element, or to actuate in that same process, if it has an actuator. As the transducer definition suggests, this element can be used to either designate a sensor or an actuator. A smart transducer has a set of characteristics that allows it to perform functions such as: amplification, filtration and data processing; communication with other elements through a network, autonomous operation or in collaboration with other elements interconnected through the same network.

The power module described in the previous section is an essential building component of a smart sensor. An MCU is the central element around which all other modules are developed. In addition to having the function of managing the power module, as already described, the MCU manages the remaining modules as shown in Figure 4.85.

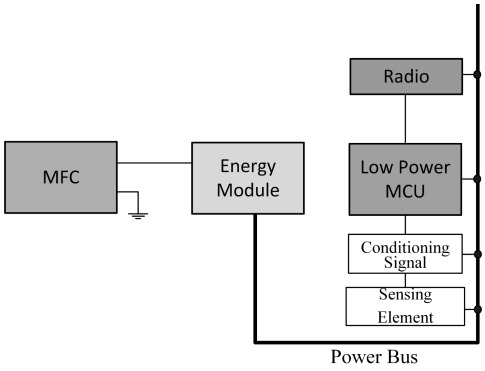

Figure 4.85 – General overview of the smart sensor on discussion.

The measurement chain links the sensor element to the MCU. It is through this channel that the acquired information is first amplified and filtered in the analog domain to, after being converted to the digital domain, be digitally processed by the MCU. The radio module connects the smart transducer to the network. It is through this channel that information requests are received and sent.

The energy available in the smart transducer needs to be managed taking into account aspects such as those discussed next. The data to be acquired can be obtained i) based on a periodic sampling process over time, ii) at the request of another process, or iii) due to the occurrence of associated events:

i) In the periodic sampling process, information is acquired with a predefined sampling frequency. The measurement process is triggered periodically. It is possible to estimate the energy cost of this process. Thus, the required energy, and given that we are using an energy collection mechanism, should never be greater than what can be acquired between samples.

ii) The smart transducer can receive a request for information over the network. In this situation, it is necessary to ensure that there is an adequate energy stock so that the measurement process can be flawlessly carried out. Ensuring that the request occurs in periods of time longer than what is necessary for the energy level to recover is mandatory.
iii) The report of an event occurrence is the sole responsibility of the smart transducer. Therefore, an adequate energy stock must be made available for the communication to happen. Ensuring that the request occurs in periods of time longer than what is necessary for the energy level to recover is mandatory.

An example of applying the solution presented in this chapter is the case of a wastewater treatment plant. At these infrastructures, data registering is necessary: water level; temperature; pH, ORP, and O_2 are some examples of chemical and physical parameters that need monitoring in order to properly meet the environmental discharge standards. In the work presented in [34,35], a network of intelligent actuators that collects the water level in a macrophyte lagoon is presented. Smart sensors are powered by an MFC and network interconnection is based on the IEEE1451 standard.

References

[1] V. Watson, G. Estadt, Graphite Fiber Brush Anodes for Increased Power Production in Air-Cathode Microbial Fuel Cells, 41 (2007) 3341–3346.

[2] W. Yang, W. He, F. Zhang, M.A. Hickner, B.E. Logan, Single-Step Fabrication Using a Phase Inversion Method of Poly(vinylidene fluoride) (PVDF) Activated Carbon Air Cathodes for Microbial Fuel Cells, Environ. Sci. Technol. Lett. 1 (2014) 416–420. https://doi.org/10.1021/ez5002769.

[3] B. Koo, S.M. Lee, S.E. Oh, E.J. Kim, Y. Hwang, D. Seo, J.Y. Kim, Y.H. Kahng, Y.W. Lee, S.Y. Chung, S.J. Kim, J.H. Park, S.P. Jung, Addition of reduced graphene oxide to an activated-carbon cathode increases electrical power generation of a microbial fuel cell by enhancing cathodic performance, Electrochim. Acta. (2019). https://doi.org/10.1016/j.electacta.2018.12.024.

[4] F. Vicari, S. Mateo, F.J. Fernandez-Morales, P. Cañizares, A. Galia, O. Scialdone, M.A. Rodrigo, Influence of the methodology of inoculation in the performance of air-breathing microbial fuel cells, J. Electroanal. Chem. 803 (2017) 81–88. https://doi.org/10.1016/j.jelechem.2017.09.024.

[5] J.R. Kim, B. Min, B.E. Logan, Evaluation of procedures to acclimate a microbial fuel cell for electricity production, Appl. Microbiol. Biotechnol. 68 (2005) 23–30. https://doi.org/10.1007/s00253-004-1845-6.

[6] V. Lanas, B.E. Logan, Evaluation of multi-brush anode systems in microbial fuel cells., Bioresour. Technol. 148 (2013) 379–85. https://doi.org/10.1016/j.biortech.2013.08.154.

[7] A. Vogl, F. Bischof, M. Wichern, Surface-to-surface biofilm transfer: A quick and reliable startup strategy for mixed culture microbial fuel cells, Water Sci. Technol. 73 (2016) 1769–1776. https://doi.org/10.2166/wst.2016.003.

[8] Y. Hong, D.F. Call, C.M. Werner, B.E. Logan, Adaptation to high current using low external resistances eliminates power overshoot in microbial fuel cells, Biosens. Bioelectron. 28 (2011) 71–76. https://doi.org/10.1016/j.bios.2011.06.045.

[9] T.R. Kuphaldt, pH measurement: Electrical Instrumentation Signals - Electronics Textbook, (n.d.). http://www.allaboutcircuits.com/vol_1/chpt_9/6.html (accessed January 14, 2014).

[10] YSI, The Dissolved Oxygen Handbook, 2009. https://www.fondriest.com/pdf/ysi_do_handbook.pdf (accessed January 11, 2014).

[11] Myron L Company, Application Bulletin: Oxidation Reduction Potential (ORP)/Redox and Free Chlorine, 2012. http://www.myronl.com/PDF/application_bulletins/orp_ab.pdf (accessed January 15, 2014).

[12] D. Walker, A.W. Bier, Oxidation Reduction Potential: Understanding a Challenging Measurement, 2009. http://www.hach.com/asset-get.download.jsa?id=7639984589.

[13] Atlas Scientific, Atlas Scientific ORP Kit, (n.d.). https://www.atlas-scientific.com/product_pages/kits/orp-kit.html (accessed January 15, 2014).

[14] Y. Fan, H. Hu, H. Liu, Sustainable power generation in microbial fuel cells using bicarbonate buffer and proton transfer mechanisms, Environ. Sci. Technol. 41 (2007) 8154–8158. https://doi.org/10.1021/es071739c.

[15] I. Gajda, J. Greenman, C. Melhuish, C. Santoro, B. Li, P. Cristiani, I. Ieropoulos, Water formation at the cathode and sodium recovery using Microbial Fuel Cells (MFCs), Sustain. Energy Technol. Assessments. 7 (2014) 187–194. https://doi.org/10.1016/j.seta.2014.05.001.

[16] P.P. Włodarczyk, B. Włodarczyk, Wastewater Treatment and Electricity Production in a Microbial Fuel Cell with Cu–B Alloy as the Cathode Catalyst, Catalysts. 9 (2019) 572. https://doi.org/10.3390/catal9070572.

[17] I. Gajda, J. Greenman, C. Santoro, A. Serov, C. Melhuish, P. Atanassov, I.A. Ieropoulos, Improved power and long term performance of microbial fuel cell with Fe-N-C catalyst in air-breathing cathode, Energy. 144 (2018) 1073–1079. https://doi.org/10.1016/j.energy.2017.11.135.

[18] R. Rossi, W. Yang, E. Zikmund, D. Pant, B.E. Logan, In situ biofilm removal from air cathodes in microbial fuel cells treating domestic wastewater, Bioresour. Technol. 265 (2018) 200–206. https://doi.org/10.1016/j.biortech.2018.06.008.

[19] V.M. Ortiz-Martínez, M.J. Salar-García, A.P. de los Ríos, F.J. Hernández-Fernández, J.A. Egea, L.J. Lozano, Developments in microbial fuel cell modeling, Chem. Eng. J. 271 (2015) 50–60. https://doi.org/10.1016/j.cej.2015.02.076.

[20] D. Recio-Garrido, M. Perrier, B. Tartakovsky, Combined bioelectrochemical-electrical model of a microbial fuel cell, Bioprocess Biosyst. Eng. 39 (2016) 267–276. https://doi.org/10.1007/s00449-015-1510-8.

[21] C. Xia, D. Zhang, Y. Zhu, Y. Guo, Models for microbial fuel cells : a critical review, (2017) 19–20. https://doi.org/10.1049/joe.2017.0533.

[22] Q. Wen, Y. Wu, D. Cao, L. Zhao, Q. Sun, Electricity generation and modeling of microbial fuel cell from continuous beer brewery wastewater, Bioresour. Technol. 100 (2009) 4171–4175. https://doi.org/10.1016/j.biortech.2009.02.058.

[23] Y. Fan, E. Sharbrough, H. Liu, Quantification of the internal resistance distribution of microbial fuel cells, Environ. Sci. Technol. 42 (2008) 8101–8107. https://doi.org/10.1021/es801229j.

[24] P.M. Domingos Serra, A. Esoirito-Santo, M. Magrinho, Energy Harvesting from Wastewater with a Single-Chamber Air-Cathode Microbial Fuel Cell, in: IECON 2018 - 44th Annu. Conf. IEEE Ind. Electron. Soc., IEEE, 2018: pp. 3847–3851. https://doi.org/10.1109/IECON.2018.8592827.

[25] J. Do Park, T.M. Roane, Z.J. Ren, M. Alaraj, Dynamic modeling of a microbial fuel cell considering anodic electron flow and electrical charge storage, Appl. Energy. 193 (2017) 507–514. https://doi.org/10.1016/j.apenergy.2017.02.055.

[26] M. Alaraj, J. Do Park, Net power positive maximum power point tracking energy harvesting system for microbial fuel cell, J. Power Sources. 418 (2019) 225–232. https://doi.org/10.1016/j.jpowsour.2019.02.042.

[27] P.M.D. Serra, A. Espírito-Santo, M. Magrinho, A steady-state electrical model of a microbial fuel cell through multiple-cycle polarization curves, Renew. Sustain. Energy Rev. (2020). https://doi.org/10.1016/j.rser.2019.109439.

[28] S.E. Oh, B.E. Logan, Voltage reversal during microbial fuel cell stack operation, J. Power Sources. (2007). https://doi.org/10.1016/j.jpowsour.2007.02.016.

[29] H.C. Boghani, G. Papaharalabos, I. Michie, K.R. Fradler, R.M. Dinsdale, A.J. Guwy, I. Ieropoulos, J. Greenman, G.C. Premier, Controlling for peak power extraction from microbial fuel cells can increase stack voltage and avoid cell reversal, J. Power Sources. 269 (2014) 363–369. https://doi.org/10.1016/j.jpowsour.2014.06.059.

[30] F. Khaled, O. Ondel, B. Allard, Microbial fuel cells as power supply of a low-power temperature sensor, J. Power Sources. 306 (2016) 354–360. https://doi.org/10.1016/j.jpowsour.2015.12.040.

[31] C.L. Nguyen, B. Tartakovsky, L. Woodward, Harvesting Energy from Multiple Microbial Fuel Cells with a High-Conversion Efficiency Power Management System, ACS Omega. 4 (2019) 18978–18986. https://doi.org/10.1021/acsomega.9b01854.

[32] H.C. Boghani, R.M. Dinsdale, A.J. Guwy, G.C. Premier, Sampled-time control of a microbial fuel cell stack, J. Power Sources. 356 (2017) 338–347. https://doi.org/10.1016/j.jpowsour.2017.03.118.

[33] J. Coronado, M. Perrier, B. Tartakovsky, Pulse-width modulated external resistance increases the microbial fuel cell power output, Bioresour. Technol. 147 (2013) 65–70. https://doi.org/10.1016/j.biortech.2013.08.005.

[34] A. Espirito-Santo, P. Serra, S. Albuquerque, B. Ribeiro, F. Santos, J. Pascoa, Low-power smart sensing in energy and water systems integration, in: 2017 IEEE Int. Work. Meas. Netw., IEEE, Naples, Italy, 2017: pp. 1–6. https://doi.org/10.1109/IWMN.2017.8078408.

[35] A. Espirito-Santo, S. Ambrosio, P.M.D. Serra, R.J.C. Pinto, Water pH Monitoring with a Smart Sensor Powered by a Thermoelectric Generator with a Phase-Change Material, in: 2019. https://doi.org/10.1109/iecon.2019.8927259.

Chapter 5

Conclusions and final remarks

Contributions of this work

Waste management and recycling are a fundamental practice to prevent environmental and health damages. Furthermore, retrieving energy from waste is an efficient strategy to recover resources and to decrease the production costs of some items. Wastewater treatment plants are a particular example of this strategy, since they can be adapted to overcome their energy deficit standard profile. The energy on wastewater is stored in its temperature, its chemical composition and its organic matter. Exploring the wastewater organic composition for energy production explores a different solution for counter-balancing the energy expenditure in wastewater treatment plants. Amid the energy producing processes related with the organic content are anaerobic digesters. These devices, although capable of producing energy in the form of biogas, also need an energy source. The use of Microbial Fuel Cells can, using the same principle as that of anaerobic respiration, eliminate that sourced energy. Repurposing bacterial respiration for maximum energy extraction through microbial fuel cells is only possible by providing specific settings. The primary condition for this to happen is to select bacteria that are capable of externally delivering the electrons produced at the end of its metabolic pathway. For that to happen, the reactor must gather the most adequate conditions for energy extraction: the material selection and proper physical and chemical environments are paramount. Although bacteria can be extremely resilient, if a specific behavior is expected, some conditions must be applied to support that outcome. Firstly, the cell's electrodes must be biocompatible, ensuring that the bacterial colony can adhere to this surface and use it to its advantage. Secondly, the reactor geometry must prevent any deposition favorable areas, so that any undesirable by-products or bacterial strains don't build-up in the reactor. On top of this, the substrate composition must also guarantee the needed biochemical settings for exoelectrogenesis. Only after these conditions are met, can the reactor be used for energy production.

Considering the previous requirements are fulfilled, the MFC can, then, be treated as a low voltage source. An electric modelling of the reactor helps estimating its internal load value and the power loss distribution for different currents and operational conditions. This information can be used to optimize the power producing profile of the reactors. Furthermore, this investigation also showed that, for particular settings, the reactor exhibits a capacitive behavior. The internal characteristics of the reactor, although briefly addressed in this work, can't be significantly manipulated in real world applications: the wastewater composition, temperature and biochemical settings can greatly vary throughout the day and seasons. Forcing a specific set of these conditions may result in unwanted side effects, like added pollutants, decreased cleaning efficiency, increased energy expenditure or higher economic investments. As such, a more

consensual optimization strategy can be applied when treating the reactor as a black box, considering only its electrical equivalent.

Energy extraction from MFCs can be grouped in two different modes of operation: continuous and interrupted. In continuous operation, current is uninterruptedly extracted from the reactor, even though presenting some fluctuations. Even so, and while an organic energy source is available, this current is never equal to zero and always flows from the reactor to the external load. This translates to a continuous energy production. Supplying current to the reactor is also possible. This may be useful when improving wastewater treatment strategies - for instance for recovering added value compounds, like gold and other heavy metals – but it does not contribute to decreasing the energy consumption of the process. In continuous operation mode, and to ensure maximum energy production, the reactor should be forced to operate at its maximum power point. As shall soon be discussed, there are several alternatives to reach this goal. In the intermittent operation mode, the reactor's operation is commuted. As proved, there is an optimal frequency and duty-cycle capable of improving and maximizing the energy production. This happens due to the biofilm capacitive characteristics, allowing it to storage charge when the reactor is disconnected from the external load. The reactor reconnection forces the biofilm discharge, momentarily improving the reactor's energy production capabilities.

Forcing the reactor's operation in an optimal point is possible by different strategies. The maximum operating point of any reactor can be experimentally determined, by varying the external load of the reactor and measuring its output in voltage and current. The substrate availability, the medium pH and the temperature are examples of factors impacting this point. This optimum operation happens, theoretically, when the MFC's internal load is matched with the external load. Subjecting the MFC to that optimal operation is possible by conditioning the parameters that affect that load matching. Several research teams have presented mathematical models that allow simulating the reactor's internal behavior. The simplest models show a single internal equivalent resistance while the most complex add the capacitive effect of the biofilm. Tracking the MFC operation status is paramount, if efficient MPPT strategies are to be applied to the reactor. This tracking may comprise the instantaneous measurement of voltage or current. This information may then be used by a computational algorithm to determine the changes to apply to the reactor so as to shift its operating point towards the optimum. This data acquisition and processing is only possible with microprocessors and the respective electronics. The energy cost of this devices and procedures must be kept to the minimum, considering the main goal of making the reactor fully autonomous.

The energy extraction from the reactor can also be optimized by using a DC/DC converter. Several different types of converters have been tested and discussed in several published works. The main challenge to overcome is the low output voltage of the reactor. This characteristic may hinder the converter functioning, leading to an inefficient operation or no operation at all. Another suitable alternative is the combination of reactors. It was made clear that the reactor volume or electrode

area are not directly related with the amount of energy produced. As such, joining several reactors in series and in parallel may be a suitable solution to increase the technology's voltage levels. The series association of MFCs presents challenges connected with voltage reversal and the working with more than one reactor simultaneously forces the tracking of the maximum operating point individually.

An improved operation of the MFCs as power sources can also be achieved by combining different operational strategies, adjusting it to the final use of the energy. As was determined by the experimental trials, a single (or a set of) reactor(s) should be operated in a commuted manner in order to be applied to a DC/DC converter capable of improving and regulating the sourced power. Such a choice of controlled functioning presents a significative advantage when compared with the continuous operation: the bacterial colony is more evenly required to discharge a larger number of electrons, greatly diminishing the exoelectrogenic stress and current fluctuations. This steady charge can then be stored in a capacitor and timely used. If this energy was not converted to a regulated and predictable value, no useful guarantee of application could be provided, rendering the power source as useless. This work has addressed several topics, ranging from economics to electronics. The list below points to the most significant subjects in discussion:

- Discussion of the relationship between energy and wastewater, in the energy-water nexus panorama;
- Comprehensive state-of-the-art review and discussion of microbial fuel cell elements and designs and corresponding energy extraction solutions;
- Design and test of MFC reactors built from of-the-shelf components;
- Design and test of 3D printing MFC reactors;
- Development of an instrumentation platform used for polarization studies and biochemical and physical measurements;
- Study of biofilm development strategies;
- Evaluation of the cathode biofouling impact on power development;
- Comparison between substrate feeding options;
- Proposal of methodologies for the development of the steady-state and transient model of microbial fuel cells;
- Performance comparison between small and large volume reactors, with an adjusted number of anode brushes and cathode area figures;
- Voltage, current, power and energy performance comparison between single and grouped reactors, both in series and in parallel associations;
- Voltage, current, power and energy performance comparison between continuous and interrupted operation of MFCs;
- Determination of a reference value for duty cycle and frequency parameters in interrupted operation of MFCs;
- Study and discussion of operation similarities for a load or a capacitor connected at the MFC terminals;

- Proposal and discussion of a power management solution to guarantee that an MFC can be used as a reliable, regulated and intermittent power energy.

A future work section follows this discussion and materializes another contribution of this work, by highlighting where further research is more important and showing an application example for this technology.

Research trends and future work

According to the ISI Web Of Knowledge data [1], the first article published on microbial fuel cells dates back to 1962 and belongs to Davis and Yarbrough [2]. Their investigation studied if ethane and glucose could feed bacteria and produce an electrical output.

Since then, the number of publications on the subject has increased dramatically: from all the 10310 results for a search with the topic "microbial fuel cells", 9272 (about 90%) of them have been produced since 2010. In fact, more than 50% of the articles were published in the last 5 years. The MFC topic is under intensive investigation: countries like China, the USA, and India being the ones with the highest number of contributions. Figure 5.1 shows the continent-wise distribution of publications.

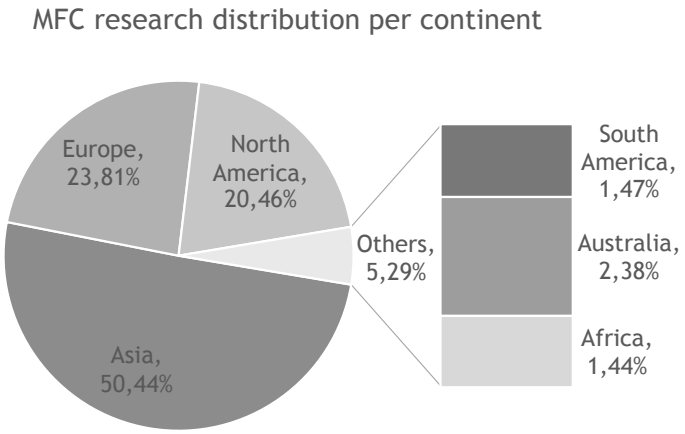

Figure 5.1 – General overview of the continent-wise research distribution in the topic of Microbial Fuel Cells, from 1962 until august of 2020.

Overall, two major areas for future research work can be identified: materials and reactor structure (configuration; dimensions); and energy conversion and regulation processes. Both investigation lines aim to increase the reactor's energetic production capability. Energy efficiency can be achieved with the development of new electrodes, where the main goal is to increase the electric potential difference between the anode and the cathode, whilst lessening the electrical losses. There seems to be an optimal relationship between the areas of the two electrodes. Nevertheless, the limiting factor for power production is the cathode area. The cost-effective relationship also has a top priority when choosing and developing electrode materials. The volumetric size of the reactors is another improvement aspect, having a direct impact on production capability. However, there are limits beyond which the capacity ceases to have a

directly proportional relationship. The reactor configuration (single, double, tubular camera) has a direct impact on the energy production capacity as well, particularly for electrode distance, disposition, and number.

Another research path related to power production optimization has been the improvement of diverse DC/DC converter topologies. The main issues to tackle are common to those found in other applications: the low starting voltage value and the adequacy of maximum power point methodologies, which invariably occur at the midpoint of the open-circuit voltage. It is also important to consider that the value of the open-circuit voltage depends on the energy availability and the operating conditions of the reactor. Therefore, it is crucial that automatic adjustment mechanisms are available to find a new relative optimum operating point of MFCs throughout its operation. This mechanism has an energy cost, which in some way reduces the overall efficiency. Alternatively, it appears that the conversion in intermittent mode, in counterpoint with the conversion in continuous mode, used by most of the early researches, seems to have a higher yield. This operating methodology provides higher operating voltages, and, for specific timeframes, allows extracting a greater amount of energy. It is, therefore, necessary to determine the relationship between the periods of charge and discharge that offer a more efficient mode of operation.

The idea of being able to harvest significant amounts of energy directly from the ambient is now achievable. This most certainly supports the development of modular designs, may they be big or small, for several different applications. Modularity allows more versatile applications and broader influence areas, which, in turn, leads to decreased costs and increased autonomy.

For instrumentation applications, energy harvesting powers more meaningful data acquisition designs: the control, quality and output of a process, irrespective of its dimension, is highly dependent on the degree to which it can be enhanced and monitored. The operation of wastewater treatment plants can be highly improved with the introduction of a monitoring system. Typically, the area of operation to cover is wide and, at the same time, data acquisition spots are inaccessible. These two reasons justify by themselves the introduction of wireless energy networks. This introduction is limited by the energy availability, which can restrict the usefulness of widely disperse monitoring systems. Devices powered by batteries require the periodical replacement of this component. This task adds cost to the operation of the system. At the same time, a monitoring system's service time is usually mainly limited by its power source's operating life.

Microbial Fuel cells technology adapts perfectly to the operation of wastewater plants. Monitoring of the wastewater biochemical parameters in key treatment steps can decrease operational costs and increase the efficiency of the cleaning process. Furthermore, analyzing the constitution of wastewater on key moments of its treatment may give greater insight as to why and how some processes can be enhanced and the treated wastewater can comply with the strict legislation parameters currently in place.

A wireless sensor network (WSN) using the MFC technology as its power can help to answer to the above challenge without meaningful expenses, as pictured in Figure 5.2. A sensor unit of that WSN would have two modules: the module comprising power source and regulation and the module for instrumentation and communication. As previously discussed, the communication feature needs a careful planning and design as it can account for major energy drainage. In the work presented in [3], [4], a network of intelligent actuators that collects the water level in a macrophyte lagoon is described by the authors. Smart sensors are powered by MFC and the network interconnection is based on the IEEE1451 standard.

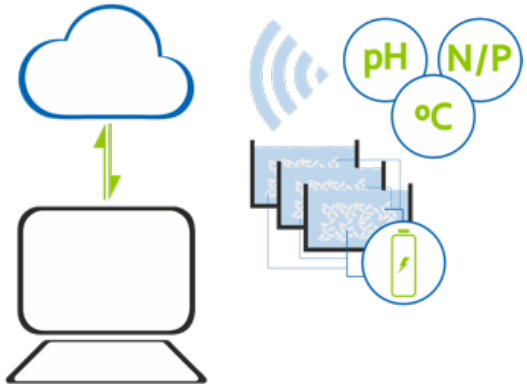

Figure 5.2 – A generic description of a wireless sensor network incorporating microbial fuel cells as a power source for biochemical sensors.

The wastewater composition can also be diverse, guaranteed an organic source is present. This solution can also be applied to other settings besides wastewater treatment plants: golf courses, natural reserves and ponds are particular examples. An estimated cost of approximately 83 euros per reactor[1] also promotes this technology as an interesting power source to apply in underdeveloped countries, where organically enriched water is more common than drinking water. As reviewed, the microbial fuel cell setup can also be explored as a transducer, providing biochemical measurements.

The inherent knowledge supporting this technology can be applied in different manners for different goals, while using the same materials. The ability to manipulate the bacterial metabolism to our needs is the greatest achievement of this research. As reviewed, the research paths rising from this topic are not strictly bound and can, due to a wide range of subjects, be addressed by scholars closer to biology, chemistry, engineering or even physics.

[1] The estimated cost for a single chamber air cathode MFC explored in this work was:
Anode=6.64€/brush, Cathode and membrane = 1.43€/7 cm², Acrylic reactor = 74.25€/ 28 mL, Titanium wire = 0.31€/ 5 cm.

References

[1] "Web of Science [v.5.35] - Principal Coleção do Web of ScienceResultados." [Online]. Available: https://apps.webofknowledge.com/Search.do?product=WOS&SID=F69UKci4pR5u1JvS8lI&search_mode=GeneralSearch&prID=bea0fd17-eb73-46d1-b89b-aca11e317d2c. [Accessed: 21-Aug-2020].

[2] J. B. Davis and H. F. Yarbrough, "Preliminary Experiments on a Microbial Fuel Cell.," *Science*, vol. 137, no. 3530, pp. 615–6, Aug. 1962.

[3] A. Espirito-Santo, P. Serra, S. Albuquerque, B. Ribeiro, F. Santos, and J. Pascoa, "Low-power smart sensing in energy and water systems integration," in *2017 IEEE International Workshop on Measurement and Networking (M&N)*, 2017, pp. 1–6.

[4] A. Espirito-Santo, S. Ambrosio, P. M. D. Serra, and R. J. C. Pinto, "Water pH Monitoring with a Smart Sensor Powered by a Thermoelectric Generator with a Phase-Change Material," 2019.